Origin of High Groundwater Salinity in the Omo Delta and its Surroundings (Southwestern Ethiopia) Hydrochemistry and Isotope Approaches

Abebayehu Tadesse

A Dissertation Submitted to
The School of Earth Sciences
Addis Ababa University

Presented in Partial Fulfillment of the Requirement for the
Degree of Doctor of Philosophy in Earth Sciences (Hydrogeology)
Addis Ababa, Ethiopia
September 2020

ADDIS ABABA UNIVERSITY
COLLEGE OF NATURAL AND COMPUTATIONAL SCIENCE, SCHOOL OF EARTH SCIENCES

Origin of High Groundwater Salinity in the Omo Delta and its Surroundings (Southwestern Ethiopia) Hydrochemistry and Isotope Approaches

A Dissertation submitted to the School of Graduate Studies of Addis Ababa University in partial fulfillment of the requirements for the Degree of Doctor of Philosophy (Ph.D.) in Hydrogeology

By Abebayehu Tadesse

Advisors: Dr. Seifu Kebede (main)

Prof. Asfawossen Asrat (Co-advisor)

September 2020

DECLARATION

I, Abebayehu Tadesse, hereby declare that the dissertation, which I hereby submit for the degree of Doctor of Philosophy (Ph.D) of science in Hydrogeology at the University of Addis Ababa, is my original work. To the best of my knowledge and belief, except as acknowledged in the text, the dissertation does not contain any written work presented by other persons whether written, pictures, graphs or data or any other. I also declare that I have complied with the rules, requirements, procedures and policy of the university.

Abebayehu Tadesse signature

Addis Ababa University
School of Graduate studies

Origin of High Groundwater Salinity in the Omo Delta and its Surroundings (Southwestern Ethiopia) Hydrochemistry and Isotope Approaches

By Abebayehu Tadesse

Approved by board of examiners:

Dr. Balemual Atnafu signature_____

Chairperson Date_____

Dr. Seifu Kebede Signature_____

Main advisor Date_____

Prof. Asfawossen Asrat Signature_____

Co-advisor Date_____

Examiners:

Prof. Tenalem Ayenew Signature_____

Internal examiner Date _____

Prof. Osman Abdalla Signature_____

External examiner Date _____

Abstract

The groundwater of the Omo Delta is characterized by the presence of fresh and saline groundwater side by side and the success of having fresh water is well below 50%. Therefore, most wells are abandoned due to elevated salt content. However, research on the origin of groundwater salinity and salinization processes, detail hydrochemical and isotopic composition of the Delta groundwater are lacking. The main objective of this work is to characterize the source of salinity and mechanism(s) of salinization in the Omo Delta (Southern Ethiopia) groundwater giving special emphasis on characterizing various morphological units and depositional environments recognized in the area and their implication on groundwater salinity. To achieve the objectives converging pieces of evidences from the conventional hydrogeological investigation, litho-hydrostratigraphic relationships, water chemistry, and isotope hydrology were used to elucidate the cause of groundwater salinity. The geochemical dataset and isotope were analyzed using different but complementary, approaches that allowed for insights into the process of salinization of groundwater in the study area. The correlation matrices of major anions, cations, and physical parameters of water indicate that elements chloride, sodium, fluoride, sulphate, and bicarbonates contributed from mineralization processes. The dominant effects of rainfall, rock weathering, and evaporation play a major role in the geochemical evolution of groundwater. Rock weathering was the main mechanism controlling the chemical compositions of the Hammer basement groundwater whereas; evaporation–crystallization is in the Delta aquifer groundwater system. The saturation index of anhydrite, aragonite, calcite, dolomite, gypsum, and halite shows that the groundwater in the study area was below the saturation with anhydrite, gypsum, and halite, indicating that these minerals are anticipated to dissolve. Moreover, groundwater samples were saturated to over-saturated with aragonite, calcite, and dolomite, implying that the three major carbonate minerals may have affected the chemical composition of groundwater in the study area. The variation of the hydraulic parameters at different locations and layers have been resulted from aquifer materials formed under different depositional environment. These deposits represent different aggradations and degradation phases that were usually accompanied by lake level changes. Groundwater movement and recharge are highly dependent on geomorphic features and depositional environments. Groundwater that is close to surface water sources

(River and Wadies) is fresh relative to other farther away from it, in the alluvial fan geomorphic feature, the fan apex is characterized by fresh groundwater compared to fan toe, which is more saline. The thickness of clay layers significantly affects the salinity of groundwater as it acts as the adsorption media and filtering membrane for groundwater in the Delta. The isotopic composition of most groundwater samples from sediment plot slightly far from the Global meteoric water line (GMWL) compared to the waters from the Hammer basement indicating that evaporative fractionation before recharge the sediments. The increase in groundwater salinity due to evaporation has resulted in a simultaneous isotopic enrichment. Both hydrochemical and isotope techniques indicate the dominance of local recharge and flow systems. The radon-222 concentration in groundwater samples showed a very wide range from 58.7 to 982.5Bq/m3 compared to the River and Lake Water samples that are range from 18.65 to 105.2Bq/m3 and 10.49 to 10.85Bq/m3 respectively. The highest concentration was found in the samples that were collected from wells close to the Omo River. From converging evidence of geology, hydrogeology, hydrochemistry, and stable isotopes of water, three processes are responsible for the salinization of groundwaters in Omo Delta: salinity originated from water-rock interaction, evaporation at or near the surface, and clay membrane filtration. The results of this study will also be useful to the development of a sound management plan for water resources and the direction of further research in the study area.

Keywords: Geomorphology, Hydrochemistry, Isotope, Omo Delta, Radon-222, and Salinity.

Acknowledgements

First of all, I thank God almighty, who provided me unlimited mercy and strength to go this long journey of the academic career. I have the greatest appreciation for my main advisor, Dr. Seifu Kebede for his guidance and support throughout the course of the study. A special thanks addressed to my co-advisor, Prof. Asfawosen Asrat, who invested his time, appeal knowledge, and energy in upgrading the manuscript of the Ph.D. thesis.

Thanks also go to Dr. Mulugeta Alene (former graduate program coordinator), Dr. Bayessa, Dr. Tarun Raghuvanshi, and members of the Ph.D. Supervisory Committee for their continuous follow-up. Thanks also go to Dr. Balemwal Atnafu, Head of School of Earth Sciences. I also appreciate the support I got from Mr. Worku and other members of the School. I am thankful to Dilla University for the opportunity given to me to pursue this study. I would also like to take this opportunity to thank South Regional State Water, Pastoral community development, and Agriculture bureaus for their support during fieldwork and laboratory analysis of water samples. Special thanks go to the Gedeo zone administration for their financial support during field works. Ministry of Water, Irrigation, Electricity, and National Meteorological Agency dually acknowledged for providing relevant data.

The author is thankful to the useful comments of Dr. Dessei Nedaw, Prof. Tenalem Ayenew, and Dr. Tilahun Azagegn. All family and friends (Tilahun Kebede, Nigatu Dansa, Dr. Behailu Berehane, Yohannis Degu, Debele Abera, Dr. Mersha Alemu, Befikadu Mekuria, and Desalegn Kekebo) who have been there for me deserve special appreciation.

Gratitude and love go to my wife Aster W/giorgis, for her love and courage, my children: Biniam, Tihunzer, and Bemihret deserve special thanks for their time-sharing and patience. My father, brothers, and Enaye deserve special appreciation for their prayer and courage. I thank brothers and sisters in Jesus Christ who have been prayed for my success, God bless you.

Table of Contents

List of Figures

List of Tables

List of Acronyms

Amsl	Above mean sea level
BH	Bore hole (well with depth more than 80 meter)
BoWI	Bureau of Water and Irrigation
DEM	Digital Elevation Model
EMA	Ethiopian Mapping Agency
FAO	Food and agriculture organization of United Nations
GIS	Geographic information system
GMWL	Global Meteoric water Line
GNIP	Global Network of Isotopes in Precipitation
GSE	Geological Survey of Ethiopia
HDW	Hand dug well (well with depth less than 10 meter)
IAEA	International Atomic Energy Agency
ITCZ	Inter-Tropical Convergence Zone
JJAS	June July August September
Kms	Kilometers
LMWL	Local Meteoric Water Line
MAMy	March April May
meq/l	milli-equivqlent per liter
mg/l	milligram per liter
NMA	National Meteorological Agency
OND	October November December
SW	Shallow well (well depth in between 10 to 80 meter)
SWWCE	South Water Works Construction Enterprise
TDS	Total Dissolved Solids
UNDP	United Nations Development Program
USGS	United States Geological Surveys
WHO	World health organization of United Nations

1. INTRODUCTION

1.1. Background

The provision of safe drinking water, as well as water of acceptable quality, remain prime targets for both advanced and developing countries. The presence of naturally occurring elements in excess amount in drinking water limit the acceptance for domestic and agricultural use. Smedley (1996), made an overview of the relationship between groundwater geochemistry and health and point out that not only anthropogenic source that create health and acceptability problems but also the natural baseline geochemistry of groundwater also playing a crucial role. In arid and semiarid environments, salinization of water resources becoming the forehead problems of water quality deteriorate. Rates of salinization vary broadly: in some cases, it is a lasting phenomenon concomitant with geologic processes; in others, it is induced by human activities and thus very topical. Due to a high level of salinity, many aquifers and river basins in the world become unfitting for human consumption (Vengosh et al., 1994; Ranjan et al., 2006; Sowers et al., 2011; Vengosh, 2014).

Diverse aspects of our lives are affected by water salinization. It worsens surface and groundwater supplies, restrict irrigation, municipal and industrial uses requires treatment and become costly, riverine ecosystems disturbed, salt-tolerant replaces the freshwater plants, fisheries used for a recreational and commercial purpose have been affected (Williams, 2001; Williams et al., 2002; Vengosh et al., 2014). It also enhances the mobilization of potentially toxic elements in groundwater, mainly due to the formation of metal-chloride complexes (Plant et al., 2003; Bäckström et al., 2004). In some areas, high saline groundwater is associated with high radium activity (Krishnaswami et al., 1991; Moise et al.,2000).

Lack of sufficient flushing in the unsaturated zone in arid and semiarid environments resulting in building up of salts on the ground. Many investigations (e.g. Nativ et al., 1997; Leaney & Herczeg, 2005) and in fracture surfaces (Weisbrod et al., 2000) reviled that salt accumulation and efflorescent were observed in many unsaturated aquifers in arid

environments. The different processes result in the formation of salt: Surface evaporation as described in (Allison and Barnes, 1985), Wetting and drying cycles include (Monjezeri, 1978), soil capillary, and capillarity transport of water and salts from the bulk rock matrix towards fracture surfaces (Weisbrod et al., 2000).

Many studies of regional aquifer systems show a general sequence of major ion evolution from low-salinity Ca–Mg– HCO_3 type to saline Na–SO_4– Cl groundwater along a hydraulic gradient (Herczeg et al., 1991; Mazor, 1997; Hendry and Schwartz, 1988; Kebede et al., 2007). Leaney & Herczeg (2005) demonstrated the increase of Na+ and Cl- ion ratio compared to other dissolved salts ($Na^+ + Cl^-$/TDS) along flow direction in Murray aquifer-Australia. Several processes are responsible for the increase of salinity and chemical modification of groundwater from bicarbonate type towards sodium and chloride ions. Some of them are (i) advection and diffusion of saline waters trapped in an aquitard that is associated with dynamic aquifer and (ii) dissolution of soluble salts such as gypsum and halite minerals within the aquifer. The entrapment of saline fluids in geological units of low hydraulic conductivity that is connected to active aquifers may result in diffusion of solute and a gradual increase of salinity (Herczeg et al., 2000).

Identifying the source of the salinity is vital for model prediction and thus water management and remediation (Vengosh, 2005). Proper management of available groundwater reserves is impossible without the knowledge of the spatial distribution of fresh and saline groundwater and the processes that determine the evolution of salinity. Typically, geophysical (e.g. electrical and electromagnetic methods) and geochemical methods are used to establish the extent and sources of groundwater salinity. Electrical resistance is highly sensitive to the salinity of pore-water in the subsurface and is therefore effective in defining fresh and saltwater (Chongo et al., 2011; Zarroca et al., 2011). On the other hand, geochemical methods offer a good perspective of geochemical processes affecting groundwater quality, which is essential in locating and managing usable water supplies (Herczeg et al., 1991; Bouchaou et al., 2008).

The deltas are an ecologically sensitive region in which various water species (including groundwater and surface water, saline and fresh waters) are in dynamic equilibrium, more importantly, the groundwater in major Delta system of the world is affected by water

quality/salinity problems (Nissenbaum, 1980; Mccarthy, 2006; Milzow et.al., 2009; Al-agha et.al., 2013). It is the terminal sink of a large river system. Huge amounts of water are lost by evapotranspiration in most deltas (Gieske, 1997; McCarthy and Ellery 1998; Bauer et al., 2006). Evaporation is a fully accumulating process, i.e. all the dissolved solids remain in the residual water. Transpiration partly takes the dissolved solids away with the water uptake and partly leaves them behind, but in the long term, vegetation does not remove salt, it simply stores the salt (Milzow et al., 2009). Many researchers have been interested to understand the nature of groundwater in the Deltas because of serious problems encountered in the area of deterioration of groundwater quality and quantity (Mabrouk et al., 2013).

1.2. The Problem of Groundwater Salinization

Groundwater accounts for the largest readily available freshwater reserve of the world population (Morris et al., 2003; vanLoon and Duffy, 2005; Monjerezi, 2012). In developing countries, groundwater is preferred from surface water because it is cost-effective, needs less treatment, and reliable water resources (Appelo, 2005, Bovolo et al., 2009) for home, irrigation, and industrial purpose. In most arid and semi-arid, groundwater quality degradation is caused by the salinization of water resources (Richter and Kleitler, 1993; Vengosh, 2005). In arid and semi-arid zones and most deltas, the future exploitation of aquifers largely depends on the degree and rate of salinization (Vengosh and Rosenthal, 1994).

Groundwater salinity is commonly described by chloride or total dissolved solids content (TDS) (Monjerezi, 2012. In some areas, high saline groundwater is associated with high radium activity (Zukin et al., 1987; Krishnaswami et al., 1991; Moise et al., 2000; Monjerezi, 2012). Long-term use of water with high content sodium for irrigation results in a significant reduction of hydraulic conductivity and hence the fertility of the irrigated soil (Richards, 1954). Similarly, the industrial sector demands water of high quality, typically with low levels of dissolved salts.

Sound geochemical understanding of the occurrence of saline groundwater resources in different geomorphic settings is of vital interest as the groundwater resources play a major

role in the water supply system and irrigation and the negative effect of salinization on their quality. Determination of the source of salt and mechanisms that redistribute the salt to other areas where it becomes the problem is challenging for the scientific community and practitioners (Gunn and Richardson, 1979; Tickell, 1997).

The salinity level of irrigation water determines its applications for agricultural uses. Many crops, such as citrus, avocado, and mango, are sensitive to salt concentrations in irrigation water (Vengosh, 2004). Furthermore, long-term irrigation with sodium-rich water consequences in a substantial decrease of the hydraulic conductivity and therefore the fertility of the irrigated soil. Likewise, several industrial sectors use require water of little salinity. The high-tech industry, for instance, requires large amounts of water with low levels of dissolved salts. Hence, the salinity level of groundwater is one of the restrictive factors that limit the suitability of water for different applications (Grieve and Poss, 2000; Kudo et al., 2010; Rengasamy, 2010).

The hydrogeological context of the Omo Delta is poorly investigated. However, Kebede (2013) studied the groundwater of the Omo Delta and pointed out that the presence of fresh and saline groundwater side by side. He also presented that the success of having fresh water is well below 50%. Moreover, most wells are abandoned due to unsuitable salt content. However, research on the linkage between geomorphic processes and the groundwater salinity, detail hydrochemical, and isotopic composition of the Delta groundwater is lacking. Besides, the questions of origin(s), the mechanism(s) that distribute the saline groundwater, its lateral and vertical distribution, and how the Delta's geomorphology affects the distribution of salt in groundwater yet not fully understood. Sound geochemical and isotopic understanding is vitally important to determine the source of salinity, their mechanism of distribution, surficial and vertical distributions in different geomorphological settings.

Recent development plans proposed and executed in the Omo Delta would call for high water demand. Moreover, the principal source of water supply for livestock and human consumption in the lower Omo and adjoining regions are highly dependent on groundwater. However, the development of groundwater is seriously challenged by a

chance of miss or hit of high salt content groundwater. This study focuses on investigating the origin of groundwater salinity prevailed in the Omo Delta and its surrounding using hydrochemistry and stable isotope of water, and thereby identify salinity safe sources.

1.3. Overview of groundwater salinization

The term "salinization" is defined as an increase in the concentrations of specific chemical constituents as well as in overall chemical content (Total Dissolved Solids) over background levels (Monjerezi, 2012). Different classifications are applied in the literature to rank water resources based on levels of salinity (Robinove et al., 1958; Davis, 1964; Carpenter et al., 1974; Carpenter, 1978; Freeze and Cherry, 1979). These classifications vary in number and label of classes, values of class ranges, and the constraints to which class ranges are linked (Electrical conductivity, Total dissolved solids, or chloride content). A classification made by Park et al (2011) was adopted in this thesis. Accordingly, Groundwater with EC < 1500 μS/cm were classified as "fresh", those having EC within the range 1500–3,000 μS/cm were classified as "brackish", and those with EC levels > 3,000 μS/cm were described as "saline." The concentration of salt in groundwater be an environmental problem when there is a source of salt, water to mobilize it, and the mechanism that redistributes the salt to the location that causes an environmental problem (Tickel, 1997). In this section, the overview of the source of salty water and salinization processes that commonly deteriorate fresh groundwater has been made.

1.3.1. Seawater intrusion

Vengosh (2014) describes that "Salt-water intrusion is one of the most widespread and important processes that degrade water quality to levels exceeding acceptable drinking and irrigation water standards, and endanger future water exploitation in coastal aquifers". Seawater intrusion is exaggerated by increase of population growth inhibit the costal land and these days, closely 70% of the world population inhabits the coastal plain zones. Human activities like irrigation, pumping, recycle of wastewater promote the rate of salinization (Jones et al., 1999). Extensive freshwater withdrawals is the main cause of the seawater intrusion in many coastal aquifers around the world. Salinity of Ocean water has

TDS of 35g/l. whereas, internal seas (Mediterranean Sea, Red Sea; have average TDS around 40 g/l) or lesser salinities. Major constituents has long residence time that seawater has uniform chemistry (Jones et al., 1999). In many situations, the saline water characterizes a Ca-chloride composition with the ratio of Ca/ (SO_4+HCO_3 is greater than 1, whereas, low ratios of Na^+, SO_4^{2-}, K^+, and B to chloride are compared to modern ocean water (Vengosh, 2014).

Base-exchange reactions with the aquifer rocks are important process that are responsible for geochemical modification of seawater intrusions (Sayles et al., 1977; Appelo et al., 1987; Appelo and Postma, 2005; Vengosh, 2014). Organic matter, clay minerals, oxy-hydroxides, and fine-grained rock materials are cation exchangers in aquifers (Custodio, 1987, 1997; Appelo and Postma, 1993; Custodio et al., 1993; Jones et al., 1999) which have mainly Ca^{2+} adsorbed on their surfaces.

During seawater intrusion to a coastal freshwater aquifer, Na^+ exchanges part of the Ca^{2+} on the solid surfaces. Consequently, Ca^{2+} is released, Na^+ is taken up by the solid phase, the solute composition changes from an Mg-chloride into Ca-chloride type water, the (Ca^{2+} +Mg^{2+})/Cl ratio increases, and the Na^+/Cl^- ratio decreases (Appelo and Postma, 1993; Custodio et al., 1993; Jones et al., 1999).

1.3.2. Mixing with saline water

The groundwater flow along a regional aquifer systems show the general sequence of major ion evolution from low-salinity Ca–Mg– HCO_3 type to saline Na–SO_4– Cl groundwater along a hydraulic gradient (Herczeg et al., 1991; Mazor, 1997; Hendry and Schwartz, 1988; Kebede et al., 2007). Many studies of regional aquifer systems Leaney & Herczeg (2005) demonstrated the increase of Na^+ and Cl^- ion ratio compared to other dissolved salts

(Na^+ + Cl^-/TDS) along flow direction in Murray aquifer-Australia. Several process are responsible for the increase of salinity and chemical modification of groundwater from bicarbonate type towards sodium and chloride ions. Some of them are: (i) advection and diffusion of saline waters trapped in an aquitard that associated to dynamic aquifer and (ii) dissolution of soluble salts such as gypsum and halite minerals within the aquifer. The entrapment of saline fluids in geological units of low hydraulic conductivity that connected

to active aquifers may result in diffusion of solute and a gradual increase of salinity (Herczeg et al., 2000).

1.3.3. Membrane filtration

Salinization of many aquifers is induced by the intrusion of underlying or adjacent saline groundwater or saline-water flow from adjacent or underlying aquifers (Magaritz et al., 1984; Hsissou et al., 1999; Vengosh et al., 1999; Kloppman et al., 2001). Maslia et al., (1990) in his study in the upper Floridan aquifer in Georgia, explain that, faults breach the nearly impermeable units of the underlying confined aquifer and allow upward leaking of saline groundwater. In the southern High Plains, Texas, USA are cross-formational flow from underlying evaporate units of saline plumes are cross-formational flow from underlying evaporate units (Mehta et al., 2000). Dissolved ions pass through the clay or shales less readily than neutral water molecules. Hanor (1994) reviled that the filtering of salt is taking place as the result of electrostatic repulsion of the dissolved ions by electrical layers around clay minerals. In upper parts of alluvial landscape, the saline groundwater table are generally deep and salt accumulation is usually at deeper depth. As progression towards the plain, the rate and amount of downward percolation of saline groundwater banned by soil texture and subsoil permeability. In coarse textured horizons, faster rates of water flow occur since the average pore diameter is larger than in fine textured soils. This phenomenon resulted in to lateral flow of water and solutes along the surface of the impermeable clay layer. When the contact between two different layers approaches the soil surface along a hill slope, the laterally moving water (with dissolved ions) will create a wet spot that eventually become saline as the accumulated water evaporated (Fitzpatrick et al., 2000).

1.3.4. Mixing with hydrothermal saline fluids

Mixing of fresh groundwater with hydrothermal saline fluids resulted in Salinization of groundwater. High salt content characterizes the thermal fluids found in marine and non-marine settings (Vengosh, 2014). Vengosh et al. (2002) investigate that, in western Turkey, the salinity of thermal water is in the range 2– 66 g/l, with a high content of boron (>50 mg/l. Edmunds et al., (2002) also explained that, in Mexico City, thermal water affects the

quality of local groundwater. Along with chloride content, thermal waters are often enriched in Na, B, F, Ar, and other contaminants that present a risk to the related freshwater resources (Vengosh, 2014).

1.3.5. Evaporation at or near the surface

Evaporation is the most influential process resulting in saline soils in arid and semi-arid environments (Deverel and Gallanthine, 1989) and groundwater where there are a shallow water table and a climate with evapotranspiration that exceeds the precipitation (i.e. net negative water balance) (Yechieli and Wood, 2002). This is the most commonly reported cause of salinity in closed basins (Sowayan et al., 1989). In closed basins, the brines start simply as recharge along surrounding highlands, which then accrues dissolved solutes through weathering and dissolution of readily soluble mineral compounds (e.g. calcite, halite) along flow paths. In addition to a net water loss, due to a negative water balance, this results in a general increase in TDS content, from low TDS Na-Ca-HCO3 recharge water to high TDS Na-Cl water in topographically low discharge areas in the center of the basins (Monjerezi, 2012).

A long-term accumulation of salts on the ground and a lack of adequate flushing in the unsaturated zone in a dryland environment is a natural phenomenon that resulted in formation of saline groundwater. In many arid areas, salt accumulation and efflorescent crusts in the upper unsaturated zone and fracture surfaces is common observations (Weisbrod et al., 2000; Vengosh, 2014). The salt formation has been attributed to wetting and drying cycles (Drever et al., 1978), surface evaporation (Allison et al., 1985), soil capillarity, and capillarity transport of water and salts from the bulk rock matrix towards fracture surfaces (Weisbrod et al., 2000).

Richter et al. (1993) point out that, along the flow path the salinity of the groundwater in the western United States that recharged typically occurs along surrounding highlands, and groundwater flows towards the basin centers, along the flow path the salinity of the groundwater rises by several orders of magnitude by both salt dissolution and extensive evaporation. The initial freshwater composition and the subsequent saturation to typical minerals (calcite, gypsum, sepiolite, and halite) determines the chemistry of the residual

saline groundwater. In Deep Spring Lake (Jones, 1965), Death Valley (Hunt et al., 1966), and the Sierra Nevada Basin (Garrels et al., 1967) it was observed that evaporation and mineral precipitation mainly control the salinity of groundwater.

1.4. Previous Studies

Geological and hydrogeological studies of the Lower Omo Basin has been poorly investigated compared to other parts of Ethiopia. However, some investigations have been conducted in connection to mapping geological units, petroleum resources, land use, paleontological interests, and accessing groundwater in the region.

The Ministry of Water Resources (2007) has conducted the hydrogeological investigation in connection with the preparation of an integrated master plan of the Omo-Ghibe Basin. In this study, attempts were made to determine the groundwater resource potential and its distribution in the Omo-Gibe Basin mainly on the upper basin to assist water resource planning. In this study, inventory has been made on the distribution of water wells and springs in the basin but their aquifer characterization and hydrostratigraphy were not described. In addition, some geophysical investigation (vertical electrical sounding) was conducted in areas, which lack subsurface hydrogeological data. This study is good to give some factual data in the basin, but they have not been interpreted.

Davidson et al. (1983) had conducted a mapping of geological units of the Omo Basin. On the "Preliminary report of the Omo project", they demonstrated details of the petrography, geochemistry, and geochronology of lithologic units that exist in the region. Tilahun (2012) predicts the possible geologic structures that can play an important role in the fluid movements using gravity data analysis in the Lower Omo Basin. This study gives very interesting clues on the hidden structures that obscured in thick sediment that cover the lower Omo Basin and Lake Turkana, which can affect the movement of groundwater in the basin.

Ebinger et al. (2000) studied the Rift deflection, migration, and propagation with the main interest to understand the linkage of the Ethiopian and Eastern Rifts. This study shows a chronology of rifting and volcanism in the zone of overlap and correlates stratigraphic sequences with those in Kenya rifting and volcanism to the south and the Main Ethiopian

Rift to the north. The distribution of seismicity and the Quaternary volcanism suggest that the Eastern and Main Ethiopian Rifts are currently linked across a 200-km-wide zone between the Omo and Segen basins. In addition to this, Ebinger et al. (2000) confirm that, all three arms of the broadly rifted zone developed during Mid-Miocene episodes of faulting, with subsequent southward propagation of the Chew Bahir-Gofa Province and Main Ethiopian Rift. The Eastern Rift propagated northward to form the North Omo and Usno basins. Butzer (1971) conducted the earliest geomorphic, hydrologic, soil, and land use-land cover work in Omo Delta. This is the most specific study of the region and gives detailed information on the geomorphology and hydrology of the Delta. However, this study did not consider the groundwater hydrology of the Delta and its environs.

Very few studies consider the groundwater hydrology of the Omo Deltas and its surroundings. The most important ones are Kebede (2009): this is a prime work that treats the Omo Delta as hydrogeological units. In this work, he addresses the hydrogeological units and hydro-chemical information on Delta groundwater. Other regional studies that cover the whole Lower Omo basin are Avery (2012), Tefera (2017), Assefa consult (2017), and Jean (2005) presented the hydrogeology of the Omo Delta and Lake chew-Bahir.

Groundwater resources play a significant role in water supply in the study area, as there is no surface water except the Omo River in the vast area of Omo Delta plain. The groundwater quality in the area is largely affected by high salt content. Moreover, the Omo Delta region is recognized as a high potential site for surface water irrigation and some irrigation projects already started. On the other hand, the groundwater underlying the vast plain of the Omo Delta contains the highest groundwater salinity. The negative effect of salinization on its quality needs an urgent and meaningful approach to the study origin of groundwater salinity. Therefore, detailed investigations on the complex hydrogeological setup, groundwater dynamics, and geochemical evolution will have great importance in the future groundwater resource development and management in the region.

1.5. Objectives

1.5.1. Main Objective

The main objective of the research is to characterize the source of salinity and mechanism(s) of salinization in the Omo Delta groundwaters.

1.5.2. Specific Objectives

The specific objectives are:

- Characterizing various morphological units and depositional environments recognized in the area and their implication on groundwater salinity.
- Investigating the interaction between groundwater and surface water in the Delta.
- Identifying sources of salinity water in the lower Omo Delta aquifer.
- Investigating potential flow mechanisms and pathways for the movement of groundwater and examine the relationship between salinity and hydraulic head and permeability zones.
- Investigating the geochemical evolution of the groundwater chemistry following the regional groundwater flow direction.

1.6. Research Questions

The main questions of this research include:

- What is the source of salinity in the Omo Delta groundwater?
- How is saline groundwater distributed?
- How does hydrochemistry vary and evolve from the headwater to discharge areas?
- Is groundwater flow pattern continuous across geologic terrains?
- How do micro-geomorphologies affect the salinity of the groundwater in the Delta?

1.7. The Significance of the Research

For the scientific community, dealing with the challenges of groundwater management, the major challenge facing hydro-geochemical investigations of saline groundwater is the determination of the source of salt. Moreover, the groundwater salinity problem in most Deltas of the world is salt-water intrusion due to sea level rises and excess exploitation. This is not the case in the Omo Delta, and the Turkana Lake level has been declining and over-exploitation of groundwater is not currently a serious concern. Therefore, the output of this research can be used as a baseline regarding groundwater salinity in the inland Delta's of Ethiopia.

Large-scale economic activities are being undertaken in the upper catchment and within the Delta. The Kuraz sugar irrigation project, resettlement of pastoralist community, and oil and gas prospecting are some of such activities. Moreover, the population of rural communities and small villages are depend on shallow and deep groundwater resources for safe drinking water supply. These indicate the vital significances of the Omo River water and groundwater of the Delta in the socio-economic activities of the region. To sustain these significances, an accurate understanding of the source and distribution mechanism of saline groundwater in the Delta is very important in safe sourcing. This has a significant contribution to the development of the resource usually characterized by failures of hit and miss identification of appropriate borehole sites. The major output of this research is therefore crucial in this respect.

1.8. The Structure of the Thesis

This thesis is organized into seven chapters. Chapters 1 mainly provide background information on the nature of the problem of groundwater salinity; the literature review and objectives of the work. Chapter 2 gives detailed information on-site characterization of Omo Delta including geology, geomorphology, climate, the evolution of Omo Delta. Chapter 3 deals with the methodology used in this study: Water stable Isotopes, hydrochemistry, Radon-222, and classical hydrogeological methods are described in detail.

Chapter 4 discusses the sampling, sampling analysis, and the data used in this research. Chapter 5 discusses the results of major element chemistry, Radon-222 from groundwater and the River, Water stable isotopes, piezometric levels maps. Chapter 6 is a discussion on the results of hydrochemistry, stable isotopes of water, and Radon-222 with respect to research objectives: The role of the Omo River on freshening, geochemical evaluation and relation to groundwater flow, Origin of salinity in groundwater, quality of groundwater prevailing for different purpose, groundwater management challenges and implication for water management. Finally, the thesis ends with chapter seven containing the conclusion and recommendations, giving more emphasis to the basic results achieved and issues to be improved for further work by scientific research and intervention of decision-makers.

2. METHODOLOGY

Delta environments are so complex that morphologic suites, overall geometry, sediment properties, and lake level fluctuation creates a very dynamic environment (Basan et al., 1985) which resulted in dynamic geologic setups and hydrogeological environments. This needs the application of various hydrogeological and hydrochemical methods to understand and conceptualize the cause of groundwater salinity in the Delta system. Thus, an effort has been made to apply various disciplines and synchronize results from each dataset to describe the pattern, dynamics, and origin of groundwater salinity in the study area.

The general emphasis is put on the characterization, analysis, and interpretation of hydro-geochemical and isotope data in understanding the groundwater salinization processes. Each source of salinity has a unique and distinctive chemical and isotopic signature. The underlying principle in all geochemical techniques used for tracing salinity sources is the assumption that the chemical and isotopic signature (or fingerprint) of the original saline source is preserved during the salinization process. However, water-rock interactions may modify the original composition of the saline source and therefore mask its identity (Monjerezi.et al, 2012).

2.1. Geochemical tracers

The major and minor elements occur in distinct ratios in different sources of salinity (Richter and Kleitler, 1993). Permutations of ratios of major and minor constituents such as Br^-/Cl^-, B/Cl^-, Na^+/Cl^-, I/Cl^-,Mg^{2+}/Cl^-, K^+/Cl^-, $Ca2^+/Cl^-$, SO_4^{2-}/Cl^-, Cl^-/NO_3^- and $(Ca^{2+}+Mg^{2+})/SO_4^{2-}$ can be used to distinguish between the major sources of salinity. Successful examples are given in Saffigna and Keeney (1977), Howard and Lloyd (1983), Hill (1986), Richter and Kreitler (1986), Novak and Eckstein (1988), Bassett (1990), Vengosh et al. (1991a, b, 1992, 1994). João et al., (2015) show that groundwater can acquire their composition through the progressive concentration of dissolved ions by evaporation, and studies by (Pereira et al., 2006; Machado et al., 2007) pointed out the importance of the contact between water and rock as the origin of the salts dissolved in groundwater.

Chloride is preferentially partitioned over bromide into sodium, potassium, and magnesium halogen salts during precipitation (Siemann and Schramm, 2000). Therefore, brine formed by the dissolution of halite, are associated with low Br/TDS (Rittenhouse, 1967) and Br/Cl ratios (Hanshaw and Hill, 1969; Worden, 1996). On the other hand, brine derived from evaporated seawater are characterized by high Br/Cl (Carpenter et al., 1974; Stoessell and Carpenter, 1986; Kharaka et al., 1987; Moldovanyi and Walter, 1992). Similarly, an intermediate Br/Cl signature is associated with contributions from both sub-aerially produced brines and brines generated by the dissolution of halite (Egeberg and Aagaard, 1989).

The geochemical modeling program PHREEQC.v3 (Parkhurst and Appelo, 1999) was implemented with MINTEQ.v3 database (Allison et al., 1991), to calculate saturation indices (SIs) to the main mineral phases.

2.2. Isotope tracers

Stable isotopes of water (O, and H) were used as tracers for the source of salt and distribution mechanism. The original values of $\delta^{18}O$ water and $\delta^{2}H$ water of saline sources are usually modified by mixing (dilution) with meteoric water (Banner et al., 1989; Bergelson et al., 1999). The δD-$\delta^{18}O$ relationships are used to calculate mixing relationships between saline and fresh groundwater e.g. in case of saltwater intrusion (Jones et al., 1999; Yechieli et al., 2001) or reflect agricultural return flows (Davisson and Criss, 1993). The stable isotopes of water may also be used for investigating the degree of water-rock exchange (Hanor, 1994). They may also be used to assess the effect of evaporation on groundwater or finding a water source subjected to evaporation since the groundwater subjected to evaporation is enriched in $\delta^{18}O$ and $\delta 2H$ (Hanor, 1994; Vengosh et al., 1999; Butler, 2007). To evaluate the sources of groundwater salinity (Z-Kattan, 1996), the chloride concentration is plotted against $\delta^{18}O$ values. This plot suggests the processes for increasing salinity. Enrichment by evaporation and enrichment due to soil salts dissolution: stable isotope concentration does not change with increasing chloride concentration.

Isotopes are forms of a given chemical element that have different atomic masses. For a particular element, the isotopes have the same numbers of protons and so have the same atomic number. However, each isotope has a different number of neutrons and therefore has a different atomic mass. Stable isotopes are those isotopes that do not undergo radioactive decay. Therefore, their nuclei are stable, and their masses remain the same. However, they may themselves be the product of the decay of radioactive isotopes. In hydrological studies, the stable isotopes of interest generally relate to H, C, N, and O. In terms of the water molecule itself, oxygen has three stable isotopes, ^{16}O, ^{17}O, and ^{18}O; and hydrogen has two stable isotopes, ^{1}H and ^{2}H (deuterium). The relative abundances of the lighter isotopes of hydrogen (^{1}H=0.999) and oxygen (^{16}O=0.997) are naturally high(Kendall and Mcdonnel, 1998). The stable isotopes of ^{18}O (oxygen-18) and ^{2}H (deuterium) are used to provide information on hydrological processes, including groundwater-surface water interactions. The use of isotope tracers in hydrogeological studies has been increased dramatically. Some detail information on the application of environmental isotopes in hydrological investigations can be obtained from Fritz and Fontes (1980), Fontes and Edmunds (1989), Coplen (1993), Gat (1996), Mazor (1997), Clark and Fritz (1997), Kandall and Mcdonnel (1998), Cook and Herczeg (2000), Mazor (2005), Kebede (2013), Yasine (2015), Jemila (2017) and Others. Salinization of water resources is one of the most prominent causes of groundwater quality degradation, particularly in arid and semi-arid regions (Richter and Kleitler, 1993; Vengosh, 2005). Future exploitation of aquifers in many water-scarce regions, such as the arid and semi-arid zones, depends largely on the degree and rate of salinization (Vengosh and Rosenthal, 1994). A critical component in assessing freshwater is knowledge of the water cycle; how water supplies are recharged (occurrence), accumulation, and distribution of groundwater resources. Water undergoes phase transitions, interacts with minerals and the atmosphere, and participates in complex metabolic processes essential to life. The isotopes of hydrogen and oxygen undergo large fractionations during these processes, providing a multiple isotopic tracer record of diverse phenomena (Clark and Fritz, 1997).

The intrinsic values of water $\delta^{18}O$ and $\delta^{2}H$ of saline sources are usually modified by mixing (dilution) with meteoric water (Banner et al., 1989; Hanor, 1994; Bergelson et al., 1999). The δD-$\delta^{18}O$ relationships are used to calculate mixing relationships between saline

and fresh groundwater e.g. in case of saltwater intrusion (Jones et al., 1999; Yechieli et al., 2001) or reflect agricultural return flows (Davisson and Criss, 1993). The stable isotopes of water may also be used for investigating the degree of water-rock exchange (Hanor, 1994). They may also be used to assess the effect of evaporation on groundwater or finding a water source subjected to evaporation since the groundwater subjected to evaporation is enriched in ^{18}O and ^{2}H (Hanor, 1994; Vengosh et al., 1999; Butler, 2007; Monjerezi, 2012).

2.3. Radon (^{222}Rn)

Radon (^{222}Rn) is typically found in higher concentrations in groundwater than in surface water, as it is released from radon-bearing rock. Therefore, radon can be used as a reliable tracer to identify local areas of groundwater input to a stream (Yoneda et al. 1991). Therefore, a relatively high 222Rn concentration in a river/seawater suggests the groundwater discharge area (Saito et.al, 2012). In this research, 222Rn was used to justify the groundwater-surface water interaction so that the dynamics of salt in the groundwater can be traced.

222Rn concentration in the water was analyzed by a widely used portable commercial α detector RAD7 and the RAD H2O accessory (Durridge Company, USA) at a spot and within 12h of sample collection. For radon concentration analysis in surface water, Big Bottle System (2.5 L), an accessory to the RAD-7 radon monitor was used. The internal pump of the RAD-7 extracts radon from groundwater and the radon circulates to the RAD-7 detector in the RAD-H2O system. 222Rn concentration in water was corrected for time-lapse between sampling and measuring as discussed in (Diab, 2019; DURRIDGE Company, 2019) and Radon in water is calculated using CAPTURE free software.

2.4. Lithological investigations and Piezometric level measurements

Changes in facies and thickness of sedimentary deposits seem to play an important role in determining groundwater flow and hydraulic continuity. Lithologic variability in the aquifer may affect water chemistry and groundwater age distributions because of its effect on rock-water interactions and directions of groundwater movement (Edmunds et al., 1997).

In this regards, the previous geological and hydrogeological works were collected and analyzed to derive information about fracture orientation, connectivity, spacing, and filling material, and lithological characteristics such as degree and depth of weathering, nature of primary porosity and nature of lithologic contact to determine the movement of saline groundwater. Based on the identified data gap, these features have been mapped, measured, or described in the field. A water table contour map is a very important tool in groundwater study as one can derive from it the gradient and the direction of the groundwater flow and possible indicator of aquifer structure (Heath, 1983; Ismail et al., 2010, Kebede et al., 2016).

3. DESCRIPTION OF THE STUDY AREA

3.1. Location

The Omo River, the main drainage for the southwestern Ethiopian highlands, originates from the Ethiopian Plateau, west of the Ethiopian Rift Valley. Its headwaters share a drainage divide with the White Nile and the Blue Nile. Along the divide with the Blue Nile, several volcanic peaks up to 3,400 m in elevation exist that have well-preserved constructional features including crater lakes (e.g., Mount Wenchi). The Omo River flows southward through a deep gorge to the Lower Omo Valley, a broad tectonic depression, and finally into Lake Turkana (Figure 3.1).

The study area is located in Southwestern Ethiopia and covers 8,291 km^2 bounded by 489486N and 650706N latitude and 161659E and 252961E longitude. A well-used tourist route Addis-Jinka accesses it. The road from Key-Afer to Omorate along the eastern foothills of the Hammer range gives easy access to the western part of the basin. In the dry season, the whole basin is drivable to off-road. Omo Delta is located at the junction of the Omo River with Lake Turkana at borders of Ethiopia, Kenya, and South Sudan (Figure 3.1). It has a total area of about 1600 km^2. Depending on the fluctuations in the level of Lake Turkana, the Delta plain has been rapidly and repeatedly submerged or laid dry during the last several centuries (Butzer, 1972; Feibel, 2011; Avery, 2012; Avery et al., 2012).

3.2. Physiography

The topography of the Lower Omo Valley is very subdued, with only the Korath Range standing ~300 m above the general level of a broad, flat region that extends ~100 km from the Hammer Range in the east to the Lorienetom Range in the west. The Omo Valley has a breadth of about 20 km and is bounded both east and west by mountains that exceed 1000 m in elevation. The land surface slopes very gradually (60 m vertically in ~90 km) from Kibish toward Lake Turkana. The Omo River course is divided into four distinct geomorphologic sections Omo River profile from Karoo Dus to Lake Turkana (Figure 3.2).

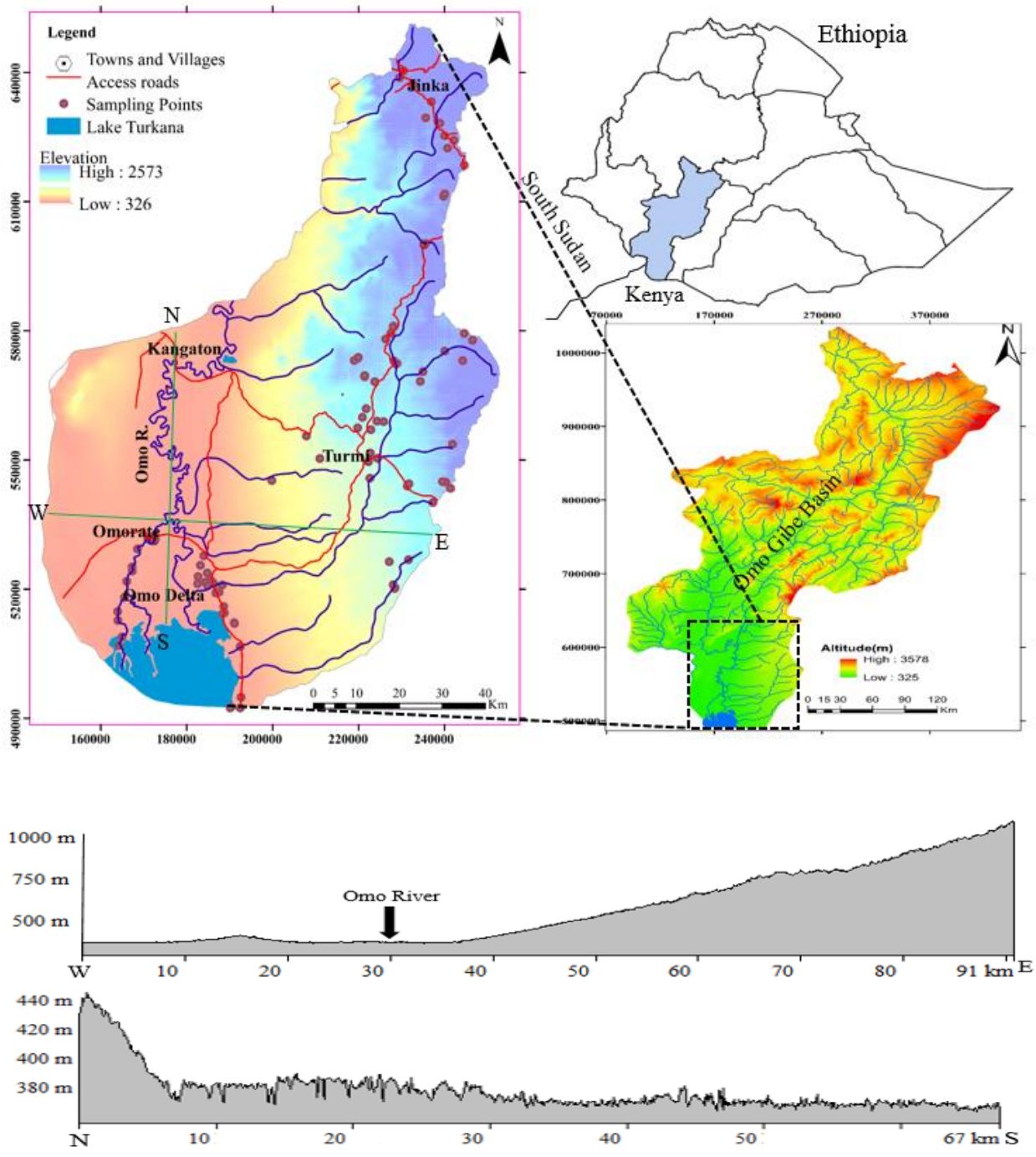

Figure 3.1 Location map of the study area and sampling points (above) and physiographic profile across line W-E and N-S (below).

Channel 0-25kms: This stretch from Kangaton to down 25km. The channel is characterized by the absence of meanders. It emerges from the deep gorges with River slope 0.54m/Km, that the water speed is sufficiently high to prevent deposition of sediments.

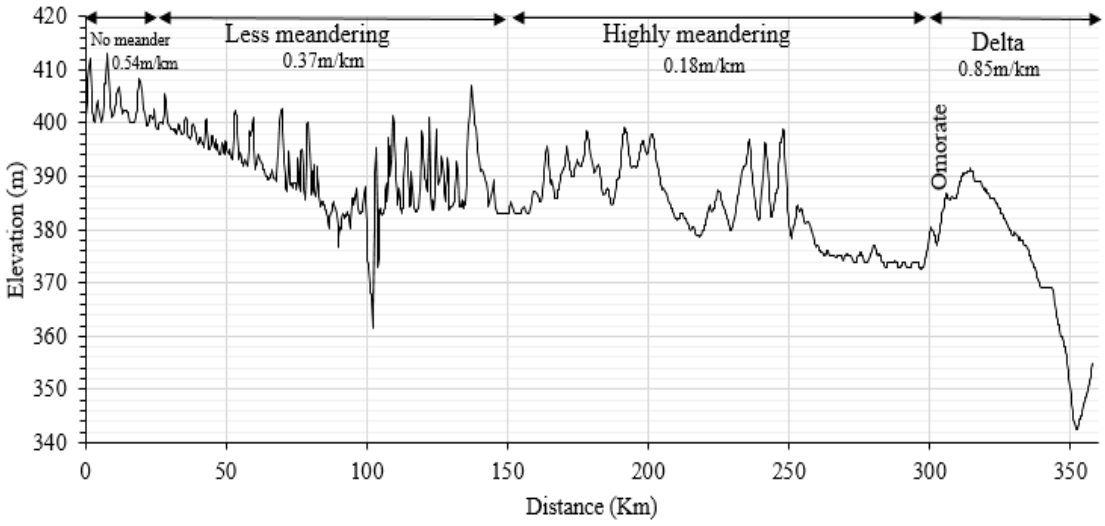

Figure 3.2 Omo River profile from Karoo Dus (Kangaton) to Lake Turkana

Channel 25-150kms: Butzer (1971) described this part of the river as "The Murle Meander Belt." It is characterized by river slope 0.37m/km, less meandering, the width of the alluvial tract is normally between 1 and 3 kilometers, and sinuosity approximates 1.9. The meanders do not move freely over an active alluvial surface but it peripherally cut into older and higher deposits. Consequently, the channel is relatively stable, with limited development of point-bar sequences and few cut-offs, while many stretches are almost straight. The levees of the Murle Meander Belt are relatively low and generally rise little more than 1 to 1.5 meters above the general level of the alluvial flats. Outside the banks in meanders, bends are normally undercut and many inside banks are as well. The narrow berms of flood silts (currently being accreted along the channel peripheries) indicate that the channel was incised in more recent times, with alluviation now restricted to the actual channel (Butzer, 1972). Some channel shortening has occurred in recent times with cutting off. Such a process is responsible for the formation of Lake Dipa.

Channel 150-300kms: This part of the River is characterized by several meanders with its course developing through recent fluvial alluvium hanging over Lake Turkana clayey riverbed. The meanders are very frequent, and their twisting and turning often invert the predominating direction of the river. In some instances, old meanders were cut off by the river adopting a higher slope through a short-cut, now providing typical ox-bow off-stream seasonal reservoirs. Butzer (1972) describes this part of the river channel as "The Shungura Meander Belt." It is characterized by River slope 0.18m/km and highly sinuous. The meander length and amplitude are usually great: 2.43 and 1.55 kilometers respectively. Mean channel width is reduced to 278 meters and presumably channel depth is greater (Butzer, 1971).

Channel 150-300kms: This is the fourth and final section formed by the Omo River entering into Lake Turkana and is characterized by River slope 0.85m/km. The River divides into several arms of islands (Agri-consulting, 2009). Islands are supposed to form from a process that is related to bedload transport in channels of the fan. Infiltration to floodplains and evapotranspiration cause a decrease of channel discharges in the downstream direction as well as an associated decrease of the bed-load transport capacity. It consists of several non-functional distributary complexes reflecting repeated channel bifurcation and divergence within a broad zone of former inter-distributary flood basins and lagoons as a function of historical Lake level fluctuations and sediment load.

3.3. Climate

3.3.1. Paleoclimate of the Study Area

Sepulchre et al. (2006) proposed that East African aridity was driven by the Late Neogene uplift in eastern Africa, blocking zonal moisture delivery east of the rift margin highlands. Cane and Molnar (2001, 2007) attributed the aridification of eastern Africa over the last ~4 Myr to the end of persistent El Niño like conditions and falling Indian Ocean sea-surface temperatures forced by the closure of the Indonesian Seaway between 4 and 3 Ma. Menocal (2004) suggested that abrupt increases in aridity and climate variability occurred at ~2.8, 1.7, and 1.0 Ma when high-latitude glacial cycles intensified.

Different authors (Menocal, (1995, 2004); Hailemichael et al., 2002; Levin et al., 2004; Trauth et al. 2005; Aronson et al., 2008) have done the reconstruction of the paleoclimate of the Omo basin and Lake Turkana. Paleosols Studies (Haesaerts et al., 1983; Cerling et al., 1988; Wynn, 2004; Quinn et al, 2007, and E. Levin, 2011), interpretation of a $\delta^{18}O$ profile of inorganic calcite from a core (Ricketts.,1996 and Johnson, 2009), analysis of diatoms from cores (Halfman, 1987; Levin, 2011; Campisanoc, 2017), lake level reconstruction (Butzer, 1971, Ferguson & Harbott, 1982; Hopson, 1982), and tectonic history of the basin (Baker et al., 1972; Strecker et al., 1990; Ebinger et al., 2000; Chorowicz, 2005; Fibel et al., 2011), indicate that Lower Omo and Turkana basin undergo different climatic history over the geologic period.

Naomi et al. (2011) interpreted the $\delta^{18}O$ record from Turkana paleosols as an indicator of climate change and basin dynamics. Cerling et al. (1988) document an increase in $\delta^{18}O$ values from the Koobi Formation (northeast of Lake Turkana), which could be due to an increase in rainwater $\delta^{18}O$ values, increased aridity, or a change in basin hydrology. Passey et al. (2010), revealed using carbonate clumped isotope thermometry, on pedogenic carbonate, from the Shungura and Nachukui formations, most paleosol carbonates from the Omo Group regardless of age or basin position, formed in soils that were hotter than 30°C. Showing that, the Omo–Turkana basin was as hot as today during the Pliocene and Pleistocene periods.

Ochieng et al (1988) show that Lake Turkana has been in existence since 4.2 million years ago. They have been provided an interesting insight into the climate change that has occurred over this time. 3.9 million years ago the Omo River flowed through the lake to the Indian Ocean, until the rifting caused further drops in the trough, leading to the lake become closed basin (Avery, 2012). 5,500 years ago, Lake Turkana was 80 –100 m higher than today and was overflowing into the Nile Basin (Ferguson et al., 1982; Johnson et al., 2009; Garcin et al., 2012). In the late 1800s, the lake was still 20m higher than its lowest contemporary level, indicating that the basin experienced a humid climate during the early to middle Holocene high stands (between 10,000 and 8,000 years before present). Renewed transgression occurred in the middle Holocene (5,000-4,000 BP), characterized by slightly lower lake levels fluctuating between +50 and +55meters and the third transgression

occurred in late Holocene (3250 before present), with high lake level +35 to +40 m. This was believed to be the last time that the lake was connected to the Nile system (Wilkininson, 1988). Gracin et al (2012) reviewed the third transgression and concluded that the Lake levels during the Tertiary period were probably tectonically controlled, whereas the level fluctuations during the Holocene were climatically controlled. The lake level has been speculated below 378 masl, which has been the result of the "arid" climate since 4,800 BP; with the lake level falling potentially bellow today's level during this period confirming that dry and wet paleo-climate scenario was taking place in the basin (Avery, 2012).

Butzer (1972) studied the fluctuations of Lake Turkana in a climatological context. The basic assumption for this was the level of closed lakes could be expected to reflect the climate of their drainage basins. Several climatic variables have been examined within the Omo-Turkana Basin: (a) rainfall over the upper and middle Omo Basin (b) direct rainfall on the lake and (c) evaporation from the lake. It can be observed from Figure 3.3 that the initial rise of Lake Turkana in 1961 was parallel by a slight increase of rainfall at Wush-Wush that reached a maximum for the year 1961-63. After a low in 1964-66. A new striking maximum was attained in 1967-69. For the brief period of comparison, the overall directions of change correspond well with the changes in the level of Lake Turkana, but the amplitudes are quite of proportion. Though the metrological stations measuring the variable was absent, it can be safe to conclude that the basin got higher precipitation in the early 1900s and there were dry dominant seasons between the 1940-1960s by observing only the lake level hydrograph.

3.3.2. Recent Climate Condition

Equatorial eastern Africa is considered as one of the more meteorologically complex parts of Africa (Levin et al., 2009). The main factors influencing rainfall in eastern Africa are low-level air streams, convergence zones between these airstreams and topographies.

The three major air streams for eastern Africa are: (1) the northeast monsoon that brings predominantly dry air (2) the southeast monsoon system from the Indian Ocean, and (3) westerly southwesterly humid Congo air (Nicholson, 1996). The Intertropical Convergence

Zone (ITCZ) separates the northeast and southeast monsoons, whereas the Congo Air Boundary separates westerly flow from easterly low-level flows (Figure 3.4).

In Ethiopia, the 'big rains' or Kiremt last from June to September and are sourced by moist south-westerlies and westerlies, whereas the Belg is the shorter rainy season, which occurs during March through May and is associated with the southeastern monsoon (Gamachu, 1977; Griffiths, 1972). The Belg rains lose their influence in northern Ethiopia, where only one annual peak of rainfall that lasts between June and September. However, in southeastern Ethiopia, rainfall is evenly distributed between the two rainy seasons in March-May and in July–October (Gamachu, 1977).

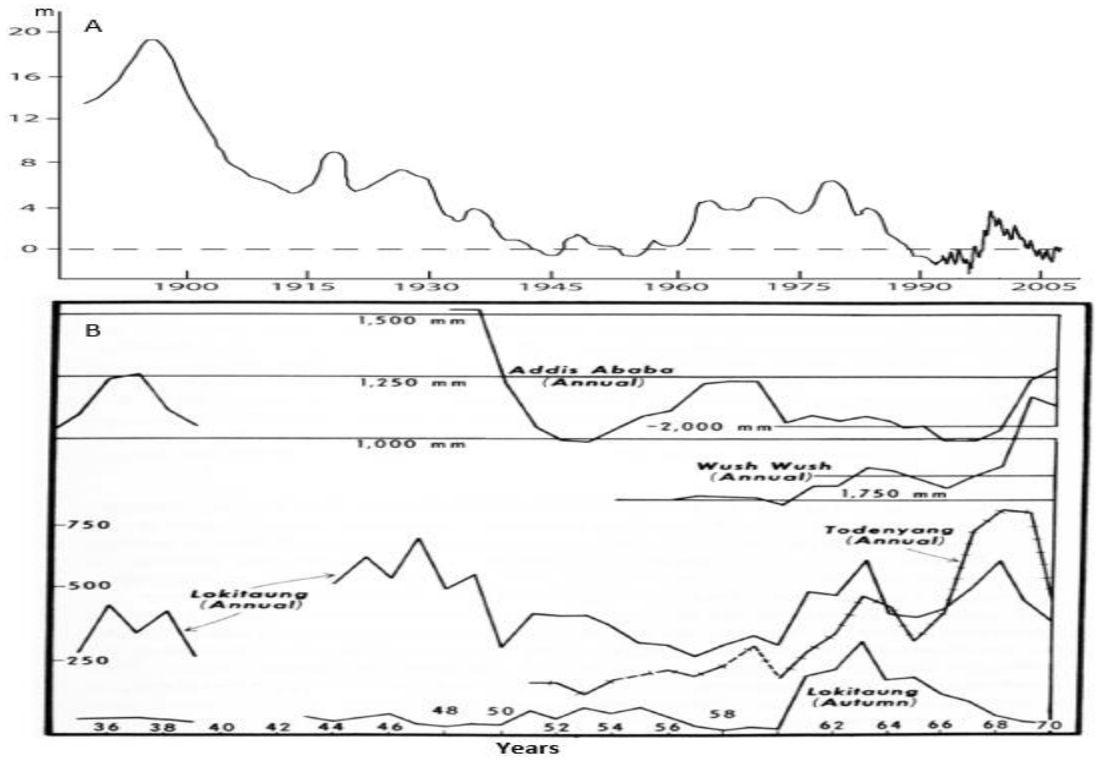

Figure 3.3 Historic Lake level fluctuations from 1893-2006 (A) and Stations in Ethiopia and Kenya: 3- year running means of precipitation (B). (Source: Butzer (1972)-B and T.C. Jhonson (2009)-A)

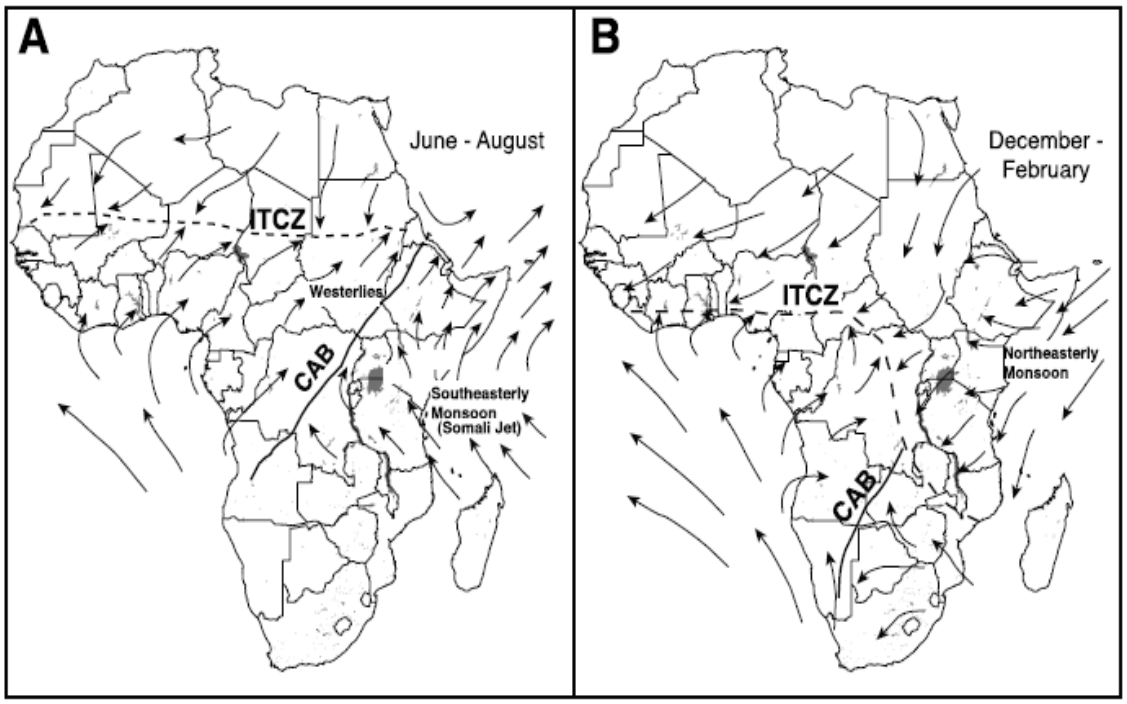

Figure 3.4 Schematics of low-level mean wind directions for tropical Africa in (a) the boreal summer (June–August) and (b) the austral summer (December–February). The approximate positions of the Intertropical Convergence Zone (ITCZ) and the Congo Air Boundary (CAB) are marked in addition to airstreams (Source: Levin et al., 2009).

The high plateaus, mountains, and varied topography in Kenya and Ethiopia affect regional climate by channeling or blocking low-level airstreams, orographic lifting of air masses, convective heating, and rain shadow effects. The highlands have a critical influence on the Somali Jet, which is part of the southeasterly monsoon system that moves into Kenya from the Indian Ocean, travels northward, and curves northeast toward Somalia and the Arabian Sea, becoming the southwest monsoon of the Indian subcontinent (Figure 3.4). At the equator, the Kenyan highlands block the Somali Jet from penetrating farther west and the Ethiopian highlands are the Jet's northern limit before it moves eastward again. The highlands also block moist westerly air from reaching the eastern portions of Ethiopia and Kenya (Levin et al., 2009).

Climate plays a dual role, as it is a driver for the upstream basin and for the Delta itself. Different authors (Butzer, 1971; agriconsulting, 2009; and Avery, 2018) have studied

climatic conditions of the Delta and its surroundings. However, the availability of representative metrological data hampered the quality of the study. In the northern part of the Omo Basin, precipitations show a marked unimodal distribution with a pronounced peak in July/August and a long dry season from November to March. In the central part, a trapezoidal distribution observed with a quite constant rainfall from May to September and a less pronounced dry season from December to February. In the southern part, a marked bimodal pattern is visible with a higher peak in April and a secondary peak in October (Figure 3.5). The northern part of the basin is situated in the highlands. It receives large amounts of precipitation (up to 2,000 mm/year), which contributes practically all the runoff. The southern parts of the basin are semi-arid and the catchment lying within contributes almost no discharge.

The variation of the rainfall pattern in the watershed contributes to the natural regulation of the Lower Omo River flows, which plays a major role in sediment transportation and the Delta progradation. Studies (Butzer, 1971; Ricketts, 1996; Jack T. 2006; Johnson, 2009; Avery, 2012; Worku, 2014; Avery, 2018) show that the historic lake level fluctuations were reflected on the Omo river inflow pattern, which contributes about 90% of water to the Lake. Rainfall on Lake Turkana is very much lower than within the middle and upper Omo Basin, which receives up to 2000mm/yr in the wetter western parts of the middle and upper basin.

The bi-modal rainfall pattern observed in the Lower Omo Basin was similarly reflected in the Turkana rainfall stations (Figure 3.5). Local precipitation is important as it raises groundwater levels, thus determining how fast a flood can propagate through the wetlands.

Omo River has a strong seasonal flow variability, which is a reflection of the variability of rainfall patterns on the basin with low flows in January-June (between 137 and 435m^3/s) and high flows in April-May (between 480 and 1400m^3/s). The mean flow for the period 1956-1998 was 541 m^3/s (Figure 3.5). The strong inter-annual variation of peak flows contributes to the yearly variability in seasonal flooding. A long-term cyclic behavior pattern appeared in the inflow data with a maximum in the 1960s and a minimum in the late 1990s. The flow of the River is influenced largely by the upper moist catchment

rainfall, which is uni-modal, and to a lesser extent by the lower drier catchment, whose rainfall is bi-modal.

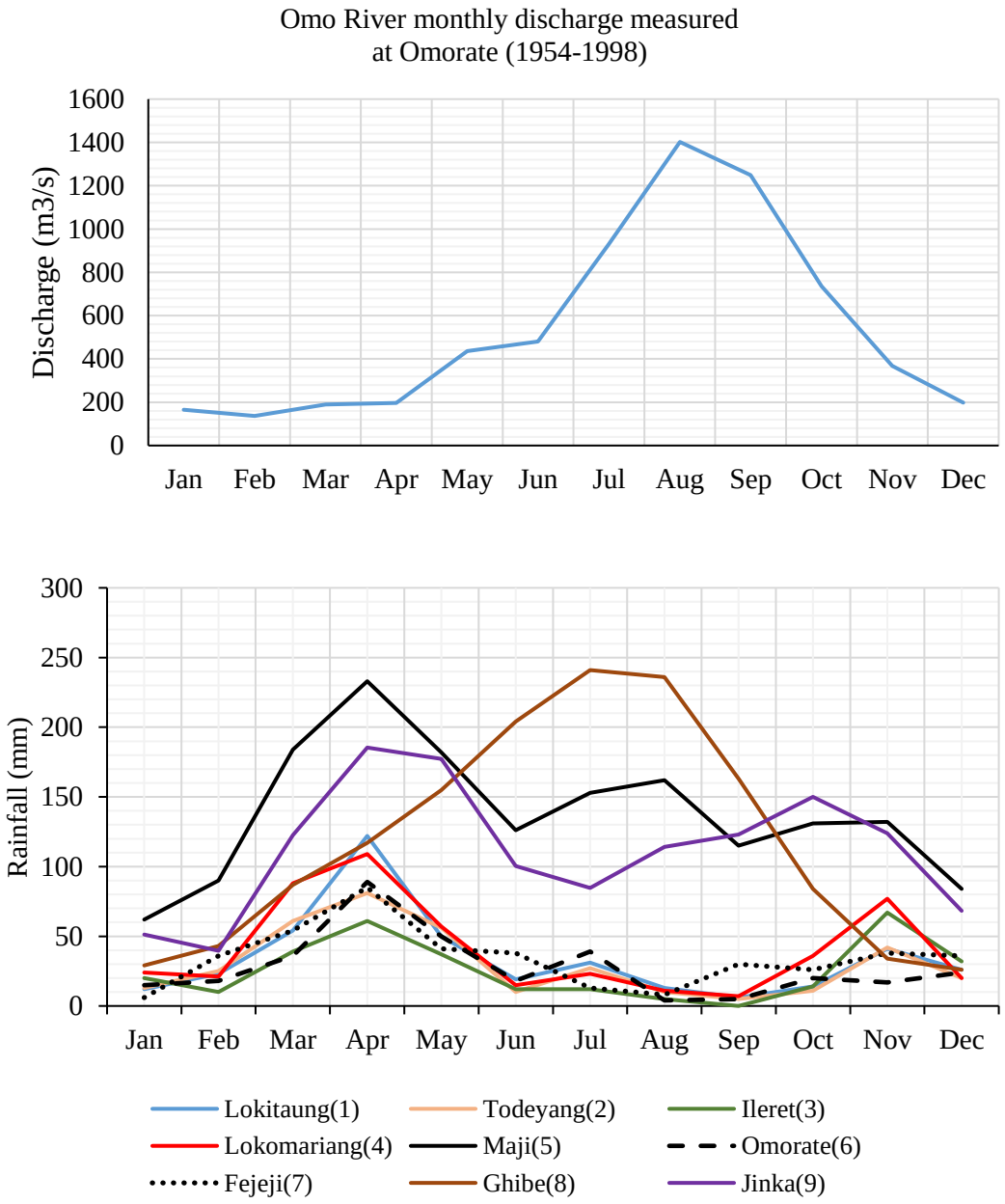

Figure 3.5 Typical annual pattern of average monthly Rainfall at 9 metrological stations. (Data sources: For 1, 2, 3, and 4, Avery 2012; 7, Butzer 1972; 5, 6, 8, and 9 EMA, 2017). Location of metrological stations out of Ethiopia is located at Figure 2.7.

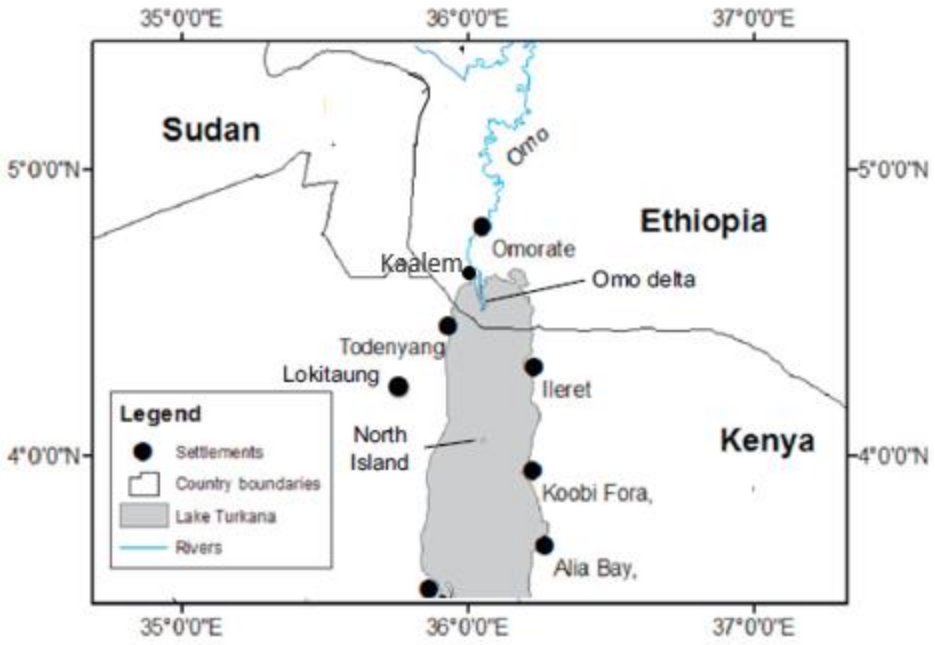

Figure 3.6 Location of metrological stations found out of Ethiopia used for this study.

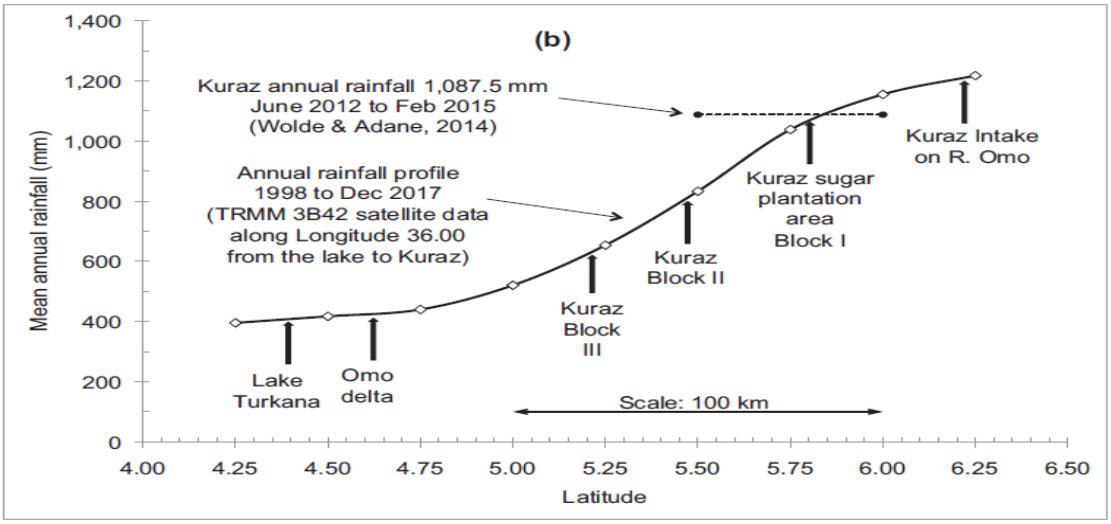

Figure 3.7 Longitudinal mean annual rainfall profile along Longitude 36.00 from Kuraz to L.Turkana (Source: Avery, 2018).

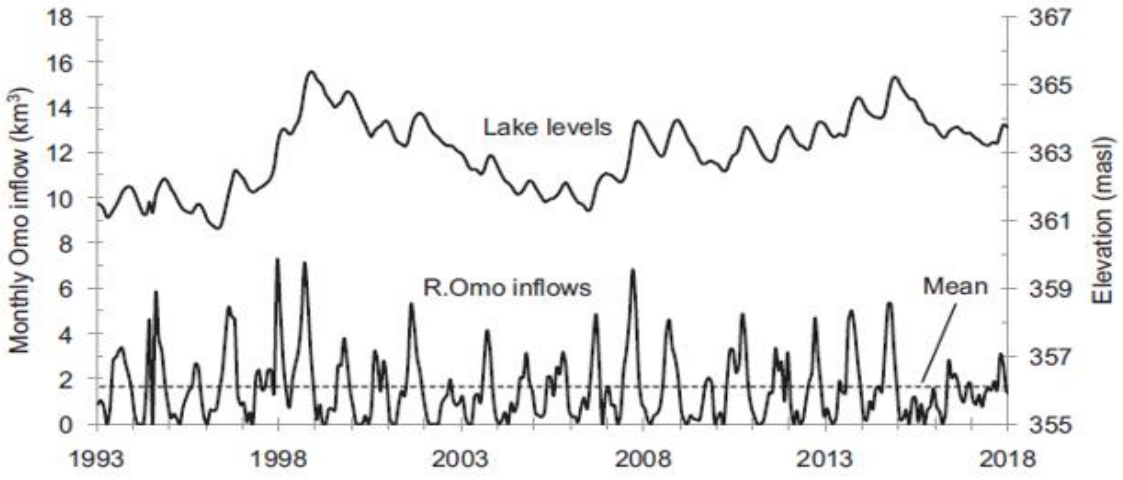

Figure 3.8 Historical Turkana lake level fluctuations from 1993 to 2016 (Source: Avery S.T et al., 2018)

Because of low elevation, the temperatures of the Delta are among the highest in the Omo Basin. The highest monthly temperature is recorded from February to March and July to August (27.7-30.2^{0}c) (see Figure 3.9). The high temperature also means very high evaporation rates, which considerably diminish the value of limited rainfall available. The negative water balance (Figure 3.11) may lead to the accumulation of salts in the soil profile in the areas there is a shallow saline water table, via capillary action. Saline-sodic soils occur in some low-lying areas (Butzer, 1971).

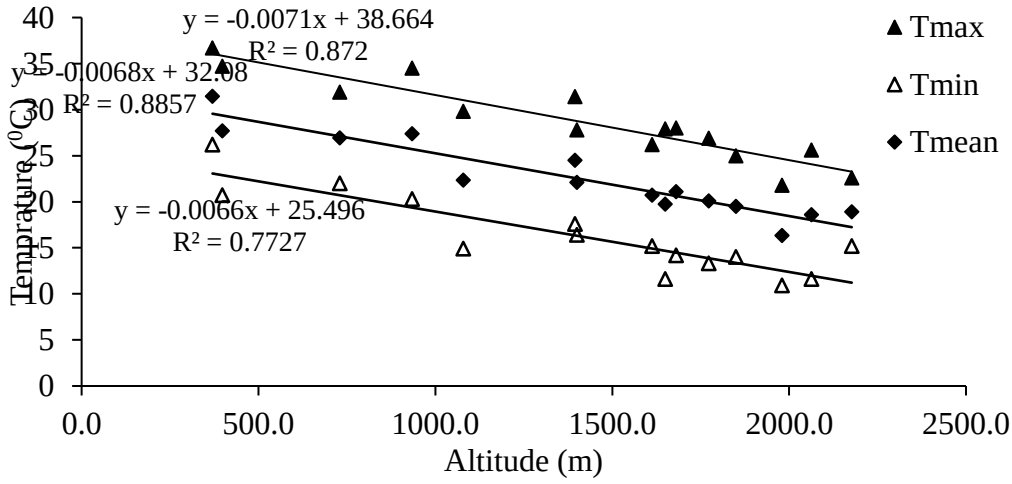

Figure 3.9 Altitude –temperature relation of some stations in the basin.

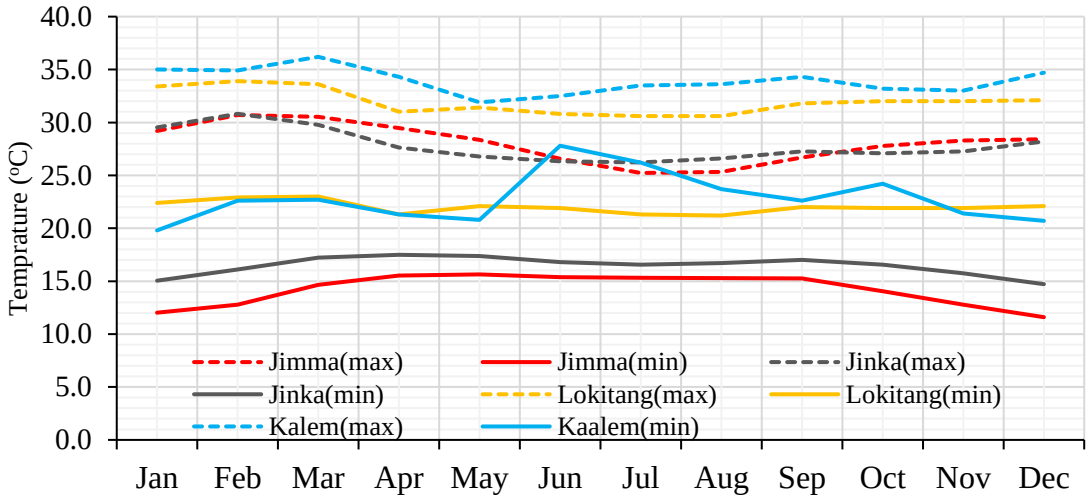

Figure 3.10 Average monthly variation in minimum and maximum daily air temperature at Jimma, Jinka, Lokitang and Kaalem (Best representative of the Delta). *Data sources: Jimma and Jinka from EMA, Lokitang, and Kaalem (Butzer, 1972).*

Butzer (1972) revised the materials on a Thornthwaite moisture-balance; the Lower Omo Basin has an arid mega thermal climate, with no water surplus at any time (Figure 3.11). The Ethiopian plateau enjoys a humid mesothermal climate with little or no water deficiency. By the KÖppen system, the boundary in the Omo lowlands lies near the 390 mm isohyet. Consequently, the Delta plain has an arid tropical climate, the adjacent higher plains, the semi-arid counterpart, both with a double rainfall maximum. Similarly, the highlands would be classified as summer-moist subtropical, with little annual temperature variation. If one looks at the water balance of the Omo Delta (see Figure 3.11) evapotranspiration by far exceeds precipitation in yearly and monthly means. Groundwater recharge in non-flooded areas is therefore quantitatively and temporally limited. Evaporation accumulates both salinity and heavier stable isotopes (due to the fractionation occurring with the phase change of water).

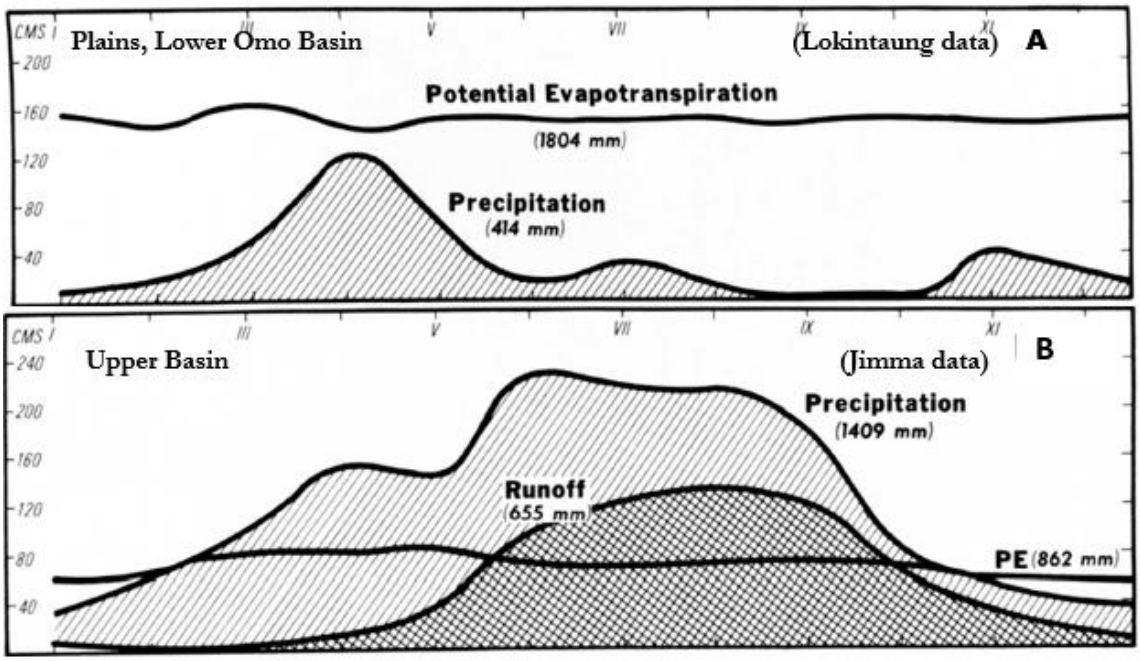

Figure 3.11 Annual water-Balance for the "Upland" plains of the Lower Omo Basin, after the Thornwaite-Mather method from Lokingtang (730m) station (A) and for the Upper Omo Basin from Jimma (1680m) station (B) (Source: Butzer, 1972).

3.4. Regional Geology and Tectonics

Different investigators with different objectives have studied the geology of the study area; geological structures and tectonic system in relation with Kenyan rift system studied by Butzer (1969, 1972) , Moore and Davidson (1978) , Wolde-Gabriel and Aronson (1987) , Bosworth (1992) , Brown & Fuller (2008), Wynn et al. (2014), and Abbate et al. (2015). Davidson and Rex (1980) defined the major rift structure in the region. Feibel et al. (1989) studied the Pliocene–Pleistocene deposits of the area. Heinzelin (1983) investigated major sedimentary deposits that are represented by the Pliocene–Pleistocene Omo and late Pleistocene Turkana Groups. Heinzelin (1983), Brown and Feibel (1986), Harris et al. (1988) and others studied different lithologic groups and formations present in the region.

The Omo Delta lies within the topographic saddle between the Ethiopian and Kenyan domes (Figure 3.12), associated with the East African Rift System (EARS). The region has

a long history of basin development, beginning with the Jurassic-Paleogene Central African Rift System (CARS), which transected the area as a northwest-southeast basin complex (Ebinger et al., 2000; Feibel, 2011; Leakey, 2003). The CARS basins were responsible for sedimentary accumulations preserved from the Late Cretaceous and may have remained an important structural influence into Miocene times. The CARS continued to affect sediment accumulation patterns through the Neogene as pre-existing rift structures and topographic lows constrained both basin morphology and fluvial corridors, particularly the Anza Graben leading to the Indian Ocean (Butzer, 1971; Feibel, 2011).

Tectonic activity delineating the modern Turkana Basin began in Early Pliocene times, with subsidence related to the EARS that quickly took on a pattern of alternating half-graben trending north-south. Several significant pulses of tectonic activity are recorded in earliest Pleistocene times when the Hamar uplift developed and in a Middle Pleistocene phase of activity that culminated in the modern basinal configuration (Feibel, 2011; Mammo, 2012; Johnson & Malala, 2015). During this time, the most recent phase, subsidence along the basin axis, has left structural blocks along the margin in topographically higher positions and subject to erosion, which has exposed Plio-Pleistocene sediments, fossils, and sites. The bio-geographic and sedimentary pattern suggests that up to the Middle Pleistocene reorganization, the Turkana Basin preserved elements of the CARS hydrography, including an outlet to the Indian Ocean. Only in the last few hundred thousand years has the basin become a contributory system to the Nile drainage (Abbate et al., 2015; Wynn et al., 2014). Following extensive research, including seismic analyses tied to hydrocarbon exploration (Morrissey, 2014) the detailed structural configuration of the basin is now well understood in many areas.

The geological history of the Omo-Gibe Basin constructed by previous workers indicates that the region is built up of > 1000 meter, and perhaps as much as 2000 m, thick successions of volcanic lava flows, unconformably overlying scattered fluvial-lacustrine sediments and Precambrian crystalline basement rocks, as well as more widely distributed Tertiary 'flood basalts'. Unlike conditions in northern and eastern Ethiopia, Mesozoic marine deposits have not been encountered in southwestern Ethiopia including the Omo-Gibe Basin (Davidson, 1983). Instead, terrestrial sedimentation, rifting and volcanism

seem to have dominated geological processes during the Mesozoic era. According to Cerling and Powers (1977), as rifting, volcanism and sedimentation continued, the zone of tectonism and crustal extension migrated from the south towards the Main Ethiopian Rift Valley.

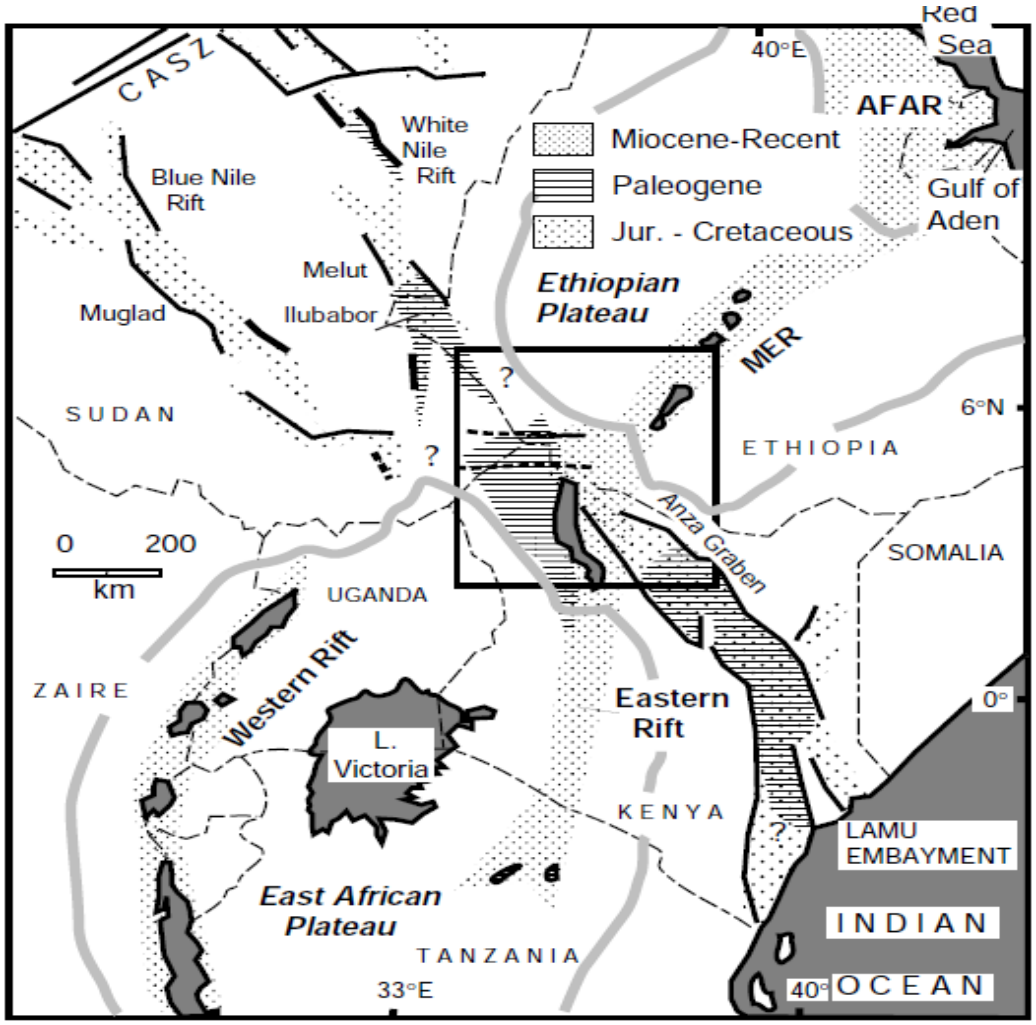

Figure 3.12 Regional tectonic setting of the Turkana region in southern Ethiopia (box) for Mesozoic and Tertiary rifts and Tertiary volcanic provinces. Shaded bold lines enclose plateau elevations greater than 1000 m. Mesozoic–Tertiary border faults (bold) and strike-slip faults (dashed) are marked (Source: Bosworth, 1992). CASZ—central African shear zone.

3.4.1. Geology of the Study Area

3.4.1.1. Crystalline Basement

Crystalline basement rocks, predominantly gneisses of several kinds cover the northeastern part of the study area. They are intruded locally by syn and post-tectonic plutons, chiefly granitoid in composition, although minor gabbroic and ultramafic intrusions are present. Their metamorphic grade is mainly middle to upper amphibolite facies but has reached granulite facies. These basement rocks classified by Davidson et al. (1976) as the "Hammer domain" based on lithological, metamorphic and structural contrast.

Dark gneisses, usually rich in hornblende and poor in or lacking quartz underlie east of Omo River. Amphibolites and mafic hornblende gneiss are interlayered in various ratios and at different scales within most of this unit. Metasedimentary gneiss, including aluminous types, calc-silicate gneiss and marble, are present as thin layers locally. Southwest of Turmi, a relatively uniform mass of dark hornblende gneiss represents deformed and metamorphosed gabbroic to quartz dioritic plutonic rocks. The layering through compositional, it is tectonically transposed that it cannot be construed as original bedding. In the field, a gradational passage from primarily black, grey, and white hornblende gneiss to pyroxene is a common observation. Gneiss and granulite of metasedimentary origin are prominent in the study area, particularly in the eastern part. They are traceable mainly because of their well-layered character and the presence of rusty zones. Compositional layering in this unit is generally very well developed and straight (Figure 3.13).

Areas mapped as metasedimentary gneiss and granulite contain a much greater amount of interlayered biotite gneiss, with or without garnet. Other metasedimentary types such as pelitic gneiss with muscovite and/or sillimanite and garnet are included. Many of the quartz-rich and biotitic gneiss carry graphite and pyrite or pyrhotite, the latter producing easily recognized rusty weathering zones. These distinctive types of gneiss provide marker horizons that help to outline the regional structure (Figure 3.13). One notable marker is a layer of blue-white, graphite-bearing dolomite marble in the southern range that can be

traced continuously for at least 20kms. The continuous nature of layering in contrasting metasedimentary gneisses suggests that it is a relict stratigraphy in this unit.

Figure 3.13 Gneisses rock exposed at road cut (Turmi-Kangaton) the compositional layering is observed.

Some dykes are strongly foliated and even mylonitized parallel to their margins, even where they cut cleanly across gneissic laying in the adjacent rocks, suggesting that they occupy restricted shear zones and were emplaced during shearing. Thin sections of specimens from dykes and plutons from these units show a range in composition from granodiorite to granite. Biotite is the prevalent mafic mineral, along with minor hornblende in some rocks. Plagioclase composition is in the oligoclase range, but secondary albite occurs in some rocks, likely formed by recrystallization from unmixed perthitic k-feldspar (Davidson, 1983).

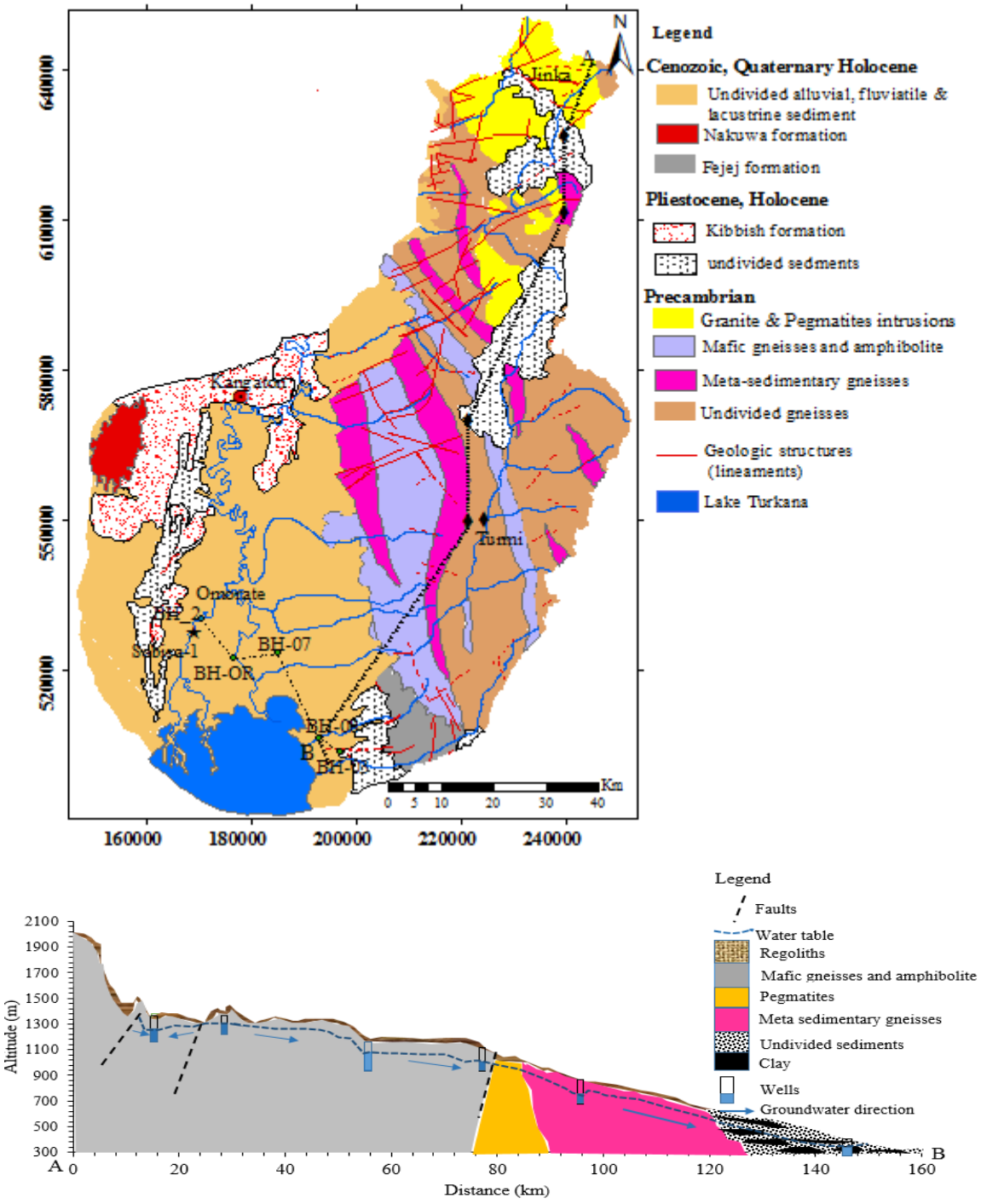

Figure 3.14 Geological map of the study area (modified after Davidson, 1983) and a lithological and hydrogeological cross-section along section A-B.

3.4.1.2. Volcanic succession

The pre-rift volcanic succession exposed in the southeastern part of the study area. The ultimate cause of the eruptions of these basaltic materials is most likely stretching of the lithosphere in the area, which has been modeled by Hendrie et al. (1992). Davidson (1983) mapped this succession (Fejej Formation) at the southeastern region of the study area. The thickness of basalt flows ranges about 150 m. The flow is in part columnar, and some are less than 20 m thick. The flows dip very gently southwestward along their northern margin. However, to the south are warped about northerly trending axes. In the main exposure area, the Fejej and succeeding formations are cut by several sets of faults with minor displacements. The same basalts appear again on the tops of the Chew Bahir rift and probably continue beneath the Quaternary sediment that fills the rift floor. The basalt flows are very similar to one another; it is dark grey, aphanitic to very fine-grained, generally aphyric though locally carrying plagioclase phenocrysts. It is rarely amygdular with opal or chalcedony filling.

Davidson (1983) and Butzer (1971), mapped Mount Nakwa in the middle of a chain of very recent and well preserved volcanic cones known as the Korath range, lies in the western part of the study area. These cones standing 400 m above the mountainous surrounding plain are the effusive vents for volcanic rocks of basic alkaline affinity, named Nakiwa Formation, and surmount an apron of lava flows. The main lavas are basanite with minor tephrite, both carry phenocrysts of plagioclase and augite, in addition to which the basanite has olivine and the tephirite has titanian amphibole phenocrysts (Brown and Carmichael, 1969).

3.4.1.3. Quaternary sediments

Quaternary alluvial fans have flanked the edge of the crystalline basement east of the lower Omo plains. Based on the clastic detritus accumulated there, this region must have been and still be a major source of sediment for the Turkana Basin. These fans to be of several ages, overlapping one another, the older ones being incised by the more recent drainage. Each of the confluence of the Omo River built a large system of fans through time. These

sediments have much the same appearance as red sediment cover on the northern parts of the western Hammer pains.

Fluvial and lacustrine deposits with interbedded tuffs and minor local conglomerates make up the Kibbish Formation (Figure 3.15). Butzer (1971) recognized that a sequence of horizontal sediments related to major fluctuations in the level of ancestral Lake Turkana lies unconformably above the various formations of the Omo Group, and has been dissected and in turn overlain by late Holocene deposits. Butzer et al. (1969) divided the Kibish Formation into four members, numbered I to IV from the base upward. The thickness of each member varies laterally because each member was deposited on a landscape with a relief of 20–25 m that developed between episodes of deposition.

According to Butzer and Thurber (1969) and F.H. Brown (2008), the lowest unit, Member I, is at least 31 m thick; it has gravelly sand at the base, followed by alternating clay, silt, and sand, in part laminated and ripple-marked, and containing reworked tuffs close to the base. Member II, 22 m thick, is composed predominantly of massive silts, deposited on a basalt tuff that blanketed the dissected surface of Member I. Member III, 46 m thick, records two cycles of advance and retreat of Lake Turkana, separated by a prominent subaqua tuff bed approximately 3 m thick. Member IV is divided into two units: it comprises sands, silts, and clays with a gravelly base with minor tuff. The two sub-members represent transgressions of Lake Turkana, separated by regression to close to the present lake level (Davidson, 1983).

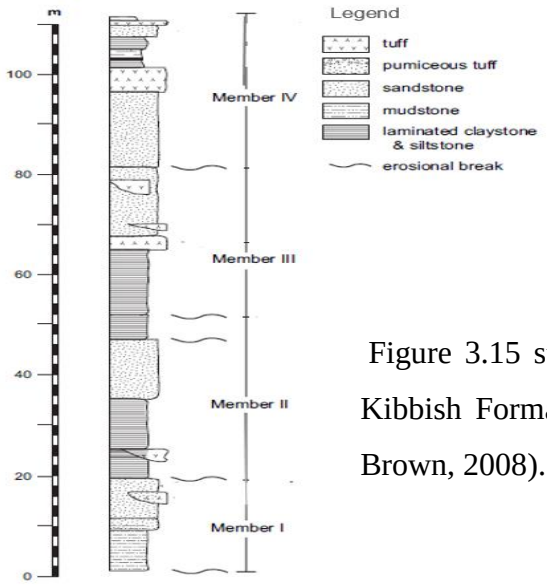

Figure 3.15 stratigraphic column of the Kibbish Formation (Modified after F.H. Brown, 2008).

Ancestral Lake Turkana was able to overflow to 80 meters above the present level (Butzer, 1976). According to him, the overflow level was last reached toward the end of the time of deposition of Member IVb of the Kibbish Formation, about 3250 years ago. At the same stage between this time and the present, the lake retreated and then rose again, perhaps by as much as 40 meters, enough to flood northward along the east side of the Turkana depression into the Usno plain. Lacustrine sediments of this stage named by Butzer (1971) are now exposed in the banks of the Omo River south of the Usno River confluence. They are in part covered by a thin veneer of littoral sediment, arranged in stripes indicating lake retreat to the southward the ancestral embayment known as Sanderson Gulf, south of the Korath range. The channel scars are likely related to the earlier regression of Lake Turkana following the deposition of Kibish Member IVb. During the advance when the Kibish-Dipa beach was formed and the Usno plain flooded, therefore, the Omo River changed its course eastward and then northward around the south end of the Nyalibong range, building its delta on the top of lacustrine deposits of Usno embayment from the north at this time.

3.4.2. Geologic Structures

The Turkana rift continues into southern Ethiopia in the Lower Omo Valley, that the Gregory rift of Kenya links to the north with the Chew Bahir rift and that the main Ethiopian rift terminates to the south and does not join directly with the Gregory-Chew Bahir rift (Moore and Davidson, 1978). The Turkana rift in Ethiopia has three branches, respectively named Kibbish, Omo, and Usno. They are lying in the west, the central and northern parts of the study area respectively. According to Ebinger et al. (2000), the Kibish branch oriented northwesterly, terminates at the west side of the Maji Highland, although its bounding faults continue a long way beyond its end. The Omo branch continues a short distance of the study area, terminating in the highland region between Bonga and Mizan Teferi. The Usno branch also terminates just north of the area. West of the Weyto-Bala sector, a series of southwest-oriented tilted fault blocks that separate the Chew Bahir and Turkana rift systems (Figure 3.14).

In retrospect, the Omo Delta plain is situated syncline between two structural provinces: the Amaro-Kokke horst to the east, the basin-and-range structure of the faulted, plunging folds to the west. The northeast-trending faults are through-going, truncating shorter northwest-trending faults, but in many places, right-angled spurs and re-entered to appear to have formed simultaneously. The modern Omo Delta is bounded by several sets of en-echelon faults to the east, and by a system of fractured (Butzer, 1971) plunging folds to the west. East of the Delta plain lies the Amar-Koke Highland, with elevations of 1000 to 2000 m, forming a horest-like structure between the Omo River and Lake Chew Bahir. The fractures adjacent to the Omo Valley is more difficult to pinpoint among alluvium-veneered pediment surfaces cut into the basement complex, and a major set of en-echelon faults appears to strike almost due north, delimiting the late Cenozoic fill and basement complex to the east of the Omo Delta and the Omo and Usno floodplains.

Northwest and north of the Delta, the strata of the Omo Group are fractured by 3 or more major faults striking N 0 to 250 E (De Heinzelin et .al., 1971). The Nakwa volcanics were probably extruded along a related tensional fissure during the late Pleistocene. The synclinal depression farther to the west of the Delta include the Lotogipi plain the Kotome and Lomogol valleys, and Sandrson's Gulf.

3.5. Soil and Vegetation

Different authors Butzer (1971), Woodroofe Vol.Part1 (2007), FAO (http://www.soilgrids.org/) studied the soil of the Omo Basin. The plateau soils of the higher Omo Basin (above 1500m), depending on the topography and to a lesser extent on variations of the volcanic parent material are classified as vertisols. It is found primarily on valley floors and seasonally –flooded intermountain plains. Vertisols are marked by dark greyish brown A- horizons that maybe 70 to 180 centimeters deep, resting on a dense, whitish zone of decomposing basalt. In the dry state, crack networks penetrate to a depth of 80 cms, whereas the soil is swollen and impermeable when wet. The plateau soils are of primary interest to this study since they provide the bulk of the Omo sediment (see Figure 3.16). To understand the dynamics of contemporary soil development and in the adjacent Ethiopian Rift at the height of the rainy season.

Overall, it appears that the materials carried by the Omo floodwaters are produced in the Ethiopian highlands by sheet wash, accelerated forms of a mass movement, and stream erosion that primarily attack the dark topsoil of deep residual mantles. The combination of high available relief and heavy protracted rains lens, provides exceptional energy to fluvial processes. This would be so with undisturbed vegetation but is, even more, the case given the thorough and almost ubiquitous human disturbance. Only the intensity of chemical weathering maintains a deep residual mantle so that the Omo River is primarily supplied with suspended rather than bed-load sediments. It appears that the vertisols and some of the fresher, humic Ferrisols contribute to the major part of this load.

This can be inferred directly from the clay minerals now deposited by the Omo montmorillonite with only a little kaolinite; it is further suggested by the dominance of rather weak elements among the heavy minerals, namely hornblende, pyroxenes and biotite that are presumably provided by fresh weathering of basaltic rocks. Altogether, it seems that accelerated erosion of montmorillonite soils from the rolling plateau surface provides the bulk of the sediments.

The zonal lowland type can be described as a non-calcic, arid brown soil. It appears to be widely associated with the thorn savanna of the better-drained Omo and Turkana lowlands, and the frequency of truncated profiles or raw mineral soils indicates that "accelerated" soil stripping and local gullying is "normal" in response to overgrazing and burning. Dark cracking clay soils of "intra-zonal" type are characteristics here, though such vertisols show considerable lateral variation in response to facies changes or surface drainage. In particular, there is a sub-surface accumulation of sodium salts (Butzer, 1972). In central Delta flats, the surficial sediment with fossilized brown, silty, clay loams soils is typical. Most of the surface is veneered with silts, but this doesn't impede the development of the great crack networks widespread on the Delta Flats. They occur singly as well as polygonal or rectangular arrangements. Individual cracks have vertical sides and drain by subterranean piping.

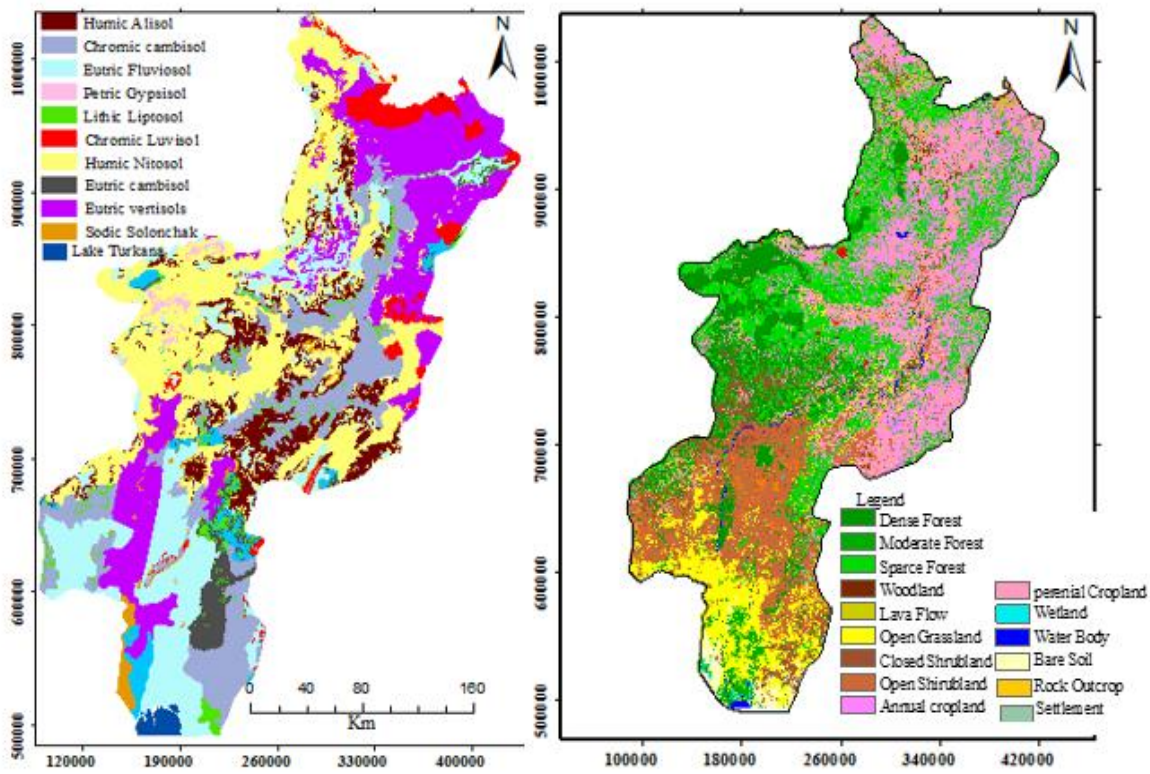

Figure 3.16 Soil map (Left) and Land Use Land Cover (Right) of Omo Basin. (Source: EMA, 2009)

The giant crack network is associated with clayey subsurface soils or tracts of vertisols. Due to low rainfall and sparse vegetation, these soils are poorly developed, infrequent leaching, and low organic content. Salinization is widespread, resulting in the concentration of mineral salts at or near the surface (Figure 3.17).

The Lower Omo Basin plains are in some part well-drained and seasonally wet in others. The well-drained, lowland surface at beach ridges and higher inter-ridge terrain, have a tree-shrub savanna, with many succulents and much bare ground present in rapidly drained "badlands" or on excessively permeable substrata. The lower-lying plains are characterized by grassland savanna or less waterlogged soils. In contrast, the levees of the Omo River and flood plains have a closed galleria woodland (Figure 3.16). The Delta flats and food basins are significantly more disturbed and mantled with tree-shrub savanna, shrub-steppe or shrub thickets, and open water (Butzer, 1971; FAO, 2008).

Figure 3.17 Sub-surface accumulation of salts at Delta flats.

3.6. Geomorphology and Development of Omo Delta

3.6.1. Geomorphology

Whether or not a river is sufficiently large and transports sufficient quantities of sediment to produce, a major delta depends largely on the nature of the drainage basin. Drainage basin climate, geology, relief, and area are all critical determinants of river discharge. Unless the drainage basin experiences significant precipitation for at least part of the year, no river can arise. Lithologic resistance, combined with drainage basin pedology and vegetation, determines the rate at which sediments can be eroded from the basin to be supplied to the river (Basan et al., 1985). The Omo River with a drainage area 78,773 km^2 and much of its catchment 60,234 km^2 (76.5%) is lies at elevation >1000m. The waters of the upper basin tumble over a series of cataracts through the 160-km canyon of the Omo, through gorges up to 600 meters deep. After merging with the waters of the Gojeb, the canyon gradually opens up into an entrenched valley and ultimately to emerge onto a broad tectonic depression at the northern end of the Turkana trough. The level of Turkana is about 370 meters, giving the Omo drainage basin considerable potential energy. Understanding the landforms and the processes that create them is important to have a good

picture of the hydrogeology of the Delta. Butzer (1972) did a detailed study on the geomorphology of Omo Delta, and Kebede (2013) did some reviews. In this study, the classification and description made by Butzer (1972) were adopted. Butzer (1971) identified seven conspicuous geomorphic units: The meander belt, the eastern flood plain, the delta flat, the delta fringe, the beach ridge plain, the Murle Lake plain, alluvial fans, and wadis.

3.6.1.1. The Meander Belt

The Meander Belt is part of the convex, Omo floodplain with meandering channels, with natural levees, numerous cut-off meanders, occasional ox-bow lakes, or clay plugs, and restricted flood basins. The southern and northern parts of this belt are markedly convex; the central sector tends to be flatter, with point-bar ridges and swales well developed. On their relative position, Butzer (1971) names them as northern (Murle), southern (Narok Meander Belts), and central (Shungura Meander Belt) (Figure 3.18). The sinuosity of the channel is shortening with cutting off the incised channel and the formation of a new surface water body. Lake Dipa and other Ox-Bow Lakes were produced by these processes. Levees are frequently breached by diverging overflow channels along outside banks. These features reserve the River overflow and subject to evaporation that resulted in saline water.

The evolutional history of the Omo Delta plain finds a substantial record in its meander belts (Butzer, 1972). The present configuration of the meander belt was already established in 1899 when most of the ox-bow lakes and other cut-offs had already been detached from the main Omo channel. The Lake Dipa cut-off, and several of the other more prominent meander scars, showed that these features were relatively younger. Butzer (1971) classify this evolution based on the sinuosity of the channel, links with the presence channel, and the vegetation of cut-offs and meander scars.

Figure 3.18 Meandering Belts of Omo River

3.6.1.2. The Eastern Flood Plain

The Eastern Flood plain overflows channels, breach the eastern levees of the Meander Belt and drain over very gentle inclines (0.2-2.00) into the low flood basin via dispersal streams. The lowlands, in turn, are marked by two back swamps in the northern, Shungura sector, with an increasingly efficient network of gathering streams in the central and southern, Narok sector.

Corresponding to the increasing amount of seepage water, the southern part of these flats are covered by dense woodland, contrasting with savanna and grassland to the north. This geomorphic Meso-environment serves as a flood basin for the meander belt and by a strict definition also function as part of the Omo Floodplain. However, it has served as lagoonal mudflat of the Delta as recently as 1900 and forms an integral part of the overall Delta Plain.

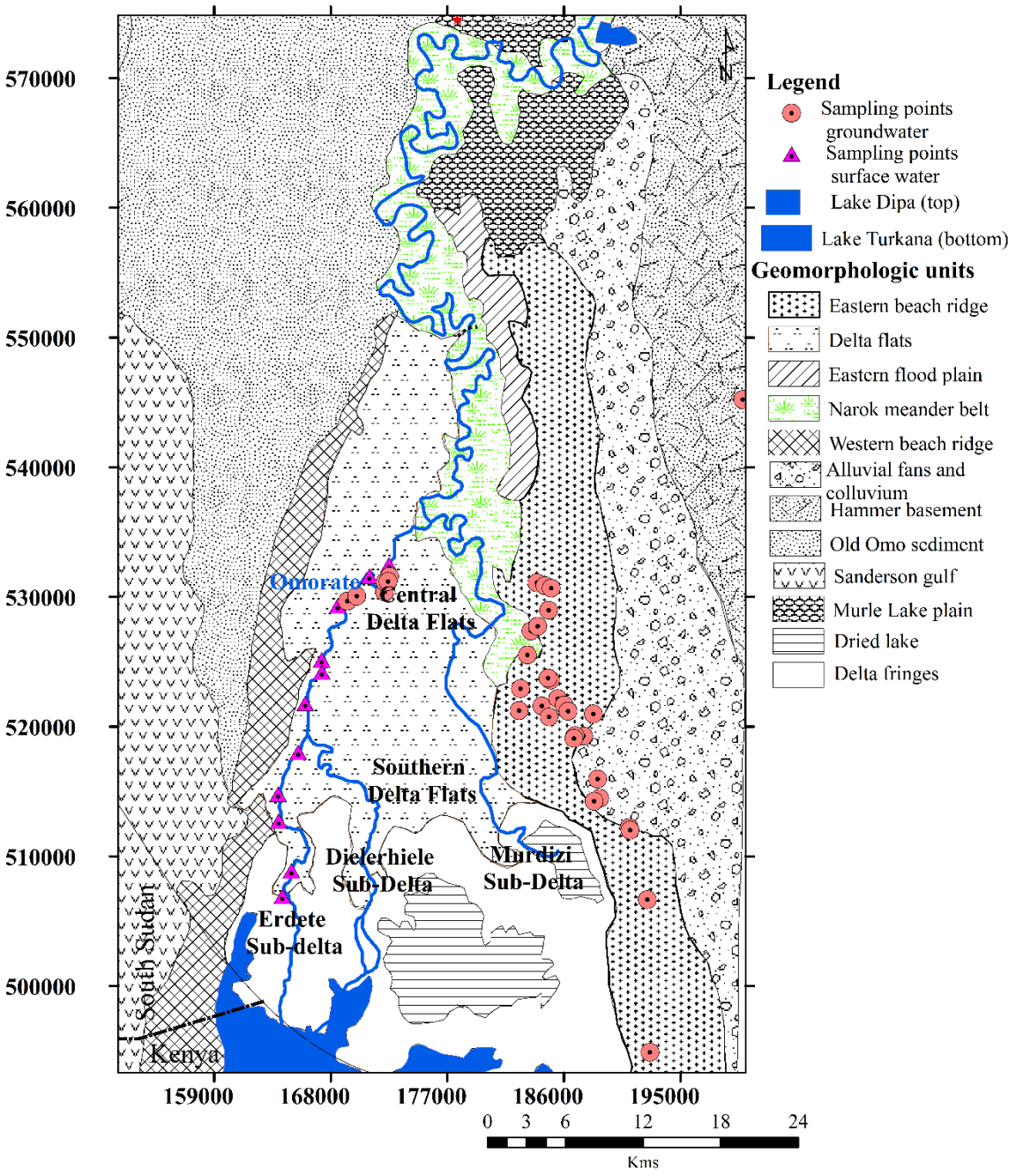

Figure 3.19 Geomorphic units observed around Omo Delta (Modified from Kebede 2010 and Butzer, 1971)

3.6.1.3. The Delta Flats

The Delta Flats are notable by their subdued topography, with local relief of 1 to 4 meters. They consist of several non-functional distributary complexes reflecting repeated channel bifurcation and divergence within a broad zone of former inter-distributary flood basins

and lagoons. Most of the surface is veneered with silts, but this does not impede the development of the great crack networks widespread on the Delta flats. Such cracks are 2 to 1.5 meters wide and as much as 5 or more meters deep. They occur singly as well as polygonal or rectangular arrangements. The cracks are enlarged by headwater erosion, soil falls and piping, eventually leading to a dendritic system of tributary master rills. The Omo floodplain is relatively narrow compared to the width of the channel. The seasonally inundated alluvial surface is largely confined to inter-channel flats or silt berms that lie between the levees and high-water channels (see Figure 3.20) many of them representing abounded river segment. The water from Omo backs up into this deltaic basin during the flood stage, with normal drainage at other times of the year.

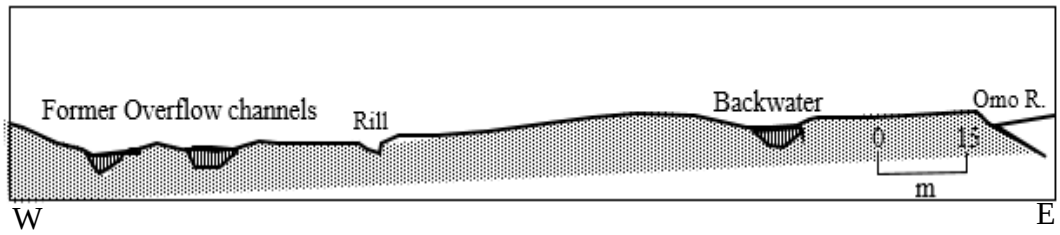

Figure 3.20 Section of Omo River at Omorate

Figure 3.21 The satellite image of Omo Delta (A) and Typical Bifurcation of the channel at Delta (B). It can be noted from the figure that bifurcation and joining are taking place frequently as River water drain to the Lake.

The evolution of the Omo Subdeltas is reflected in many atrophied delta complexes within the Omo Delta plain documenting the history of shifting river channels and fluctuating lake levels. Based on: distributary bifurcations, multiple major distributaries and conspicuous convexity of terrain, Butzer (1971) recognized 10 subdeltas. Morphologically and functionally, these subdeltas grouped into three categories (Figure 3.19). Active, primarily subdeltas, including the contemporary Erdete and Dielerhiele embouchures in the now partly submerged Delta Fringe.

3.6.1.4. The Delta Fringe

The submerged delta fringe is the most important of the deltaic environment of the Omo River because it elucidates the processes operating past and present in the transitional fluvio-lacustrine environments of the Omo delta plain.

The extreme bird foot profile of the contemporary shoreline is largely due to the Dielerhiele distributary extending 12 kilometers out into the lake rivaled by the Erdete branch, with a projection of over 6 kilometers, and by the remnants of the Murdezi channels. The older aerial photography also exhibits a bird foot profile, but far less pronounced and with notable differences.

Sediments are a mixture of organic and mineral sources, as vegetation colonizes these flats, trapping and binding suspended sediment. The resulting deposits normally consist of a finely bedded to massive, brown clay, with very coarse angular blocky to a prismatic structure. Sodium salts, with a little gypsum, are precipitated in ponds or stagnant waters during periods of desiccation and, it would seem, particularly during times of receding lake level. Such salty waters can be more widely disseminated by wind-driven lagoonal waters (Butzer, 1971).

Figure 3.22 The Badland topography observed at Delta Flats NNE of Omorate.

3.6.1.5. Beach Ridge Plains

The littoral sub-environment of Lake Turkana includes the delta fringed shorelines, the leeward low wave-energy eastern coast, and the windward, high wave-energy western shores. Above watermark, low ridges of well-sorted, course sands extend for several hundreds of meters inland, with very gentle slopes and few coherent patterns. The sands appear to be primarily of eolian facies, but wave reworking is apparent at the shore and true fluvial beds are found both at depth and further inland. Quartz is dominant but ferromagnesian minerals and feldspar are present. The lee slope rises abruptly from a smooth sandy or lag-strewn surface, separating a chain of lagoons and ponds from the open lake. During the low-water season, these ponds are often evaporated and reduced to Saltpans.

The functional beach ridge built of moderately to well-sorted coarse sands or gravelly sands, including a component of shell debris, feldspars, heavy minerals, and basalt sand,

with cobble gravel intercalations near stream mouths. The development of the eastern beach ridges is highly variable according to location and sediment source. These ridges consist of very coarse sand, in part rich in fine gravel, and owe most of its sediment and some of its prominence to a now eroded alluvial fan from the eastern drainage lines.

3.6.1.6. The Murle Lake Plain

The non-functional deposits of the Murle Lake plain are the oldest visible within the confines of the Delta Plain. The older beds and surface consist of coarse sands and sandy loams with gravel inclusions and generally rise 10 meters and more above the Murle Lake Plain. The soil sample analysis carried by Butzer (1971) shown the fine gravel lenses consists of subrounded, macro to mesocrystalline quartz, pegmatite, and gneiss. Traces of salt efflorescence on peds.

3.6.1.7. Alluvial Fans and Colluvium

Alluvial fans and wadis composed of sands, gravels, and pebbles. The alluvial cover extends for variable distance on the elevated areas with increasing thickness towards the lowlands and overlies on the lacustrine sediments. But in places where tectonic uplifting is clearly seen (westerly dipping uplift) as in around Ashewa Village of Lokoro Kebele, the alluvial cover on top of the lacustrine sediments is thin and deposited on the top few meters and in depressions along with river courses and flatlands. The seasonal flooding is restricted in them and the results of local runoff. The alluvial materials are found at the confluence of the wadi beds draining the Hammer Koke highlands in the east and the Omo Valley. The alluvial fans contain distributary channels and sand bars. The volcanic clasts are rare and most deposits are eroded from the Turmi plain crystalline basement. The groundwater recharged from the local precipitation of the upper catchment of Turmi has significant importance in addition to the intermittent streams drain from the highlands. These alluvial fans are a good source of shallow groundwater with good water quality.

3.6.1.8. Hammer Basement

Extensive North-South trending high-grade metamorphic rocks underlie the Hamer-Koke block. It covers the highlands of the study area, from the East and West by the Omo and the Chew Bahr tectonic depressions filled by alluvial-lacustrine sediments. In the Hammer-Koke block, permeability related to foliation is absent. However, the basement rocks are high grade (granite to granulite facies). The syncline and anticline structures are important in the deposition of sediments and strip erosion respectively. The Wadi beds consist are important geomorphic features that store the groundwater in the Hammer basement. They extend from the highlands of Alduba and Turmi to Murdazi delta with a total length of 365kms and an average width of 10kms.

3.6.2. Geomorphologic Evolution of the Omo Delta

Every delta consists of a subaqueous delta and a subaerial delta, even though the relative areas of these may vary considerably. The subaqueous delta lies below the low-tide water level. In general, the subaqueous delta is characterized by seaward fining of sediments, sand being deposited nearest the river mouths and fine silts and clays settling farther offshore from suspension in the water (Basan et al., 1985; Wang et al., 2009). The subaerial and subaqueous deltas can also be subdivided into active and abandoned zones. The active delta plain is the accreting portion occupied by functioning distributary channels. The abandoned delta plain results when the river changes its lower course causing a shift in the locus of river-mouth sedimentation.

The river mouth is the most fundamental element of a delta system because it is the dynamic dissemination point for sediments that contribute to delta progradation. In Omo Delta, when the River discharges into receiving Lake Turkana, its momentum is dispersed by its interaction with Lake Water. The result is the deceleration of the effluent, consequent loss of sediment-transporting ability, and deposition. As one goes from Delta plain to front, it can be observed progressive Lake Ward decrease in the concentration and grain size of the sediments transported and deposited by effluents (see Figure 3.23). This resulted in a decrease in the flow rate of the groundwater in the Delta relative to alluvial deposits. Hence,

the gradual increase of groundwater salinity is a result of advection and diffusion of saline fluids entrapped in impermeable zones.

The distributary network patterns exhibited in the Omo Delta are Bifurcating and Rejoining (Figure 3.21). Bifurcations tend to be most frequent when offshore slopes are flat or when sediment load consists of a high proportion of coarse material.

The Omo Delta is situated in a complex tectonic depression, known as Lower Omo Basin and forming an extension of Lake Turkana trough. It has been created along essentially modern lines during the first part of the Pliocene period, a serious of deltaic, fluvial and lacustrine sediments were already accumulating by 4.4 million years ago. The Delta Plain has been submerged or laid dry during the last several centuries depending on the fluctuations in the level of Lake Turkana (Butzer, 1972). Lake Turkana has been relatively low for 3,000 years B.P. dropping rapidly, in successive stages, below the threshold of the probable Nile Overflow.

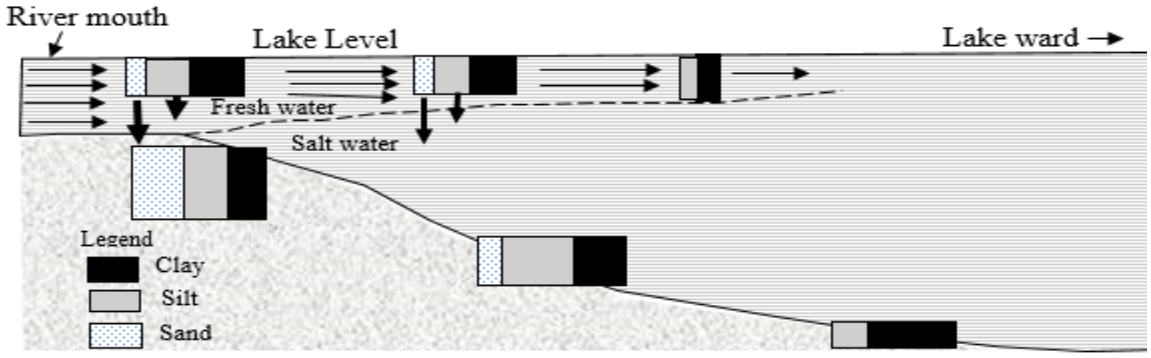

Figure 3.23 Model of depositional and sorting of sediments at a river mouth.

Concomitantly, the Lower Omo River cuts down its bed by as much as 52m before it could begin to aggrade its modern floodplain and Delta. Consequently, the modern Delta Plain is a remarkably recent phenomenon. Major Delta has been situated somewhere in the Lower Omo Basin for most of the last 5 million years. The recent history of the Omo Delta Plain finds a substantial record in its meander belts. Innumerable meanders scars and other channels. The earliest evolution of the meander belts can be interpreted with a falling lake level immediately following the recession from the Murle Lake Plain. Many atrophied delta

complexes within the Omo Delta Plain document a history of shifting river channels and fluctuating lake levels. Currently, the river divides into several arms forming about 31 islands (Agriconsulting, 2009). Starting from flat surfaces islands are supposed to form from a process that is related to bedload transport in channels of the fan. Infiltration to floodplains and evapotranspiration cause a decrease of channel discharges in the downstream direction as well as an associated decrease of the bedload transport capacity. Bedload is thus deposited on the channel bottoms, leading to aggradation. Channels are flanked by a thick layer of peat and vegetation, which stabilizes the bed and filters suspended sediment. These stable sidewalls allow the channels to rise to a higher level than the surrounding floodplains. This results in aggradation of channels over time and is accompanied by the upward growth of the vegetated channel margins, creating vegetation levees, which continue to confine the channels. During the life of a channel, peat can accumulate in this way. As the channels aggrade, they become increasingly less efficient in moving water. Ultimately, they fail and become overgrown, and water diverts elsewhere, forming new channel systems (Mccarthy, 2006).

Figure 3.24 Channel bifurcation and joining at Delta (A) and vegetated channel margins (B). (Source: Avery, 2012)

3.6.3. Recent Submergence of Delta

Omo Delta was undergoing frequent emergence and submergence through geologic period depending on the climate, tectonics, Lake level fluctuations, and anthropogenic activity that affect the volume of Omo River water and sediment input from upper catchment. The satellite images taken at the different time shows very interesting changes in Delta over time (Figure 3.25). In 1973 large part of Delta can be seen submerged, this could be associated with the lake level rising following the 1940s and 1950s low period. In 1989 the Lake level was 3.7m lower than in 1973 which is very close to the lowest ever level and hence much larger delta area is exposed by the lower water level. In 1995 the Lake level was 2.4m higher than in 1989 and 1.2m lower than in 1973. The Delta not reduced much since 1989, but much larger than in 1973. Recently in 2018, the lake level was 1m higher than in 1995 and the Delta is larger in the western part as it was in 1995.

Reduced Lake water levels will lead to down-cutting of inflowing river channels in response to the increased hydraulic gradient resulting from the drop in the water table. As the lake level is lowered, River-Lake equilibrium is disturbed and the river starts losing its sediment before it reaches the interface resulting in increasing the Delta area exposed. It is evident from the satellite image maps at different time scale and lake-level change (Figure 3.25), reduction in the volume of water, resulting in the shrinking of the shallower northern end of the lake in which Omo River joins the Lake. This will cause the River Omo to deeply incise through the existing Delta, and there will be an extension of the Delta south into Kenya. This was evidenced by Ferguson's Gulf which was left dry after the lake level lower more than 3.1m below the 1972 zero datum (z=365.4 masl).

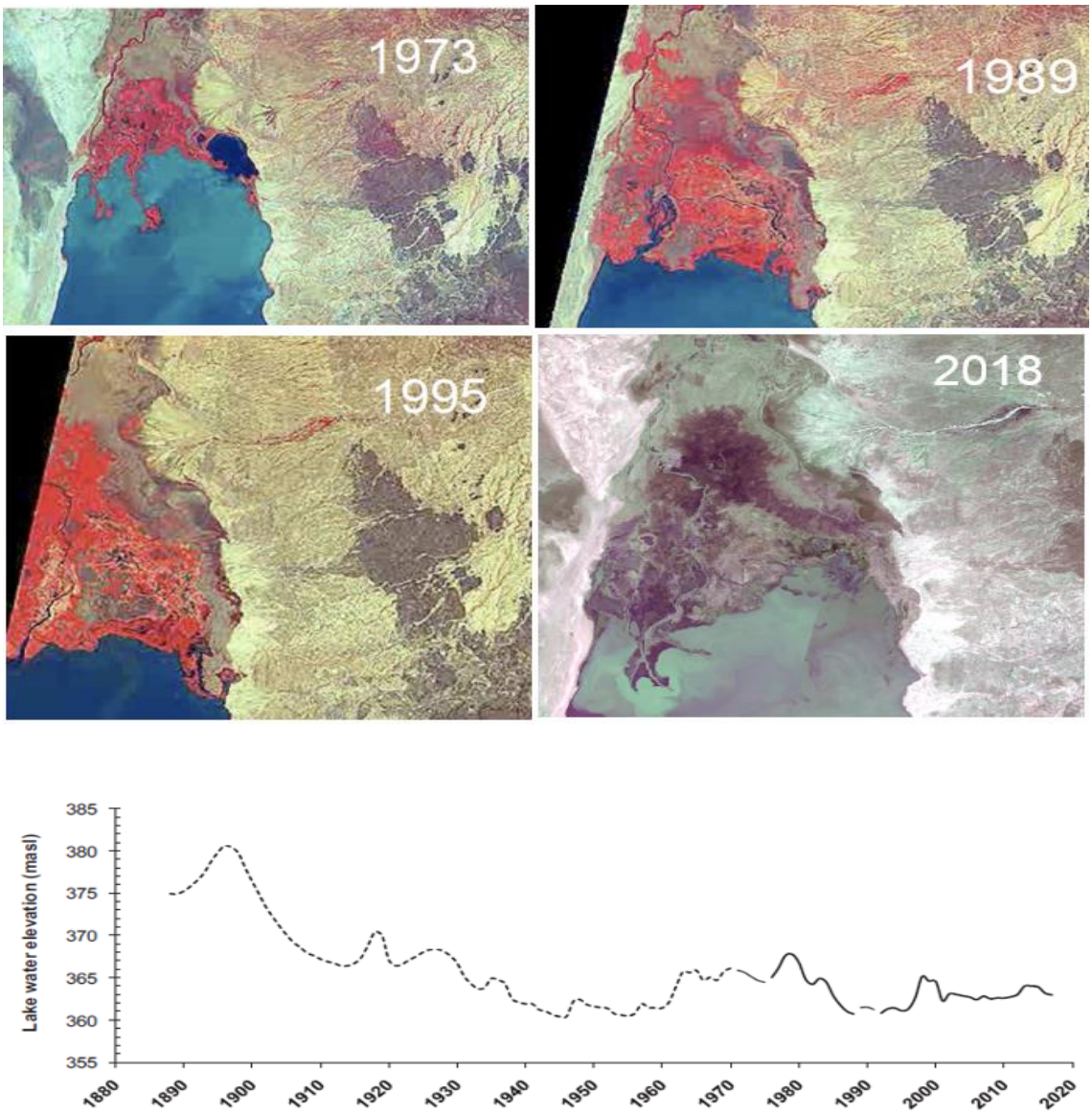

Figure 3.25 Omo Delta imagery showing changes over time all images are taken at January (above) and Turkana Lake level fluctuation (below) from pieced together from explorer's maps and colonial documents, Water level gauge first installed, water levels since 1992 remotely sensed at ten-day intervals by satellite radar altimeters (Source: Avery, 2018).

3.6.4. Delta Sediments and Stratigraphy

The geology below the Omo Delta is virtually masked by a thick blanket of alluvium, colluvium, fluviatile and lacustrine sediment grouped called quaternary sediments (Butzer, 1972; Davidson, 1983). The geological rock descriptions are derived mainly from rock

outcrops in the nearby areas, and their spatial distribution below the Delta is mainly inferred from gravity geophysical data (Mammo, 2012 and Alemu, 2017) and borehole data to supplement these two data sets. From the interpreted results, the Lower Omo Basin and the Delta, has west tilted basement and sedimentary sequences. N-S the basement and the deposited sediments are undisturbed. However, E-W the basement is uplifted in the middle that forms southern and northern sub-basins. The sedimentary sequences thin up-dip towards the eastern edge of the basin (Tullow Oil Ethiopia, 2010 and Mammo, 2012).

The occurrence of clay material act as groundwater flow barriers as shown by the steep hydraulic gradients across the faults. The change in lithology of the high conductive layer on the east side of the Delta (Figure 3.26 and
Figure 3.27) to a low conductive layer on the west, grading from weathered basalt to clay material. This results in a slow rate of flow of the groundwater and gradual increase in salinity in groundwater as the result of advection and diffusion of saline fluids entrapped in impermeable zones. A fence diagram is drawn (
Figure 3.27) with lithologies and borehole coordinates in the Delta revealed that the second aquifer (sand) occurs at shallow depth in the eastern and central part area and laterally thins out completely towards southwestern. In the southeastern portion of the area (Fejeji), the second aquifer weathered basalt occurs deeper to the ground surface (greater than 20 meters) and pinch out toward the lake indicating gradational deposition of sediment during the Delta formation. Three cross-sections drawn with shallow well logs from the Delta and Environs further reveal lateral changes in the thickness of aquifers in parts of the study area. Tefera (2017) and Tilahun (2012), clearly indicate that sedimentation in the Lower Omo Basin was controlled by the basin geometry and the marginal bounding fault. The fault created accommodation zone for the accumulation of sediments. Sediments were thick at the central part of the Delta (>3000m) on the N- S bounding fault and thin out towards the eastern side of the basin. The contact between the basement rocks and sedimentary sequences within the basin was determined and was found to be at relatively shallower depth along both on the western and eastern side of the basin.

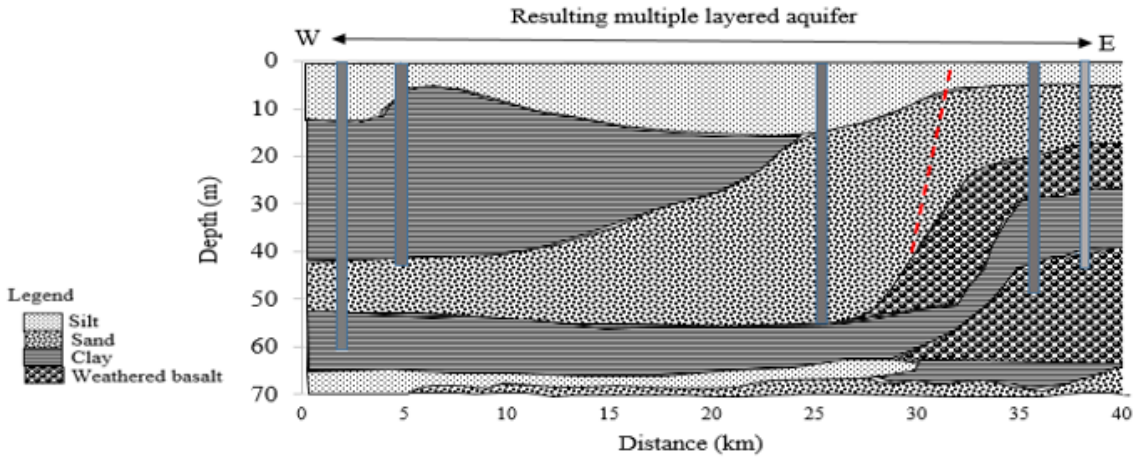

Figure 3.26 Schematic alternating fluvial and lacustrine depositional cycles have resulted in a multilayered aquifer system as observed in cross-section (W-E) in Delta groundwater wells.

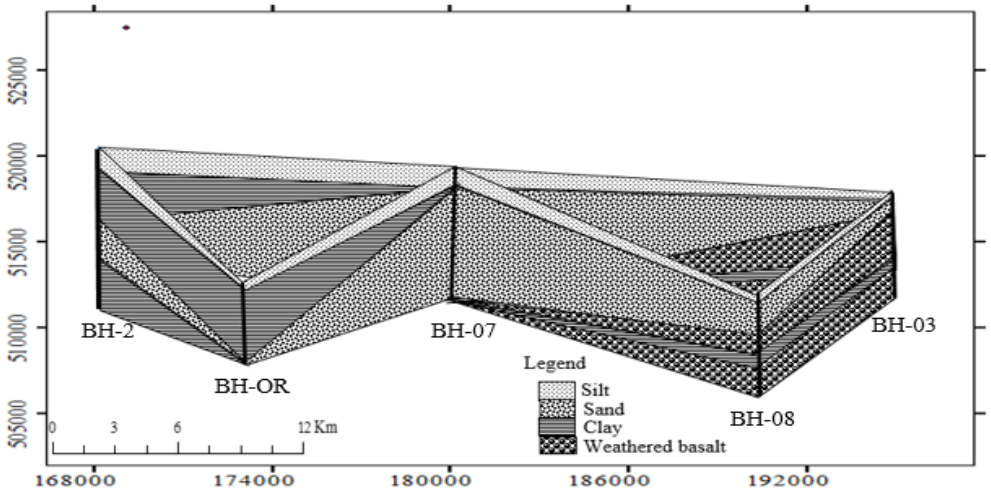

Figure 3.27 Fence Diagram Showing a 3-Dimensional Geometry of Lithology and Aquifers in Omo Delta. The Well locations are presented in the geological map of the study area (fig.2.15).

Lithological ages of the sediments are assigned from the result of drilling of Sabisa-1 well (2082 m test well drilled at Delta by Tullow Oil Ethiopia (see annex 3), has the following lithological units:

Precambrian basement rocks-The regional basement is formed by Pre-Cambrian metamorphics, primarily gneisses, and amphibolites with intrusions of granites and pegmatite. They form the base of Lower Omo basin and they are found to be high on both the western and the eastern sides of the basin and specifically in the northeastern part of the study area.

Lower Miocene sediments-From the well logs of Sabisa-1 these sequences of rocks overlie the Precambrian basement rocks unconformably. They consist of fluvial-lacustrine sediments that contain shales.

Upper Miocene fluvio-lacustrine sediments-These sediments overlie the Lower Miocene with intercalation of claystone and sand/sandstone.

Early and Middle Pliocene sediments-These Early Pliocene sediments are lake sediments of Pliocene age represented by a fluvial conglomerate and sandstone in the basin (Davidson, 1983). They are one of the older Omo Group sediments. From the lithological log of Sabisa-1 well these sediments are located at depth 1170- 1725m. The middle Pliocene sediments as described in the lithological log of sabisa-1 are found at depth of 850-1170 m. The geological descriptions of these sediments are also claystone and sand. This could be the next deposited Omo Group sediments.

Late Pliocene sediments-These sediments are intercalation of claystone and sand and they found at depth of 680-850 m in Sabisa-1 well log.

Pleistocene sediments (Kibbish formation)-The horizontal sediments related to major fluctuations in the level of ancestral Lake Turkana lies unconformably above the various Formation of Omo Group. Butzer (1969) name this sequence the Kibbish formation. It comprises four members. In Sabisa well-1 it is found at depth range 200-400m representing the early Holocene and late Pleistocene.

Holocene sediments - Holocene sediments constitute the youngest sediment in the basin. They cover most of the Lower Omo basin particularly the Delta. They exposed in banks of the Omo River confluence, on recent littoral, deltaic, alluvial fan and fluviatile deposits.

3.7. Hydrostratigraphy and aquifer configuration

The heterogeneous lithologic, geomorphic, and structural pattern of the study area resulted in various groundwater localization, quantity, quality, and flow. Therefore, it is key to understand the physical frameworks of these rocks that comprise this region. Hydrogeology of this region is under the infant stage of an investigation. Published materials and reports are scanty. Characterization of the aquifer lateral and vertical property should be supported by: exploratory drillings, pumping tests, hydrochemistry, stable isotopes of water, and radioactive isotopes. Studies in such quality are unavailable, and a few regional studies (Woodroofe & Associates, 2007; MOWR, 2006; Kebede, 2013; EGS, 1988; Asefa consult, 2015) are some of the works that address the hydrogeology of the area in part. After a thorough review of these works and fieldwork, the description of major hydrostratigraphic units has been made.

3.7.1. Basement Aquifers of Hammer

Hydrogeology of Basement rocks in Ethiopia have been discussed in different researchers (Jones, 1985; EIGS, 1988; Wright, 1992; Cherinet, 1999; MoWE, 2007; Deyassa et al., 2013; Woldemariyam et al., 2016) are some of them. These authors discussed different zones of basement aquifers in the country based on the development of regolith, degree of fracturing, type of metamorphic rocks or grades, and sustainability of recharge and topography.

The Hammer domain metamorphic rocks are basement rocks that are highly deformed and metamorphosed and reach granulites facies (Davidson, 1983) implying they belong to the high-grade belt. This belt is chiefly composed of various coarse-grained and foliated rocks. These rocks grouped into syn to late-tectonic granites, diorite, gabbro, as well as gneiss and migmatites mostly of amphibolite and granulite facies (Kazmin, et al., 1978). The Hamar domain gneisses generally dipping toward the east-northeast but show some variations from place to place. West of the Chew Bahir rift system (Hamar range); overturned and recumbent isoclinal folds have themselves been folded into open antiforms and synforms that trend and plunge northward. Foliation is generally sub-parallel to the layering (Kebede, 2009).

Among 113 tube wells sited on the Omo Delta and its surrounding, 61 wells (53.9%) are drilled on this domain. These shallow tube wells (depth range: ~16-83 m below ground, the thickness of the weathered zone and sediments above the basement varied from 4.5 to 42m below the surface with a mean of 18.3 m, The static water level varies from 2 to 29 m below the land surface. The mean static water level was 10.9m, the borehole yield range 0.5–5 L/s. The lowest yield of 0.2 L/s occurred in mafic gneisses which hydrogelogically categorized in aquifers with limited storage and the highest yield has occurred at Turmi. This 46m tube well was drilled near to "Kaskie" stream and the lithologies encountered were 0-12 m coarse sand and 12-46 gneisses with minor fractures. Both water striking depth and the static water level was 1.9m. This confirms that the "Kaskie" recharges the groundwater in nearby. Depending on the local condition of geologic structures and sediment thickness, we can have a good yield on Basement aquifers.

The availability of high recharge of precipitation (1100mm), deeply weathered surface, dense vegetation cover, and availability of tectonically induced fractures make the Hammar domain can enhance groundwater storage both in the regolith and fractured bedrock. For example, the 82.5m well drilled at Turmi (UTM 224511 E, 224511N) on this domain, the weathered clay part is 5m. From 5m up to 32m fractured granite and the rest are gneiss of different degree of fracturing. The water striking depth was at 20, 31, and 37 meters, and the main water-bearing formation is highly fractured granite. The pump test was conducted with Constant pumping rate of 3 L/sec was registered for the 8 minutes and progressive changes in water level reached at 82.5meter with the total drawdown of 67.9-meter reference to the SWL, 14.6 meters, and the wells recovered 98% by 720 minutes. This well has been recommended to pump at a rate of 0.2 L/s at pump position 82m. Another well sited on this domain is at Kako (UTM 0239667 E, 0626547 N) which has 55m depth. The upper weathered regolith (clay and sandy clay) reached up to 14m and the rest are gneiss of different compositions. The constant pumping rate 1.5 L/sec and 2.2 L/sec were registered for 13 and 2 hours respectively. The progressive changes in water level recorded following the time specified. With the given discharging rates and time the water level reached 6.37 and 12.10 meters respectively. The well recovery measurement was taken for 80 minutes after the shutting down of the pump and the water level recovered up to 3.85 meters the percentage of recovery was estimated at 87.7%. The Transmissivity well was

determined using Theis and Jacob as 1.85 x 10^{-2} M^2/min and its hydraulic Conductivity is 3.70 x 10^{-3} M/min and it is recommended that to pump this well at 2 L/s discharging rate. From these two wells, it can be observed that though, the depth of Turmi well is much deeper than Kako but the thickness of regoliths in Kako well is three-fold that gives higher discharge than Turmi.

The extensive wadi beds that exist in the dry river channels of Hammer Koke lowlands are the result of active stripping. They are developed parallel to the regional NW-SE running foliations or follow contacts between the different units of the basement rocks; there is no obvious deep penetrating fracturing (Kebede, 2013). This geomorphic feature is acting as the temporary groundwater storage and most shallow wells and hand-dug wells are sited close to these features. The groundwater recharge to the wadi beds and the broad basement takes place from occasional flash floods generated in the higher ground high rainfall area in the north. The principal source of water supply for livestock and human consumption in the Hammer basement and lower Omo regions are riverbed excavations and hand-dug wells drilled adjacently to the riverbeds. Based on the storage and permeability, total dissolved solids (TDS), the geometry of aquifers, and the availability of recharge. Kebede (2013), classify this domain into four aquifer units (Figure 3.29).

1. Aquifers with limited storage and permeability but characterized by low total dissolved solids.
2. Aquifuges composed of basement intrusions and granitoids.
3. Fractured aquifers with limited lateral and vertical extent.
4. Lithologies with higher inter-granular porosity but dry because of lack of recharge.

The hydraulic gradient reflects topography and permeability. In general, the piezometric contours indicate a regime of groundwater flow towards the central axis of the valley i.e. towards Omo River (Figure 3.29). The groundwater flow is confined in wadi beds and they are developed parallel to NE- SW running foliation or follow contacts between the different units of the basement rocks, there is no obvious deep penetrating fracturing, regoliths thickness is in the order of 15m maximum. The groundwater recharge to the wadi beds and the broad basement takes place from occasional flash floods generated in the higher ground

and high rainfall area in the north. Water quality is often of low TDS and in the order of less than 1500mg/l.

3.7.2. Quaternary Sediments

Three types of Quaternary sediments are recognized and mapped by Davidson (1983) namely: alluvium (e.g. alluvial fans), lacustrine silt and clay, and fluvial sand and silt (Figure 3.14). The alluvial sediments, in general, are thick and extensive in the Omo Valley. This is particularly true in the tectonic depressions in which the delta is situated. Besides, there are alluvial fans and wadis composed of sands, gravels, and pebbles. The unconsolidated alluvial formations produce a complex hydrogeological framework comprising alterations of silt, sand, clay, and gravel layers of variable thickness. The alluvial materials are found at the confluence of the wadi beds draining the Hammer Koke highlands in the east and southeast of the study area. They contain distributary channels and sand bars. These quaternary sediments are results of different geomorphic activity and resulted in the different salinity patterns of groundwater in the Delta. The unconsolidated alluvial formations produce a complex hydrogeological framework comprising alternations of sand, silt, clay, and gravel layers of variable thickness. The complexities arising out of the various depositional environments that the area has faced owing to Lake level changing, changing the course of the river and the changes in the associated sub-environments like estuaries, lagoons, floodplains, Ox-bow Lakes.

The borehole drilled some 18 km northeast of the former Ethio-Korean State Farm (36o 13'E, 4o 26'N) is considered representative of this hydrogeological unit. This borehole, penetrating to 40 m, revealed the following lithological sequence: 0-8 m light yellow silt, 8-15 m silty-fine to medium-grained sand and gravel, 15-27m slightly silty gravel and fine to coarse-grained sand, 27-31 m fine to medium-grained sand with some pebbles, 31-40 m fine to coarse-grained sand and gravels. With the water table at 25.4 mbgl, the sand and gravel beds below 25 mbgl are considered as the main aquifer, which is reported to contain water of "good" quality.

Figure 3.28 Children are digging a dry river bed for gathers water (left) and the livestock watering is also done from these excavations (right) at Bubua (near Fejeji).

The analysis of pumping test data revealed a composite aquifer transmissivity of about 57 m^2/day, with the borehole supporting a yield of 3.9 liters per second at a drawdown of about 8.5 m.

Groundwater potential in this hydrogeologic unit can be explained by water stored in both the alluvium and underlying lacustrine sediments. The groundwater availability in parts of Delta: around Fejeji and Omorate can be represented by such aquifer type; where groundwater is stored in both the top alluvial aquifer and the bottom lacustrine sediment. The aquifer in such a condition seems to have a continuous nature but variable in water quality from top to bottom and from the highland side towards the Lakeside. Freshwater is stored up to a depth of 70 to 80 meters usually in such cases and the water below that is saline rich water (Assefa, 2017). Although recharge from the intermittent streams partly neutralizes the water, the white incrustation seen in dry sediments in dry creeks indicates that the sediments have a high proportion of dissolvable materials that highly affect the groundwater quality from such lacustrine sediment dominated aquifers. The knowledge of the nature of deep aquifers in Omo Delta is blurred due to limited data that represent the basin.

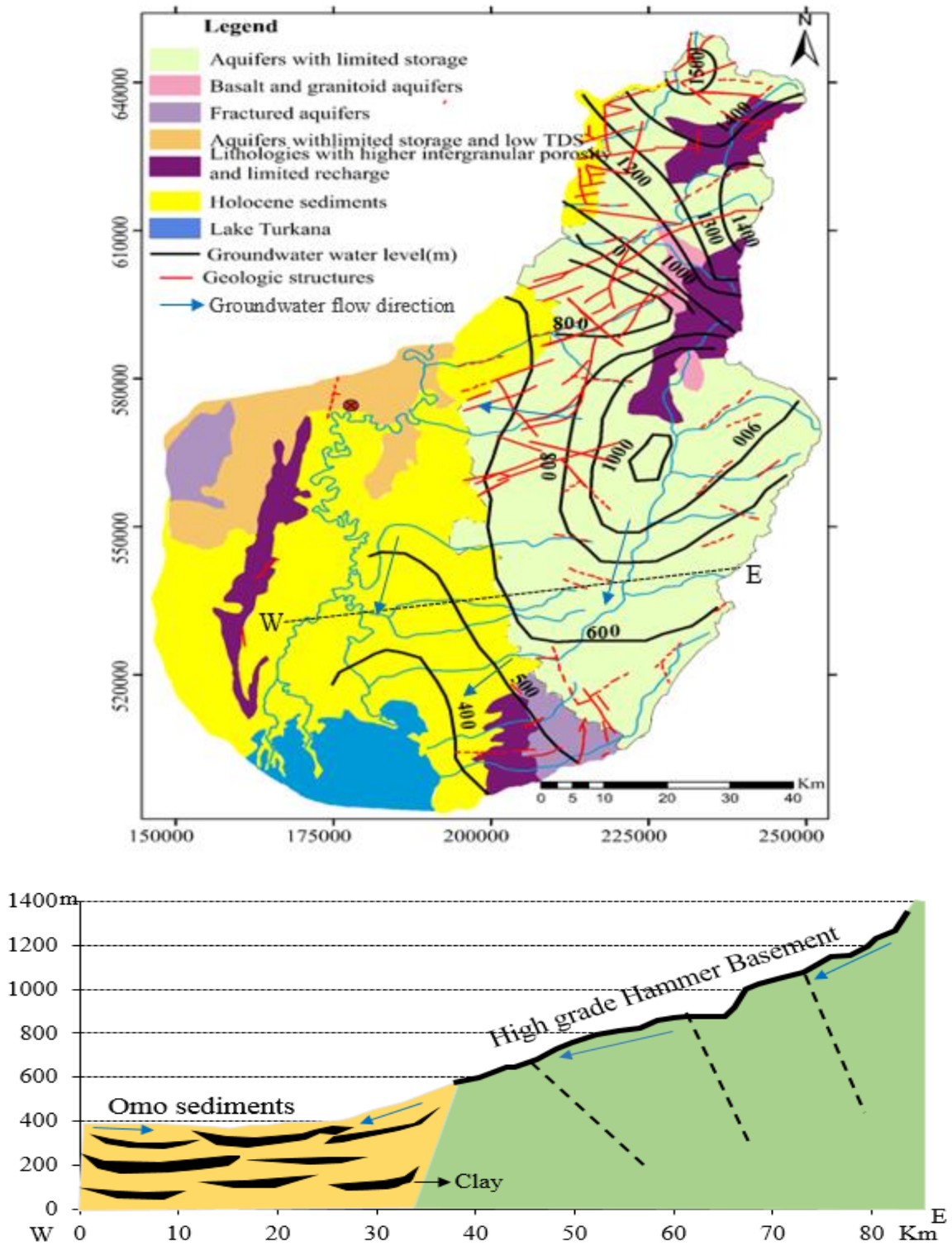

Figure 3.29 Hydrogeological map of the study area. (Modified after Kebede, 2013).

4. SAMPLING, SAMPLE ANALYSIS AND DATA

4.1. Sampling

Mapping the spatial variation of geological outcrops, water point inventory, and hydrochemical sampling of water points are major activities undertook in fieldwork. The water sampling of existing wells done from available water points, though the population of wells is scarce because the area is highly underdeveloped and less populous. Surface water sampling was carried out along Omo River and Lake Turkana about 50cm below the water surface. The river water was obtained from the middle part of the river. Lake water was collected as far as possible from the shore. Along with the sampling, in situ water quality parameters measurement was made with a portable HANNA instrument with a multi-parameter probe (T, pH, and EC).

Groundwater samples from 62 existing all functional wells have been collected from the Delta and its environs to understand the hydrochemical system of the Delta. Similarly, 72 shallow wells, 2 cold springs, 11 River samples, and nine Lakes samples were collected for stable isotope analysis. Although the wells are used extensively, we have pumped the wells for 10 min before sampling to obtain fresh groundwater. At each sampling point, the plastic bottles were completely rinsed with the source waters to be sampled.

Secondary data collection and organization from previous regional research articles, books, maps, and reports consisting: well log data, pump test data, chemistry data, isotope data is used for the preparation of base map and identification of data gaps for fieldwork. Hydrochemical parameters from 52, 3, and 3 shallow drilled wells, Lake Turkana and Omo River respectively, collected from secondary data sources. Major hydrometeorological data consisting of rainfall, the temperature in the Omo River/Lake Turkana Basin was collected from the Ethiopian Meteorology Agency.

^{222}Rn concentration in the water was measured by a widely used portable commercial α detector RAD7 and the RAD H_2O accessory (Durridge Company, USA) at a spot and within 12h of sample collection. For radon concentration analysis in surface water, Big Bottle System (2.5L), an accessory to the RAD-7 radon monitor was used (Figure 4.1). The internal pump of the RAD-7 extracts radon from water and the radon circulates to the RAD-

7 detector in the RAD-H_2O system. ^{222}Rn concentration in water was corrected for time-lapse between sampling and measuring as discussed in (Diab, 2019; DURRIDGE Company, 2019) and Radon in water is calculated using CAPTURE free software.

Figure 4.1 RAD 7 and its accessory used for ^{222}Rn concentration measurement.

Existing geological and hydrogeological information was also used. Geologic units of the exposed area (fault scarps, river cuts, and erosion gullies), lithologic contacts and faults, and water points were mapped using materials such as Garmin GPS 72 and 1:50,000 scale topographic map. The pictures of lithological units were taken from the routes for correlation of the units. The inventory of water points was made for the generation of the data sets including the location of water points, water level, well discharges, and physical characteristics of water samples. This resulted in the spatial distribution of groundwater level, its flow direction, hydraulic property, hydrogeological and structural elements used to prepare the geological, hydrogeological maps, and cross-sections.

4.2. Sample Analysis for Hydrochemistry and Isotope Hydrology

The major ions in water samples were analyzed at the South Region water development bureau water quality department laboratory. Calcium and magnesium were determined using a Jenway 6405 UV/Vis spectrophotometer, while sodium and potassium were determined by atomic absorption spectrophotometer. Sulfate ion was determined by a Jenway 6405 UV/Vis spectrophotometer. Alkalinity and Chloride were determined by titration. The anion-cation charge balance was checked to be of ±5% for all samples. Water samples environmental isotopes of δD and δ18O were analyzed by LGR Water Vapor Isotope Analyzer; in Addis Ababa University School of Earth Sciences and reported relative to the VSMOW Standard (Vienna Standard Mean Ocean Water) in peril (‰). The analytical error is less than 0.2‰ and 0.03‰ for δD and δ18O, respectively.

4.2.1. Database editing procedures

Data quality must be assessed before proceeding into complex statistical data analytical procedures. Even though computers do much of the computational work, some degree of knowledge of the statistical methods used is also necessary to be able to produce the required type of results. Unfortunately, there is no single procedure or method that can be employed to prove that data are or are not usable. Randomness in data may either be due to naturally occurring randomness, which exists in the geological environment or to measurement errors introduced by analytical procedures or instruments used (Guler, 2002).

For this study, a five-step methodology was followed to support these activities. These steps were:

i. Data Collection
ii. Database Editing Procedures
iii. Data-Gap Filling Procedures
iv. Percent Charge Balance Error
v. Data Characterization and Screening.

4.2.2. Data Collection

This study commenced with a through primary field sampling and literature search and compilation of published and unpublished relevant hydrologic and water chemistry information, well-drilling reports, and water quality data to create a comprehensive hydrochemical database for the Omo Delta area. Secondary data compiled for this study collected from different sources and time assuming that adequate quality control measures were undertaken at the time of original data collection and analysis. Some data are compiled from the hardcopy and others from a digital format. The samples collected by different researchers and institutions used by this study were not selected based on a rigorous statistical procedure. The area is poorly developed and populated. Moreover, the shallow wells drilled for water supply abandoned due to high salt content and non-functional, making the sampling impossible. Therefore, the hydrochemical and drilling history data at the time of construction is important to address the objective of this study. After entering all the pertinent data into the database editing process was initiated.

4.2.3. Database Editing

No missing data values (a complete water analysis result) is mandatory for the effective use of the methods that are utilized in this study and means of establishing that were addressed in the following sections.

4.2.3.1. Uncertain Sample Locations

Since water chemistry data without a location cannot be evaluated in a spatial context; samples with uncertain locations were located by using reports and maps or eliminated from the database when such information was not available.

4.2.3.2. Different Unit Reporting Formats

Inconsistent unit of measurement between different data sets causes difficulties in compiling the water chemistry database. All values were converted to an internally consistent format (all units are in mg/l in the hydrochemical database) before entry into the main database to be able to produce meaningful statistical analysis results. Common reporting units observed within disparate data sets were mostly weight-per-volume units

(milligrams per liter (mg/l) and micrograms per liter (µg/l)), equivalent-weight units (milliequivalents per liter (meq/l) and micro equivalents per liter (µeq/l)), and weight-per-weight units (parts per million (ppm), parts per billion (ppb), and parts per trillion (ppt)). Mazor (2005) gives conversion factors for the calculation of a unit from the other units is used for this study. The flowchart below summarizes the methodology used for compiling and editing the hydrochemical database.

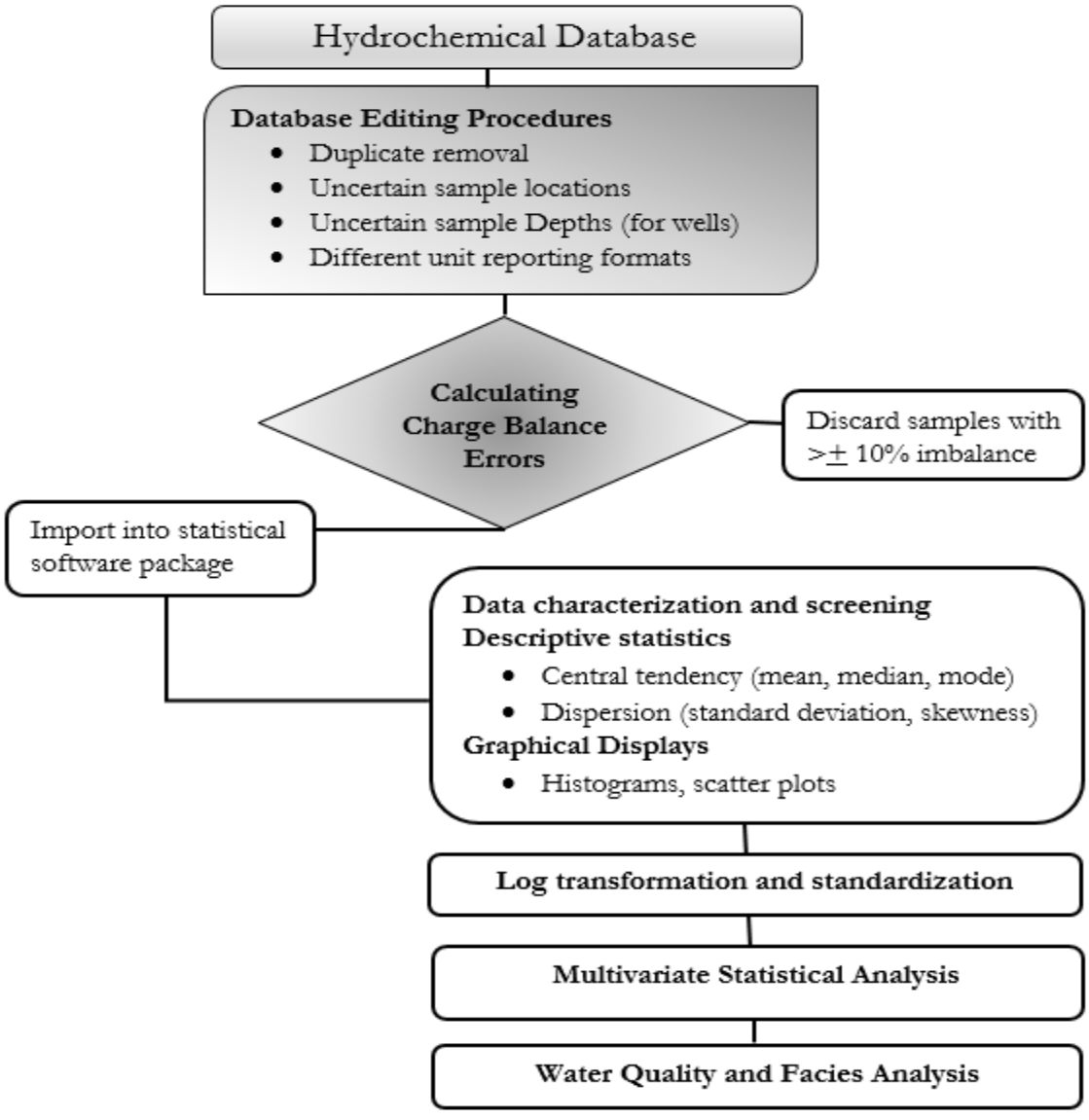

Figure 4.2 The methodology used for compiling and editing the hydrochemical database.

4.3. Data-gap Filling

The effective use of many of the methods requires complete water analysis (no missing data values). Missing data values may hamper the construction of graphical water chemistry evaluation techniques or limit the quality of the statistical and non-statistical analysis techniques, and thus, provide an important challenge in database construction (Mazor, 2005). During the statistical analysis, most statistical software packages replace those missing values with means of the variables or prompt the user for case-wise deletion of the valuable analytical data, both of which are not desirable. This can bias statistical analyses if these values represent a significant number of the data being analyzed (Guler, 2002). Therefore, it is important to make sure that every variable and object in the database have numerical values. If this is not possible, then the easiest option is to use variables and samples with no missing values.

There are statistical methods and chemical relationships that can be employed to estimate missing values to fill the data gaps that exits in the database. For instance, the missing Specific Conductance data were calculated from the total dissolved solids (TDS) data by using a simple linear regression method. The conventional approach to regression analysis involves fitting a straight line that minimizes the sum of squares of the vertical distances from data points to this regression line. This minimum sum of squares value often is referred to as the error sum of squares of the residual sum of squares. The linear regression analysis method was utilized for predicting the value of one variable, called the dependent variable, from the knowledge of the value of another variable, called the independent variable.

4.4. Data Characterization and Screening

In this study, Statistica® Release 12.0 (StatSoft, Inc., 2013) commercial statistical software package was utilized for the data characterization and screening purposes. This software is a comprehensive, integrated statistical data analysis, graphics, database management, and custom application development system featuring basic and advanced analytic procedures for science, engineering, and data mining applications, which supports data import/export

compatibility with other database and spreadsheet formats such as dBASE, Excel, Lotus, Paradox, and QuattroPro. Data screening is a critical part of data preparation that utilizes univariate and bivariate statistical methods to assess each variable independently and variable pairs. The purpose of data screening is to evaluate the distribution characteristics of each variable in the database.

Statistical procedures can help reveal the insufficiency of data and information gaps that commonly found during hydrochemical evaluations. Within the various data sets, measurements of individual physical and chemical properties were evaluated using the basic statistical measurements of the central tendency (mean, median, and mode) and dispersion (standard deviation, skewness) and by graphical displays such as histograms, scatterplots, probability plots, and box plots.

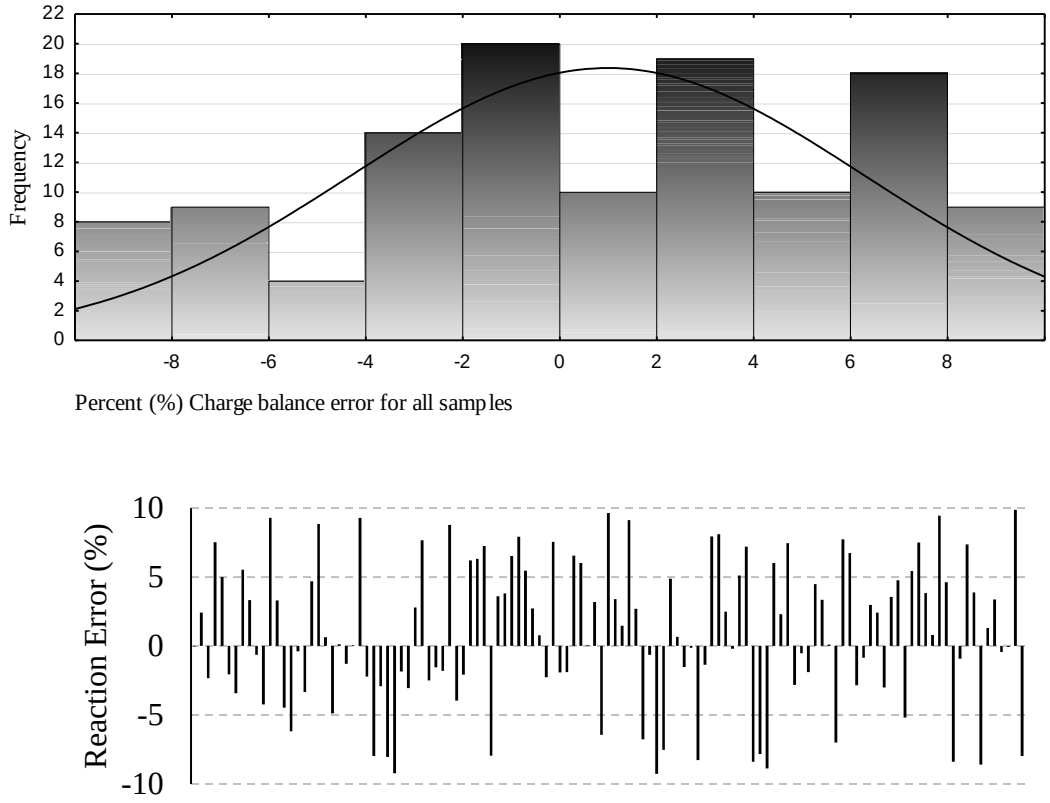

Figure 4.3 Histogram of percent of charge balance error (top) and Charge balance error percentage (bottom) and for samples used in this study.

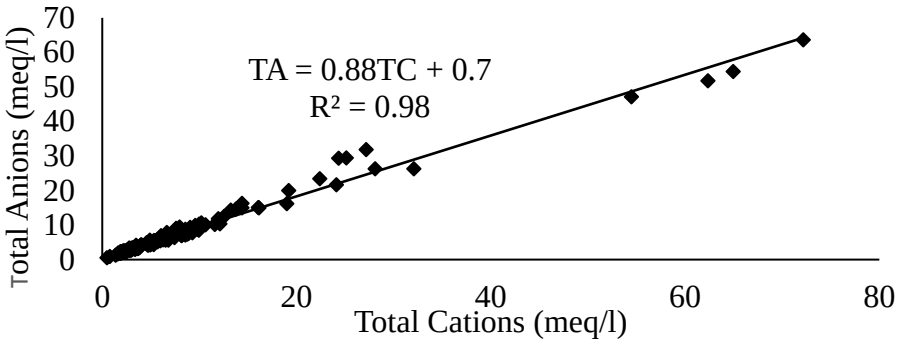

Figure 4.4 Correlation for ions.

The data screening showed that the data used in this study were universally skewed positively; the data contained small numbers of high values. This result was expected since most naturally occurring element distributions follow this pattern (Miesch, 1976). The data were log-transformed (except for pH) so that they more nearly corresponded to normally distributed data. Then, all variables were standardized by calculating their standard scores (z-scores) as follows:

$$z_I = \frac{X_I - \bar{X}}{s} \qquad (4.2)$$

In Equation (4.2) the Z_I is the standard of sample I, X_I the value of sample I, $\bar{x}$ the mean, and s the standard deviation.

4.5.1 Basic Statistics

A basic data-screening task was undertaken to determine the accuracy and utility of the chemically balanced water chemistry analyses in the hydrochemical database. Raw and transformed (log-transformed and standardized) surface and well water data were evaluated, basic statistics were calculated, and histograms were plotted. Linear relationships between variable pairs were examined (for both raw and transformed data) using scatterplots and correlation coefficients. Two data sets were created for both water type (surface and well water) for basic statistical analysis, one containing original raw data values and second containing transformed data in which the data were first log-transformed and then standardized by calculating their z-scores. All the data sets were formatted to be used by Statistica® 12.0 (StatSoft, Inc., 2013). Ten variables (Electrical Conductance, pH, Ca, Mg, Na, K, Cl, SO4, HCO3, and F) were statistically evaluated for each data set.

Calculated basic statistics included a number of samples, mean, minimum and maximum values, standard deviation, and skewness.

4.5. Correlation Coefficients

Associations among variables can be demonstrated statistically by correlation analysis. In correlation analysis, correlation coefficients are calculated for all possible pairs of variables, and those numbers can be presented in an easily comprehensible table format (correlation coefficient matrix). Correlation is the ratio of the covariance of two variables to the product of their standard deviations (Davis, 1986). A resulting correlation coefficient is a unitless number that ranges between −1.0 and +1.0. A value of −1.0 represents a perfect inverse relationship between the two variables. A value of +1.0 occurs when the two variables react in the same way as their values change. A correlation coefficient of 0 suggests that the two variables are independent of each other.

Most of the common statistical software packages perform correlation analysis and significance tests simultaneously. In the resulting correlation coefficient matrix, statistically significant correlation coefficients are highlighted and easily recognized. This widely used type of correlation coefficient is also known as the "Pearson product-moment Coefficient" or "Pearson r". Correlation coefficients of both raw and transformed data sets were calculated by using the Statistica® 12.0 "Basic Statistics and Tables" algorithm and by choosing the "Correlation Matrices" option. This algorithm computes correlation coefficients for pairs of variables, thus defining the linear relationship between them.

5. RESULTS

5.1. Physical Properties

To investigate the hydrochemical composition, flow processes, and evolution of groundwater in the study area, a systematic survey, and analyses of the physical (EC, TDS, P^H, and T) properties of water have been conducted.

5.1.1. Temperature

To obtain necessary information on the nature of aquifers that groundwater is pumped out from measuring the physical parameters, as the temperature is important because it is sensitive to aquifer depth and is most useful in distinguishing different water systems (Hem, 1980; Mazor, 2004; Anderson, 2005; Constantz, 2008). Therefore, if wells show variable groundwater temperature within small spatial distance, then the waters come from different aquifers (i.e. Temperature remained constant, indicating pumping remained constricted to a single aquifer). Whereas, the temperature suddenly increased, indicating water from a warmer (probably lower) aquifer breached in.

In the study area, the temperature of the groundwater ranges from a minimum 34.4 and 21.9 ^{0}c to a maximum of 39.4 and 31.5 ^{0}c for Delta and basement groundwater respectively. The maximum temperature was recorded in Delta groundwater from two wells sited at Delta Flats (OD8 and OD9) and the minimum value measured from two wells close to each other (OD4 and OD5). In the case of Hammer basement aquifer, the maximum temperature was measured at the shallow well (OD19) and the minimum was observed at contact spring at Jinka (OD28). It can be observed that in Delta groundwater temperature vary significantly within few changes in altitude (dot circle B in Figure 5.1) as compared to the Basement aquifer, in which groundwater temperature variation is small compared to change in altitude (dot circle A). This can be explained that the groundwater at Delta is characterized by a multilayer aquifer system. The spatial variation of temperature reflects the northeastern part (recharge area) is characterized by relatively low temperature and the temperature increases towards the Delta. The relationship between electrical conductivity and temperature of groundwater in the study area also shows interesting relation (Figure

5.1). One can observe that Delta groundwaters are characterized by relatively high EC and temperature values (Circle C in Figure 5.1) as compared to Basement aquifer groundwater (Circle D).

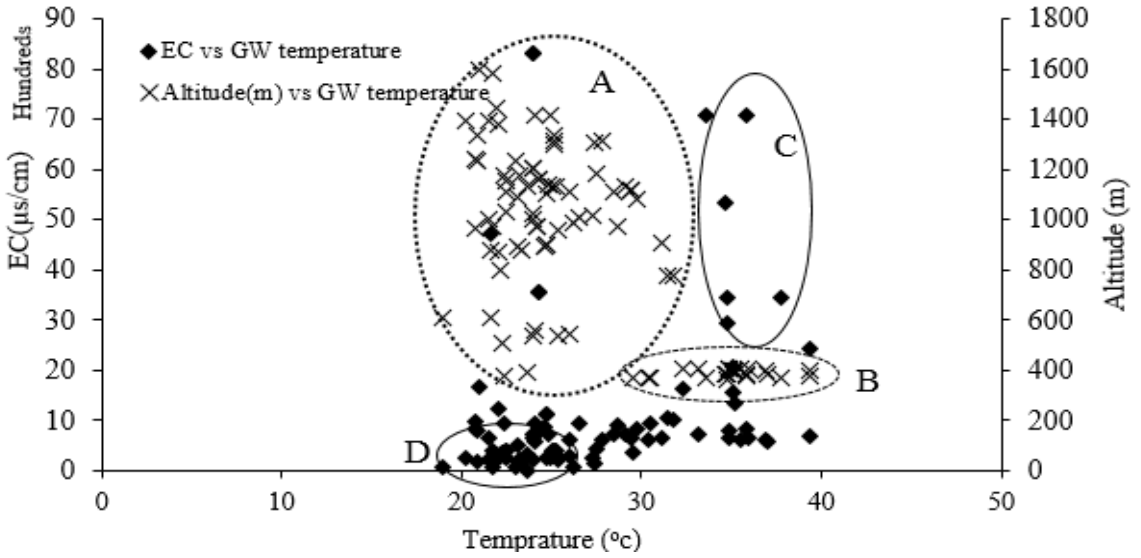

Figure 5.1 The relation between the temperature of groundwater in the study area as a function of altitude and electrical conductivity.

5.1.2. Hydrogen-ion Activity (pH)

The pH of a solution indicates the effective concentration of hydrogen ions, H^+. The pH is controlled by various reactions and the presence of different compounds. In freshwater systems, the carbonate system CO_2-HCO_3-CO_3 plays a primary role in determining the pH. In other cases, the presence of H_2S or its oxidized form, sulfuric acid determines low pH. The pH value is an important parameter in water quality assessment concerning corrosion problems and taste (Mazor, 2004). The hydrogen-ion activity in an aqueous solution is controlled by interrelated chemical reactions that produce or consume hydrogen ions. The dissociation equilibrium for water is always applicable to any aqueous solution, but much other equilibrium and non-equilibrium reactions that occur in natural water among solute, solid and gaseous, or other liquid species also involve hydrogen ions. The pH of natural water is a useful index of the status of equilibrium reactions in which the water participates (Hem, 1985).

P^H in the study area ranges from 4.9 to 9.25 and 7.67 to 8.23 for groundwater and Omo River respectively. The highest value measured at Delta flats and the lowest value was measured at well sited at mafic gneisses and amphibolite. Generally, wells at Delta have higher pH values relative to wells at the Basement. High pH values tend to facilitate the solubilization of ammonia, heavy metals, and salts. It can be observed that the Delta groundwater, which is generally characterized by high salinity, also shows alkaline nature. The precipitation of carbonate salts is encouraged when pH levels are high (Hem, 1985). Low pH levels be likely to rise carbonic acid and carbon dioxide and concentrations. Lake Turkana is alkaline with an average (pH=9.25). The high pH of the lake results in the precipitation of $CaCO_3$ and hence the loss of Ca from the water column.

5.1.3. Total Dissolved Solids (TDS)

A measure of the amount of dissolved material in the water column is defined as total dissolved solids (TDS). Dissolved salts such as sodium, chloride, magnesium, and sulfate contribute to higher residue values. The acceptability of water as a drinking source and irrigation supply determined by concentrations of total dissolved solids (Arad, 1984; Monjerezi, 2012). Total Dissolved Solids (TDS) signifies the salinity behavior of water because it is the index of the concentration of the dissolved ion in the water. There is also a relationship between TDS and Electrical Conductivity (EC). This relation is used to estimate TDS after having field EC measurement or vice versa and it also helps to check the reliability of laboratory results using a certain constant (A). A is mostly between 0.55 and 0.75; the higher values generally being associated with water high in sulfate concentration (Hem, 1985). The relationship of these parameters can be valued by the next equation:

$$\mathrm{TDS}\left(\frac{\mathrm{mg}}{\mathrm{l}}\right) = \mathrm{kxEC}\left(\frac{\mu_s}{\mathrm{cm}}\right) \qquad (5.1)$$

The increase of the concentration ions in water resulted to increase the value of k. Where k is correlation between EC and TDS, which is range from 0.55-0.7 for various water type. However, the correlation between total dissolved solids and electrical conductivity is not straight linear; it depends on the activity of specific dissolved ions average activity of all ions in the liquid and ionic strength (Rusydi, 2018). As discussed in (Rusydi, 2018)

electrical conductivity (measured in-situ) and total dissolved solids measured in the laboratory had a good correlation coefficient ($R^2 = 0.99$) (Figure 5.2) and this indicates that total dissolved solids and electrical conductivity can be used exchangeably in the following discussion. It also shows that the parameters measured in the field and lab harmonized very well.

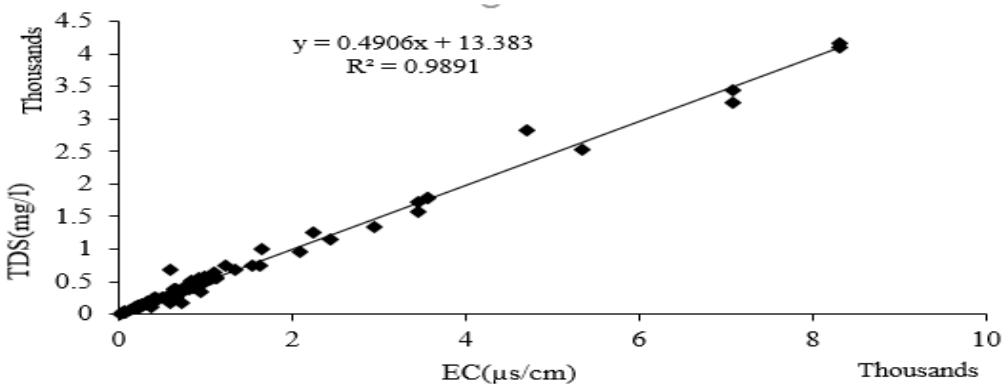

Figure 5.2 Scatter plot on the top-right represented the TDS-EC relationship for all water samples in the study area

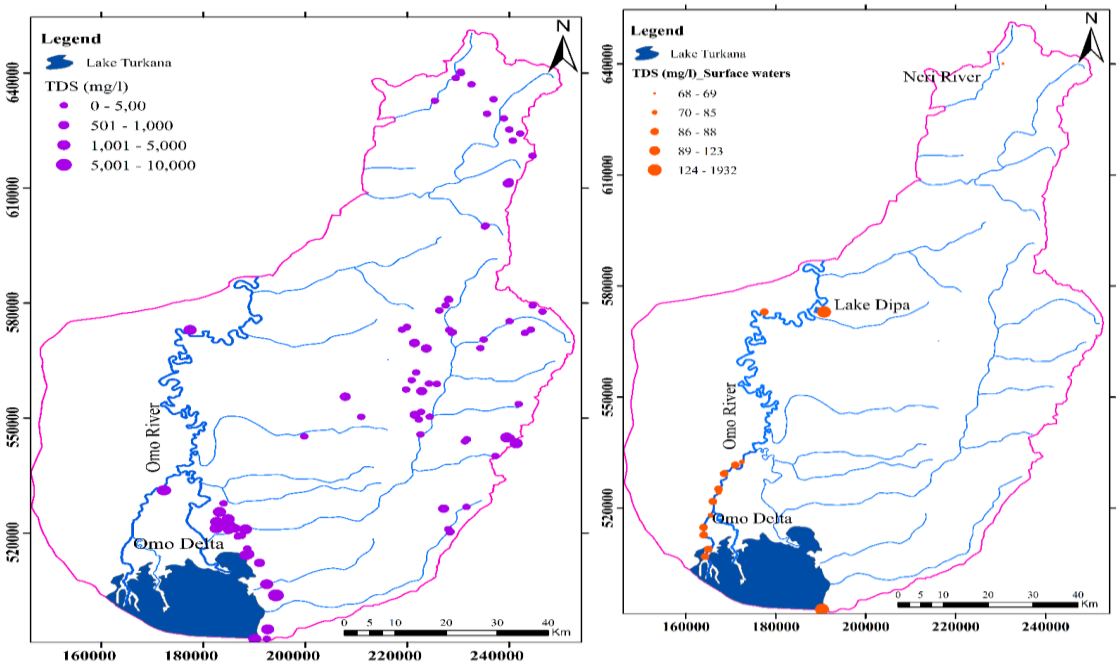

Figure 5.3 TDS of groundwater (left) and surface waters (Right) in the study area.

Similarly, the TDS of surface waters was measured and the highest value (1932 mg/l) was measured at Lake Turkana. Whereas the TDS of Lake Dipa was not high as expected (122.3mg/l) this is due to Omo River seasonally flooded through small natural channels, which cross the riverbank. Unlikely, Lake Turkana lies in an enclosed basin with no surface outlet, as a result, the concentration of solutes increases continually. TDS values indicate that the concentration of solutes is increasing at a much slower rate than expected; over a longer period, relatively low conductivities in the lake are maintained by sediment-water interactions (Hopson, 1982).

The TDS of Omo River was measured along the river course from Kangaton (north) to Delta fringe (south). Moreover, it can be observed that there is a slight increase in TDS (Figure 5.4) as the River stretches from Kangaton to Delta (18.6mg/l) this is likely caused by the contribution of saline groundwater and the River water subject to intense evaporation prevails enrichment insoluble minerals.

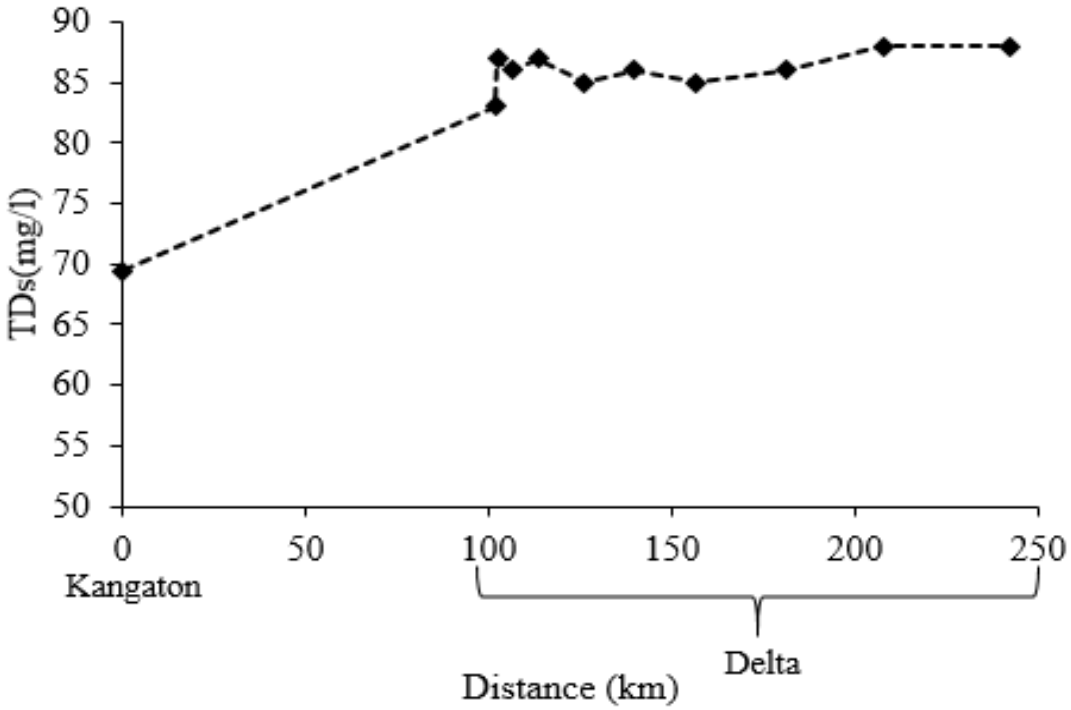

Figure 5.4 Variation of TDS along Omo River.

5.1.4. Electrical Conductivity (EC)

The electrical conductivity of water is the ability of the water to conduct an electric current. The presence of charged ionic species in water makes the water conductive (Mazor, 2004). As ion concentrations increase, the conductance of the water increases. Therefore, the conductance measurement provides an indication of ion concentration in the water (Hem, 1985).

EC values of the groundwater samples of the study area are in the range of 56.9μs/cm to 10,240μs/cm. The optimum values are much higher than the maximum permissible range of the standard EC value set by the World Health Organization (WHO, 2011) for drinking water, which is 1,500μs/cm. The electrical conductivity (EC) values in the investigation area showed an increasing trend from recharge to discharge area (Figure 5.3). As discussed above, total dissolved solids (TDS) and EC (Electrical conductivity) can be used interchangeably so that interpretation for EC variation is similar to that of TDS described in the above section.

5.2. Major Element Geochemistry Characterization

The chemical composition of the surface and groundwater is controlled by many factors that include the composition of precipitation, mineralogy of the watershed and aquifers, climate, and topography (Guler, 2002). These factors combine to create diverse water types that change in compositional character spatially and temporally. In the study area, there is a variety of climatic conditions (cold to desert), hydrologic regimes (alluvial basin-fill aquifers, fractured rocks, and basement aquifers) and geologic environments (volcanic rocks, metamorphic rocks, and sedimentary deposits). Accordingly, the samples from the area could possibly denote a variety of water types providing an opportunity to test the performance of many of the available graphical and statistical methodologies used to classify water samples.

The hydrochemical lab. analysis result of major ions (Na^+, Ca^{2+}, Mg^{2+}, K^+, Cl^-, F^-, SO_4^{2-}, HCO_3^-, and NO_3^-) of ground and surface water were obtained from primary and secondary data. Depending on the climatic condition, hydrologic regimes, and geologic environment, their concentration varies as discussed in the next session.

5.2.1. Graphical Methods

Graphical methods are designed to simultaneously represent the total dissolved solids (TDS) concentration and the relative proportions of certain major ionic species (Hem, 1989). They use a limited number of parameters, usually a subset of the available data, unlike the statistical methods that can utilize all the available parameters. The chemical constituents in each water sample under investigation are well understood by comparing their similarity and differences in the concentration using different graphs. The chemical processes responsible for variation in composition, detection of mixing of water from different sources, and aquifers are well explained by graphs. In this study, different graphical methods are used for the presentation and interpretation of hydrochemical data in the region.

The Piper diagram is the most widely used graphical form (Piper, 1944). The diagram displays the relative concentrations of the major cations and anions on separate trilinear plots, together with a central diamond plot where the points from the two trilinear plots are projected (Guler, 2002). The central diamond-shaped field (quadrilateral field) is used to show the overall chemical character of the water (Hill, 1940; Piper, 1944). Back (1961) and Back and Hanshaw (1965) defined the subdivisions of the diamond field that represent water type categories that form the basis for one common classification scheme for natural waters. The mixing of water from different sources or evolution pathways can also be illustrated by using this diagram (Freeze and Cherry, 1979). Symbol sizes can be scaled to TDS on the diamond-shaped field to add even more information (Domenico and Schwartz, 1997).

Figure 5.5 shows the results of plotting the 112 Groundwater samples on the Piper diagram. The data are broadly distributed rather than forming distinct clusters. Employing the water classification scheme of Back and Hanshaw (1965), the samples are classified into a variety of water types including Mg-HCO_3, Ca-Mg-HCO_3, Ca-Na-HCO_3, Na-HCO_3, Na-Ca-HCO_3, Na-Cl, and Ca-Mg-SO_4 types, with no dominant type. The groundwater samples clustered in four groups and 9 subgroups based on the HCA in section 5.2.2

The groundwater samples are distributed in both the Quaternary sediment and Hammer basement aquifers. 30.4% of groundwater samples are geologically located in the Quaternary sediments. Whereas, the rest 65.6% are from Hammer basement. The water type from the Quaternary sediment aquifers is characterized by 52.9, 32.4, and 11.8% mixed, sodium chloride, and sodium bicarbonate types respectively. The majority (82.1%) of groundwater from Hammer basement are magnesium bicarbonate type. The remaining, 11.5% and 6.4% are mixed and sodium bicarbonate type respectively, showing that the water type in this hydrogeologic unit is bicarbonate type of recharging type. Figure 5.5 also indicates that the groundwater in the Hammer basement is characterized by shallow depth and unconfined aquifers representing the local flow groundwater system for the region.

Figure 5.5 shows that group1 groundwater comprises 61.3% and 69.2% from all and the Delta groundwater samples respectively. They are characterized by low EC, and in close association with dry river channel in Hammer basement aquifers. They are from shallow groundwater wells and unconfined basement aquifers. In the case of the Quaternary sediment, this group is found in association with the Eastern beach ridges, which is characterized by alluvial fan and fan deposits. Group2 groundwater accounts for 28.6 % of groundwater in the study area. They characterize low salinity and almost all samples found on the Hammer basement aquifers. These samples show a slight evolution than group 1 samples.

Group 3 and 4 samples are characteristics of the Delta groundwater with salinity range from brackish to saline. They are prevalent in Central Delta flat and Delta fringe geomorphologic features of the Delta where the Quaternary sediments comprise the aquifer material at different proportions. It can be observed from Figure 5.5 that unlike to Hammer basement, the Quaternary sediment aquifer comprises a variety of groups in close association.

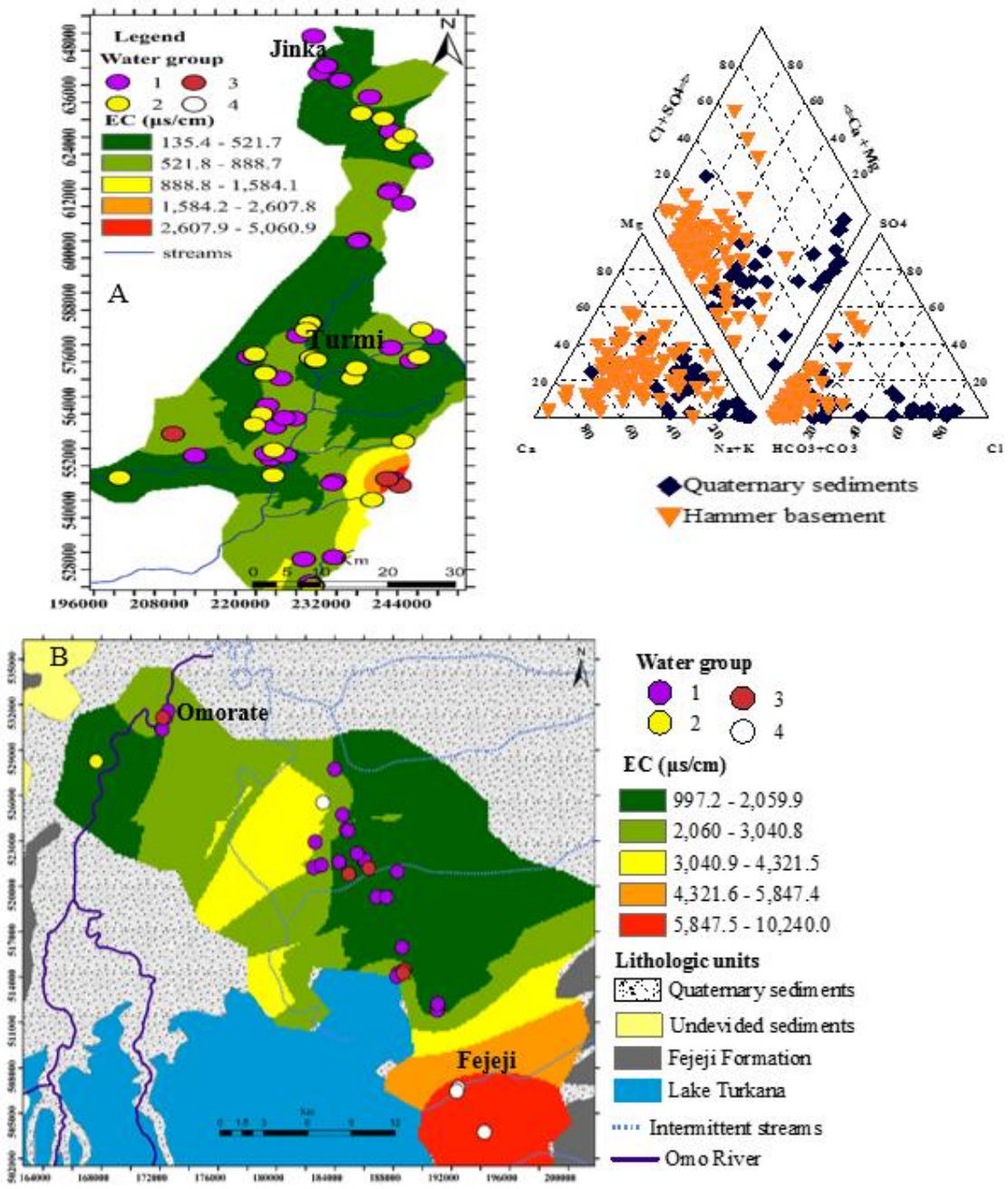

Figure 5.5 The spatial distribution of EC and its relation to water groups: Delta (A) and Hammer Basement (B). The geologic units and other features explained in Figure 2.14. Surface map created using Kriging using ArcGis 10.4 and the Piper diagram that showing the division of groundwater based on geology they exist. Water groups are generated based on Dendogram developed in section 5.2.2.

5.2.2. Cluster Analysis

Statistical techniques, such as cluster analysis, can offer a great tool for analyzing water chemistry data. These methods can be used to test water quality data and determine if samples can be grouped into different populations (hydrochemical groups) that may be important in the geologic framework, as well from a statistical perspective (Guler, 2002; Kebede, 2004; Monjezeri, 2012).

The assumptions of cluster analysis techniques comprise homoscedasticity (equal variance) and normal distribution of the variables (Alther, 1979). An equal weighing of all variables requires the log-transformation and standardization (z-scores) of the data as discussed in Chapter 4. The classification of samples according to their parameters is termed Q-mode classification. This approach is commonly applied to water chemistry investigations in order to define groups of samples that have similar chemical and physical characteristics because rarely is a single parameter sufficient to distinguish between different water types.

In order to determine the relationship between groups, the r × c matrix (r samples with c variables) is imported into a statistics package. The Statistica ® 12 (StatSoft, Inc., 2014) has seven similarities/dissimilarity measurements and seven linkage methods and supports up to 300 cases for the amalgamation process in the cluster analysis. Individual samples are compared with the specified similarity/dissimilarity.

The linkage rule used for this study is Ward's method (Ward, 1963) for hierarchical clustering. Linkage rules iteratively link nearby points (samples) by using the similarity matrix. The initial cluster is formed by the linkage of the two samples with the greatest similarity. Ward's method is distinct from all other methods because it uses an analysis of variance approach to evaluate the distances between clusters. Ward's method calculates the error sum of squares, which is the sum of the distances from each individual to the center of its parent group (Judd, 1980) and forms smaller distinct clusters than those formed by other methods (StatSoft, Inc., 2014).

HCA classifies the data in a relatively simple and direct manner, with the results being presented as a dendogram, an easily understood and familiar diagram (Davis, 1986). For

this study, the selection of the number of groups was based on visual examination of the dendogram. Figure 5.6 shows the grouping of each data set samples from the HCA cluster analysis. In Figure 5.6, the resulting dendogram was interpreted to have classified the 112 groundwater samples into four major groups (I to IV) and nine subgroups (1 to 9) using 12 variables; this, however, is a subjective evaluation. Greater or fewer groups could be defined by moving the dashed horizontal line (phenon line) up or down. In addition, the dendogram does not give information about the distribution of the chemical constituents that form each group, a distinct limitation when compared to the graphical techniques.

Group I (G1) Na- Ca- HCO_3 rich water types have five subgroups SG1 (Na-HCO_3), SG2 (Na-Cl-HCO3), SG3 (Na-K-HCO_3), SG4 (Ca-HCO_3), and SG5 (Ca-Na-HCO_3). The subgroups are dominant in aquifers of highland (Hammer basement) and Meander Belts recharge areas in the basin. The former gets its major recharge from precipitation and the latter from Omo River. In subgroup2, which comprises 19 samples, are mainly distributed at eastern Delta flats geomorphic units. They are characterized by a high range of EC values 4,906 µs/cm, a high percentage of Na^+ ion (25.1%), and (25%), and HCO_3^- (34.8%) (Table 5 1). The groundwater type of this subgroup is 36.8% are mixed, 31.5% are sodium chloride, and 10.5% are magnesium bicarbonate and no calcium chloride type water. The average proportion of ions of the Group1 waters is Na (15.9%) > Ca (5.9%) > Mg (3.2%) and HCO_3 (55.8%).

Group I water types are circulating in shallow depth (82m maximum in Basement aquifer and 90m in Quaternary sediment) and dilute having less residence time and short groundwater flow paths within weathered and fractured media of gneisses and sediments. These waters are recharged by highland rainfall and have a low average EC of 1122µS/cm and temperature of 29.9 ^{0}c (table 5-1). The higher variability of EC among samples in a group is related to the occurrence of the waters in weathered gneissic rocks (1233µS/cm, OD59) and Holocene sediment (3,450 µS/cm, OD10).

Group II water samples are Na-Ca and HCO_3 dominating water types occurring on northern and northeastern inter-mountain and stream channels (Figure 5.5). The samples from this group showed 14.7% was sodium bicarbonate and the rest 85.3% are magnesium bicarbonate type. Some water types of Hammer ridge areas are Ca and HCO_3 dominating.

Whereas towards the central and south part it becomes Ca-Na and HCO_3. This group groundwater characterized by low EC with a mean value of 333μS/cm. A higher value (1079 μS/cm) is registered at well OD23, which is located at Delta flat near Omo River. The lower EC value and the recharging type water chemistry of this group reviled that the groundwater of this group is the recharging type with a local flow system. This group groundwater sample have average ion percentage of Na^+ (10.4%), Ca^{2+} (11.1%), SO_4 (4.4%), and HCO_3 (66%).

Group III water samples occurred at the eastern water divide between the Omo Basin and lake Chew-Bahir (figure 5.5). The number of samples on this group is only six and they show significant peculiarity to other groups that are associated with Hammer basement. It has two subgroups (SG7 and SG8). Both subgroups characterized by high EC values with the mean values of 2288 and 5940 μS/cm respectively. The subgroups are found at different lithologic units. Subgroup7 Na-HCO_3 type water occurred at Delta fringe; it comprises six samples and characterized by high TDS (3,239 mg/l maximum and 2658mg/l average) value. The 83% of samples of this cluster found in the Delta fringe zone of geomorphic units.

Table 5-1 Statistical summary of hydrochemical parameters of groundwater of clusters resulted from Q-mode HCA analysis (TDS, cations and anions in mg/l; temperature in ^{0}C, and % is percent of ions relative to corresponding cations and anions)

Group	Subgroup	No. sample	Variables	EC(µs/cm)	TDS	T (0c)	pH	Na^+	Ca^{2+}	Mg^{2+}	K^+	Cl^-	SO_4^{2-}	HCO_3^-	NO_3^-
I	SG 1	9	Min	270	140	27.3	7.51	41.7	21.3	16	5.68	3.5	4.07	260	0.4
			Max	852	411	39.4	8.33	124	48.2	43.9	56	28.4	52.3	482	12.8
			Mean	644	313	34.4	8.05	71.5	30	31.3	30.9	17.5	29.3	362.7	5.6
			% ion					12.3	5.2	5.4	5.3	3	5.1	62.6	0.96
	SG 2	19	Min	434	229	21.6	6.91	18.2	2.9	0	1.8	6.38	4	73.2	0
			Max	940	2830	37.8	9.25	560.3	51.2	32.4	7.68	847.26	115.58	872	97
			Mean	869	1050	32.5	8.14	172	18.9	8.6	5.2	177.3	36.9	237.9	26
			% ion					25.1	2.8	1.3	0.8	25.9	5.4	34.8	3.8
	SG 3	2	Min	1508	843	33.5	8.6	172.4	4.8	1	112	43	61	224	19.2
			Max	1836	1108	35.6	9	358	9.6	2	143	168	65	817.4	20
			Mean	1672	976	34.6	8.8	265.2	7.2	1.5	127.5	105.5	63	520.7	19.6
			% ion					23.9	0.6	0.1	11.4	9.5	5.7	46.9	1.8
	SG 4	21	Min	56.9	28.5	20.2	6.74	20.3	4	3.2	1.4	1	1	256.6	0.1
			Max	1654	992	30.5	8.62	138.5	98	46.58	37.5	86.1	97.5	561	16.3
			Mean	701	362	24	7.57	57.1	65.8	28.6	8.4	16.5	23.07	422.8	4.4
			% ion					9.1	10.5	4.6	1.3	2.6	3.7	67.3	0.7
	SG 5	22	Min	56.9	28.5	20.2	6.74	20.3	4	3.2	1.4	1	1	256.6	0.1
			Max	1654	992	30.5	8.62	138.5	98	46.58	37.5	86.1	97.5	561	16.3
			Mean	624	339	24.9	8.28	48.8	36.3	11.6	16.7	16.7	17.6	253.3	5
			% ion					9.1	10.5	4.6	1.3	2.6	3.7	67.3	0.7
II	SG 6	28	Min	59	30	18.9	5.9	4	4	2.916	1.3	1.25	0	68.5	0
			Max	1079	521	29.7	8.57	60	62.4	16.8	15	18.982	54.6	292.8	16.5
			Mean	333	172	24.1	7.02	29.1	31.1	8.3	5.1	5.9	12.3	184.7	2.4
			% ion					10.4	11.1	3	1.8	2.1	4.4	66	0.9
III	SG 7	6	Min	1012	506	31.8	7.13	37	30	33.5	6.9	1.3	44.55	366	0.9
			Max	7070	3239	39.4	7.94	262.1	178	72.7	28.8	249.9	125	1202	334.4
			Mean	2658	1295	34.8	7.31	157.5	88.8	53.3	11.8	99.1	72.5	632.4	123.4
			% ion					12.7	7.2	4.3	1	8	5.8	51	10
	SG 8	2	Min	3560	1780	24	7.65	35	320	26.73	14.5	75	520	475.8	0.3
			Max	8320	4100	24.3	8.1	120	360	30.132	24.5	155	560	488	9.2
			Mean	5940	2940	24.2	7.87	77.5	340	28.4	19.5	115	540	481.9	4.8
			% ion					4.8	21.1	1.8	1.2	7.1	33.6	29.9	0.3
IV	SG 9	4	Min	6150	3431	32.6	7.27	1224.6	3.63	3.09	6.32	1119.5	54.19	817.4	13
			Max	10240	5734	35.8	8.05	1645.3	30	28.8	15.64	1583.91	131.24	988.2	62
			Mean	7635	4144	34.8	7.74	1417.7	12.9	11.6	8.9	1286.3	94.3	904.1	43
			% ion					37.5	0.3	0.3	0.2	34	2.5	24	1.1

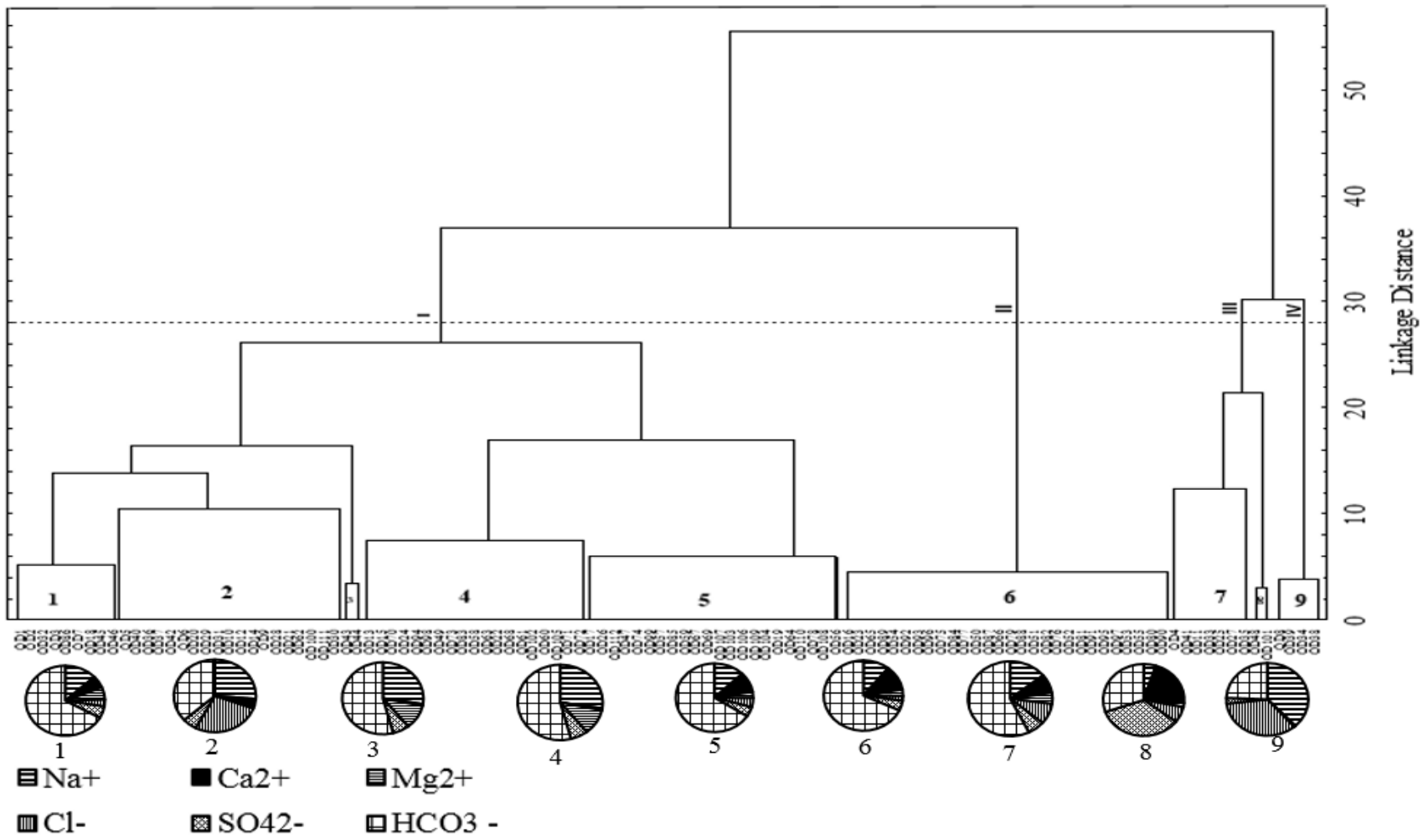

Figure 5.6 Dendogram from Q-mode HCA for 112 groundwater samples. Link of asterisks defines “phenon line” which is defined by analyst to define groups or subgroups.

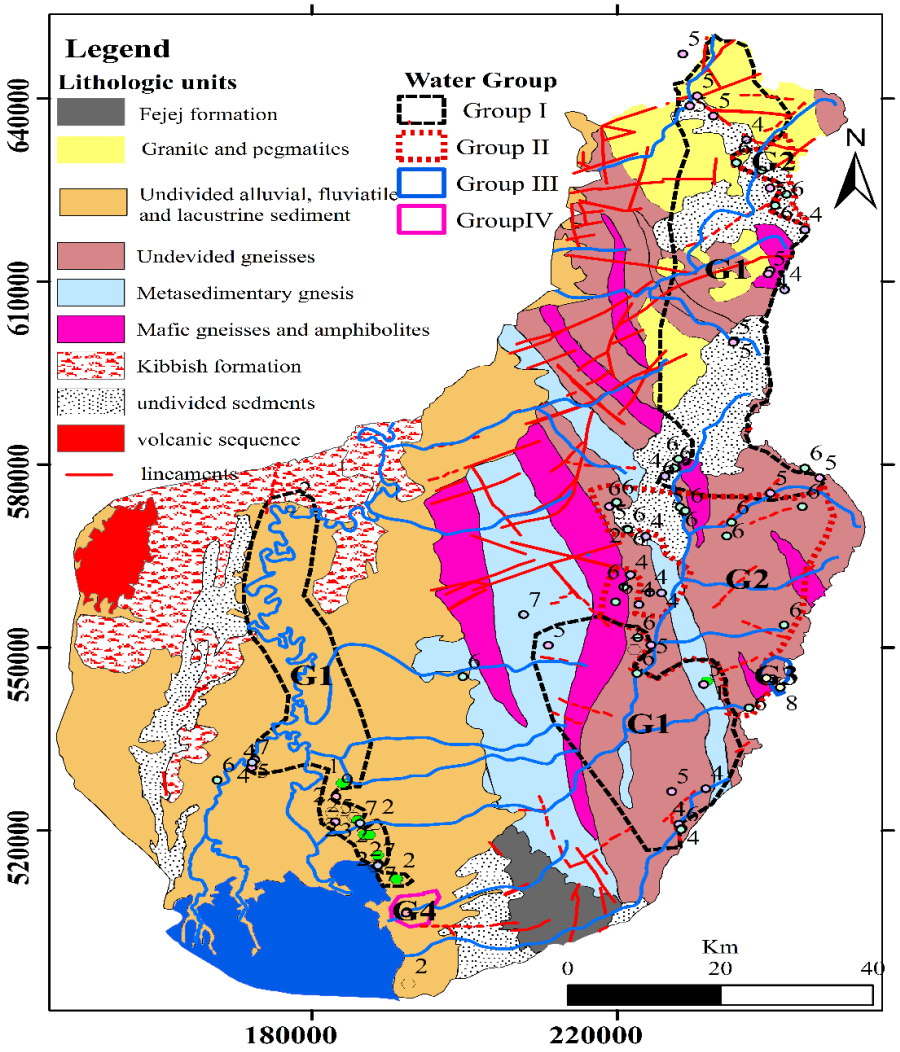

Figure 5.7 Map view of HCA-derived subgroup and group values for the groundwater Samples over a geologic map of the study area. The symbol indicates group, numbers subgroups.

Group III are collected from the undivided alluvial, colluvial, and lacustrine sediment geologic units. The plotting on the Piper diagram (figure 5.5) for the samples from the group1 shows 20.5% are mixed, 9.5% Sodium chloride, 4.1% sodium bicarbonate, and the rest 65.9% are magnesium-bicarbonate type. Subgroup8 $Ca\text{-}SO_4\text{-}HCO_3$ type water found at structurally affected Hammer basement.

The fourth group (G4) water samples are highly evolved Na-Cl type. They are localized at Delta fringe and characterizes the highly saline groundwater of the Delta. The maximum EC value

measured was 10,240 and the mean value is 7,635 μS/cm. High EC values are associated with the dissolution of evaporating lenses accumulated along with the lacustrine beds. The percentage of ionic ratios of this water is Na (35.5%), Cl (34%), and HCO_3 (24%).

Except for a few samples, chemical water types are closely related to the geographical, geomorphological/hydrogeological regime. The relationship of the statistically defined groups and subgroups of samples to the geographic location was tested by plotting the groups and subgroups value for each sample on a geological map of the study area (Figure 5.7). The figure shows that there is a good correspondence between spatial locations and the statistical groups as determined by the HCA.

It can be observed that one cluster of Group1 groundwater samples is found in the contour line greater than 750m. In addition, they are characterized by low TDS and geologically found in basement aquifer that represent the recharge zone of the study area. The second cluster of Group1 groundwater is associated with Omo River and its intermittent effluents. This Group of groundwater shows an interesting pattern, which characterizes the Omo Delta in which the fresh (magnesium bicarbonate-recharging) water and saline (sodium chloride) water in close association. It can be observed that the Group1 groundwater Clusters around the Omo River meander belt and alluvial fans geomorphologic units. Therefore, it is safe to conclude that the river and its intermittent effluents are playing a major role in recharging the groundwater in the Delta. Subgroup1 groundwater samples, which comprising 9 samples, are mainly associated with the eastern beach ridge geomorphologic unit.

5.2.3. Principal Components Analysis

The principal component analysis is probably the oldest and best known of the techniques of multivariate analysis. It was first introduced by Pearson (1901) and developed independently by Hotelling (1933). The main idea of principal component analysis is to decrease the dimensionality of a data set in which there are a large number of correlated variables while retaining as much as possible of the variation exist in the data set (Jolliffe, 2002). The axis of greatest variance becomes the first principal component (PC1), and the axis of second-greatest variance becomes the second (PC2), and so on. A bivariate plot of PC1 vs. PC2 will thus summarize the greatest amount of

variance in the dataset and be a more comprehensive summary of that dataset than a plot of any two of the original variables (Grunsky et al., 2014; Yousef et al., 2015).

The number of principal components to be retained in the analysis is based on Kaiser Criterion. As per this criterion, principal components (Fi) having the latent root or Eigenvalue (denoted by λi) greater than one are considered essential and are retained in the analysis. Factor loading is the standardized values of the original number of variables (Yousef et al., 2015). High factor loadings (value of a close to ±1) indicate a strong relationship (positive or negative) between the variable and the factor. In this study, PCA was carried out in the standardized data sets and sorted by using Eigenvalues greater than 1.0 as these are considered significant influences towards the hydro-geochemical processes (Sahu et al., 1998; Panigrahy et al., 1999; Sundaray et al., 2006).

The PCA was performed on 106 standardized data set of twelve hydrochemical variables. Four principal components (PC1, PC2, PC3, and PC4) accounting for 70.03% are retained having Eigenvalues greater than unity out of 12 where 8 have Eigenvalues less than unity (PC5 to PC12) (Table 5-3).

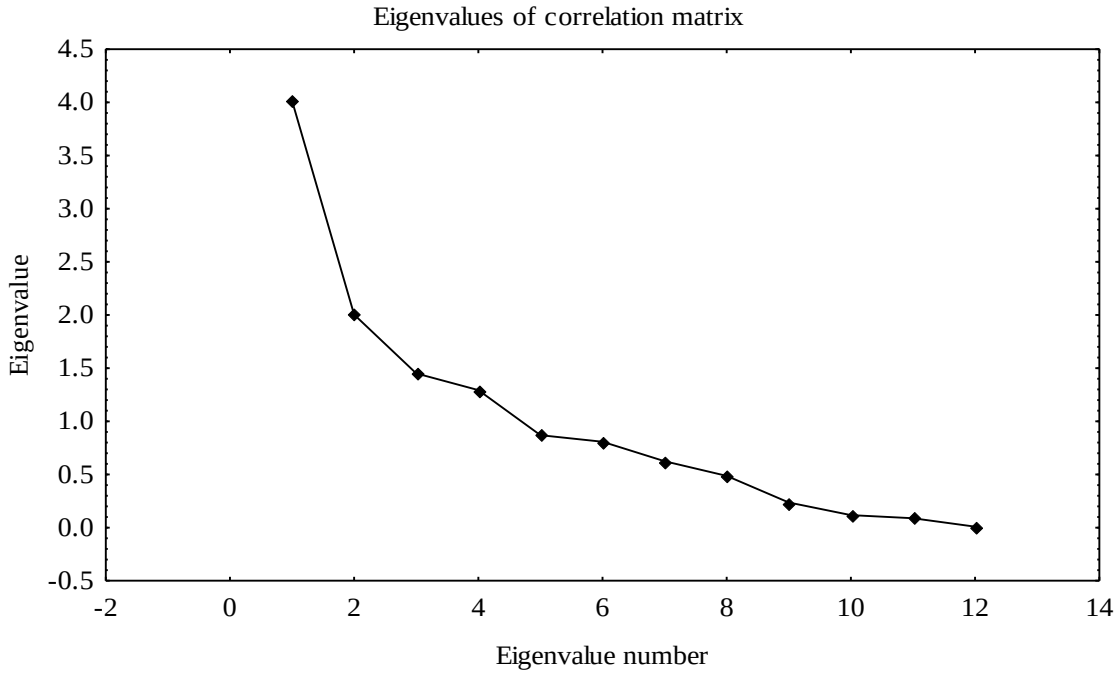

Figure 5.8 Graph of Eigenvalues of 12 principal components.

Table 5-2 Eigenvalue of PCs

	PC1	PC2	PC3	PC4	PC5	PC6	PC7	PC8	PC9	PC10	PC11	PC12
Eigenvalue	4.01	2.0	1.5	1.3	0.9	0.81	0.62	0.5	0.24	0.12	0.09	0.008
% Total	33.8	16.6	12.09	10.8	7.3	6.7	5.2	4.1	2.0	1.0	0.7	0.07
Cumulative %	33.5	50.2	62.3	73.0	80.3	87.0	92.2	96.3	98.2	99.2	99.9	100

The factor loadings obtained after varimax orthogonal rotation from the data set of 12 variables and processes which have been interpreted from the factor loadings are given in Table 5-3. The factor includes both positive and negative loadings. Loadings close to ±1 indicate a strong correlation between a variable and the principal component. Loadings higher than ±0.75 are considered strong correlation, loadings between ±0.5 and ±0.74 are considered moderately correlated and loadings approaching 0 indicate weak correlations (Jolliffe, 2002, Mohopatra et al, 2011). Based on the significant factor loadings (greater than ±0.5), each principal component is assigned a process in which the significant variables are likely to be associated with the component.

PC1

PC1 is strongly loaded with EC, Na^+, Cl^-, F^-, SO_4^{2-} and HCO_3^- that account for 33.38% of the variability in the dataset. This principal component has a strong positive loading for EC, Na^+, Cl^- and HCO_3^- and moderate positive loading for F^-, T, and SO_4^{2-}. The other loadings in this PC are all positive less than 0.5 and have a weak correlation Table 5-3. Substantial positive loading of EC, Na^+, Cl^- and HCO_3^- indicated silicate weathering and cation exchange reactions. The least positive loading of Ca^{2+} and Mg^{2+} compared to Na^+ and K^+ is related to increased ion exchange along the groundwater flow direction. Elevated temperature and rock-water interaction in aquifers facilitate the release of Na^+ and K^+ to groundwater and precipitation of Ca^{2+} in the aquifer matrix. This also tends to increase HCO_3^- towards the Delta.

The difference in the association of Na^+ and K^+ is related to the resistance of K-minerals to hydrolysis/weathering in solution (Hem, 1992) and hence K^+ is lower. An increase in F^- is related to lower Ca^{2+} in the waters. Increased SO_4^{2-} and Cl^- in the solution could also be related gypsum and evaporate dissolution respectively. The hydro-geochemical process assigned to this component is base ion exchange, which responsible for the formation of Group III and Group IV

clusters. The clusters are highly mineralized where the groundwater has undergone maximum evolution.

Table 5-3 PC loadings obtained after varimax orthogonal rotation.

Variable	PC1	PC2	PC3	PC4
EC	**0.93**	0.02	0.19	0.03
T	**0.51**	-0.27	**-0.51**	-0.22
pH	0.17	-0.04	0.21	**-0.73**
Na^{+}	**0.86**	-0.42	0.06	0.14
Ca^{2+}	0.26	**0.92**	0.16	0.05
Mg^{2+}	0.22	**0.50**	**-0.56**	0.08
K^{+}	0.16	0.009	-0.31	**-0.76**
Cl^{-}	**0.83**	-0.40	0.09	0.17
F^{-}	**0.56**	-0.02	0.48	-0.01
SO_4^{2-}	**0.50**	**0.69**	0.20	-0.09
HCO_3^{-}	**0.80**	0.140	-0.14	0.0005
NO_3^{-}	0.33	0.07	**-0.61**	0.26
Eigenvalue	4.01	2.0	1.5	1.3
Proportion	0.34	0.167	0.12	0.10
% proportion	33.38	16.64	12.09	10.8
Cumulative	33.38	50.2	62.3	73.1

PC2

PC2 explains 16.64% of the variability and has a strong positive correlation with Ca^{2+} and moderate positive correlation with Mg^{2+} and SO_4^{2-}. Other parameters show poor correlation. The negative and low correlation of Na^{+} indicates the reduction of ions influenced by the increased concentration of Ca^{+2} and Mg^{2+} in the water. The increment of Ca^{2+} and Mg^{2+} is due to the dissolution of gypsum and dolomite respectively in aquifers of the highland basement. Low loading of F^{-} is due to enriched Ca^{2+} trapping the ion from the solution in PC2. Aquifers of the highlands have low temperature and less chloride derived from the rain. PC2 represents the formation of Group I and Group II clusters. Due to silicate weathering of basement rock minerals, which are less mineralized having low EC at an early stage of hydrochemical evolution.

PC3

PC3 showed a moderate negative correlation with Mg^{2+}, NO_3^- and T. It represents a significant proportion of variability in a data set (12.1%) and explains important correlations with respect to the groundwater contamination. All other variables are poorly correlated that plotted around zero. A negative sign of NO_3^- suggest decreased concentration because of denitrification.

PC4

PC4 explains 10.8% of the variability and has a moderate negative correlation with pH and K^+. Other parameters show poor correlation. The negative and low correlation of K^+ indicates the reduction of ions influenced by ion exchange for Na^+. Low EC is related to the shallow circulation of Group I and II waters. This water characterized by relatively low pH conditions.

The graph of PC1 Vs PC2 on the unit circle (figure 5.9) indicated that Na^+, EC, Cl^- and HCO_3^- are positively correlated with the first component, PC1 (the horizontal axis) where variables are plotted on the unit circle close to 1. This indicated that the variables showed better variance when close to 1 and poor when closer to 0 as K^+ and pH for both PC1 and PC2. Ca^{2+}, Mg^{2+}, and SO_4^{2-} are positively correlated to the PC2 (vertical axis).

The groundwater samples were plotted on the PCA correspondence according to their group to which they belong to investigate the similarity or dissimilarity between clusters. The vertical axis represents the second principal component (PC2) which accounts for 16.64% of the total variance and the horizontal axis represent the first principal component (PC1) which accounts for 33.38% of the total variance of the data set. From left to right along the PC1, the group1 (G1) groundwater samples are clustered at the middle part of the graph to that of group 2, group 3, and 4. The graph in Figure 5.9 revealed that salinity gradient increase from left to right as TDS increases and groundwater samples gradually progress from bicarbonate to brackish types. The loading factor of the chemical elements presented in Table 5-3 shows that component 1, loadings are dominated by Na^+ (0.86) and Cl^- (0.84). The positive and negative loading for component 2 constrains chemical elements in two distinct clusters: Cluster 1 (positive load): Ca^{2+}, Mg^{2+}, K^+, HCO_3^-, and NO_3^- and cluster 2 (negative load): Na^+ and Cl^- . Chemical element loadings for component 1 and 2 are plotted on the correspondence circle in Figure 5.9. The distribution for group1 fits with the distribution of samples for G3, and the distribution for group2 fits with the distribution of samples for G4. G3 (Group3) samples represent exclusively to brackish groundwater collected from

quaternary sediment aquifer. Their distribution in Figure 5.9 suggests that chemical elements in cluster1 (Ca^{2+}, Mg^{2+}, K^{+}, HCO_3^{-}, and NO_3^{-}) characterizes samples in G3 (Group3) and chemical elements in cluster 2 (Na^{+} and Cl^{-}) specially characterizes samples in cluster 4. This conclusion also suggests that an increase of salinity enhances the fingerprint of the rock type aquifer on the groundwater chemistry.

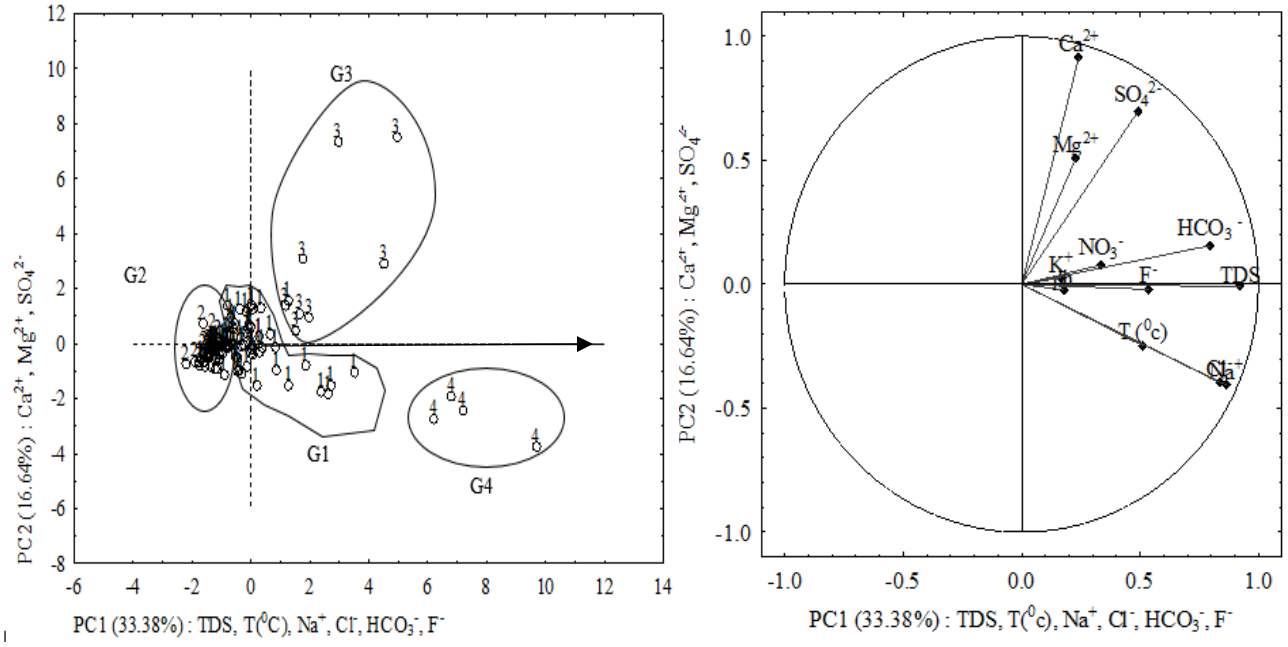

Figure 5.9 Graphical presentation of the first two components derived from principal component analysis (PCA). Component 1 (TDS, T, Na^{+}, Cl^{-}, HCO_3^{-}, F^{-}) explained 33.38% of the total variance of the data set while Component 2 and the vertical axis corresponds to the second principal component (Ca^{2+}, Mg^{2+} and SO_4^{2-}) explained 16.64%. A, PCA diagram of samples classified by cluster membership. B, PCA presenting the chemical element loadings.

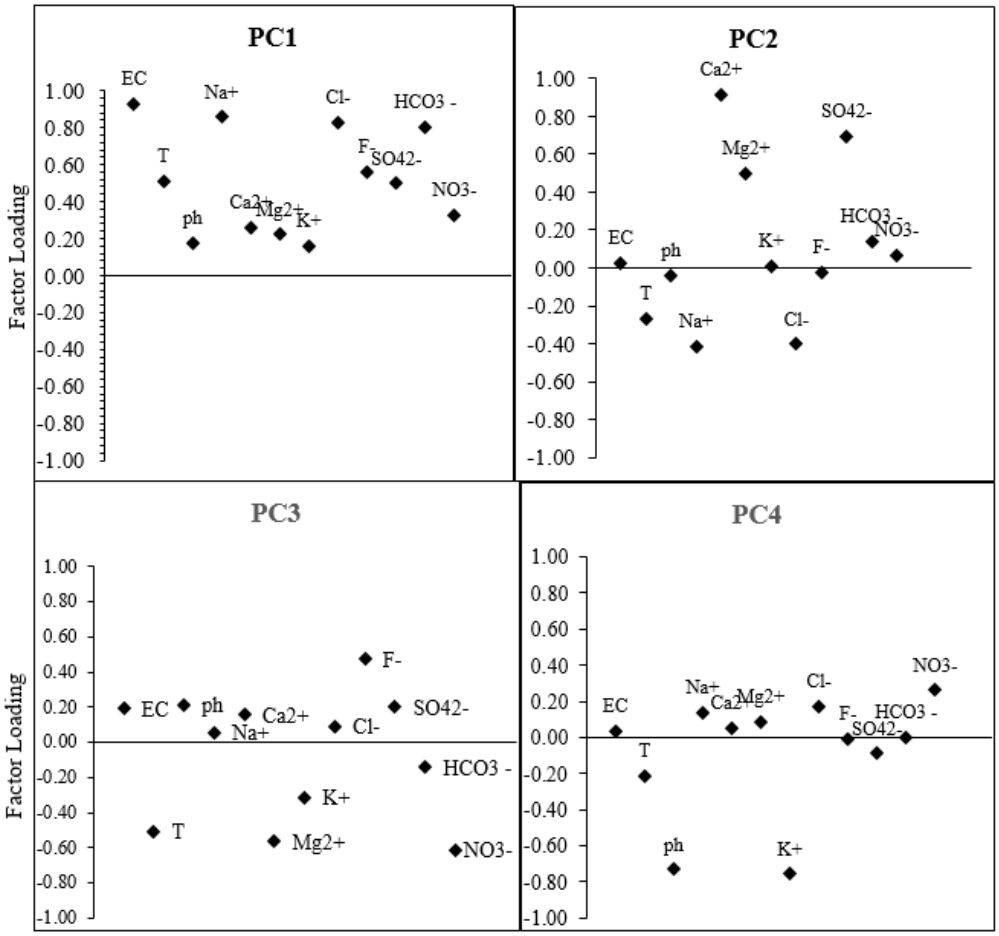

Figure 5.10 PCA representing the chemical elements with high loading factors.

5.2.4. Correlation Analysis

Reactions between groundwater and aquifer minerals have a significant role in water quality. The *p*×*p* correlation matrix, revealing the existence of bivariate linear correlations between variables, allows a better understanding of the dominant water-rock interactions or source of the ions (APPELO and D. POSTMA, 2005; Guseva et al., 2017; Jamila et al., 2017; Modibo et al., 2019; Umar et al., 2019).

Table 5-2 non-parametric test (Wald-Wolfowitz) method to characterize samples.

Variable	Wald-Wolfowitz Runs Test Marked tests are significant at p <.05000				
	Valid N-Q	Valid N-H	Mean(Quaternary sediments)	Mean(Hammer basement)	p-value
EC(µs/cm)	34	76	2407.03	733.16	0.002459
TDS	34	76	1253.25	382.90	0.000086
T (0c)	34	75	33.94	24.43	0.000000
ph	34	75	7.90	7.60	**0.772270**
Na^+	34	76	311.04	40.41	0.000001
Ca^{2+}	34	76	30.67	50.97	**0.092843**
Mg^{2+}	34	76	18.35	17.49	**0.314069**
K^+	34	72	20.23	6.38	0.004428
Cl^-	34	76	270.25	13.18	0.000000
F^-	30	72	1.11	0.8	**0.837708**
SO_4^{2-}	34	76	41.94	35.15	**0.913815**
HCO_3^-	34	76	424.65	279.13	**0.218195**
NO_3^-	34	70	39.22	4.88	0.001378

Prior to this, a nonparametric test (Wald-Wolfowitz) was used to test whether there is a significant difference in groundwater composition between the Quaternary sediment and Hammer basement aquifers sources, using several samples ANOVA (Table 5-2). The Wald-Wolfowitz runs test assesses the hypothesis that two independent samples were drawn from two populations that differ in some respect, i.e., not just with respect to the mean, but also with respect to the general shape of the distribution. The null hypothesis is that the two samples were drawn from the same population (Rice, 1995). Results obtained (table 5-2) show that there was no significant difference in pH, Ca^{2+}, Mg^{2+}, F^-, $SO_4^{2-}$and HCO_3^- concentrations between Quaternary sediments and Hammer basement aquifer groundwater. Whereas, the other parameters show a significant difference as their p-value <0.05. Therefore, it is important to characterize the two-aquifer systems individually in order to elucidate the source of mineralization of groundwater in the basin.

Table 5-3 Correlation matrix of physicochemical parameters of the Quaternary sediment groundwater.

Parameters	TDS	EC	T (0c)	pH	Na^+	Ca^{2+}	Mg^{2+}	K^+	Cl^-	F^-	$SO4^{2-}$	$HCO3^-$	NO_3^-
TDS	1.00												
EC	**0.99**	1.00											
T (0c)	0.13	0.14	1.00										
pH	-0.02	-0.01	0.44	1.00									
Na^+	**0.91**	**0.88**	0.13	-0.01	1.00								
Ca^{2+}	0.00	0.06	-0.06	-0.38	-0.21	1.00							
Mg^{2+}	-0.04	-0.01	0.26	-0.28	-0.13	**0.52**	1.00						
K^+	-0.09	-0.07	-0.02	-0.16	-0.13	0.29	0.19	1.00					
Cl^-	**0.89**	**0.86**	0.12	-0.02	**0.97**	-0.22	-0.11	-0.14	1.00				
F^-	**0.55**	**0.55**	0.15	0.41	0.46	-0.17	-0.28	-0.18	0.41	1.00			
SO_4^{2-}	**0.51**	**0.54**	0.32	-0.15	**0.51**	0.40	0.30	0.12	0.45	0.09	1.00		
HCO_3^-	**0.82**	**0.85**	0.13	-0.10	**0.70**	0.33	0.23	0.15	**0.60**	0.47	**0.60**	1.00	
NO_3^-	0.03	0.02	0.08	-0.35	0.03	0.40	0.35	-0.11	0.01	-0.11	0.41	0.08	1.00

Values in bold are significant at ≥ 0.50

Table 5-4 Correlation matrix of physicochemical parameters of Hammer basement groundwater

Parameters	EC	TDS	T (0c)	pH	Na^+	Ca^{2+}	Mg^{2+}	K^+	Cl^-	F^-	$SO4^{2-}$	$HCO3^-$	$NO3^-$
EC	1.00												
TDS	**0.99**	1.00											
T (0c)	0.04	0.02	1.00										
pH	0.29	0.31	-0.18	1.00									
Na^+	0.26	0.27	0.43	0.01	1.00								
Ca^{2+}	**0.78**	**0.74**	-0.07	0.19	0.22	1.00							
Mg^{2+}	0.28	0.28	0.29	0.14	0.63	0.30	1.00						
K^+	0.22	0.20	0.17	0.12	0.13	0.26	0.22	1.00					
Cl^-	**0.74**	**0.71**	0.27	0.11	**0.54**	**0.62**	0.41	0.22	1.00				
F^-	0.47	0.44	0.14	0.26	0.04	0.39	0.13	0.10	0.24	1.00			
SO_4^{2-}	**0.79**	**0.75**	0.01	0.16	0.28	**0.89**	0.22	0.32	**0.67**	0.36	1.00		
HCO_3^-	0.37	0.36	0.18	0.18	0.61	**0.52**	**0.78**	0.19	0.34	0.27	0.26	1.00	
NO_3^-	0.19	0.20	0.40	-0.01	0.59	0.01	0.42	-0.03	**0.64**	-0.06	0.02	0.25	1.00

Values in bold are significant at ≥ 0.50

The correlations established between the TDS and concentrations of major elements for Quaternary sediment groundwater aquifers (Table 5-3) show that the TDS is well correlated with the concentrations of chloride (r^2 = 0.89), sodium (r^2 =0.91), Fluoride (r^2 =0.55), Sulphates (r^2 =0.51), and Bicarbonates (r^2 =0.82). The high correlation of TDS with chloride, sodium, fluoride, sulfate, and bicarbonates indicated that these elements are mostly contributed by mineralization.

These ions have been dissolved into groundwater continuously and resulted in an increase of total dissolved solids. The contribution of calcium and potassium is negligible (r^2 = 0.0 and r^2 =–0.09,

resp.). The low correlation between TDS and pH suggests that the dissolution of the salts is not related to acidic conditions of groundwater, but it is related to their degrees of solubility. Bicarbonates are not correlated to calcium r(HCO_3-Ca) = 0.33 indicating another source other than the calcite dissolution. However, high correlation coefficients between sodium and chlorides r (Na-Cl) = 0.97 suggest halite dissolution. Considerable correlation between Sodium and sulphates r(Na-SO_4)= 0.50 and sodium and bicarbonate r(Na-HCO_3) = 0.7 suggests that dissolution of miralbite ($NaSO_4.10H_2O$) and sodium bicarbonate salts which are common in closed basin lakes (Hem, 1985).

Likewise, the correlations established between the TDS and concentrations of major elements for Hammer basement groundwater aquifers (table 5-4) show that the TDS is well correlated with the concentrations of chloride (r^2 = 0.71), calcium (r^2 =0.78), and sulphates (r^2 =0.75). The high correlation of TDS with chloride, calcium, and sulphate indicated that these elements are mostly contributed by mineralization. The strong correlation between calcium and sulfate (r^2=0.89) and calcium and bicarbonate (r^2=0.52) suggest that gypsum and calcite dissolution are the main source respectively. A positive correlation between sodium and chloride (r=0.54) suggests that some parts of sodium are derived from halite. The poor relation in calcium and TDS in Quaternary sediment aquifer but strong relation in Hammer basement indicates that Hammer basement groundwater representing recharge type water. Whereas, Quaternary sediments represents an evolved water type.

5.3. Stable Isotope Composition of Waters in the Study Area

Isotope hydrology has provided the best new insight in understanding hydrological processes such are recharge rate and recharge mechanism, surface water-groundwater interaction, the time scale of processes, origin of pollution, and pathway of water movement (Gat & Carmi, 1970; Vitvar & Aggarwal, 1998; Levin et al., 2009; Kebede, 2013; Cary et al., 2015; Jamila et al., 2017; Prajapati et al., 2018). The tool is even more powerful when used in the understanding of the hydrology of arid and semi-arid regions. Given that, half of Ethiopia is an arid or semi-arid region; isotope hydrology could provide the much-needed knowledge for groundwater resources management (Dansgard, 1964; Levin et al., 2009; Deressa, 2012; Kebede, 2013; Worku et al., 2014; Woldemariam & Ayenew, 2016). As discussed in section 3.3, in this study the result of stable isotopes of waters from different sources is presented.

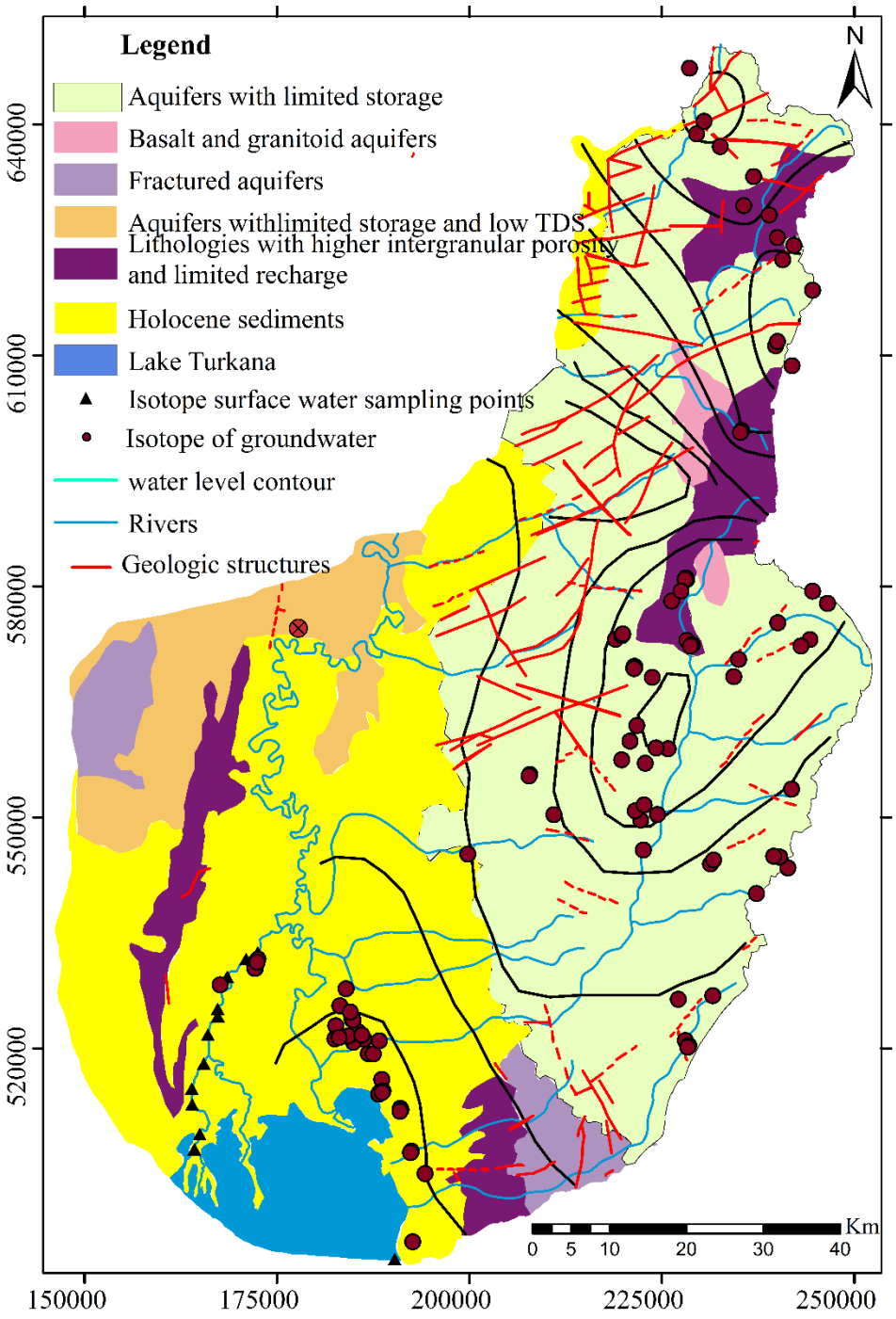

Figure 5.11 Spatial distributions of isotope data points for groundwater.

5.3.1. Stable Isotope Composition of Meteoric Waters in the Study Area

Ten rainfall isotope samples collected during the field sampling campaign lasting June to October 2018, Which are considered as the rainy season in the study area as discussed in chapter 2. The samples are taken from the possible data points that represent the highlands of Jinka (recharge area), Turmi-Kangaton (intermediate), and Omorate (the Delta). The mean isotopic composition of precipitation is $\delta^{18}O$ = 0.3‰ and $\delta^{2}H$ = 7.55‰, and the maximum enriched δ value relative to VSMOW ($\delta^{2}H$= 26.8‰ and $\delta^{18}O$ = 2.85‰) was measured at Jinka in June. And depleted value relative to VSMOW was measured at Kangaton with $\delta^{2}H$= -14.9‰ and $\delta^{18}O$ = -3.28‰.

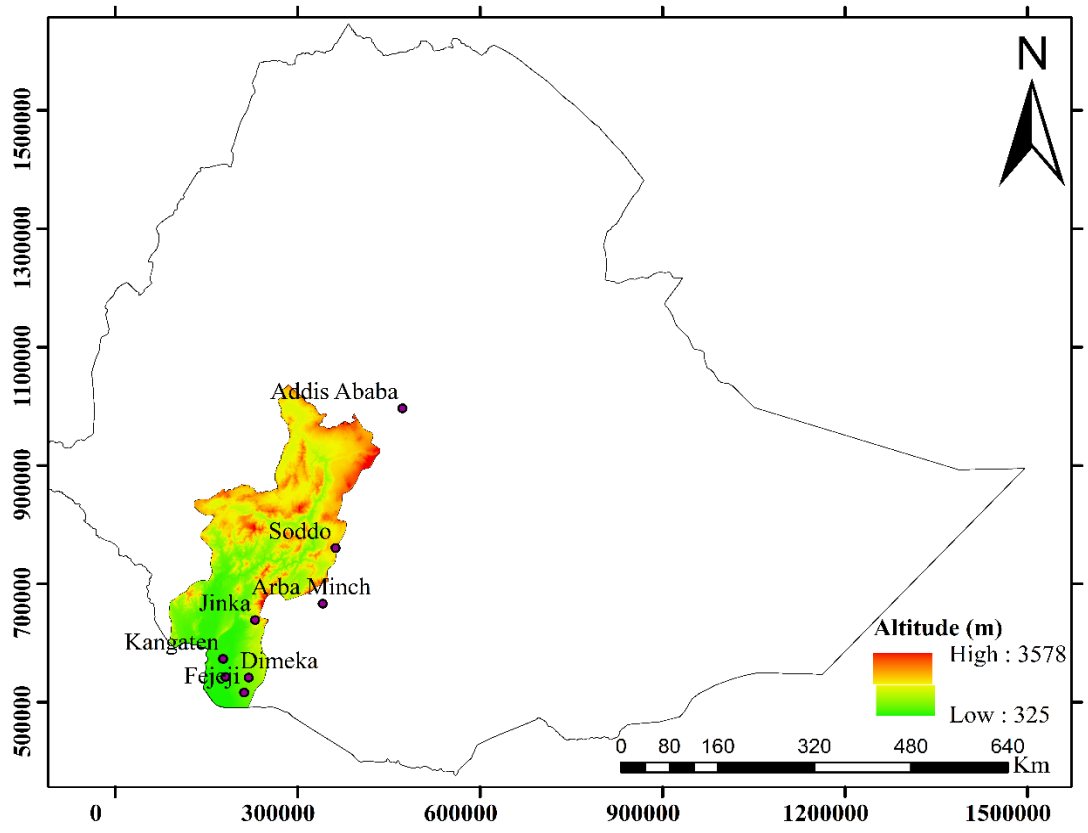

Figure 5.12 Location of IAEA stations used for study area (Addis Ababa, Soddo, Arbaminch) and rainfall sampling sites (Jinka, Kangaten, Turmi/Dimeka, Fejeji, Omorate).

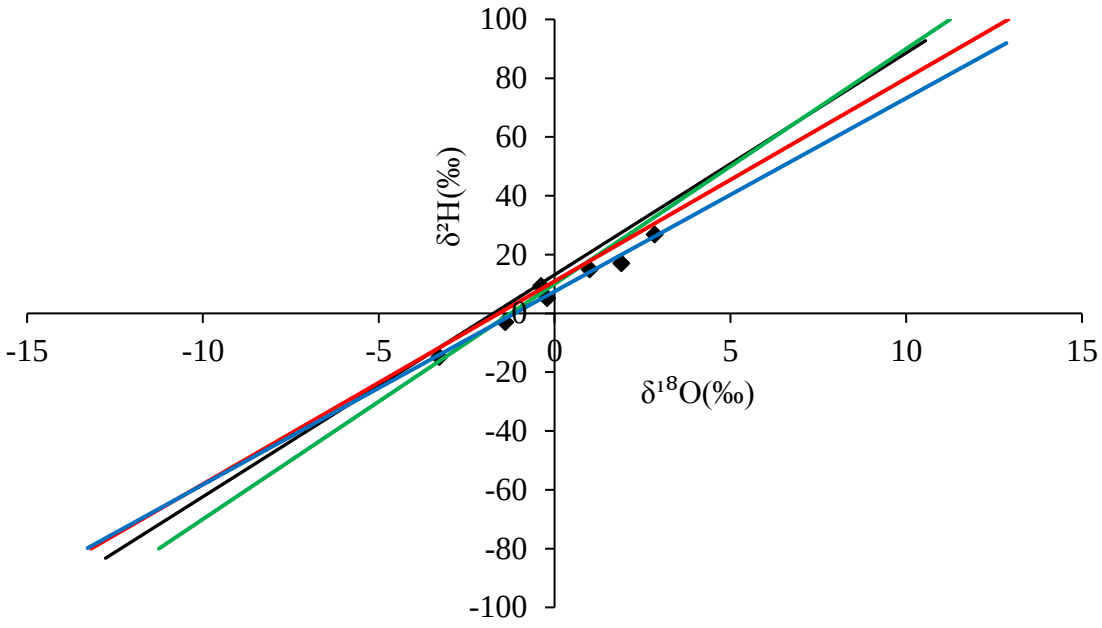

Figure 5.13 Linear relation of $\delta^{18}O‰$ vs $\delta^{2}H‰$ of precipitation at three GNIP stations with regression line: green-GMWL, black-Addis Ababa LMWL, red-Soddo LMWL and blue-LMWL with equation ($\delta^{2}H= 6.57\delta^{18}O+ 7.46$) constructed using an isotope of precipitation (black squares) in the study area for comparison.

The stable isotopes of local rainwaters showed a wide range of variations from -2.38‰ to 2.85‰ for $\delta^{18}O$ and from -14.9‰ to 26.8‰ for $\delta^{2}H$ (Figure 5.13). Most samples are plotted below GMWL indicating that precipitation experiences evaporative loss. It observed that the remarkable enrichment of isotope value despite high altitude at Jinka characterizes the high isotopic value.

The average values of ($\delta^{18}O‰$, $\delta^{2}H‰$) of fifty-five years (1961-2016) local precipitation stations of Addis Ababa (-0.38‰, 9.48‰) and one-year (1999-2000) Wolaita-Sodo (-1.44‰, -0.96‰) showed deviation from GMWL. The GMWL and three LMWLs (Figure 5.13) intersect at the ($\delta^{18}O‰$, $\delta^{2}H‰$) axes at different points. The slope and D-excess of the yearly precipitation for the stations of Addis Ababa (7.54 and 13.12‰) and Wolaita-Soddo (6.9 and 10.93‰). Similarly, the local meteoric water line constructed from one season precipitation in the study area had (6.57 and 7.46‰) value. The variation in average isotopic composition, slope, and D-excess of each LMWLs with the GMWL is related to the change in isotope value of the source and/or season. Similarly,

the rate of evaporation of source, the isotopic evolution of air mass and relative humidity during precipitation also affects isotopic composition of the waters (Kendall et al., 2001; Kebede et al., 2007; Levin et al., 2009; Kebede and Travi., 2011). The difference in D-excess may reflect a higher kinetic (non-equilibrium) effect during evaporation of the moisture along the trajectory of the two main moisture sources of the region: the monsoon from the Atlantic and Indian oceans to southern Ethiopia. The regression lines for the stations of Soddo and the study area are plotted to the right of the GMWL because of substantial evaporative enrichment.

5.3.2. Stable Isotope Composition of Surface Waters

The water in most rivers has two main components: (1) recent precipitation that has reached the river either by surface runoff, channel precipitation or by rapid flow through the shallow subsurface flow paths; and (2) groundwater. The relative influences of these sources vary in each watershed or basin and depend on the physical setting of the drainage basin (e.g. soil, topography, depth to bedrock, type, fractures, vegetation, etc.), climatic parameters (e.g. temperature, seasonal variations in precipitation, precipitation amount, potential evapotranspiration, etc.), and antropogenic activities (Kendal et al., 2001).

The $\delta^{18}O$ and $\delta^{2}H$ of rivers will reflect how the relative amounts of precipitation and groundwater vary with time, and how the isotopic compositions of the sources themselves change over time. Seasonal variations will be larger in streams where recent precipitation is the main source of flow, and smaller in streams where groundwater is the dominant source (Sklash et al., 1976; Kendall and McDonnell, 1998).

The isotope samples were collected from Omo River water during a field survey at a suitable location (accessible) at approximately 5km intervals (Figure 5.22). This helps to describe the spatial variability in $\delta^{18}O$ and $\delta^{2}H$ of the river, to compare the river isotopic data with available precipitation isotope data, and to investigate the interaction between surface water and groundwater in order to understand the dynamics of groundwater-surface water in the Delta. The isotopic values ranged from 8.2 to 10‰ for $\delta^{2}H$ and -0.32 to 1.87‰ for $\delta^{18}O$. The Omo River water tends to be isotopically enriched relative to rainfall because of surface water evaporation (Leaney & Herczeg, 2005). The contribution of local precipitation should be a major source of water for the river. while evaporation would increase the oxygen and hydrogen isotope ratios of

the residual fraction and the residual surface water to produce systematic linear deviations from the local meteoric water line (LMWL), which can be used to trace the source of water and as footprint of hydrogeological processes (Clark and Fritz, 1997; Wassenaar et al., 2011). The δ^2H-δ^{18}O plots of the data from the Omo River are shown in Figure 5.14 shows that the data are plotted at Sodo/Addis Ababa Local Meteoric Water Line (LMWL) except for samples at the lowest part (circled) of the river, which is subject to evaporation.

Along the Omo River, EC showed a general tendency of increasing from a minimum of 166 to a maximum of 178 μs/cm (Figure 5.15). The pick values are measured between 0 to 5 km, 5 to 10km, and 25 to 30 km. Similarly, δ^{18}O‰ pick values have been measured at distance between 0 to 5km, 5 to 10km, 10 to 15km, and 25 to 27kms. The mid-River, characterized by (around 15kms), low EC value compared to others, and increase of isotopes of δ^{18}O‰. This might be attributed to the mixing with low EC and enriched by heavy isotopes in groundwater at the beginning of the mid-river.

Table 5-5 The Stable Isotopic composition of the Omo River along the River stretch. SOB (south of Omorate Bridge and sampling point location can be seen at Figure 5.11).

Sample ID	Sample source	X	Y	Z	Distance (km)	EC (μs/cm)	T(ºC)	δ2H in ‰	δ18O in ‰	D-excess
104	Omo R. at Omo bridge	172493	532479	372	0	166	30	9.7	0.2	8.1
105	Omo R(0.9kms)SOB	170983	531615	374	0.9	175	29.9	9.9	0.21	8.22
106	Omo R(3.8kms)SOB	168541	529321	368	3.8	170	30.5	9.8	0.24	7.88
107	Omo R(7kms)SOB	167297	525156	363	7	173	30.4	10	0.34	7.28
108	Omo R(12.7kms)SOB	167317	524214	365	12.7	169	30.3	9.6	0.33	6.96
109	Omo R(13.8kms)SOB	831735	521788	367	13.8	173	30.2	10	-0.23	11.84
110	Omo R(16.8kms)SOB	831230	518024	367	16.8	170	30.4	9.9	-0.32	12.46
112	Omo R(24.4)SOB	829763	512708	367	24.4	171	30.2	8.2	1.87	-6.76
113	Omo R(26.7kms)SOB	830781	508870	368	26.7	178	30.8	8.5	1.43	-2.94
115	Omo R(34.7kms)SOB	830102	506897	369	34.7	176	30.5	8.9	1.23	-0.94

Whereas, the local precipitation is plotted to the left of the Global meteoric water line and Omo River samples. These show that the waters in Omo River are mainly coming from the precipitation from the highlands of the basin.

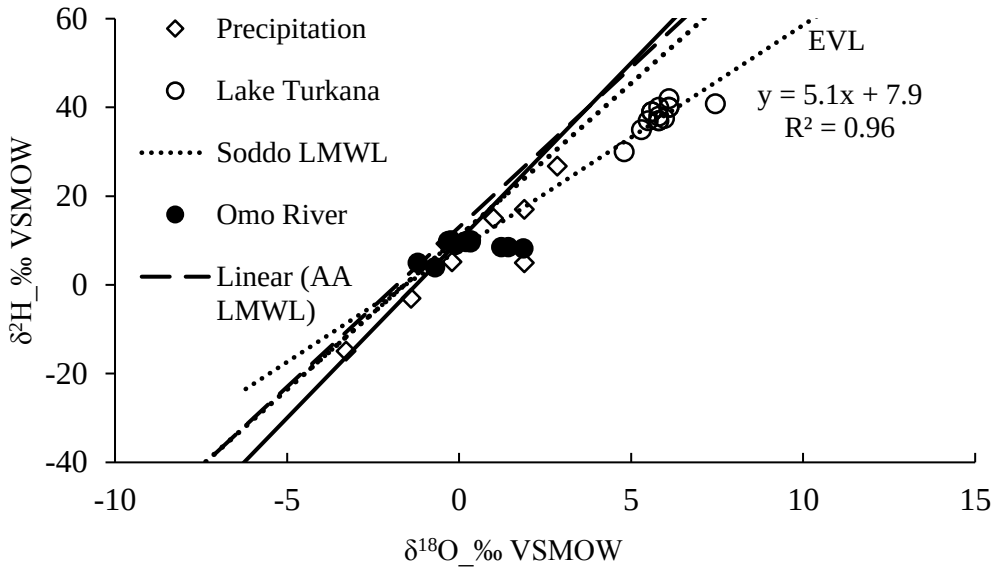

Figure 5.14 The δ^2H‰ vs δ^{18}O‰ plot of surface waters relative to the GMWL, LMWL Addis Ababa and LMW of Soddo.

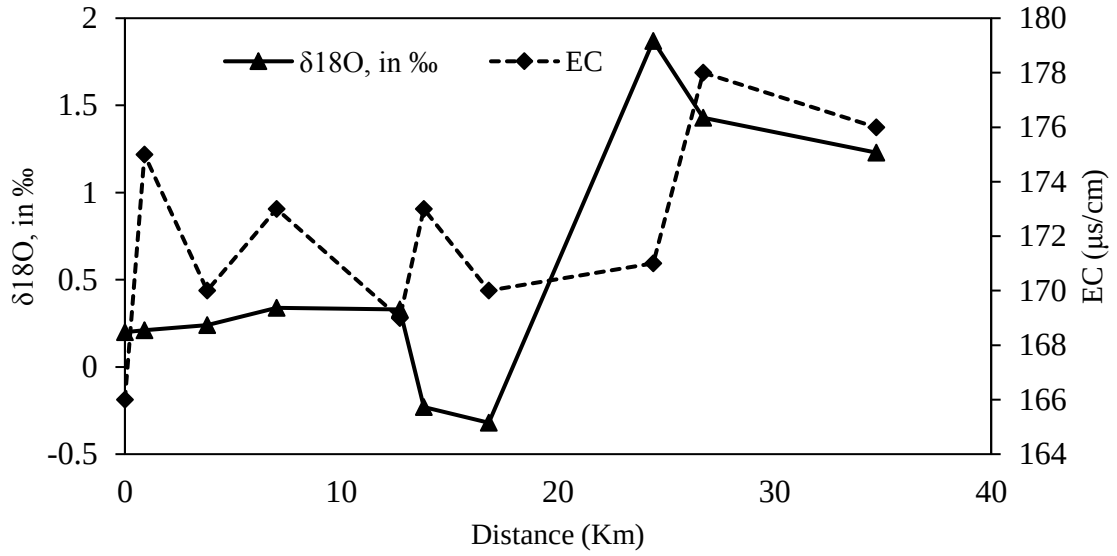

Figure 5.15 The relationship between the EC and the stable isotopes (δ^{18}O in ‰) along the Omo River.

Lake Turkana is Africa's fourth-largest lake and the world's largest desert lake. It is a closed basin within the East African Rift Valley. The lake water is slightly saline, being unsuitable for domestic

use, agriculture, and livestock (Avery et al., 2018). About 90% of the lake surface water inflow derives from the Omo River in Ethiopia (Avery, 2010). The lake waters are well mixed, due to the strong prevailing SE winds, and consequently, the waters are well oxygenated in the upper layers, and there is limited temperature stratification (Avery et al., 2018).

The $\delta^{18}O$ and $\delta^{2}H$ enrichment in lakes are the results of isotope fractionation that takes place during evaporation (Craig and Gordon 1965). However, the intensity of enrichment, the absolute isotopic content and the slope of the Local Evaporation Line (LEL) are the result of the interplay of processes involving the isotopic composition of inflow waters, ambient vapors, and humidity. The initial isotopic composition of inflow waters which represent the composition of meteoric waters in the region can be retrieved from the intersection of the LEL with LMWL (Kebede, 2013).

Water samples from Lake Turkana have been collected and analyzed for $\delta^{18}O$ and $\delta^{2}H$ in this study and some data from previous studies (Cerling, 1999, and IAEA wiser/gnip) used for analysis. It can be observed that the lake water samples are more evaporated (range +4.8 to +7.45‰ for $\delta^{18}O$ and +37 to 42.0‰ for $\delta^{2}H$); this is essential because Turkana Lake is a closed basin with no drainage. The surface water samples plotted in two distinct locations in Figure 5.14 below the meteoric water lines indicated that the lake has undergone intense evaporation. The evaporation line (EVL) can be fitted as $\delta D = 5.1\delta^{18}O‰ + 7.9$ with ($R^2 = 0.96$) with river and lake water samples sourced from the Turkana Basin. The crossing point of EVL and GMWL, which represents the isotopic composition of the water source for surface water, is significantly similar to the rainfall isotopic values of Soddo and Addis Ababa (Figure 5.14), implying that the river is recharged by recent precipitation.

5.3.3. Isotope Composition of Groundwater

In order to understand the source of groundwater salinity and variability of hydrogeological systems in the Omo Delta and its surroundings, the isotopic composition of ($\delta^{18}O$, $\delta^{2}H$, and d-excess) of groundwater samples (74 wells and 2 cold spring) is used. Hydrogeologically, these samples are distributed in both the Quaternary sediment (33 samples) and Hammer basement aquifers (41 samples). The groundwater samples are sampled from 54 shallow wells, seven boreholes, 13 hand-dug wells, and two springs.

The results from the water isotopes are used to gain an insight into the groundwater recharge source and mechanism (Rozanski et al., 1993; Jamila et al., 2017); groundwater flow and evolution direction (Edmunds et al., 1992; Fausto et al., 2006), lake–groundwater relations (Kebede et al, 2002) and elucidating origin of groundwater salinity (Dongmei et al., 2011; Shojaeya et al., 2011; Mongelli et al., 2013; Petelet et al., 2013; Vengosh, 2014; Ait et al., 2015; Alcala et al., 2017; Sahu et al., 2018).

The stable isotopic compositions (δ^2H and oxygen $\delta^{18}O$) of groundwater samples in the study area were shown in Figure 5.16 and Annex 1. The isotopic values range from -1.5 to 3.3 ‰ for δ^2H and -2.08 to -1.23‰ for $\delta^{18}O$, -17.3 to 5.9 ‰ for δ^2H and -3.96 to -0.74‰ for $\delta^{18}O$, 0.5 to 13.2 ‰ for δ^2H and -0.79 to 2.57‰ for $\delta^{18}O$ 0.1 to 0.6‰ for δ^2H and to -0.01 to -0.77‰ for $\delta^{18}O$ for Boreholes, Shallow wells, Hand-dug wells, and springs respectively. This shows that the isotopic composition of the boreholes and spring samples collected in the study area lies within a narrow range, confirming that these groundwater samples had the same recharge source. The boreholes are found in basement aquifer that only groundwater flow through fracture openings and regoliths that dominantly reflect the recharge sources. Shallow groundwater in both aquifer systems show similar isotopic compositions except those hand-dug wells recharged directly from Omo River suggesting a hydraulic connection between shallow groundwater and deep groundwater as observed from the chemical data. Based on their isotopic composition, two types of groundwater samples were identified.

The first group is relatively depleted in isotopic values and includes samples with $\delta^{18}O$ and δ^2H values plotted at the meteoric water level line. This may be explained by the fact that non-evaporated water is rapidly infiltrated to the saturated zone. The second group, whose $\delta^{18}O$ and δ^2H values plotted below meteoric water level line are relatively enriched isotopic values demonstrate that this groundwater is affected by evaporated open water or soil water (Figure 5.17 circled). The hand-dug wells at Delta and Hammer basement exhibit such kinds of characteristics.

Figure 5.17 shows the $\delta^{18}O$ and δ^2H contents of the waters from the two-aquifer units. The graphs show that the groundwater in Hammer basements is distinct from waters of the Quaternary sediments in that:

- Most waters of Quaternary sediment plot in systematic clusters near the global meteoric water line (GMWL) compared to the waters from the Hammer basement. Indicating that local precipitation and Omo River are the main recharge source.
- The groundwater from the Hammer basement is plotted at/near-global meteoric water line indicating that precipitation from rainfall is the main recharge source of the groundwater.

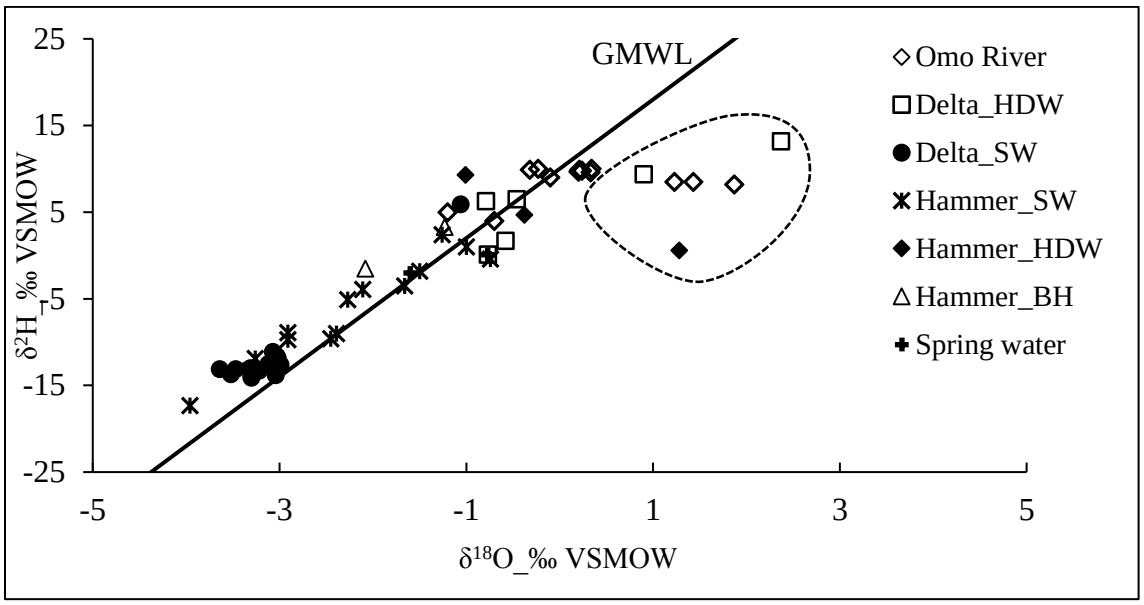

Figure 5.16 The isotopic relationship of groundwater in the study area (BH-bore hole, SW-shallow well, HDW-Hand dug well, SP-Spring water, and GMWL-Global meteoric water line).

The isotopic data for the groundwater collected linearly fit using the regression equation δ^2H ‰ = 4.6 $\delta^{18}O$‰ + 4.6 (R^2 = 0.83) (see Figure 5.18). This regression line can be interpreted as the groundwater evaporation line (GEL). The GEL has a $\delta^2H/\delta^{18}O$ slope <8, which reflects evaporation during or after rainfall and/or mixing with an external water source (e.g., Waddies and marshes) with high $\delta^{18}O$ and δ^2H values. Furthermore, the GEL of the groundwater intersected the GMWL at values of $\delta^{18}O$ = −1.59‰ versus V-SMOW and δ^2H= −2.72‰ versus V-SMOW.

These values are estimated as the baseline for δ^2H and $\delta^{18}O$ in recharging rainfall. If samples are plotted above the lines, a significant groundwater evaporation process can be confirmed (Jamila et al., 2017). The increase in groundwater salinity due to evaporation can thus result in a simultaneous increase in heavy isotopes (GAT, 1996; Kebede et al., 2007; Xiaoyi et al., 2017).

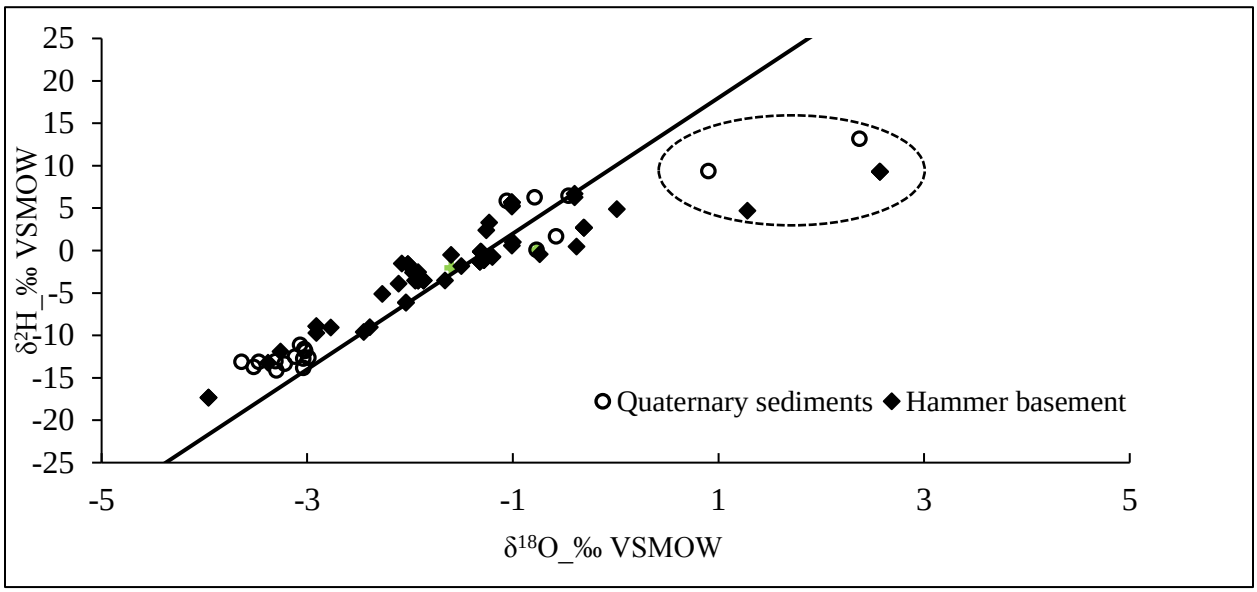

Figure 5.17 Isotopic relationship of quaternary sediment and hammer basement aquifer groundwater

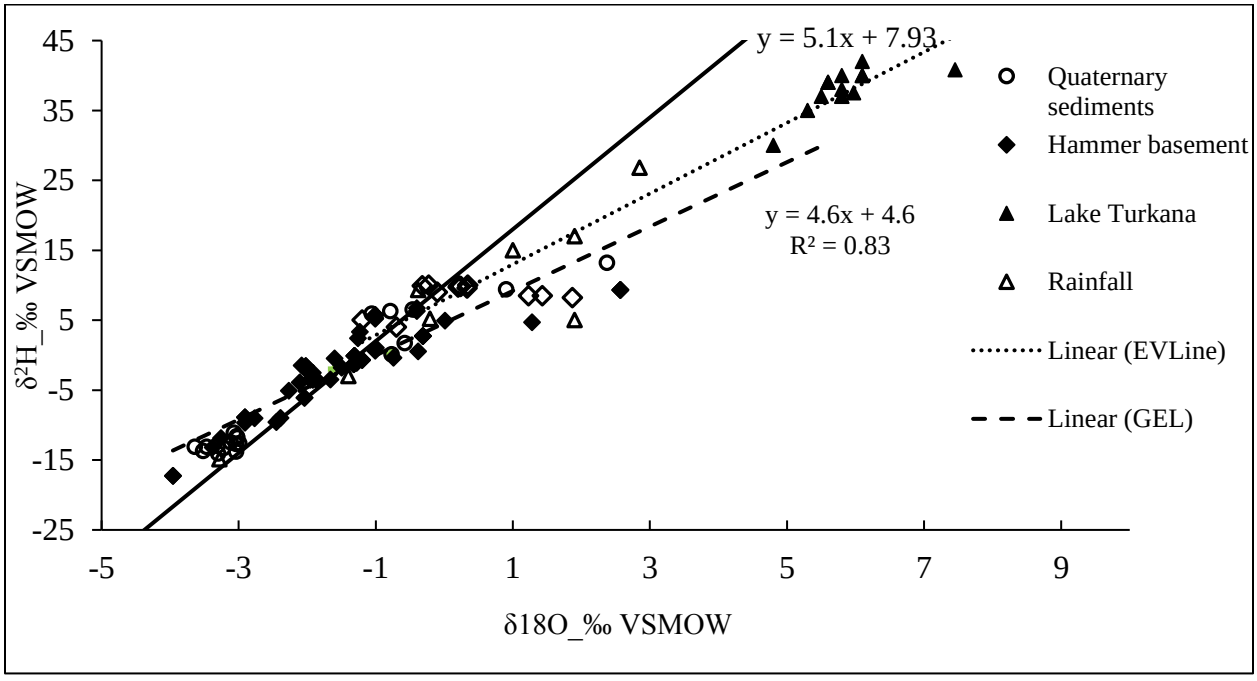

Figure 5.18 The groundwater evaporation line (GEL) with respect to other samples.

Additionally, the isotopic data from the Delta (quaternary sediment aquifer) were linearly fit using the regression equation δ^2H (‰) = 5.4∗ $\delta^{18}O$ (‰) + 5.3 (with a correlation coefficient R^2 = 0.93). The GEL has a smaller slope than the GMWL because evaporation tends to enrich heavy isotopes in water. It can be observed from Figure 5.19 that 47.5% of the groundwater samples were plotted above the baselines and this demonstrates that evaporation has a significant contribution to groundwater salinity in the study area. The GEL of the Delta groundwater intersects the GMWL at values of $\delta^{18}O$= −1.8‰ versus V-SMOW and δ^2H= −4.46‰ versus V- SMOW, which are chosen as baselines (Figure 5.21).

The deuterium excess, defined as d-excess = $\delta^2H - 8*\delta^{18}O$ (where δ^2H and $\delta^{18}O$ denote the deuterium and oxygen-18 abundance relative to VSMOW – Vienna Standard Mean Ocean Water). It is a second-order isotope parameter that is specifically sensitive to the conditions during the evaporation of water from the ocean surface i.e. the moisture source conditions (Merlivat and Jouzel, 1979; Johnsen et al., 1989; Pfahl and Wernli, 2008; Pfahl & Sodemann, 2014).

Furthermore, the deuterium excess has been widely used in hydrological studies. Secondary processes that affect the atmospheric vapor content in the evaporation–condensation cycle in nature is identified by using the d-excess. The plot of d-excess against $\delta^{18}O$ shows a negative relationship for all set of samples (Figure 5.20). High d-values indicate low humidity and rapid or kinetic evaporation effects on the isotopes. The decrease in d-excess suggests that evaporation has happened during the recharge process, which again confirms the earlier results.

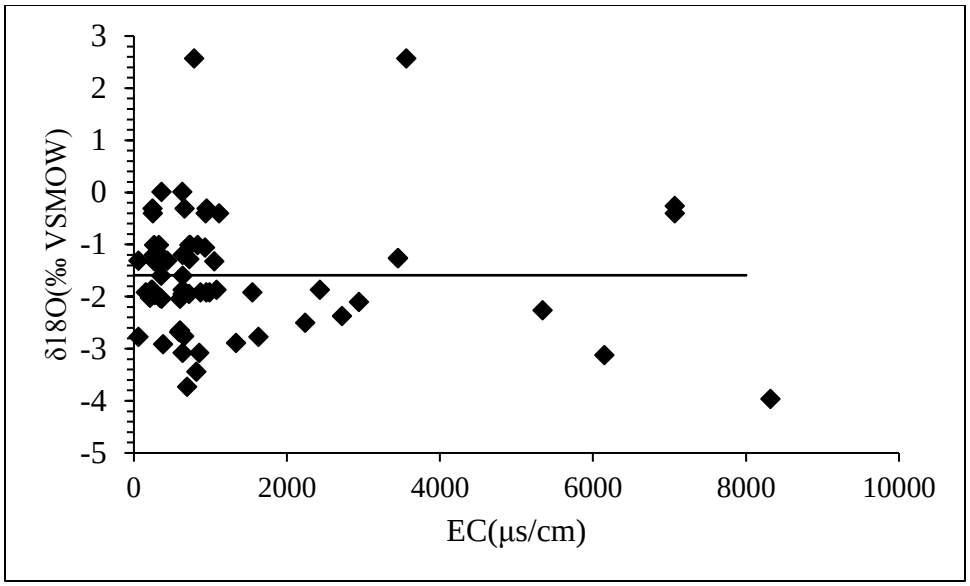

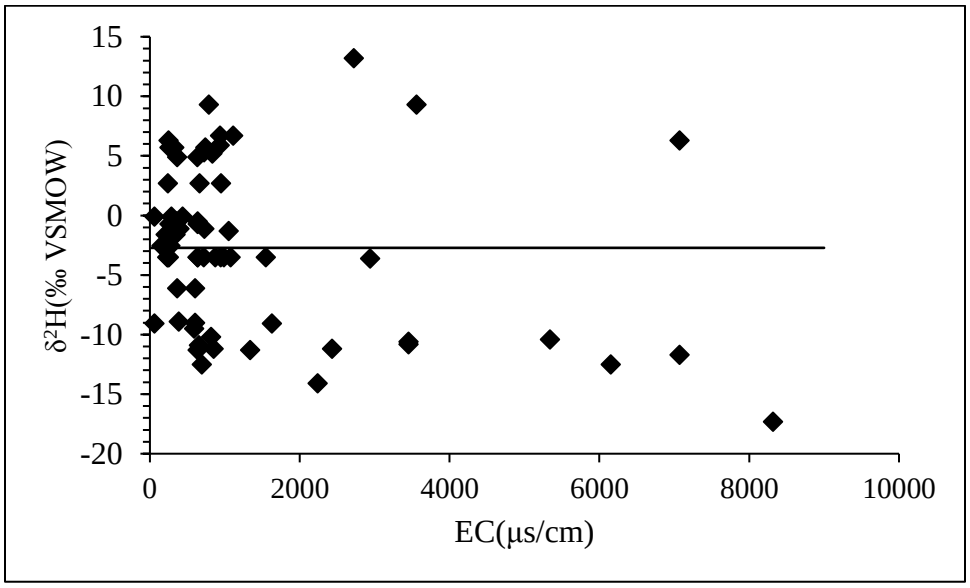

Figure 5.19 Isotopic relationships of all groundwater in the study area.

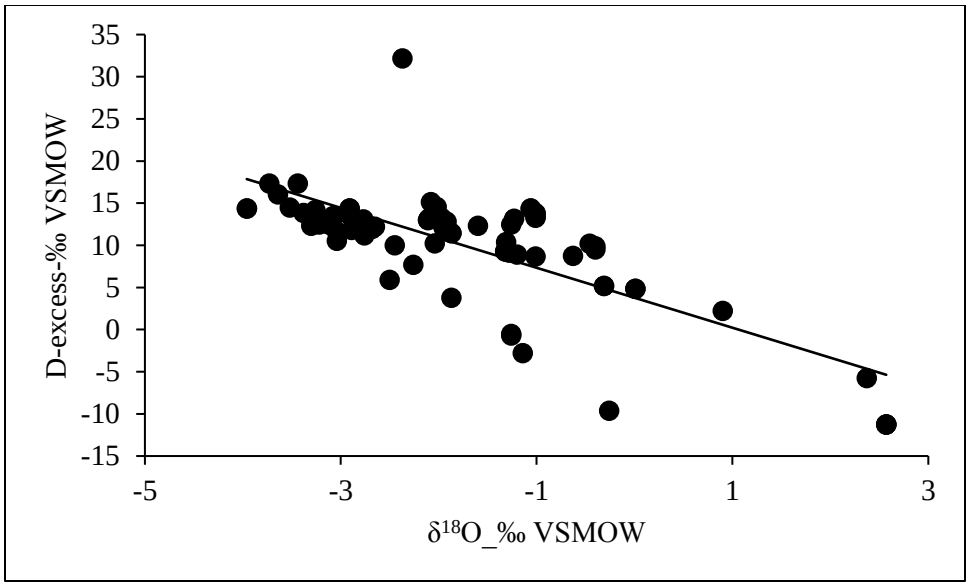

Figure 5.20 The D-excess plotted against $\delta^{18}O$.

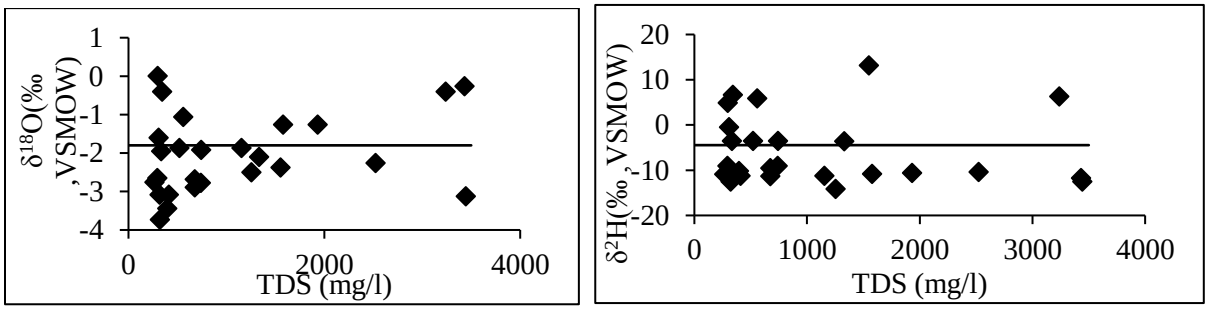

Figure 5.21 Isotopic relationships of groundwater in the Delta.

5.4. Radon (^{222}Rn) concentration in ground and surface water

Radon is a soluble, colorless, gaseous, unstable isotope with a half-life of 3.8 days (H. Martindale & Raaij, 2018). It is generated naturally as part of the uranium decay series and is therefore present in most rocks and soils. Radon released from the aquifer matrix into groundwater, resulting in elevated radon concentrations, but upon entering a river system the radon gas quickly degasses such that surface waters have negligible concentrations of radon (Kies et al. 2005). Surface waters that contain elevated concentrations of radon indicate locations where groundwater is discharging or has discharged slightly upstream of the sampling site. It is, therefore, a useful tool for identifying where groundwater is discharged into a river or stream.

Radon concentrations can vary considerably within groundwater systems and are affected by the uranium content and radon emanation potential of the aquifer material. Generally, geological units with more uranium will result in groundwater with higher radon concentrations. Radon emanation potential can be described as the ease in which the radon can move from the minerals into the water. When the parent material (Radium-226) decays from uranium, it emits a radon particle and an alpha particle. This release of energy can cause the radon particle to diffuse out of the rock grain if it is housed close enough to a surface of the material (Cecil and Green, 2000). Due to the contrast between radon concentrations in discharging groundwater and the low concentrations of radon in surface water recharging into the groundwater, ^{222}Rn can be used as a tracer to identify locations of groundwater discharge to surface water as well as the recharge of surface water to groundwater (Heather Martindale, 2015).

5.4.1. Factors Affecting Radon Concentration in Groundwater

While radon is prominent in groundwater, the release of this hydro-chemical tracer into water is highly variable (Asikainen, 1981). Even where groundwater is essentially coming from the same aquifer, with the same bedrock material, radon concentrations have been shown to vary greatly (Folger et al., 1996). The factors affecting radon concentration relate to the physical and chemical characteristics of the aquifer as well as the uranium content of the bedrock/aquifer material (Asikainen, 1981; Ellins et al., 1990). Obviously, rock materials higher in uranium, such as granites, have the potential to produce groundwater with relatively higher concentrations of radon compared to lower uranium-bearing rocks such as sands or clays (Cecil & Green, 2000). The radon concentration in the groundwater is dependent on where the uranium and the decay product radium-226 are housed within the rock/sediment material. Radium, which is positioned on rock fracture surfaces, produces groundwater higher in radon concentrations because the radon is able to emanate out of the rock material and into the groundwater. Thus, the concentration of radon in groundwater is dependent on the concentrations of radium-226 and uranium-238 housed on the fracture surface of subsurface materials (Heather Martindale, 2015; Martindale & Raaij, 2018).

Both the chemical conditions of the aquifer and the locations of fractures within the subsurface materials influence the mobility of radium-226 and uranium-238 (Asikainen, 1981; Folger et al., 1996). Uranium can adopt many forms depending on hydrochemistry. Uranium is present in the +4 oxidation state at low temperatures and pressures (Skeppström & Olofsson, 2007). In oxidizing

environments, uranium adapts to the +6 oxidation state, which is mobile. The mobile U (VI) can then form strong complexes with Fe and other commonly occurring ions in the groundwater (Skeppström & Olofsson, 2007). When pH is low and total dissolved solids are low, radium remains mobile in the groundwater (Ellins et al., 1990). The preference for mobile radium and uranium to bind to fracture surfaces contributes greatly to the concentration of radon. Radium has a particularly strong affinity to clay minerals and iron oxides (Yanase et al., 1995).

In this study, the radon-222 measurement was conducted on both surface and groundwater in the Delta in order to understand the surface water-groundwater interactions in the Omo Delta groundwater system.

5.4.2. ^{222}Rn in Ground and Surface Water

The concentration of radon-222 (^{222}Rn) in groundwater is much higher than in surface water, the use of ^{222}Rn was examined as an indicator for the analysis of the interaction between surface water and groundwater (Hamada, 1999; Taylor et al., 2009; and Zhao et al., 2018). In the study area, the radon-222 concentration in groundwater samples showed a wide range from 58.7 to 982.5Bq/m^3 compared to the River and Lake Water samples, which are ranged from 18.65 to 105.2Bq/m^3 and 10.49 to 10.85Bq/m^3 respectively (table 5.8).

The average radon-222 concentration was about 424.7 and 31.4 Bq/m^3 for ground and surface waters respectively. The distribution of radon-222 was shown in the graphs (Figure 5.24) along the Omo River stretch and groundwater in the Delta. The highest radon concentration was found in the samples that were collected from wells close to the Omo River (e.g. OD23 and OD24).

These points represent groundwater discharge zones that area close to the Omo River. It can be observed that the groundwater wells that are sited on the fan apex had high radon concentration than those at fan toe (Figure 5.23). This is because samples collected from alluvial fan apex lithologically located in sediments that consist of a poorly sorted mixture of clay, sands, and gravels. Because of heterogeneous lithology and highly porous gravels, the radon emanated is easily dissolved in infiltrated water that reaching the groundwater.

In addition to radon, other physiochemical parameters like electrical conductivity (EC) and temperature were measured to find the relation of these parameters on radon concentration. There

is a positive relation between radon concentration and temperature as shown in Figure 5.23. The radon concentration was increasing if the water temperature increases.

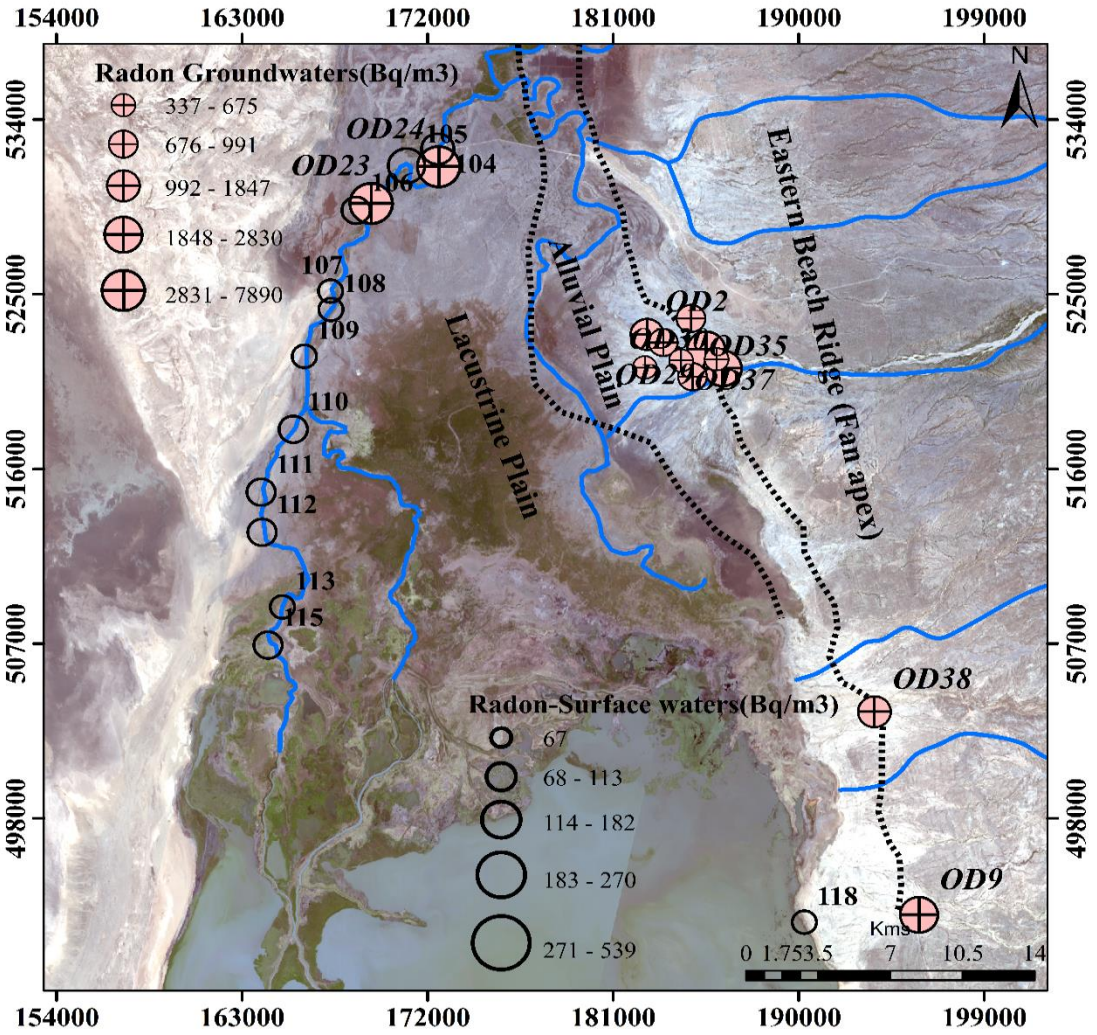

Figure 5.22 Radon-222 measuring and isotope surface water-sampling points in the study area.

Except a few wells (OD25, OD27, OD28, and OD25) a positive correlation exists between radon concentration and electrical conductivity. This is mainly because the samples come from different hydrogeological units that have distinct characteristics. Further, the lack of correlation may also be due to the mixing of groundwater from a different level of aquifers. The groundwater, which has a very low radon-222 concentration due to the connection between the surfaces, means that some of the radon spread into the atmosphere. Generally, it is observed that (Table 5-6) the shallow groundwater wells had relatively higher radon-222 concentration than deep-well groundwater.

This is because the shallow aquifers comprising sand and gravel deposit, which are mainly derived from the crystalline basement rocks rich in uranium-containing minerals from the upper catchment.

Table 5-6 Radon-222 Data used in the discussion. *SOB-South of Omo Bridge at Omorate, SW-Shallow wells, DW- Deep wells.

Sample ID	**Sample source**	**X**	**Y**	**Z**	**Distance(km)**	**EC(µs/cm)**	**T(ºC)**	**δ2H, in ‰**	**δ18O, in ‰**	**Rn-222(Bq/m^3)**
104	Omo R. at Omo bridge	172493	532479	372	0	166	30	9.7	0.2	52.66
105	Omo R(0.9kms)SOB	170983	531615	374	0.9	175	29.9	9.9	0.21	105.2
106	Omo R(3.8kms)SOB	168541	529321	368	3.8	170	30.5	9.8	0.24	25.42
107	Omo R(7kms)SOB	167297	525156	363	7	173	30.4	10	0.34	21.72
108	Omo R(12.7kms)SOB	167317	524214	365	12.7	169	30.3	9.6	0.33	18.65
109	Omo R(13.8kms)SOB	831735	521788	367	13.8	173	30.2	10	-0.23	19.49
110	Omo R(16.8kms)SOB	831230	518024	367	16.8	170	30.4	9.9	-0.32	35.17
112	Omo R(24.4)SOB	829763	512708	367	24.4	171	30.2	8.2	1.87	25.17
113	Omo R(26.7kms)SOB	830781	508870	368	26.7	178	30.8	8.5	1.43	18.78
115	Omo R(34.7kms)SOB	830102	506897	369	34.7	176	30.5	8.9	1.23	31.64
118	Lake Turkana	190283	492644	366	0	3450	34.5	40.8	7.45	11.85
OD21	SW	167663	526424	370	0.01	1079	30.3	-3.5	-1.87	503.1
OD20	SW	172197	531152	370	0.19	7070	33.6	-1.1	-1.28	932.2
OD25	DW	172170	530378	373	0.54	635	30.4	5.7	-1.01	768.3
OD27	DW	186321	521188	409	18.05	1628	32.3	-6.1	-2.04	431.1
OD18	DW	186022	521659	410	18.18	718	33.2	-10.3	-2.97	122.5
OD34	SW	183437	522512	392	14.76	1548	35.1	-3.5	-1.92	155.3
OD28	DW	182648	522929	383	15.27	2940	34.8	-3.6	-2.1	233.5
OD29	DW	184299	521592	396	14.74	1336	35.2	-11.3	-2.89	58.7
OD30	DW	182541	521233	384	13.52	5340	34.6	-10.4	-2.26	106.8
OD35	DW	184857	520745	407	17.58	655	34.9	-10.9	-2.76	136
OD24	SW	172546	531578	371	0.01	937	30.5	6.7	-0.4	932.2
OD9	SW	195842	493032	399	5.14	6120	31.5	9.7	0.2	519.8
OD38	DW	193679	503488	399	5.95	6040	33.8	-11.9	-1.14	331
OD23	SW	169270	529676	347	0.54	1058	32.3	10	0.34	982.5

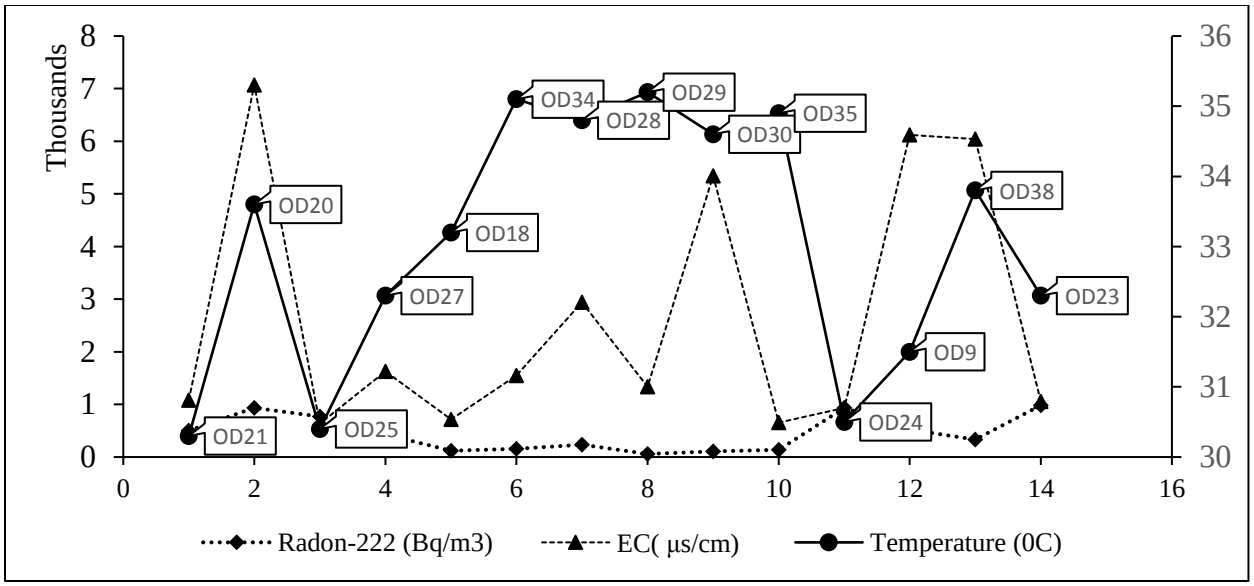

Figure 5.23 The correlation between radon-222, electrical conductivity, and temperature of groundwater in Omo Delta wells (numbers in x-axis represent the sample ID) as arranged in Table 6.8).

From the plot (Figure 5.23), it can be observed that radon concentrations are higher in groundwater close to the Omo River and decrease with distance from the river and Lake. This observation suggests that groundwater in the Delta discharge to the river and Omo River gain its water from not only upper catchment runoff and precipitation but also groundwater along with its lower basin extension too.

In this study, Radon-222 concentration was measured along the Omo River stretch to investigate the interaction between ground and surface water. The Omo River water samples obtained from the high flow season showed that the radon-222 concentration varied characteristics for different distances of the flow path (Figure 5.24). The radon-222 concentration showed a general trend of decreasing along the flow path. However, the pick values of radon were measured between distance 0 to 5km, 14 to 25, and around 35kms. This indicates that there are points in between where the groundwater discharge to the river. At the south tip of the river branching into two and the right hand (figure 5.21) are hard to reach and do not sampled. EC of the River significantly increases between points, 0-5, 5-10, 13-15, and 25-30kms, indicating that saline groundwater discharge to the River.

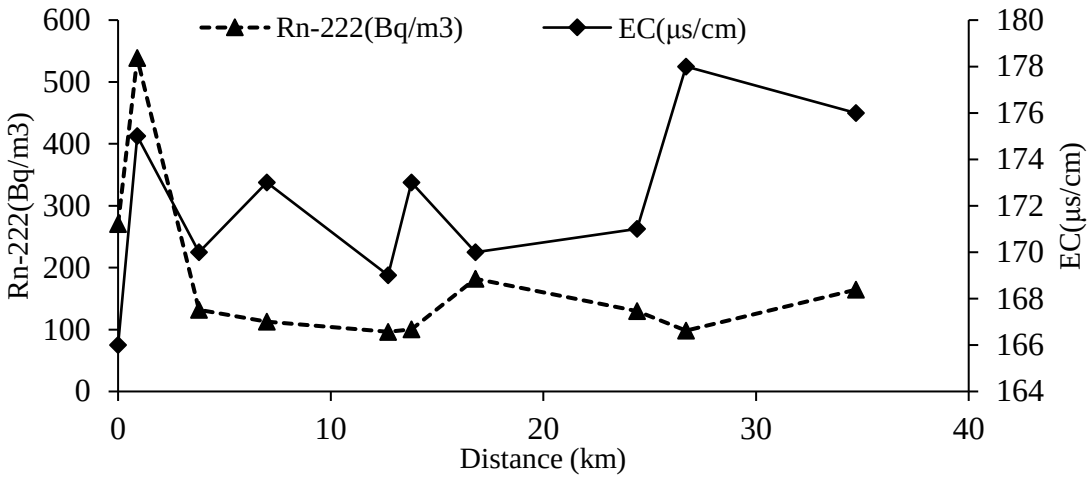

Figure 5.24 radon-222 concentration along the Omo stretch with associated electrical conductivity.

5.5. Piezometric Level

A water table contour map is a very important tool in groundwater management as one can derive from it the hydraulic gradient and the direction of the groundwater flow and possible indicator of aquifer structure (Heath, 1983; Ismail et al., 2010; Kebede et al., 2016). A water table contour map or a contour map of the potentiometric surface of an aquifer is a graphic representation of the hydraulic gradient of the water table or potentiometric surface. The hydraulic gradients, which can be directly derived from these maps, are the basis for calculating the rate of groundwater flow through aquifer cross-sections (De Ridder, 1980, Hiscock, 2005; Naus et al., 2019). The contour lines of a water table map or a potentiometric surface map are in fact equipotential lines. Hence, the direction of the groundwater flow, being perpendicular to the equipotential lines, can be directly deduced from these maps. Furthermore, an effluent (gaining) or influent (losing) from a source (upper lands or river) and the artesian effect can be determined using these maps.

A depth-to-water table map or iso-bath map, as these names imply, shows the spatial distribution of the depth of the water table below the land surface. It can be prepared in two ways. The water level data from all the observation wells for a certain date should first be converted to water levels below the land surface. Once plotted, then the transformed data on the topographical base map near each observation point and lines of equal depth or isobaths to groundwater. Another way of preparing an iso-bath map is made by taking the difference between the topographic elevation and the depth-to water level, which gives the groundwater elevation from means sea level (datum).

Head observations of water wells in this study were done by latter means at the field and for those wells, which sealed and had drilling history report; their static water table is taken as it was during drilling to plot the piezometer of the study area. The resulting piezometric map (Figure 6.28) indicates a steep hydraulic gradient in the northern and northeastern parts of the basin and gentle in the western and southern parts. Head observations of water wells in this study were done at the field and for both those wells which sealed and had drilling history report and open dug wells. Depth to water level water table is considered and range 0 to 50m with well depth range from 2 to 97m (Table 5-7).

Table 5-7 Hydraulic heads, depth, and isotope signature of some wells in the study area. Wells are distributed at Hammer basement (Bold) and Quaternary sediment (light) aquifers.

Well Code	Depth	Hydraulic heads	$\delta^{2}H$‰	$\delta^{18}O$‰	D-excess(‰)
OD108	**16.5**	**12**	**-2.54**	**-1.92**	**12.82**
OD17	**5**	**2**	**-6.1**	**-2.04**	**10.22**
OD14	**10**	**6**	**-0.1**	**-1.31**	**10.38**
OD16	**7**	**4**	**5.7**	**-1.01**	**13.78**
OD10	**46**	**2**	**2.7**	**-0.31**	**5.18**
OD112	**82.5**	**15**	**2.7**	**-0.31**	**5.18**
OD111	18	12	13.2	-2.37	32.16
OD30	55.5	30	-10.4	-2.26	7.68
OD31	85	25	-10.9	-2.76	11.18
OD21	61.5	28	-12.7	-3.04	11.62
OD18	91	50	-3.5	-1.95	12.1
OD3	97	44	-12.5	-3.73	17.34
OD40	5	3	-10.6	-1.26	-0.52
0D9	1.9	0	-14.1	-2.5	5.9
OD38	80	34	-11.9	-1.14	-2.78

6. DISCUSSION

The main purpose of this study is to contribute towards a better understanding of the source of salinity and mechanism(s) of salinization in the Omo Delta (southwestern Ethiopia) groundwater. This chapter includes the discussion of major findings as related to the literature on the sources of salinity and the salinization process in groundwater in the inland Delta system. The socio-economic activities in the region largely depend on the availability of water with acceptable quality. To achieve this significance, an accurate understanding of the source and distribution mechanism of saline groundwater prevailing in the Delta and its surrounding is very important. This has a significant contribution to the development of the resource usually characterized by failures of hit and miss identification of appropriate borehole sites with fresh water.

The result of methods used to answer the research question: (a) what is the source of salinity in the Omo Delta groundwater. (b) How is saline groundwater distributed? (c) How does hydrochemistry vary and evolve from the headwater to discharge areas? (d) Is groundwater flow pattern continuous across geologic terrains? (e) How do micro-geomorphologies affect the salinity of the groundwater in the Delta? Revealed that there are different processes and sources of salinization in groundwater in the study area. Variation in deposition history and geomorphic processes are responsible for the formation of different parts of the Delta that characterizes different salinity pattern.

6.1. Recharge Sources of Aquifers in the Study Area

Understanding the origins of the rainfall (discussed in chapter 2), is important for the investigation of surface and groundwater hydrology. ^{18}O and ^{2}H are integral parts of natural water molecules that fall as rain or snow (meteoric water) each year over a watershed and, consequently, are ideal tracers of water (Kendall and McDonnell, 1998). Unlike most chemical tracers, oxygen and hydrogen isotopes in water are relatively conservative in reactions with catchment materials. Waters recharged at different times, in different locations, or that followed different flow paths are often isotopically distinct. In other words, they have distinctive "fingerprints." The difference in the sources and processes results in the variation of isotopic effects for local stations. The $\delta^{18}O$ and $\delta^{2}H$ composition of rainfall waters of the IAEA/WMO stations in Ethiopia studied by different researchers (e.g. Dansgaard, 1964; Rozanski et al., 1993; Kebede, 2004; Levin

et al., 2009; Kebede and Travi, 2011) with special emphasis on the anomalous $\delta^{18}O$ and $\delta^{2}H$ composition of Addis Ababa rainfall compared to other stations of neighboring countries in the region.

Time series rainfall isotopic data of Addis Ababa metrological station, which can represent the nearby recharging area for north of the upper catchment of Omo River is plotted by Figure 5.12. From the long-term $\delta^{18}O$ and $\delta^{2}H$ measurements of precipitation at the Addis Ababa GNIP station of IAEA (Data from 1961-2016), the mean isotopic composition of precipitation is $\delta^{18}O$ = -0.38‰ and $\delta^{2}H$ = 9.48‰, $\delta^{2}H$ is positively correlated with $\delta^{18}O$ measurements. The line of best fit through data points representing $\delta^{2}H$ vs. $\delta^{18}O$ values (Figure 6.1) is given by:

$\delta^{2}H‰ = 7.54\delta\ ^{18}O‰ + 13.12$ ……. (6.1)

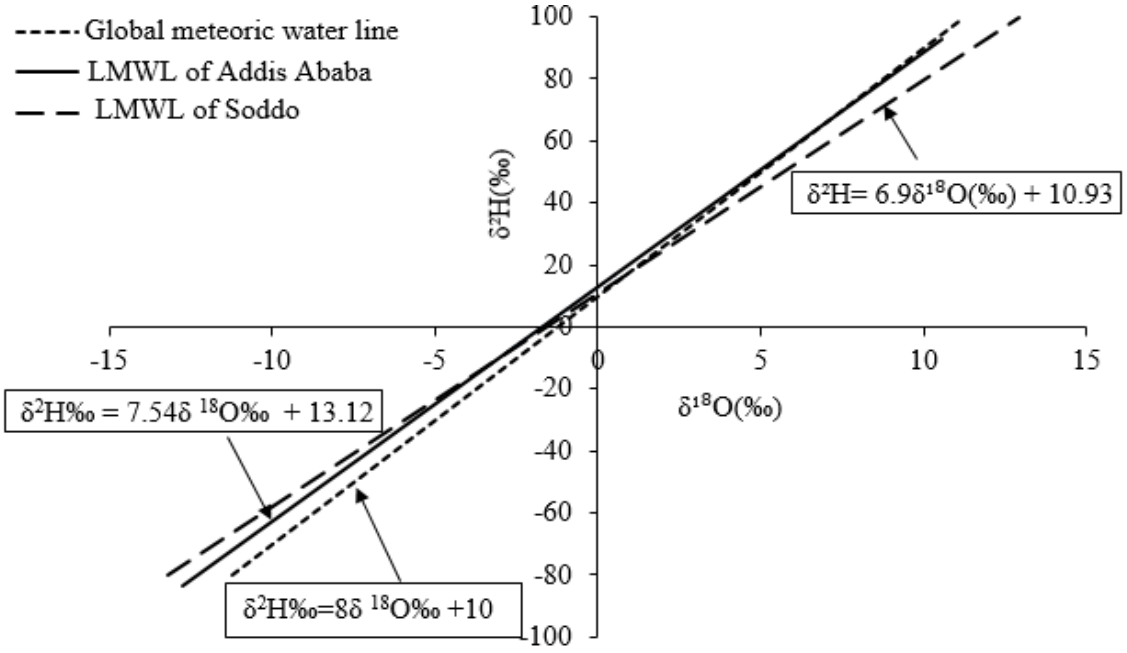

Figure 6.1 Linear relation of $\delta^{18}O‰$ vs δ2H‰ of precipitation at three GNIP station (Data 1999/2000, IAEA) for Soddo, Addis Ababa and Global Meteoric water line.

This is comparable to the global meteoric water line (GMWL) of Craig (1961), which is given by $\delta^{2}H = 8\delta^{18}O + 10‰$ SMOW, and later modified by Rozanski et al. (1993) using the regression line of IAEA GNIP stations as $\delta^{2}H = 8.17\ (\pm 0.07)\ \delta^{18}O + 11.27\ (\pm 0.65)$ ‰ VSMOW. The isotope value of precipitation is controlled by isotope value of the source, rate of evaporation of a source, isotopic

evolution of air mass, relative humidity during precipitation (Gat, 1996). As an air mass leaves its source, it cools as it rises above the continents. This cooling induces precipitation that distills the heavy isotopes.

Physiographic regions used in the interpretation of the isotope data from the water vapor in the air mass. The remaining vapor becomes progressively depleted in ^{18}O and ^{2}H. Precipitation with relatively high isotope values (compared to the air mass vapor) falls from the clouds. This results in the so-called continentality effects and the orographic effect that produces precipitation with very low values at high altitudes (Dansgaard, 1964).

Time series rainfall isotopic data is totally lacking for the Omo Basin in general and Delta in particular. There are no GNIP stations in the basin except Soddo (Figure 5.12), at the east side of the Omo Basin. However, it can't be representative of the study area. But its GNIP data are used for interpretation of isotope signature as it can represent the recharge area of the Omo Basin. Therefore, the local meteoric line couldn't be defined, and the rainfall data collected during this study are interpreted using the global meteoric water line (GMWL).

6.2. Isotopic Effects of Rainfall

Due to the absence of GNIP stations in the Omo Basin, it is difficult to understand both the moisture source and the isotopic effects along with the moisture trajectory directions. Here, only characterization using isotope signature is preferred to show the variations.

The amount of rain determines the variation of isotopic composition (Hem, 1998; Mazor, 2004; Christian et al., 2009; Liu, 2018). The amount effect where greater monthly precipitation amounts result in more depleted $\delta^{18}O$ and $\delta^{2}H$ values (Dansgaard, 1964). This could be related to the formation of clouds yielding heavier rains with depleted heavy isotopes favored by lower ambient temperature (Mazor, 2004). The relation of monthly rainfall amount to the monthly average stable isotopic composition of precipitation of Soddo GNIP stations for the year 1999/2000 (IAEA, 2000) is available to understand the variations using amount effect in the upper recharging basin of Omo River (Figure 6.2).

Wolaita-Sodo station GNIP data showed a relatively weak correlation ($R^2 = 0.56$) exist between the amount of rainfall and $\delta^{18}O‰$ on a yearly basis. The amount effect of major rainfall season (Ju, Jul, Au, S) showed a weak relation ($R^2 = 0.04$), the spring (Mar, A, Ma) season ($R^2 = 0.83$)

and the October peak (OND) season ($R^2 = 0.97$) with the $\delta^{18}O$ of the respective months. This shows that the amount effect is pronounced only for small rains and cannot explain isotope variation in the fully developed monsoon season of major rainfall events where the meteorological parameters such as (humidity and temperature) are almost uniform. This is because, in small raindrops, the amount of rainfall becomes important to overcome the re-evaporation of rainwaters. During low rainfall, re-evaporation of rainwater leads to enrichment, and therefore a clear and relatively high correlation ($R^2 = 0.97$) of $\delta^{18}O$ to rainfall amount exists (Asha, 2018).

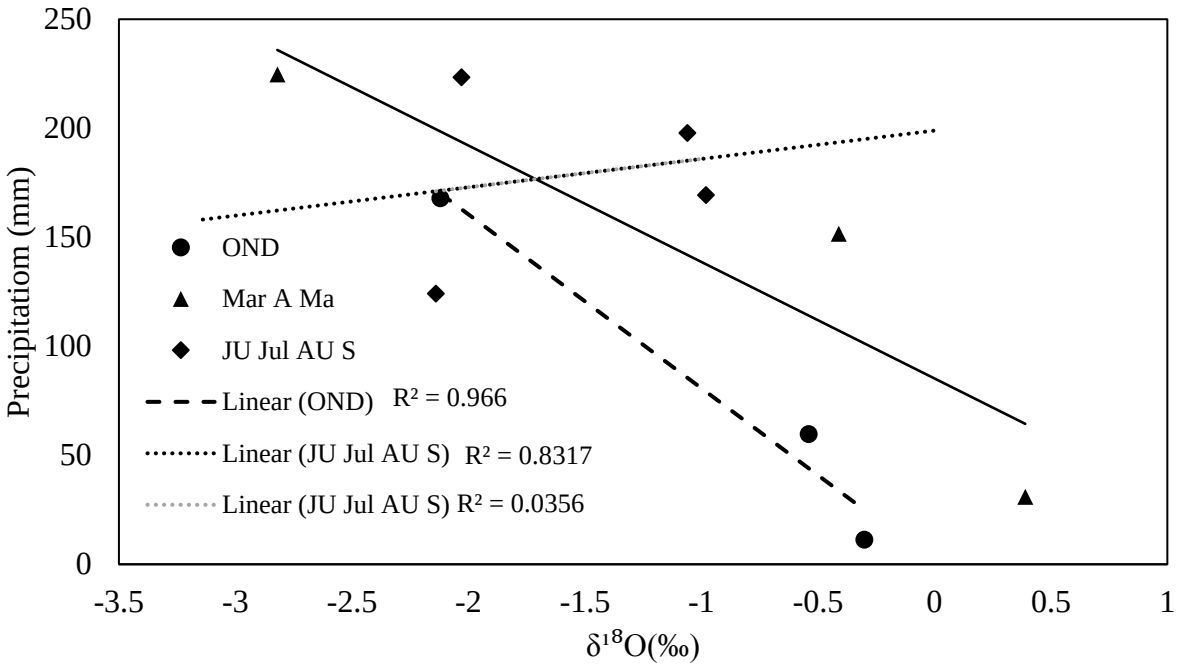

Figure 6.2 Rainfall amount and $\delta^{18}O$ variations for three seasons of Soddo.

Precipitation and shallow groundwater are used to see the altitude effect of the isotopic composition of the study area. As the clouds ascending to higher altitudes, heavier isotopes are depleted, and the residual precipitation gets isotopically lighter. The altitude effect is locally variable and turns out to be an effective tool in tracing groundwater recharge (Mazor, 2004). The spatial variation of the stable isotope could be explained by the altitude effect that leads to the difference in the composition of ($\delta^{18}O$, $\delta^{2}H$, and d-excess) precipitation.

Low d-excess values of waters from Ethiopia indicate enrichment in ^{18}O due to evaporation, as expected for a river and shallow well waters in arid regions (Levin et al., 2009). Similarly, the

variation in d-excess with altitude (Figure 6.3) could also be used to characterize the processes for a different rate of depletion per 100m. The D-excess of the shallow groundwater in the Delta aquifer exhibit high range, though the altitude range is small (see Figure 6.3 circled), indicating that the rate of evaporation before precipitation takes place at a different rate.

Evaporative enrichment of the rainfall beneath the cloud base is higher towards lower altitude where the d-excess is lower. However, along areas where the inter-mountains affect the wind flow to leeward of the summer rains, the d-excess varies greatly. It is understood that evaporation is lower around highlands where the temperature is lower. But some highland rainfall, proxies cold highland springs and shallow dug wells showed a poor correlation of altitude with the d-excess (R^2 = 0.05) in the study area. Rainfall at Jinka showed less d-excess compared to Turmi due to evaporation prior to precipitation (Figure 6.4).

The global distribution of annual mean $\delta^{18}O$‰ of precipitation based on GNIP (Figure 6.5) data indicated that there is a general trend of enrichment from the southern hemisphere ($\delta^{18}O$ = -9‰) towards northern Ethiopia and Sahel zone ($\delta^{18}O$ = +2‰). The Omo basin is situated in the range of -2 to +0‰ on the map (Kanndel, 1998). The 1969 summer (JJAS) precipitation of Kenya (Kericho) GNIP station data has $\delta^{18}O$ ranging from -0.7‰ to +0.8‰ and d- excess range of 8.84‰ to 12.8‰ (Figure 6.4). This implied that the summer precipitation is relatively enriched to the south of Ethiopia. However, when the cold summer season precipitation originated mainly from the Atlantic Ocean enters into south Ethiopia, it ascends to southwestern highlands of the Omo Basin (Jinka and Soddo) and undergoes condensation at higher altitude (>2000masl). During the processes of gradual condensation of the cloud to higher altitudes, equilibrium isotopic fractionation makes the remaining vapor and the latter precipitation become more and more depleted in $\delta^{18}O$ and $\delta^{2}H$ (Gat, 2010). The moisture continuously depletes in heavy isotopes ($\delta^{18}O$) as it moves over the western face of the southwestern Omo Valley towards Jinka-Soddo of the Omo River Basin because of the altitude effect.

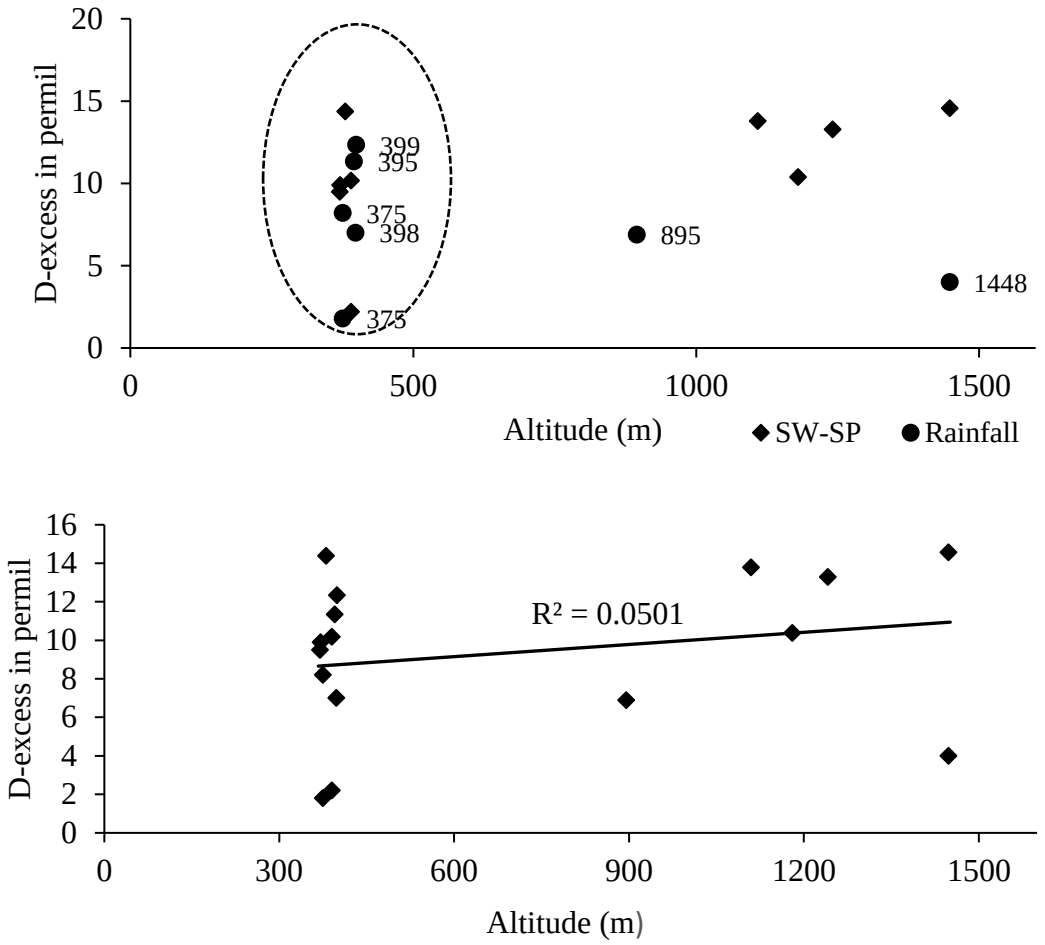

Figure 6.3 The variation of d-excess with altitude. Variations in shallow wells, springs, and precipitation (A) and correlation of d-excess with altitude (B).

Figure 6.6 revealed that, groundwater from hand-dug wells exhibits evaporation in some wells due to their shallow depth and arid climate prevailed in the area. Others are plotted near the meteoric water line indicating that their recharge source is precipitation from rainfall. For the Hammer basement groundwater, as shown in Figure 6.7, all samples (except two hand-dug samples) plot along the global meteoric water line (GMWL) and Soddo LMWL, indicating that the Hammer basement groundwater is mainly of meteoric origin. In comparison with the other groundwater samples, hand-dug well samples are relatively enriched in stable isotopes; it deviates significantly from the LMWL. The isotopic distribution of groundwater samples from the Quaternary sediments mainly shows two clusters (Figure 6.7). The first pattern is populated along the lower part GMWL (circle A) indicating that these samples are from non-evaporated water which is rapidly infiltrated

to the saturated zone , and middle part of GMWL (circle B) which are shallow and hand-dug wells that have hydraulic interconnection with Omo River (recharged by Omo River). Whereas, the samples that populated at left corner (circle C) indicates evaporation prior to recharge.

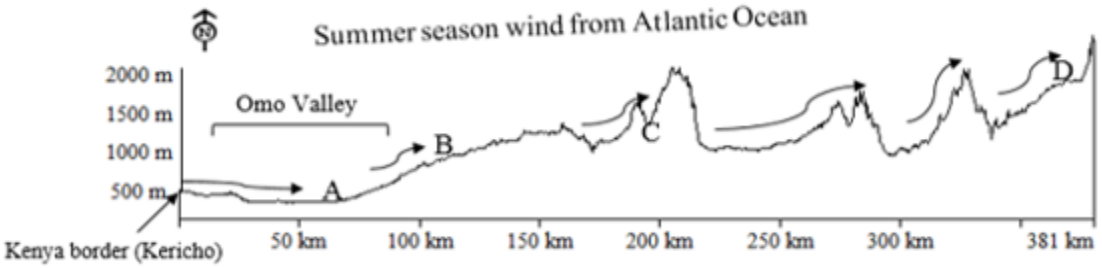

A. Omorate (P=97.3mm, $\delta^{18}O$ = -0.38 to 2.31‰, D-excess to -13.68 to 12.34‰, and T^0c= 31.9)
B. Turmi (P=71.2mm, $\delta^{18}O$ = -1.14 to -0.21‰, D-excess 6.88 to 14.32‰, and T^0c=28.5)
C. Jinka (P=151.9mm, $\delta^{18}O$ = -2.02 to 2.85‰, D-excess to 14.56‰, and T^0c=22)
D. Soddo (P= 220mm, $\delta^{18}O$ = -1.06 to -0.78‰, D- excess 13.8 to 16.84‰, and T^0c=19.6)

Figure 6.4 Conceptual profile of the summer moisture-bearing wind flow from Atlantic ocean along the SW-NE direction of Omo basin indicating altitudinal variation in $\delta^{18}O$ and d-excess of GNIP stations (Kericho, Sodo) and proxy groundwaters of Omorate, Turmi, and Jinka localities. The letters A, B, C, and D represent localities and the arrows point to the moisture-bearing wind flow direction. P and T are mean monthly rainfall and temperature respectively during isotope data analysis.

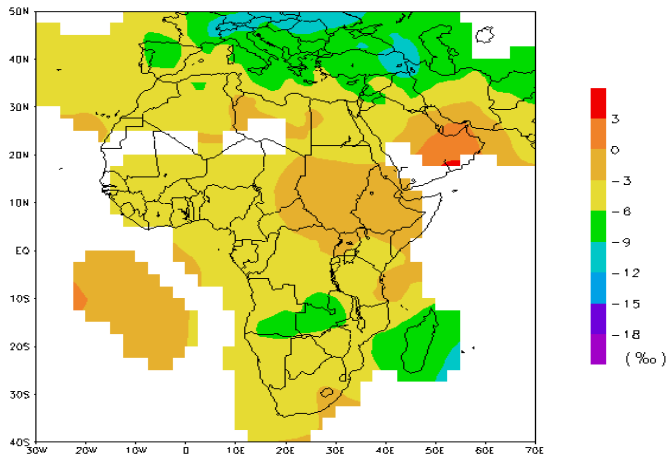

Figure 6.5 Annual mean $\delta^{18}O$‰ of precipitation based on GNIP data (Adapted from http://isohis.iaea.org)

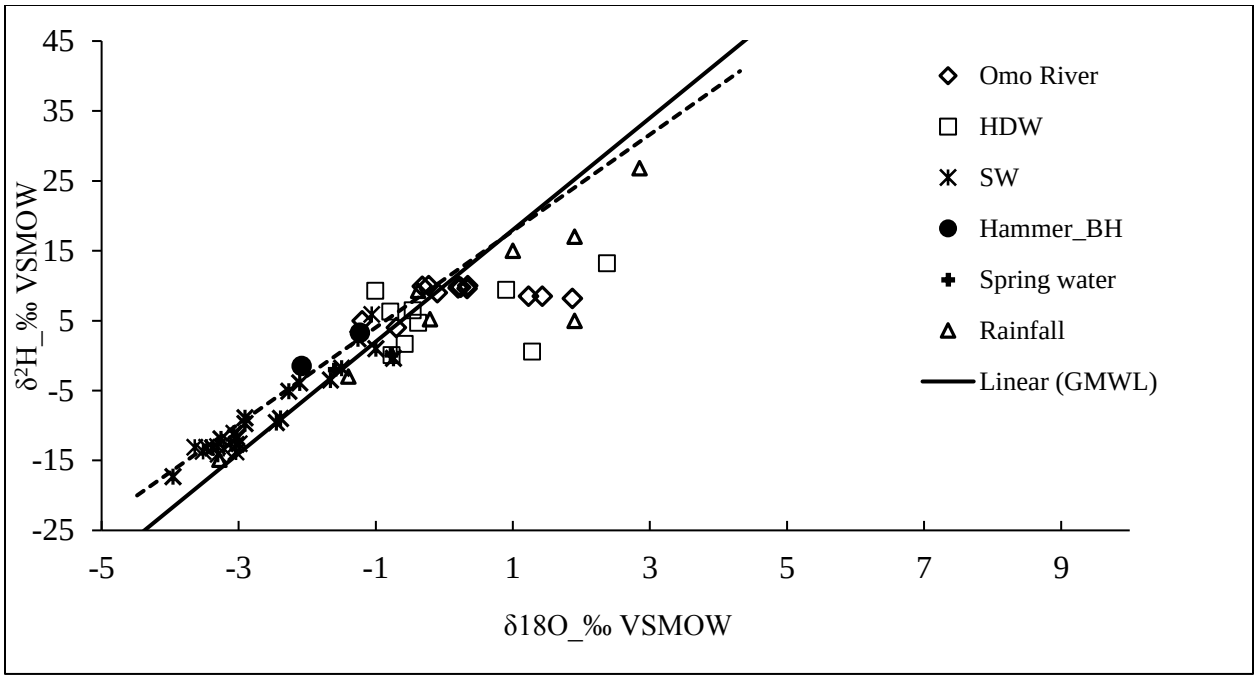

Figure 6.6 Isotopic relation of all waters in the study area

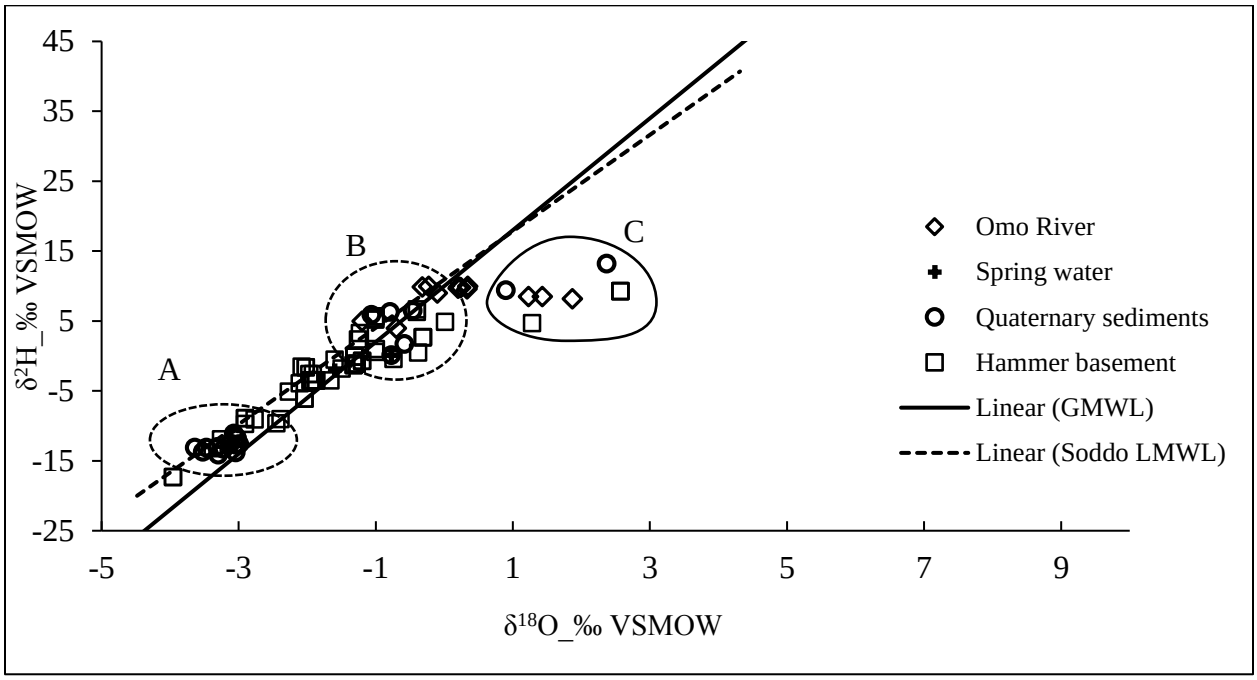

Figure 6.7 Stable isotope compositions of groundwater in two hydrogeological units.

The basement associated hydrogeological units are recharged directly by depleted highlands and escarpments summer rainfall ($\delta^{18}O‰$= -4.5 to -0.3) under cold air condition. But the degree of depletion of rainfalls varies from south to north of the basin due to basin-scale microclimatic variability (Figure 6.4). Low EC and depletion with respect to heavy isotopes of the group indicated that the waters are formed due to fast percolation of highland rainwaters favored by high hydraulic gradient and open lineaments where the residence time, rock-water interaction and isotopic fractionation are very low.

From the Hammer mountains to the Delta plain (Jinka, Turmi, Omorate, and Fejeji), there is a general progressive enrichment in the $\delta^{18}O$ and $\delta^{2}H$ composition of the groundwater (Figure 6.8). This trend suggests the progressive increase in the importance of evaporatively fractionated water recharge the groundwaters and the progressive decrease in groundwater inflow to the aquifers from the highlands. The $\delta^{18}O$ of groundwater samples from the Omorate area has no outlier values compared to other areas. This is mainly due to recharge from the Omo River is the main source. Furthermore, all basement groundwater samples are scattered around the GMWL also confirming that the recharge of this aquifer originates from the infiltration of recent precipitation from Atlantic vapor air mass.

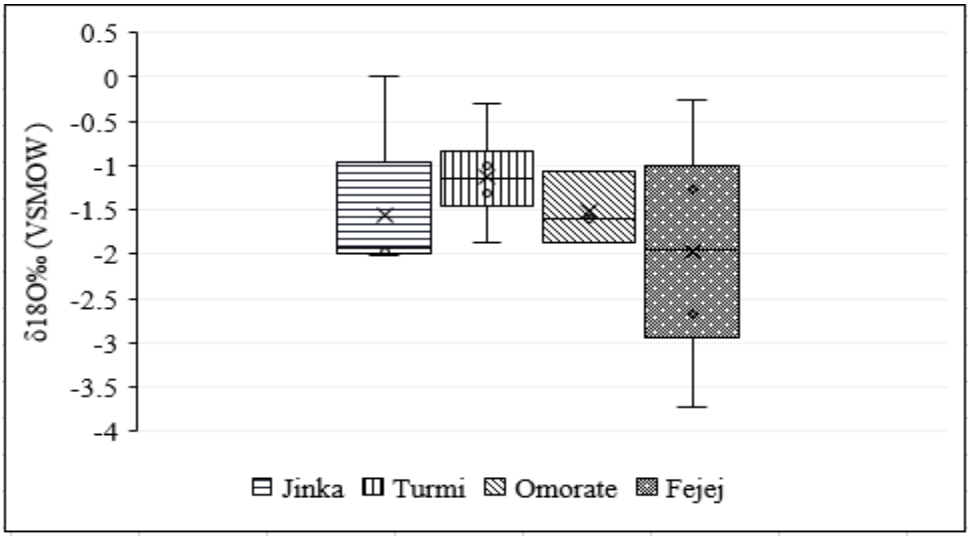

Figure 6.8 The spatial variation in the $\delta^{18}O$ in ‰ of groundwaters along N-S of the study area.

6.3. Origin of Salinity in Groundwater

An understanding of hydro-geochemical processes that determine spatial variation of salinity is essential for achieving and sustaining usable water supplies. In this context, it is imperative to constrain the effect of groundwater mixing of distinctly different sources of groundwater from contributions of water-rock interaction reactions, evaporation, dissolution, and precipitation of minerals. Preceding sections of this study in the Delta have been applied multivariate statistics on groundwater chemistry and isotope composition ($\delta^{18}O$ and $\delta^{2}H$) to constrain the contributions from water-rock interaction reactions, evaporation, dissolution, and precipitation of minerals. This part tries to summarize the main process that is responsible for salinization.

6.3.1. Salinity Originated from Water-Rock Interaction

After conducting a non-parametric (Wald-Woldfowitz) test, it has been confirmed in section 5.2.4 that there was a significant difference in groundwater composition between Quaternary sediment and Hammer basement aquifer sources. Therefore, it is important to characterize the two-aquifer systems individually to elucidate the source of mineralization of groundwater in the basin. From the correlation matrix of physiochemical parameters of the Quaternary sediment aquifer groundwater, the salinity of groundwater is well correlated with the concentration of chloride, sodium, sulphate, and bicarbonate. These ions have been dissolved into groundwater constantly and demonstrate the rise of total dissolved solids. Dissolution of halite (Na-Cl), miralbite ($NaSO_4.10H_2O$), and sodium bicarbonate salts were responsible for salinity in this aquifer system. Similarly, the salinity in Hammer basement groundwater aquifer is well correlated with chloride, calcium, and sulphate indicated that these elements are mostly contributed by mineralization. gypsum and calcite dissolution are the main sources. The poor relation in calcium and TDS in the Quaternary sediment aquifer but strong relation in the Hammer basement indicates that the Hammer basement groundwater representing recharge type water. Whereas, the Quaternary sediments represents an evolved water type.

6.3.1.1. Ionic Ratios

Complex geochemical mechanisms and processes mainly control the study area's groundwater chemistry. The dissolved ion concentration in groundwater samples is frequently governed by lithology, the nature of geochemical reactions, and the solubility of interaction rocks (Modibo et al., 2019).

The Gibbs graph (Figure 6.9) was used to understand the relationship between the composition of water and its respective aquifer characteristics according to the variation in the ratio of (Na + K)/(Na + K + Ca) and Cl/(Cl + HCO_3) as a function of TDS (Liu et al., 2015; Jamila et al., 2017; Modibo et al., 2019; Umar et al., 2019). Gibbs (1970) recommended two diagrams to assess the dominant effects of precipitation, rock weathering, and evaporation on the geochemical evolution of groundwater in semi-arid and arid regions. The distributed characteristic of samples in Figure 6.10 shows that rock weathering is the dominant mechanism in the geochemical evolution of the groundwater in the study area. The ratio of (Na + K) / (Na + K + Ca) was mostly less than 0.5 in the Hammer basement aquifer groundwater, with low TDS values indicating that rock weathering was the main mechanism controlling the chemical compositions of the Hammer basement groundwater.

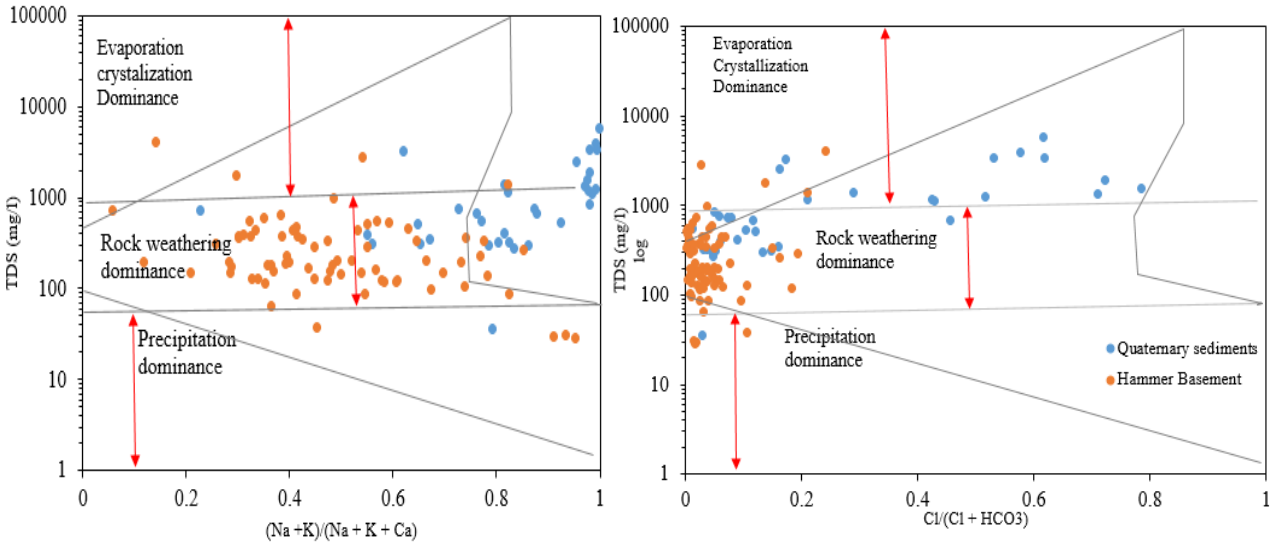

Figure 6.9 Mechanisms governing groundwater chemistry according to a Gibbs diagram: (left) TDS vs. $(Na^+ + K^+)/ (Na^+ + K^+ + Ca^{2+})$; (right) TDS vs. $Cl^-/ (Cl^- + HCO3^-)$.

In the Quaternary sediment groundwater, about 97% of samples had a ratio of (Na+K) / (Na + K + Ca) greater than 0.5 and higher TDS between 34.5 and 3965 mg/L, which indicated that the Quaternary sediment aquifer groundwater was not only controlled by rock weathering, but also by the process of evaporation-crystallization. The weight ratio of (Na + K) / (Na + K + Ca) spreads from low to high without a great variation of TDS, which indicated that cation exchange also played a role by increasing Na^+ and decreasing Ca^{2+} under the background of rock dominance. In the Quaternary sediment aquifers, groundwater is predominantly evaporative due to semi-arid climate conditions or sources of surface contamination. Na^+, Ca^{2+}, and HCO_3^- can be derived mainly from the weathering of plagioclase feldspar that is important to dominant minerals in most igneous and many metamorphic rocks. The plagioclase feldspar is typically the first primary mineral to be weathered considerably, followed by biotite and K-feldspar at a later stage, while quartz should be the most stable of all the minerals (Hem, 1989; Sasamoto et al., 2007).

The Chloro-Alkaline indices (CAI) also used to study the cation exchange between the groundwater and its host rock during a residence or travel (Schoeller, 1965; Marghade et al., 2012; Li et al., 2013). In this study, CAI 1 and CAI 2 was conducted and confirms that Na^+ and K^+ are released by the Ca^{2+} and Mg^{2+} exchange.

Which are CAI-I and CAI-II calculated by the following equations, where all ions are expressed in meq/l:

$$\text{CAI 1} = \frac{Cl^- - (Na^+ + K^+)}{Cl^-} \quad \text{.....(6.2)}$$

$$\text{CAI 2} = \frac{Cl^- - (Na^+ + K^+)}{SO_4^{2-} + HCO_3^- + CO_3^{2-} + NO_3^-} \quad \text{..... (6.3)}$$

Positive Chloro-Alkaline Indices indicate the exchange of Na^+ and K^+ from the water with Mg^{2+} of the rocks (base-exchange reaction). The CAI is negative when there is an exchange of Mg^{2+} and Ca^{2+} of the water with Na^+ and of K^+ of the rocks (Liu et al., 2015). Ca^{2+} or Mg^{2+} will be removed from the solution and Na^+ or K^+ will be released into the groundwater. At the same time, a negative value indicates the Chloro- Alkaline disequilibrium, and the reaction is known as a cation-anion exchange reaction. During this process, the host rocks are the primary sources of dissolved solids in the water. In another case, if the positive values are obtained, then the inverse reaction possibly

occurs and it is known as the base-exchange reaction. In this study, almost all groundwater samples had negative Schoeller index values (annex 5), which indicates direct ion exchange (Figure 6.10) (Chloro-Alkaline disequilibrium). The results indeed clearly show that Ca^{2+} and Mg^{2+} exchange release Na^{+} and K^{+}, which is a common form of cation exchange in the study area. This also further confirms that the cation exchange is one of the major contributors to higher concentrations of Na^{+} in the groundwater, and it is still an important geochemical process of groundwater in Omo Delta.

Cation exchange is an important process of water-rock interactions that obviously influences the major ion composition of groundwater (Liu et al., 2015). Although the cation exchange is widespread in the geochemical evolution of all groundwater, it is essential to know and identify the various changes undergo by water during their traveling processes in the groundwater system under the influence of geologic activities. In this study, the molar Na^{+} / Ca^{2+} ratio changes between 0.9 and 133.6 with an average of 33.34, suggesting the presence of Na^{+} and Ca^{2+} exchange in Quaternary sediment groundwater. It can be conveyed in the following reaction:

$$Ca^{2+} + 2Na^{+} - X = 2Na^{+} + Ca - X \quad \text{……………………………………………}(6.4)$$

Where X is sites of cation exchange.

The graph of Na^{+}/Cl^{-} versus EC (figure 6.13), the Na^{+}/Cl^{-} showed a decreasing trend with increasing EC specifically in quaternary sediment aquifers, which also indicate that the sodium ion originated from the silicate weathering process. It can be observed that most of the samples belong to the Quaternary sediments plotted parallel to the electrical conductivity axis (Figure 6.12) indicating the role of evaporation and evapotranspiration to increase sodium concentration, which resulted in the formation of salt layers related to the leaching from the soil surface during evaporation in a semiarid climate.

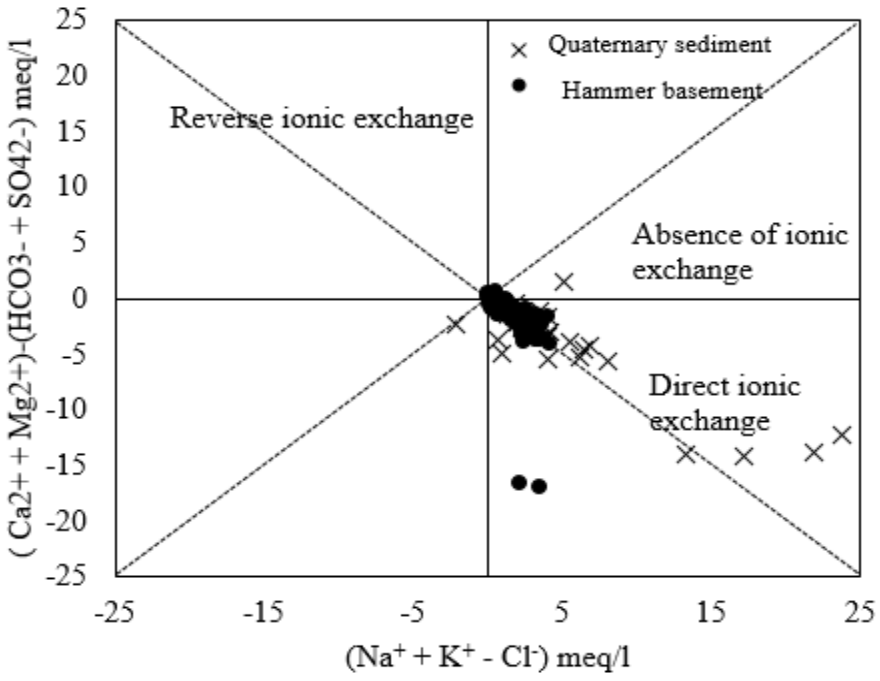

Figure 6.10 Plot of [(Ca^{2+} +Mg^{2+})–(HCO_3^- +$SO4^{2-}$)] versus (Na^+ + K^+– Cl^-) for ion exchange.

High salinity samples (Na–Cl type), which do not follow the halite dissolution line and show enrichment in sodium compared to chlorine, the Na^+ /Cl^- ratio varies from 0.45 to 95.69 meq/l with an average value of 11.14 (Figure 6.11 and Annex 5). Higher ratio exhibited in the central part of Hammer basement whereas the lower ratios are at the Delta groundwater and northern part of Hammer basement. A greater Na^+/Cl^- ratio may be ascribed to the feldspar weathering and the dissolution of other Na-containing minerals. The relatively high Na^+ concentration in the groundwater could also be illustrated by cation exchange between Ca^{2+} or Mg^{2+} and Na^+. In this study, the molar Na^+/Ca^{2+} ratio changes between 0.9 and 133.6 with an average of 33.34, suggesting the presence of Na^+ and Ca^{2+} exchange in quaternary sediment groundwater. The spatial distribution map of Cl^-/HCO_3^- ratio (Figure 6.11) indicated that the affected water mostly covered the south and southeastern side of the Delta plain, which was suspected to be affected by the fossil saline water.

The concentration of Ca^{2+} and Mg^{2+} in groundwater could be related to the presence of carbonate rock in the basin, while the weathering of carbonate and silicates may contribute Ca^{2+} and Mg^{2+} in the groundwater. The groundwater's Ca^{2+} /Mg^{2+} molar ratio can show the dissolution of calcite

and dolomite. Mayo and Loucks (1995) confirmed that when the ratio of Ca^{2+}/Mg^{2+} is equal to 1 indicates the dissolution of dolomite rocks, while the greater ratio could be attributed to the presence of calcite minerals in host rocks. The dissolution of silicate minerals resulted in a Ca^{2+}/Mg^{2+} ratio, greater than 2. In the study area, 27.3% of groundwater samples from the Quaternary sediment have a ratio greater than 2; 60.6% is less than 1, indicating the dissolution of dolomite, and 12.1% are between 1 and 2 (Figure 6.12).

Whereas, in the Hammer basement, 41.1% of samples had an ionic ratio greater than 2, showed the effect of silicate minerals that release calcium and magnesium to the groundwater, and 26% had less than 1 and 32.9% are in between which indicated that dissolution of calcite. The spatial pattern map in the ratio of calcium and magnesium showed the variation from the northern to the central and eastern parts of the Hammer basement. Wells close to the Omo River and a dry river channels ("waddie beds") at the Delta flats, attributable to the increase in calcium concentration through the weathering of silicate and carbonate rocks in the recharge area. The ratio is decreased at the southern tip of the Delta flats (around Fejej), where maximum groundwater salinity measured. Kura et al. (2013) define the dissolution of carbonate minerals, which is a common weathering reaction in carbonate rocks in natural systems by the following reactions:

$$CaCO_3\ (calcite) + H_2CO_3^- \rightarrow Ca^{2+} + 2HCO_3^- \quad \text{.....(6.5)}$$

$$CaMg(CO_3)_2\ (Dolomite) + H_2CO_3 \rightarrow Ca^{2+} + Mg^{2+} + 4HCO_3^- \quad \text{.....(6.6)}$$

$$CaCO_3 + H_2SO_4 \rightarrow Ca^{2+} + SO_4^- + H_2CO_3 \quad \text{.....(6.7)}$$

$$CaMg(CO_3)_2 + 2H_2SO_4 \rightarrow Ca^{2+} + Mg^{2+} + 2SO_4^- + 2H_2CO_3 \quad \text{.....(6.8)}$$

The plot of $Ca^{2+} + Mg^{2+}$ versus $HCO_3^- + SO_4^{2-}$ will be near to 1:1 line if Ca^{2+}, Mg^{2+},SO_4^{2-}, and HCO_3^- are derived from the dissolution of calcite, dolomite, and gypsum. If ion exchange is the dominant process, the data points tend to shift to the right due to excess of $SO_4^{2-} + HCO_3^-$. The ion exchange reaction may be explained as follows (Narany et al., 2014):

$$\frac{1}{2}\,Ca\text{- }Clay_2 + Na^+ \rightarrow \frac{1}{2}\,Ca^{2+} + Na\ \text{- Clay} \quad \text{.....(6.9)}$$

When the points are above 1: 1 line, the reverse ion exchange was the active reaction for the excess of $Ca^{2+} + Mg^{2+}$ over $SO_4^{2-} + HCO_3^-$, which represented by the following reaction:

$$Na - Clay + \frac{1}{2}Ca^{2+} \rightarrow Na^{+} + \frac{1}{2}Ca - Clay_2 \quad \text{.....(6.10)}$$

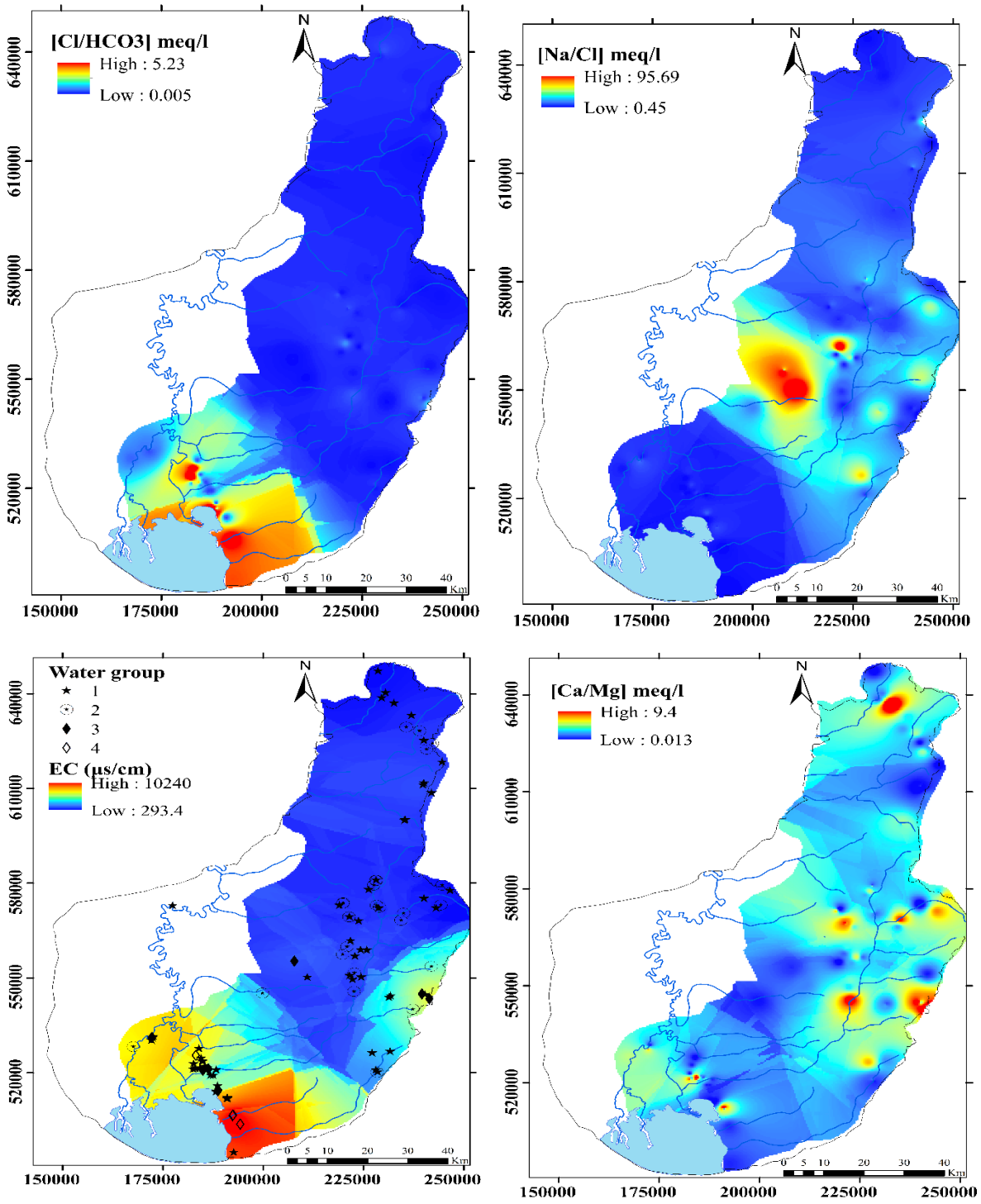

Figure 6.11 Spatial distribution of(a) Ca/Mg ratio, (b) Cl/HCO3 ratio, (c) Na/Cl ratio, and (d) electrical conductivity, of groundwater in the study area.

From Figure 6.12 it can be observed that groundwater samples from both the Quaternary sediment and hammer basin characterize differently with respect to this ratio. In the Quaternary sediment, groundwater samples points falling on the bicarbonate side, indicating the silicate weathering (Elango & Kannan, 2007). Reverse reactions tend to be a dominant reaction as explained in equation (6.10), which was responsible for the higher HCO_3^- and SO_4^{2-} concentration in groundwater.

The plot of $Ca^{2+} + Mg^{2+}$ versus Cl^- shows a significant difference in the distribution of points of Hammer basement and Quaternary sediment groundwater. The hammer basement, characterized by low ratio and salinity compared to the Quaternary sediments, which may be due to reverse ion exchange in the clay/weathered layer. The spatial distribution map of Na^+/Cl^- ratio (Figure 6.11), shows that the majority of the area is covered by a low ratio, indicating that silicate weathering is the source of sodium in the study area.

It can be observed from (Figure 6.12) that, the plot of sulfate versus calcium shows an excess of Ca^{2+} ions for the majority of the groundwater samples from Hammer basements. 70.7% of these samples ($Ca/(Ca + SO_4)$) ionic ratio greater than 0.5 ratios (from 0.52 and 0.95) confirms the ionic exchange process (Jamila et al., 2017). The ($Ca/(Ca + SO_4)$) ionic ratio close to 0.5 confirms that the main source of Ca^{2+} is the gypsum dissolution (Liu et al., 2015; Modibo et al., 2019). A bivariate diagram of sodium versus chloride reveals two main groups: for the first group halite dissolution was maintained for a slope equal to unity where a small number of the samples are situated on the 1:1straight of halite dissolution. The second group includes the high salinity samples (Na–Cl type), which do not follow the halite dissolution line and show enrichment in sodium compared to chlorine. The concentration of Cl^- is well correlated with Na^+ (r^2=0.92, for the Quaternary sediment aquifer groundwater and r^2=0.52 for Hammer basement), suggesting that the dissolution of halite may be the major source of Na^+ and Cl^-.

There is no simple pattern for increasing electrical conductivity in the study area, but it can be observed that at Delta flats (from Omorate to Fejeji) there is increasing of EC with minor fluctuation in between. The Quaternary sediment groundwater, which mainly group 3 and 4 (Figure 6.21) characterized by a higher value of electrical conductivity (salinity), whereas, the groundwater from the Hammer basement is characterized by low electrical conductivity. This

could be linked either to a shorted time for weathering and/or to the lack of sufficient amounts of soluble cation bearing minerals in the aquifer rock environment.

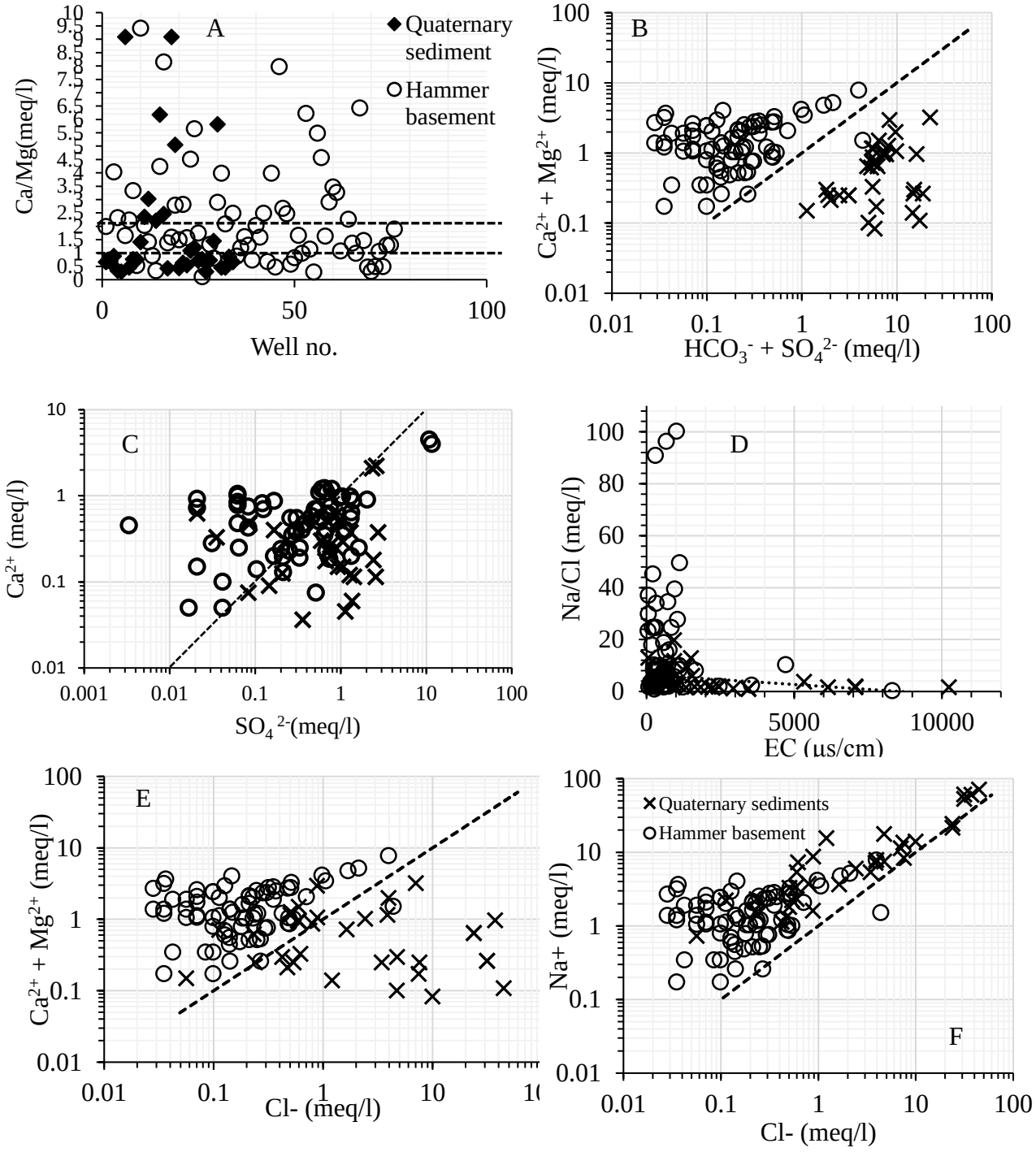

Figure 6.12 relationships between different solutes of Na^{+}, Ca^{2+}, Mg^{2+}, Cl^{-}, SO_4^{2-}, and HCO_3^{-}.

6.3.1.2. Saturation Index

The saturation index is a vital geochemical parameter in the fields of hydrogeology and geochemistry, often useful for identifying the existence of some common minerals in the groundwater system (Ayuba et al., 2013; Liu et al., 2015). In this study, saturation indices (SIs) with respect to anhydrite, aragonite, calcite, dolomite, gypsum, and halite were calculated using the geochemical computer model PHREEQC (Parkhurst and Appelo, 2004). When the groundwater is saturated with some minerals, SI equals zero; positive values of SI indicate over-saturation, and negative values show under-saturation (Appelo and Postma, 1994; Fitts, 2002).

The saturation index (SI) is a measure of how close a mineral–water system is to equilibrium (Hem, 1985; Fitts, 2002) in terms of the following equation:

$$SI = \log\frac{IAP}{Kso} \qquad \text{(6.11)}$$

where: IAP- the ion activity product

Kso- the solubility product

Where IAP is the relevant ion activity product, which can be calculated by multiplying the ion activity coefficient γi and the composition concentration mi, and Kso (T) is the equilibrium constant of the reaction considered at the sample temperature. Figure 6.14 reviled the saturation index (SI) against the total dissolved solids (TDS) for all the groundwater samples classified as Hammer basement and quaternary sediment aquifers. The computed values of SI for anhydrite, aragonite, calcite, dolomite, gypsum, and halite vary between −4.98 and −0.78, between −4.77 and -0.54, and between −9.86 and -4.29 with an average of -2.88, -2.66 and -7.08, respectively. It shows that the groundwater in the study area was below the equilibrium with anhydrite, gypsum, and halite, indicating that these minerals are anticipated to dissolve. However, the SIs of aragonite, calcite, and dolomite range from −2.06 to 0.63, −1.91 to 0.76, and −1.16 to 2.64, with averages of -0.72, -0.58 and 0.74, respectively. Overall, the groundwater samples were saturated to over-saturated with aragonite, calcite, and dolomite, implying that the three major carbonate minerals may have affected the chemical composition of groundwater in the study area. The results show that the groundwater may well produce the precipitation of aragonite, calcite, and dolomite. Saturation of aragonite, calcite, and dolomite could be attained quickly due to the existence of

abundant carbonate minerals in the groundwater system. The soluble ions in natural waters mainly derive from rock and soil weathering (Lasaga et al., 1994).

The plot of SIGypsum and SIAnhydrite versus TDS exhibits a proportional variation, whereas SIHalite parabolic shape evolution with negative values of the saturation indexes (Figure 6.14) (-4.02< SIGypsum <−1.37 and −4.76 < SIGypsum <−0.54 in the Quaternary sediment and Hammer basement, resp., and −4.19 < SIAnhydrite <−1.56 and −4.98 < SIAnhydrite <−0.76 in the Quaternary sediment and Hammer basement respectively). Thus, both calcium and sulphate are derived from the same origin, which is the dissolution of gypsum and anhydrite.

As water travels down the flow path (Figure 6.17), the electrical conductivity (EC) increases, from 645 to 6150µs/cm (OD45 to OD34) and from 564 to 10240 µs/cm (OD46 to OD38). Moreover, the figure shows that the electrical conductivity/salinity of the wells is associated with depth. It seems that the electrical conductivity/salinity distribution is not solely dependent on the aquifer's depth and other factors like additional recharge, mixing between various water types as well as water-rock interaction. Computation of the saturation index for each well shows that these minerals in different proportion characterize water chemistry in the study area. The cause of mineralization of groundwater at the Delta varies greatly as observed in Figure 5.15. The three wells (OD34, OD44, and OD45) have proportional saturation indices of SIcalcite and SIdolomite, which is saturation to over-saturation to these minerals. Whereas, they are undersaturation to gypsum and halite indicating that these minerals are responsible for the presence of soluble ions in groundwater resulted in high salinity.

A large negative saturation index value of halite in both (OD34 and OD38) wells indicates that the halite dissolution important for the mineralization of groundwater in Delta. In addition to this, it can be observed that the higher salinity in groundwater well OD34 is resulted by the increase in well depth as well as it is relatively far from the occasional floods that occur in wet summers but flows rarely reach the well relative to the other wells (OD44 and OD45) attributed to insufficient flushing of freshwater. The groundwater wells at the right-hand side (OD46, OD39, and OD38) exhibit saturated index of calcite, dolomite, gypsum, and halite in a small range, but their electrical conductivity/salinity vary significantly. This may be related to the lithologic composition in which the wells are sited and relative distance of the well from the freshwater recharge.

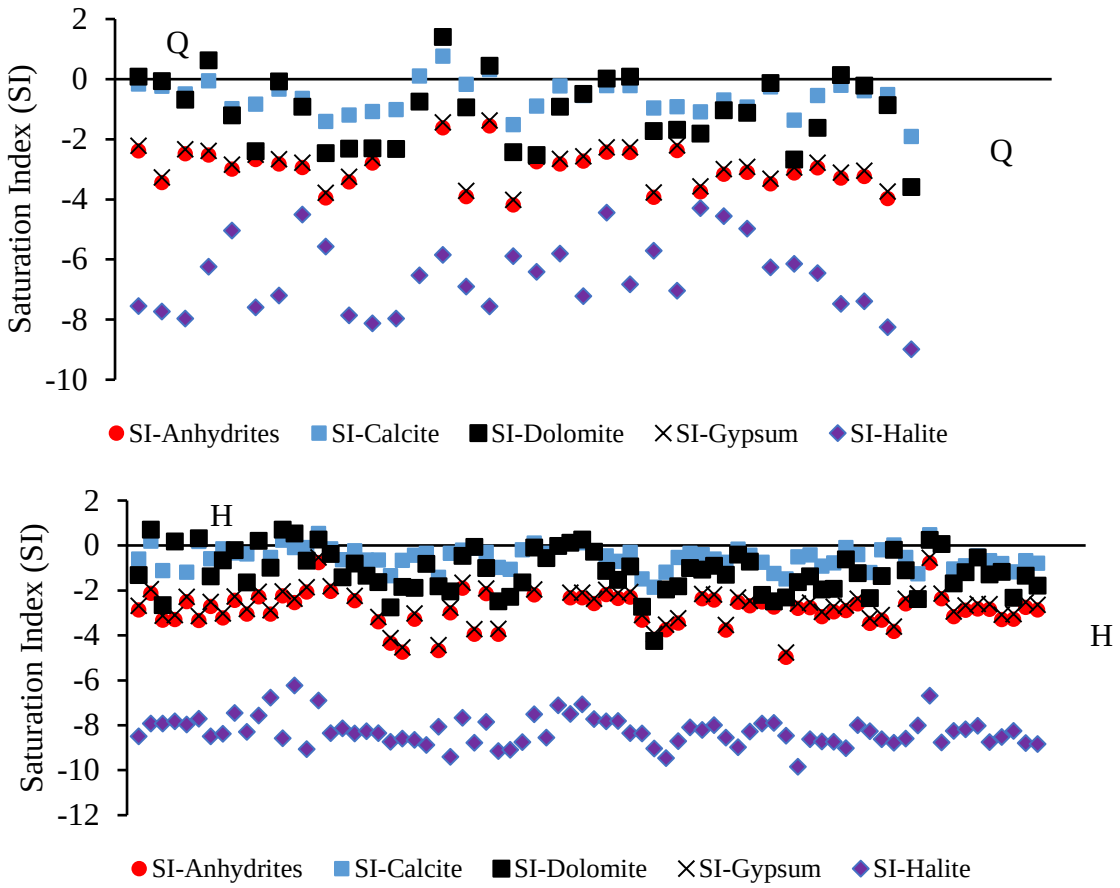

Figure 6.13 Plots of saturation indices with respect to some minerals in groundwater. Q and H represents Quaternary sediment and Hammer basement groundwater.

It can be observed from Figure 6.15 that, the saturation index of calcite, aragonite, dolomite, gypsum, and anhydrite is related to the depth of the well. As well as depth increases, the saturation index of these minerals also increases or vice- versa. This explains that the precipitation of these minerals is expected at higher depths, implying that the three major carbonate minerals may have affected the chemical composition of groundwater in the Omo Delta.

The results show that the groundwater may well produce the precipitation of aragonite, calcite, and dolomite as the depth of the wells increase. Saturation of aragonite, calcite, and dolomite could be attained quickly due to the existence of carbonate minerals in the Quaternary sediment groundwater system.

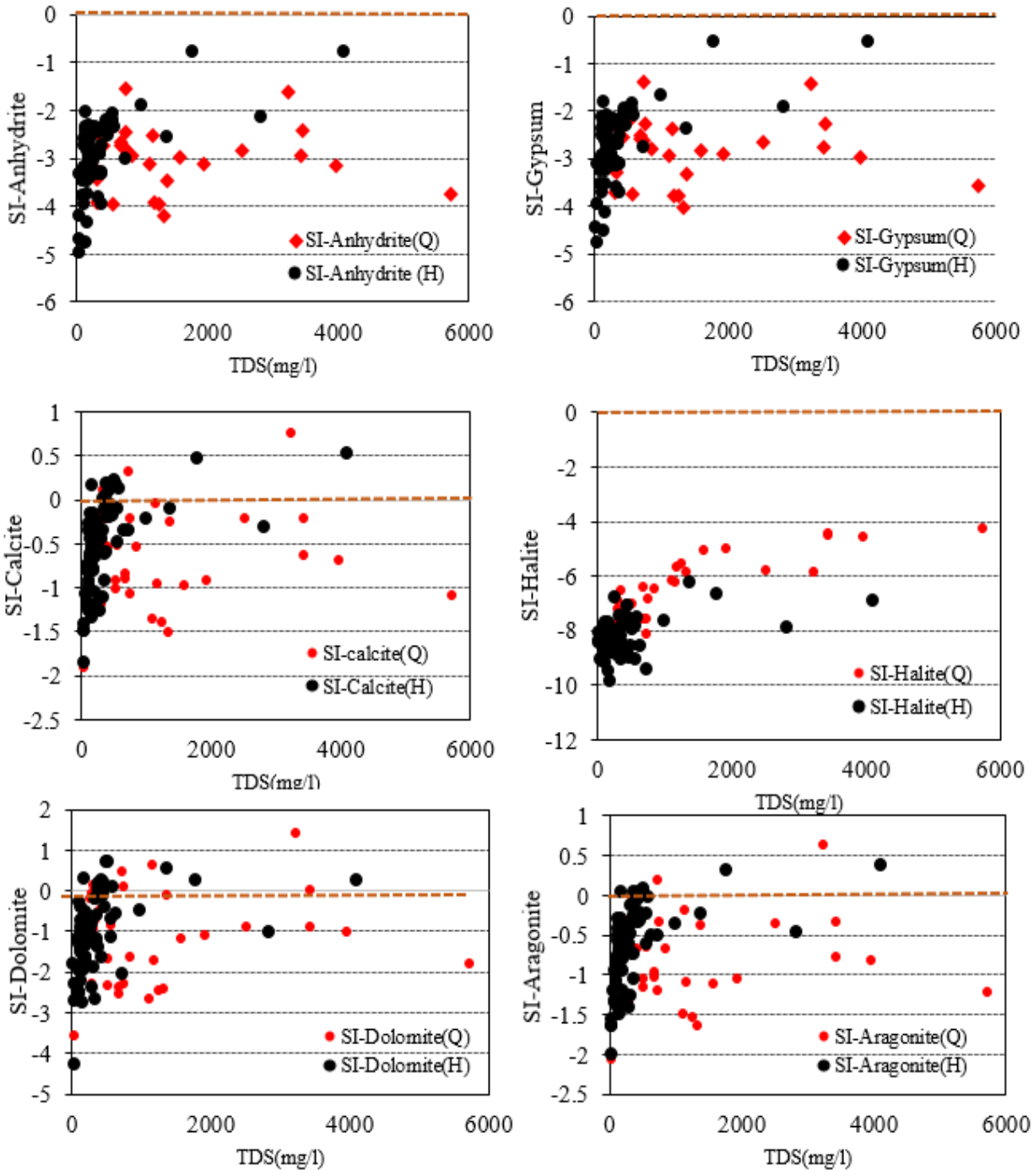

Figure 6.14 Plots of saturation indices with respect to some minerals in groundwater. Q and H represents Quaternary sediment and Hammer basement groundwater.

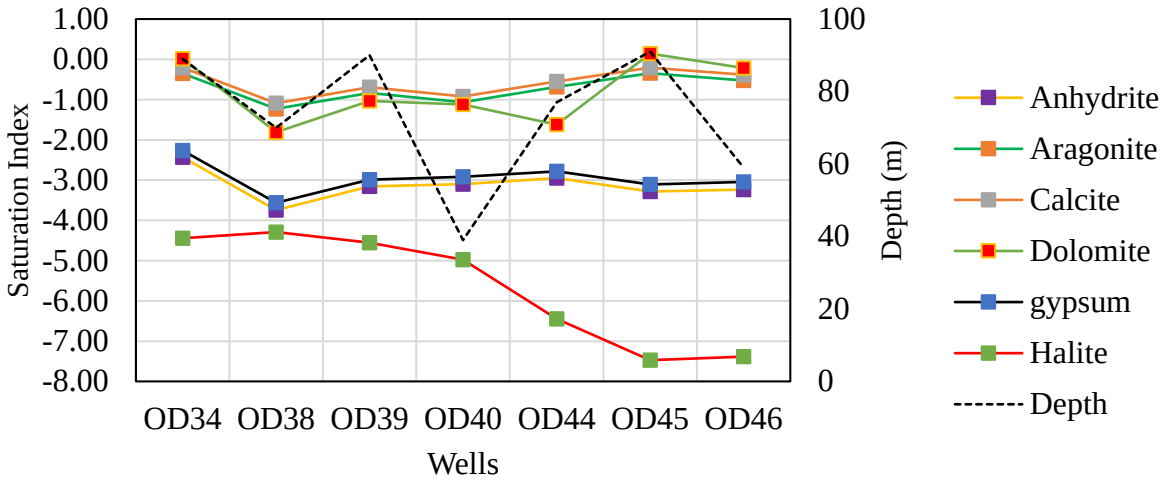

Figure 6.15 The relation between the saturation index (SI) and depth of the wells.

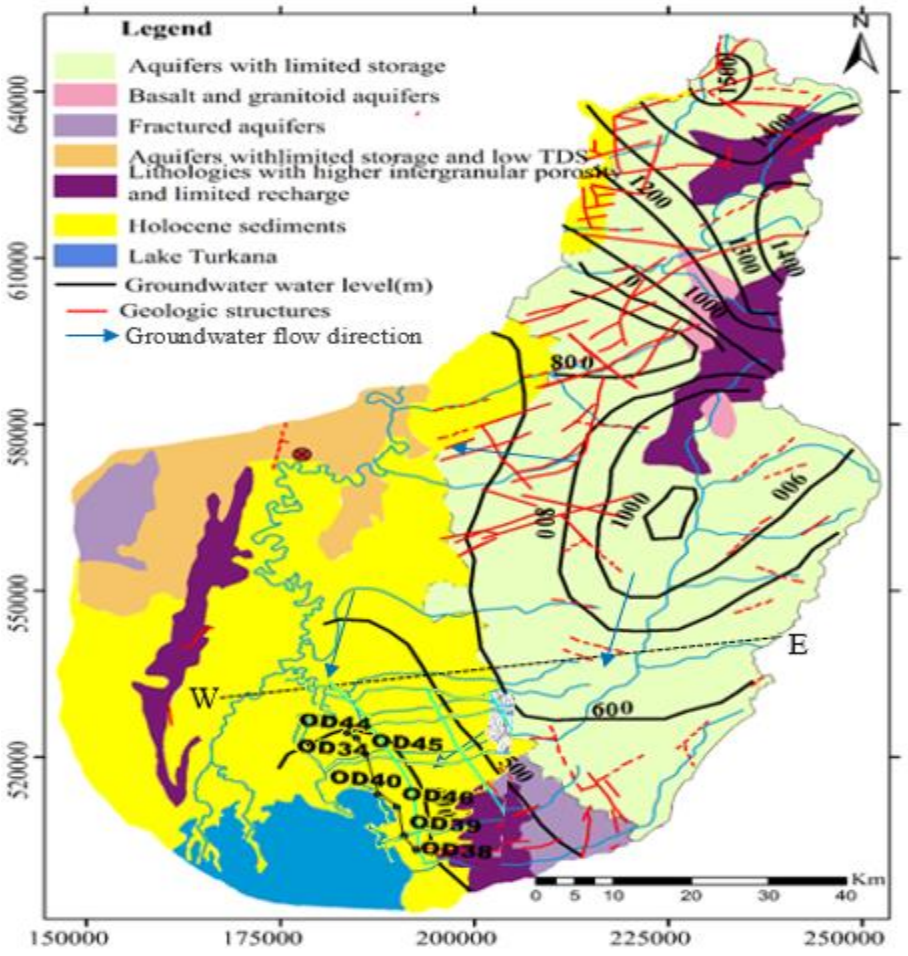

Figure 6.16 The hydrogeological map of the study area.

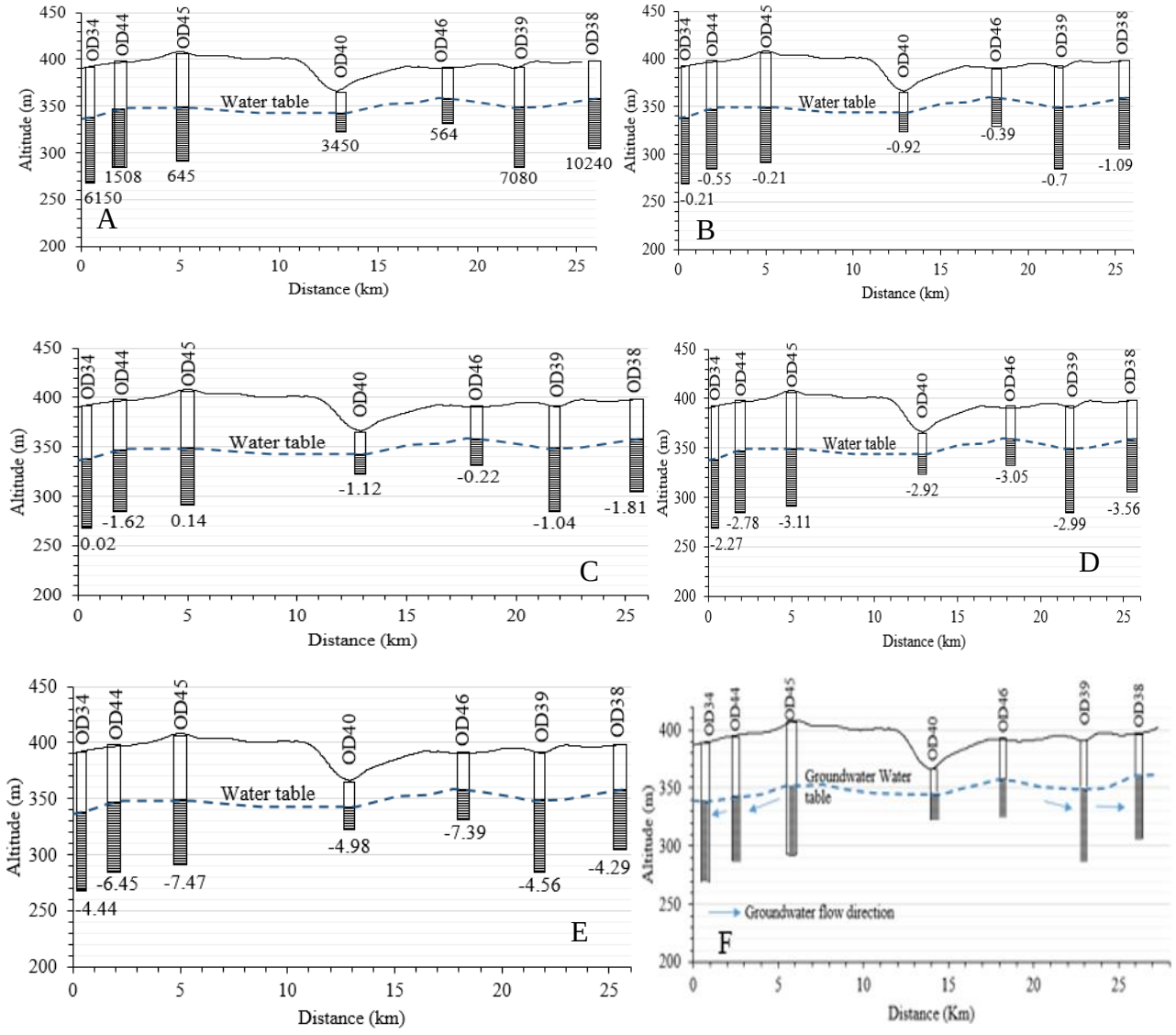

Figure 6.17 Hydrogeochemical section of groundwater wells at Quaternary sediment aquifer of Omo Delta (section line drawn from fig.2.15) A, B, C, D, E, and F are Electrical conductivity (EC-in µs/cm), Saturation index of calcite, dolomite, gypsum, halite, and groundwater flow paths respectively.

6.3.2. Salinity Caused by Evaporation at or near the Surface

Evaporation is the most influential process resulting in saline soils in arid and semi-arid environments (Deverel and Gallanthine, 1989; Mazor, 2005; and Monjezeri, 2012) and groundwater where there are a shallow water table and a climate with evapotranspiration that exceeds the precipitation (i.e. net negative water balance) (Yechieli and Wood, 2002). Salt accumulation and efflorescent crusts have been documented at beach ridge plains of Omo Delta (see section 2.6). The salt formation has been attributed to surface evaporation, wetting and drying cycles (Drever et al., 1978), soil capillarity, and capillarity transport of water and salts from the bulk rock matrix towards fracture surfaces (Weisbrod et al., 2000).

When the water balance in the scenery is changed and salt is mobilized by groundwater as it rises to the land surface resulted in evaporation induced salinity. Figure 3.17 is the picture taken from the study area near Fejej, which shows that the white strips observed are evaporative of salt at the top of the capillary zone. The rising groundwater mobilizes salt stored in a previously unsaturated part of the ground. These salts are then concentrated at the ground surface as the water evaporates. The salinity caused by this phenomenon is well expressed by hand-dug wells OD101 and OD25, which are characterized by high electrical conductivity 3560 and 7070 μs/cm respectively.

Figure 6.18 shows the relationship between Cl^- concentration, and oxygen isotope composition, which are considered as the most conservative constituent of groundwater. For low Cl^- concentrations, there is a large variation in $\delta^{18}O$, representing the variation of the isotopic composition of recharged water. This plot suggests two processes responsible for the increasing salinity as a measure of Cl^- concentration in groundwater: first, enrichment by evaporation as in the case of samples OD77, OD20, and OD101. Secondly, enrichment due to salts dissolution. In this case, stable isotope concentration didn't change with increasing chloride concentration. This is the case for many groundwater samples (e.g. OD8, OD24, OD25, OD85, and OD112). Most groundwater from the Hammer basin is characterized by a high range of $\delta^{18}O$ isotopes compared to the Quaternary sediment groundwater indicating that evaporation has a significant impact on the variation of isotope signature because of low residence time and shallow water table in the regolith. The outlier wells (broken circled), OD101 is shallow well with EC=3560 μs/cm and OD68 is hand-dug well with EC=787 μs/cm. They are found in the eastern part of Turmi, sited at

mafic gneisses and amphibolite lithologic units. Both have similar $\delta^{18}O$ isotopic value, but variation in salinity and Cl^- concentration may be due to the dissolution of silicate minerals. In addition to this, the difference of the depth has a significant impact in the salinity of groundwater as shallow well trap a significant amount of aquifer material that undergoes mineral dissolution than hand-dug well which is drilled close to dry river channel. Moreover, all wells with negative d-excess (OD34, OD5, OD8, OD40, and OD101) are characterized by higher EC (salinity value); 6040, 3450, 7071, 3450, and 3560μs/cm respectively. The presence of water that is isotopically heavy in $\delta^{18}O$, has a large negative deuterium excess and a relatively low $\delta^2H/\ \delta^{18}O$ slope, provides evidence of recharge water evaporation before infiltration (wood, 2001).

Spatial isotope variation in $\delta^{18}O$ values and EC (salinity) is examined and their variation is observed across groundwater in the Delta. The groundwater in bores intercepting the alluvium aquifer (OD27, OD1, and OD3) had remarkably consistent $\delta^{18}O$ values (Figure 6.20), confirming negligible evaporation from the saturated zone. Figure 6.20 reveals the processes responsible for the origin of salinity in the groundwater different and evaporation is not the sole process. Along cross section A-B, enrichment in isotope $\delta^{18}O$ composition of the well OD38, OD10, and OD103 relative to others is observed. Groundwater well at a lower elevation (OD38) has high salinity and enriched by heavy isotopes. Whereas, the isotope composition of groundwater wells at basement aquifers (OD10, OD94, OD109, OD14, OD17, and OD103) characterized by low salinity and relative enrichment. The relative enrichment was measured at hand-dug well OD10 is due to the fact that the well is constructed at the waddie beds (kaskie) that subjected to evaporation.

To a small extent irrigation return also play a significant role in groundwater salinity in Omo Delta. On the Omo River flood plain indigenous people practices occasional flood recession agriculture, that evaporation of irrigation return has been taking place for a long period. The salinity of soil was checked at the field at different points on the flood plain, and it was measured an average of 11,440 μs/cm with a P^H 8.46 indicating alkaline soil. The hand-dug well (OD25), sited at this plain had a higher EC value of 7,070 μs/cm, indicating that surface evaporation is resulting in the accumulation of halite mineral, an important source of salinization of groundwater in the Delta.

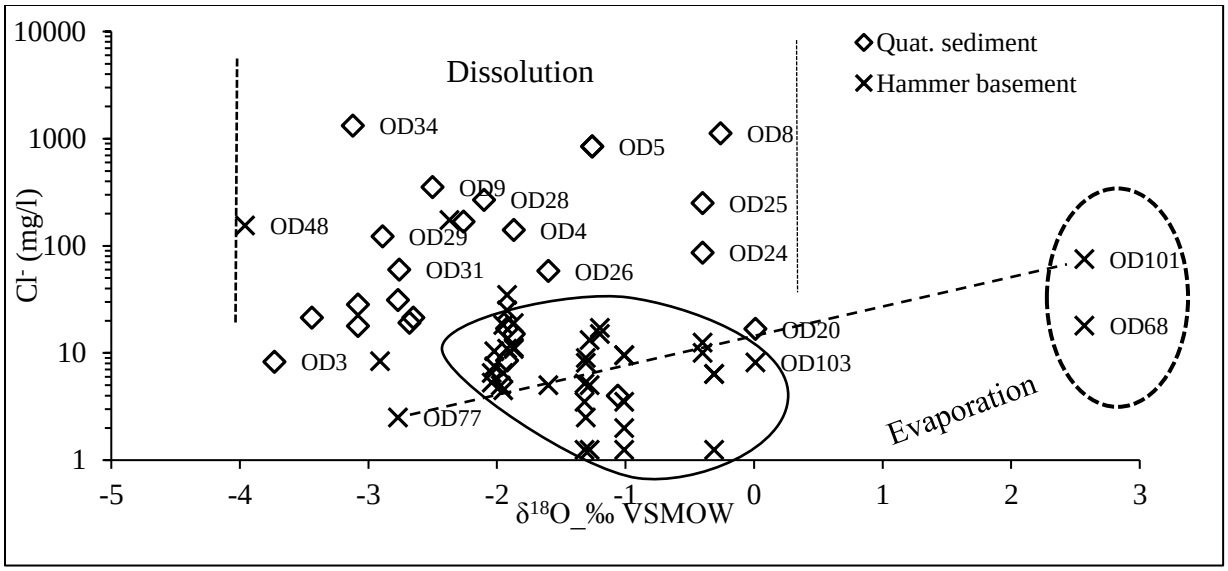

Figure 6.18 Plot of Cl versus $\delta^{18}O$ of groundwater.

6.3.3. Salinity Originated from Clay Membrane Filtration

Salinization of many aquifers is induced by the intrusion of underlying or adjacent saline groundwater or saline-water flow from adjacent or underlying aquifers (Magaritz et al., 1984; Vengosh et al., 1999; Hsissou et al., 1999; Kloppman et al., 2001). In the study area, the thick clay layer in which some wells are sited, act as adsorption surface of dissolved minerals that increase selective adsorption of minerals resulted in the higher salinity. The wells that lie at alluvial fans undergo not as much of evaporation and the clay layer is not thick, e.g. in (Figure 6.19) well (OD31) is characterized by low salinity and depletion of isotopic signature. Groundwater at wells (OD8 and OD34) show comparable EC and isotopic signature indicating that the water comes out from the same aquifer and recharge source. Similarly, the groundwater sample from well OD39 is saline and exhibits relative enrichment with $\delta^{18}O$ isotope. The clay layer and evaporation could be responsible for higher salinity observed in the area. Moreover, the geologic structures (faults) observed may restrict the movement of groundwater and have played a damming effect that the residence time of the groundwater is high and get enough time for mineralization of groundwater in the study area that characterized by high salt content.

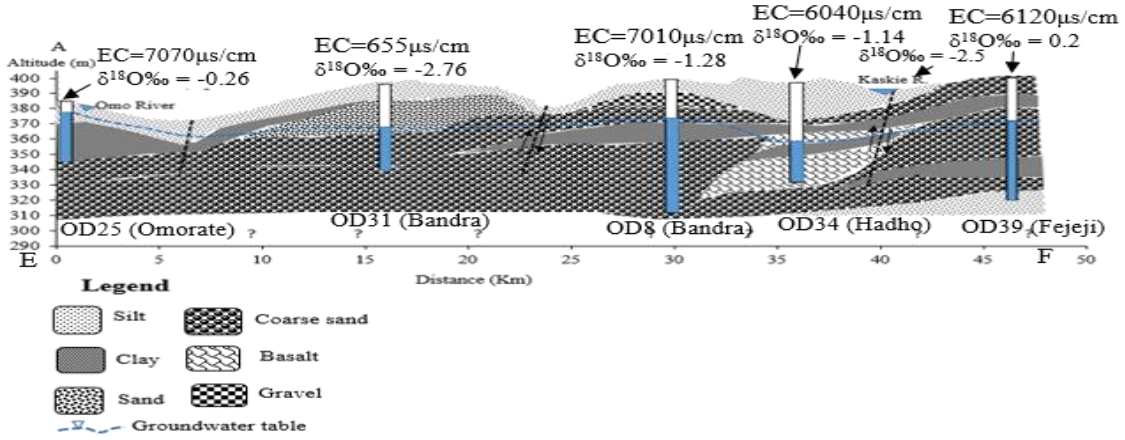

Figure 6.19 Schematic section of salinity as measured of EC, $\delta^{18}O$ and lithologies the wells taped in Omo Delta. Transect section points are shown in figure 6.16.

The geophysical study conducted by Assefa consult (2015), revealed that the saline groundwater in the Omo Delta is encountered when the drilling depth exceeds an average of 80m. The section reveals low resistivity formation at the bottom showing saline water and this appears at shallow depth on the southeastern side and deeper around northwestern (Lokoro and Nakia) VES points (Figure 6.22). The section shows dominantly sediment cover at subsurface but with some intrusive and volcanic rocks in few sites such as Lokoro, Nakiya, and partly in Hadho. The section shows the thickness variation of water-bearing material and even top material thickness variation corresponds to subsurface water quality variation across the area. This generalization is justified by wells like OD39 (91m) and is characterized by high EC (7080µs/cm).

From Figure 6.21, it can be observed that, as we go from alluvial fan apex to alluvial toe, and lacustrine plain the isotopic compositions of groundwater became enriched indicating the groundwater subjected to the evaporation process. The groundwater wells at Nakia kebele, which are sited close to dry river channel characterized by relative enrichment by heavy isotopes compared to those away from it, indicating that dry river channels “Kaskie” are playing a significant role in freshening/recharging the groundwater from occasional flooding during a summer rain.

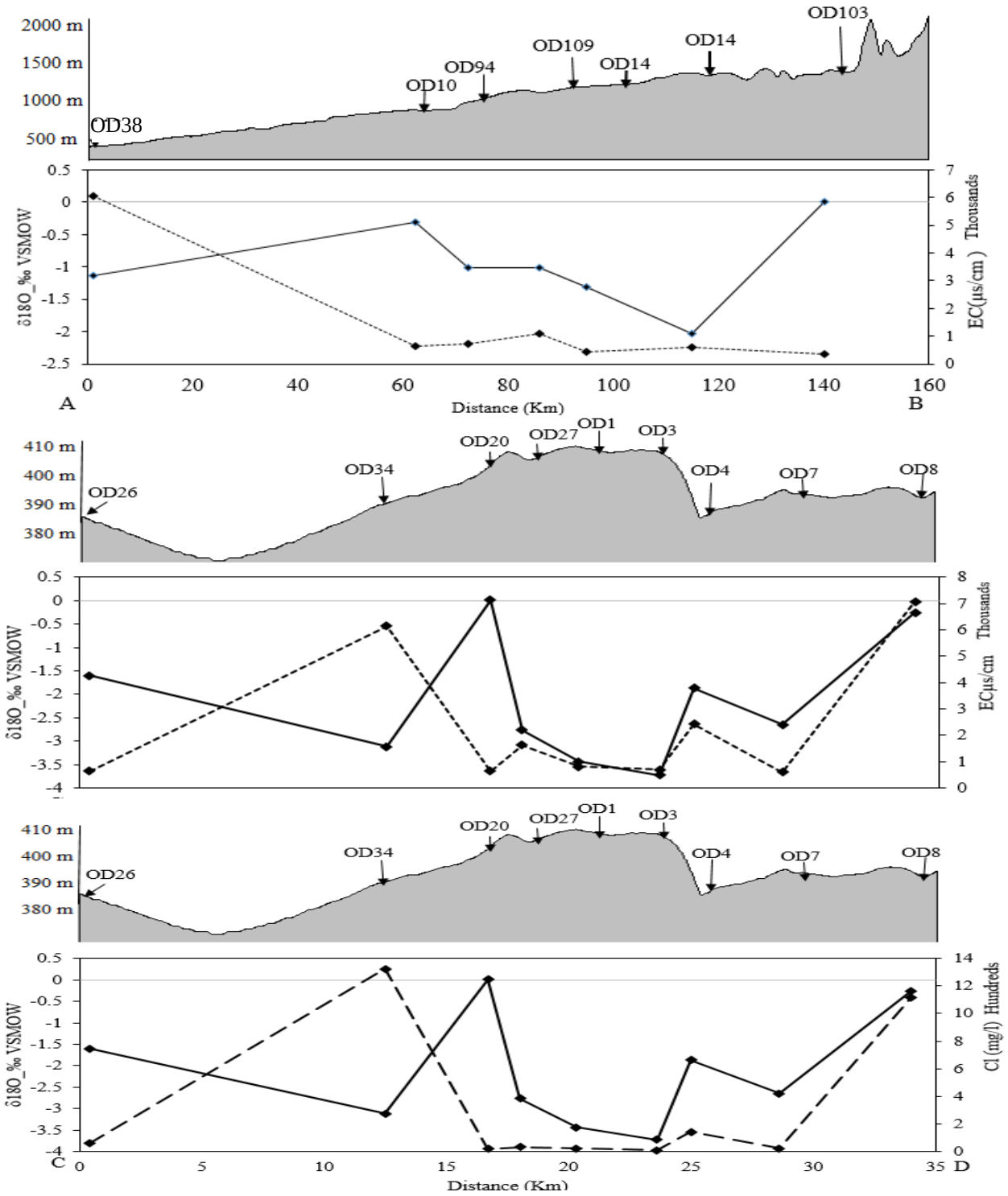

Figure 6.20 Transects along (A–B) and across (C–D) in groundwater flow direction showing a gradual change of isotope composition and salinity (see Fig. 5.3 for transect locations and altitude obtained from the DEM of the study area). The bold lines and dot lines connect the isotope of $\delta^{18}O$ and EC of groundwaters respectively and broken lines are Cl^- ion concentration.

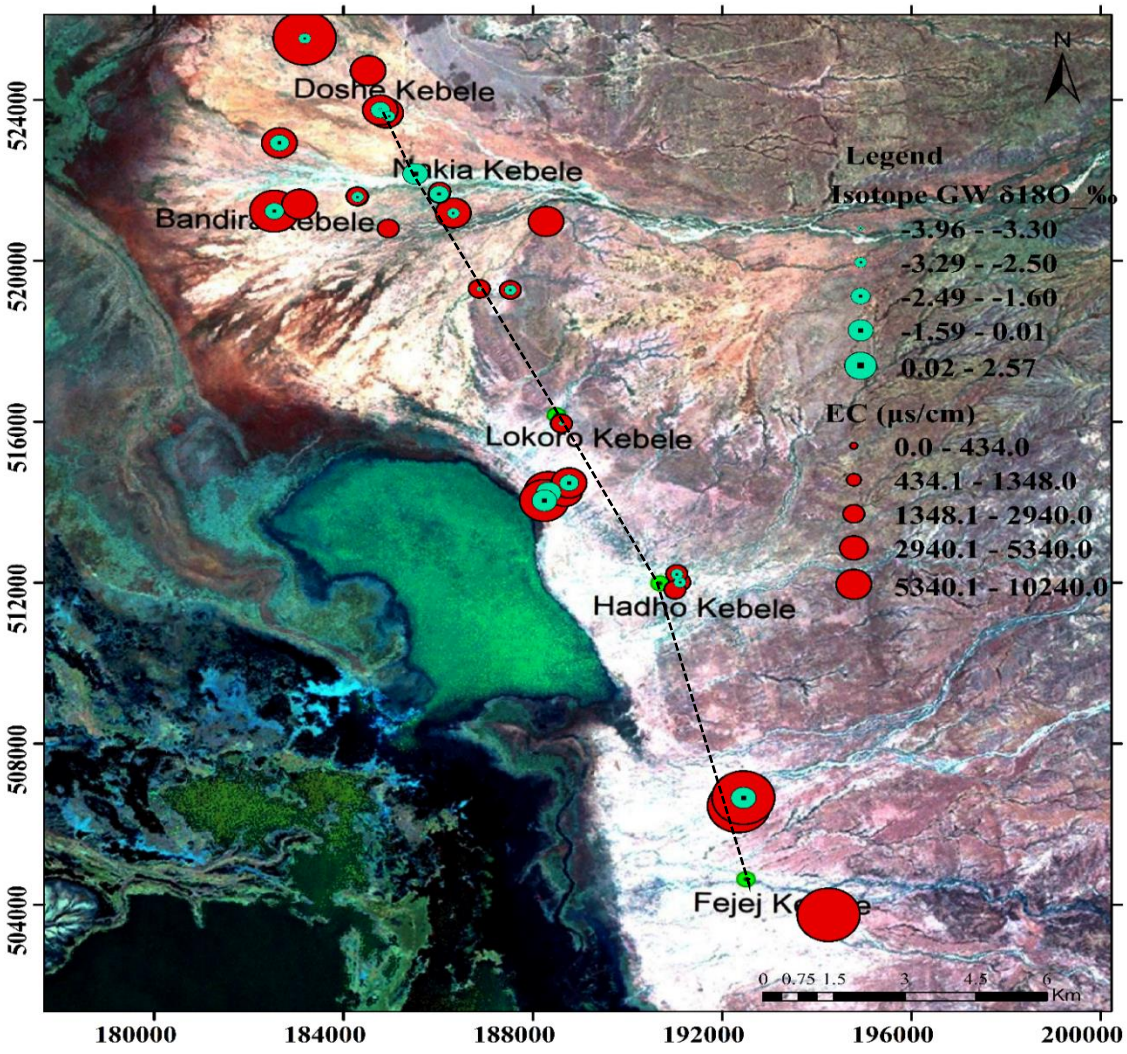

Figure 6.21 EC and $\delta^{18}O$ of groundwater at Omo Delta.

Similarly, the electrical conductivity (EC) of the groundwater shows a significant variation in relation to the alluvial geomorphic feature. As wells away from the alluvial fan apex, the EC/salinity of groundwater is increasing (Figure 6.21). This can be explained by two processes that act in conjunction: the clay layer filtration, this is because samples collected from alluvial fan apex geologically located in sediments that consist of heterogeneous lithology, a poorly sorted mixture of clay, sands, and gravels that easily infiltrated water that reaching the groundwater. In the progression of the groundwater flow along its flow path the permeability of the sediment decreases as sediment size decrease progressively to silt to clay that restricts ease flow of groundwater and increases the accumulation of dissolved ions in the groundwater (Banner et al., 1998, Vengush et al., 2004, Mirzavand et al., 2020).

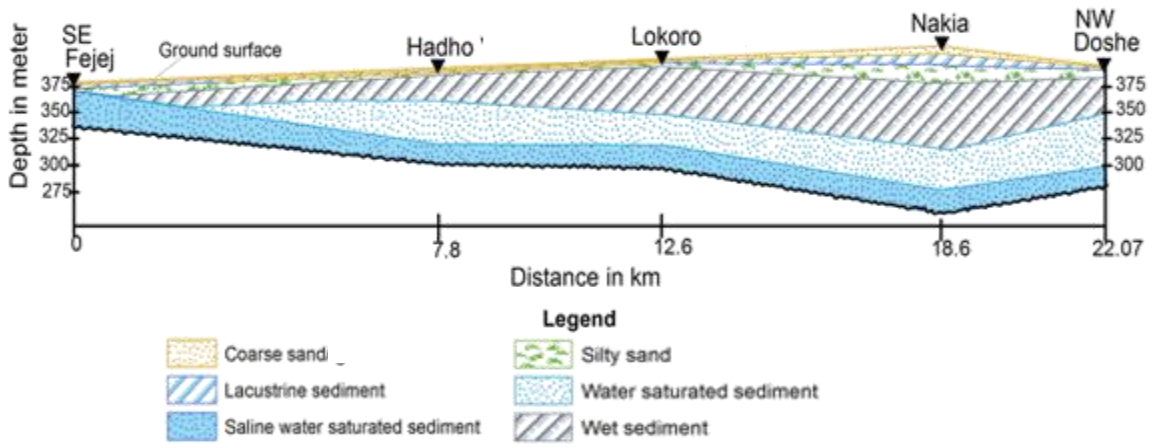

Figure 6.22 Calibrated hydro-geoelectrical section along collinear VES points (Fejej to Doshie). Adapted from (Asseffa conslt. 2017).

The second process is evaporation that resulted in concentrating the infiltrated water. This is typical in the central pain, which is rich in clay soils. Infiltration through this soil is typically slow and strong evapotranspiration forms an intermediate reservoir of saline water in under the saturated zone. Therefore, the combination of evaporation, which resulted in evaporites salt accumulation and clay membrane filtration, explains the down gradient salinity increases.

Around Lokoro kebele (Figure 6.21), one can observe that the groundwater at the top depleted isotope signature and low EC, and sited at dry river channel responsible for freshening. But at the lower part, the wells are saline and the isotope signature also indicates evaporation effect. As we go down to Hado kebele, the salinity of groundwater is less, this is possibly wells are located at an alluvial fan getting its recharge from the nearby river channel. However, the groundwater around Fejej is characterized by high salinity and enriched isotope signature. This can be explained by the saline connate water is found at a shallow depth relative to other areas, as confirmed by geophysical data interpretation in the previous studies.

The geo-electric section constructed for VES at Doshe, Nakia, and Bandra and the resulting fence diagram of the three-section (Figure 6.23) indicating that, the saline groundwater may be found at less than 100, nearly 100, and 140 meters around Bandra, Doshe , and Nakia Kebeles respectively. This shows that saline groundwater is shallow and pinching towards the Lake Turkana.

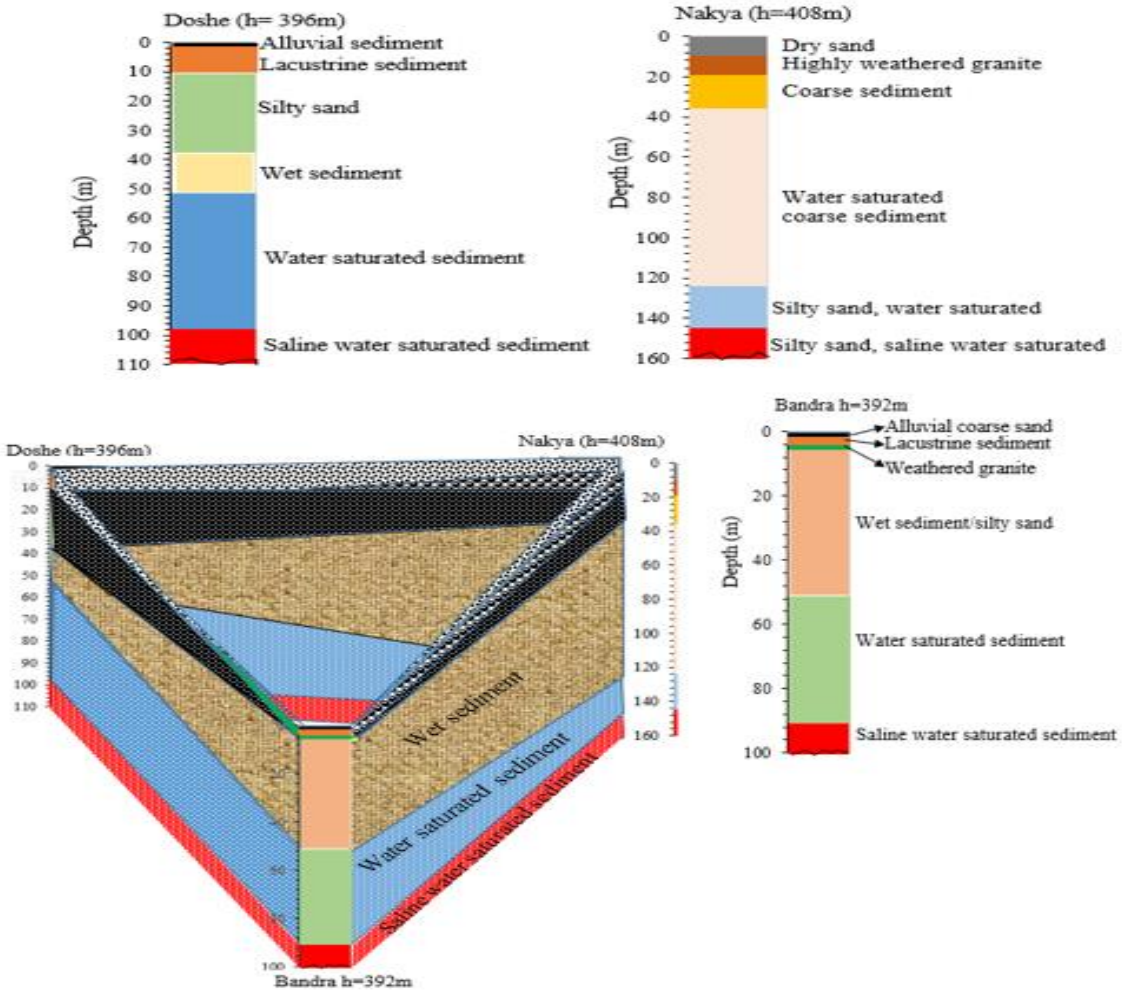

Figure 6.23 Geo-electric section of VES under Doshe, Nakya, and Bandra and the resulting fence diagram (not to scale). The VES points are indicated at figure 6.23.

6.4. Interactions between Surface and Groundwater

Effective use of groundwater and predicting its quality strongly depends on understanding the nature and extent of the surface and groundwater interaction. These two complex systems are highly interrelated and the movement, quality, and use of one body of water affect the other (Kalbus et al., 2006; Khan H. and Khan A., 2019). Large scale to channel scale studies of groundwater-surface water interaction (Kalbus et al., 2006; Antolino, 2011; Coluccio and Morgan, 2018; Zhao et al., 2018; Khan H. and Khan A., 2019) have shed some light on this complex system. Source identification, hydrologic dynamics of interchanges, as well as exchange quality and

quantity are usually the focus areas of investigation (Winter, 1998; Li et al., 2009; Martindale, 2015; Yi et al., 2018).

Various measurement techniques have been deployed to study groundwater and surface water interaction mechanisms at river channels (Scanlon et al., 2002; Kalbus et al., 2006; Zhao et al., 2018). The most frequently used techniques include: environmental isotopic tracers (Kendall and Caldwell, 1998; S. Baskaran et al., 2009; Yang et al., 2012; Peng Yi et al., 2018; and Demlie et al.,2019), hydro-geochemical tracers (Herczeg and Edmunds, 2000; Kalbus et al., 2006; Baker, 2009; Dimova et al., 2013; Shaw et al., 2013), seepage meters (Lee, 1977; Rosenberry, 2008; Santos et al., 2010), temperature sensing (Constantz et al., 2002; Anderson, 2005; Hatch et al., 2006; Kalbus et al., 2006), differential flow gauging (Hatch et al., 2006; Kalbus et al., 2006; McCallum et al., 2012), tracer injection (Davis et al., 1980; Scanlon et al., 2002; Flury and Wai, 2003; Moore, 2004), and piezometeric monitoring of hydrologic parameters (Kelly and Murdoch, 2003). Each method has limitations and uncertainties (Kalbus, 2006), which could be alleviated and minimized by applying a combination of approaches and techniques.

In the Omo Delta area, the groundwater and surface (river) water interactions were mainly recognized by radon-222, isotopes of hydrogen and oxygen, and hydrogeological characteristics along the Omo River. All river samples showed nearly the same characteristics of stable isotopic composition ($\delta^{2}H$ and $\delta^{18}O$) with groundwater from shallow wells close to the river (Figure 6.24). Four river gaining zones, between 0-5, 5-10, 13-15, and 25-30kms in the lacustrine plain were recognized along the river stretch. These were the places, where the river was partially recharged by groundwater as evidenced by the measurements of ^{222}Rn, stable isotopes of hydrogen and oxygen. It can be explained by firstly, the ^{222}Rn concentration in river water sharply increased which could be due to the mixing with the groundwater of high ^{222}Rn concentration. Secondly, the stable isotopic compositions of river water became more depleted which might be due to the mixing with the groundwater of relatively depleted isotopic values.

The study demonstrated that the radon tracer, Radon-222 played a dominant role in the determination of the groundwater discharge to the river. It was mainly because of the inert chemical characteristic of Radon-222 itself, and the quite large concentration difference between the groundwater and surface water, which both made it an ideal tool in the investigation of groundwater and surface water interaction.

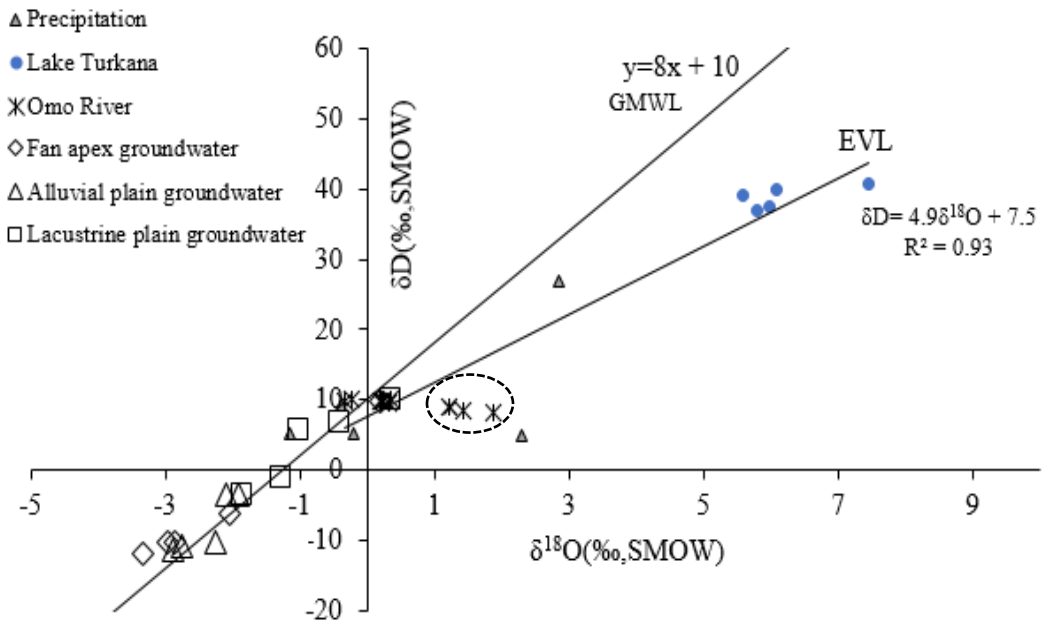

Figure 6.24 The δD and $\delta^{18}O$ distribution of water samples in the Omo Delta. EVL (evaporation water line), and GMWL (Global meteoric water line). The geomorphological location of groundwater present in Figure 5.22.

In the study area, different water types show different isotopic values. The rainwater samples with the isotopic composition (δD: 4.4‰, $\delta^{18}O$: 2.31‰), and plotted on the right of the GMWL, showing a quite enriched distinct characteristic with other samples (Figure 6.24). It might be due to sampling in June (summer in Ethiopia) as discussed in (Gat & Carmi, 1970; Levin, Zipser, & Cerling, 2009) the isotopic composition of Ethiopian meteoric water is characterized by high isotopic composition value. It is observed that lake water samples are more evaporated (range +5.97 to +7.45‰ for $\delta^{18}O$ and +37 to 40.8‰ for $\delta^{2}H$); this is essential because Turkana Lake is a closed basin with no outlet drainage. The Omo River water tends to be isotopically enriched relative to rainfall because of surface water evaporation (Leaney & Herczeg, 2005). The surface water samples plotted in two distinct locations in Figure 6.24. The evaporation line (EVL) can be fitted as $\delta D = 4.88\ \delta^{18}O + 7.48$ with ($R^2 = 0.94$) with river and lake water samples sourced from the Turkana Basin.

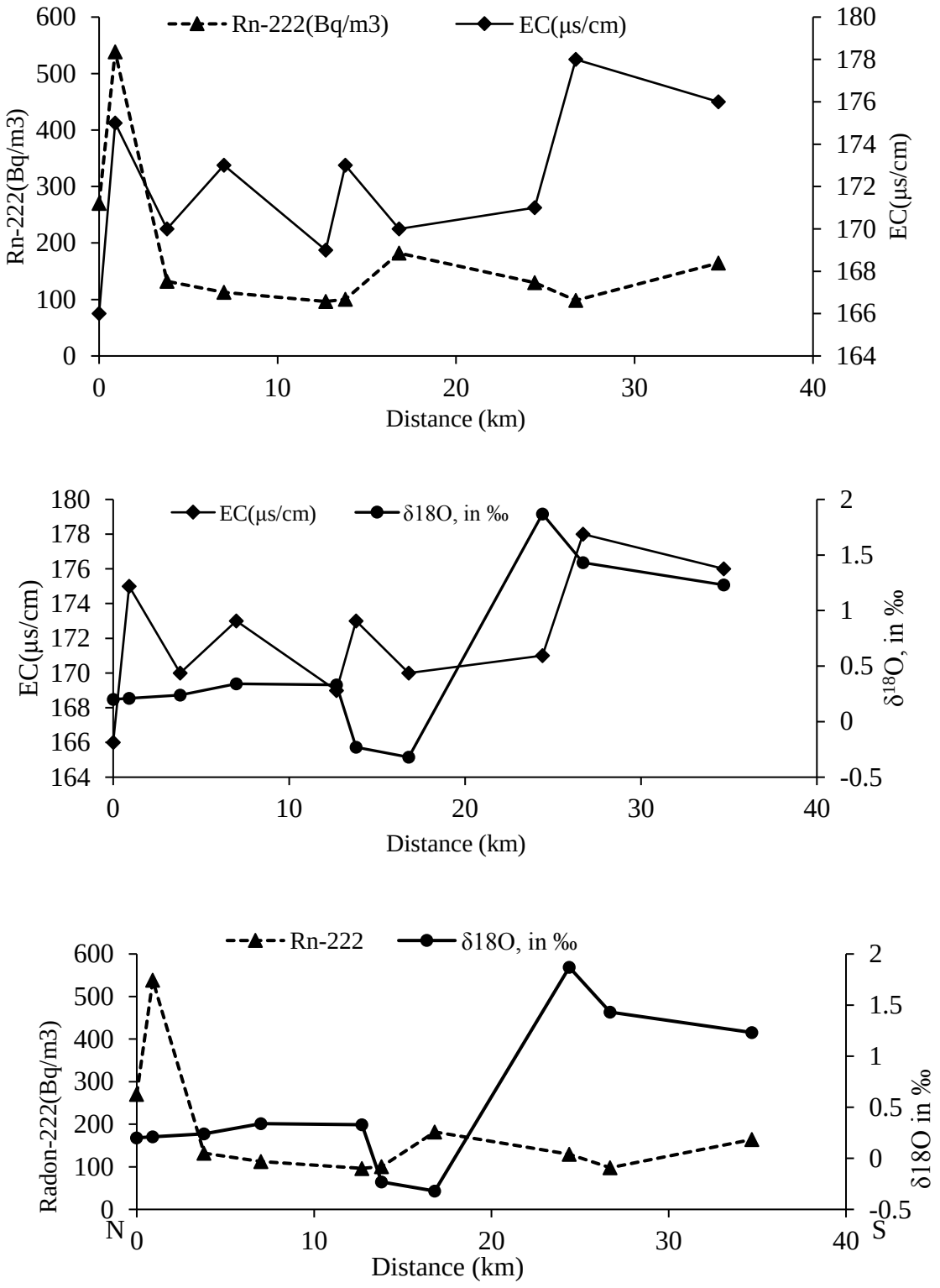

Figure 6.25 The relation between the EC, radon-222, and the stable isotopes ($\delta^{18}O$ in ‰) along Omo River.

The crossing point of EVL and GMWL, which represents the isotopic composition of the water source for surface water, is significantly similar to the rainfall isotopic values, implying that the river water is the result of overland flow during precipitation.

Groundwater wells geographically distributed close to Omo River (circled) have comparable isotopic value to Omo River (Figure 6.24). This shows that there is an interaction between the River and the groundwater wells. The river water samples showed a generally increasing trend (from 8.2‰ to 10‰ for δD, and -0.32‰ to 1.87‰ for δ18O), which indicated an evaporation effect (Clark and Fritz, 1997; Kendall and McDonnell, 1998) because it is flow in a wide bank (34m average) and sinusoidal meander, with a low flow rate of for 218kms before reaching the Delta. A drop in river isotopic values from ~15 km (figure 6.27) could be attributed to the mixing with groundwater discharge featured by more negative isotopic values.

A comparison of the deuterium and chloride data provides a greater understanding of the scale of groundwater-surface water interaction processes (e.g. Leaney & Herczeg, 2005; Mazor, 2004; Taylor et al., 2009). The chloride–deuterium plot (Figure 6.26) suggests three types of groundwater occur in the Omo Delta. These are: (a) shallow groundwater from lacustrine plain close to Omo River, characterized by low chloride and relatively enriched δD that frequently recharged by river water (e.g. OD21, OD26, OD20, OD25, OD63, and OD111); (b) groundwater from an alluvial fan which is sometimes recharged by intermittent rivers ("Kaskie") during rainy seasons. These groundwaters are characterized by low chloride and depleted δD, representing areas that are recharged less frequently by surface water more frequently by direct recharge from storms (e.g. OD30, OD32, and others); and (c) highly saline groundwaters at lacustrine plain with very high chloride and lower δD, that never or rarely receive recharge from surface water (e.g. OD34, OD30, OD5, and OD40). This result also confirms that the interaction between surface and groundwater is taking place at different parts of the Delta differently.

Figure 6.27 shows the relation between the relative distance to surface water (Omo River and Lake Turkana) and the isotopic signature in waters. It can be observed that the groundwater close to Omo River water shared similar isotopic distributions with groundwater (e.g. OD25 and OD24). Moreover, it can be observed that the isotope values of the hand-dug wells (OD25 and OD24) are characterized by similar isotopic values. Whereas, the shallow wells (OD26 and OD23) are close to Omo River show different isotopic value, indicating that the wells recharged from mixed

recharge sources. Well (OD38) found close to Lake Turkana, but its isotope signature is by far different from the Lake. This result also confirms the conclusion made by (Kebede, 2013) that the contribution of groundwater to Lake Turkana is insignificant.

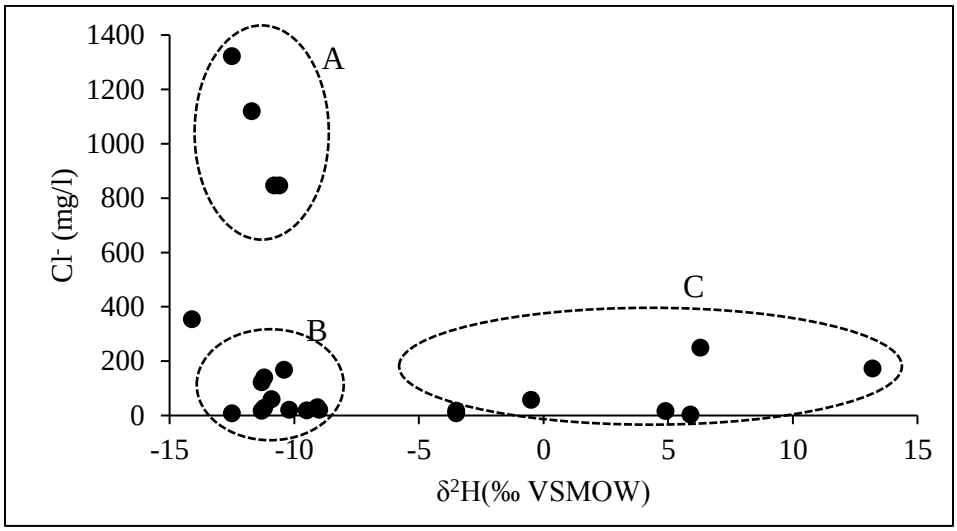

Figure 6.26 Deuterium vs Chloride concentration of groundwater in Omo Delta. Groundwater never recharged by surface water (A), Close to the surface water and recharged from it (C) and groundwater recharged from alluvial and intermittent river (B).

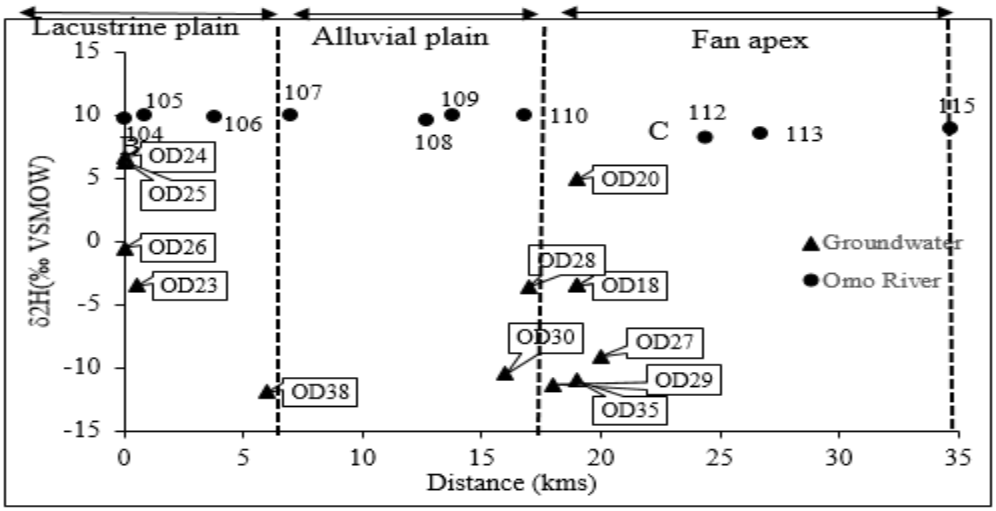

Figure 6.27 The $\delta^{18}O$ and δD changes of water samples along the Omo River and Delta. The distance was measured relative to surface water along the groundwater flow direction.

6.5. Groundwater Flow mechanisms, Salinity and Hydraulic Head

Groundwater flow at local, intermediate, and regional scale along its way from recharge to discharge area is determined by topography and hydraulic characteristics of underlying rocks (Huang & Chen, 2012; Ayenew, 2016; Jamila et al., 2017). Locating groundwater of the best quality and quantity requires understanding groundwater flow patterns (Toth, 1984; Kebede et al., 2007; Flurlong et al., 2011). Lowland aquifers are highly dependent on the regional flow and important for the water supply of the arid and semi-arid regions in which the direct recharge from precipitation is scant (Bisson and Lehr, 2004). Studying the hydrochemical pattern and environmental isotopes can be used to characterize the groundwater flow patterns (Ophori and Toth 1989, Kebede et al., 2005, Kebede, 2013).

The Omo Delta and its surroundings are characterized by complex geologic settings as discussed in section 2.4.1, which is comprised of metamorphic rocks of various grade, geologic structures with different orientations and propagation. Locating groundwater of good quality and quantity is the main concern of hydrogeological experts, especially in the Delta part in which the quality of groundwater is highly affected by salinization. A detailed study dealing with groundwater recharge and flow system is scared in the region. Specifically, hydraulic characteristics of a particular rock and its spatial association with the other units are not known. It is also difficult to establish these hydrogeological parameters with the methods that depend on well data due to the limited and incomplete water well information in the area. Therefore, in the study area, it is challenging to establish the nature of groundwater flow pattern using methods like flow modeling or based on existing groundwater levels. Back (1960, 1966) defines the concept of hydrochemical facies, placing the geochemical observations in the context of groundwater flow in aquifers of relatively homogenous hydrologic and mineralogic properties. The regional variation in the chemical composition of groundwater along the groundwater flow paths resulted from the geochemical reactions in the direction of flow (Glynn & Plummer, 2005).

As discussed in section 5.2.2 and 6.2 there is no significant signature of geochemical evolution that indicates the presence of continuous or regional flow system along N-S and NE-SW hypothetical transects. The isotopic analysis under the section (Figure 6.30) also shows that relatively depleted groundwater at Hammer basement and enriched groundwater at the Quaternary

sediments reasonably indicates the absence of flow continuity between the two regions. Both hydrochemical and isotope techniques indicate the dominance of local recharge and flow systems. A water table contour map is a very important tool in groundwater management as one can derive from it the gradient and the direction of the groundwater flow and possible indicator of aquifer structure (Heath, 1983; Ismail et al., 2010; Kebede et al., 2016). A water table contour map or a contour map of the potentiometric surface of an aquifer is a graphic representation of the hydraulic gradient of the water table or potentiometric surface. The hydraulic gradients, which can be directly derived from these maps, are the basis for calculating the rate of groundwater flow through cross-sections (De Ridder, 1980; Hiscock, 2005; Naus et al., 2019).

The resulting piezometric map (Figure 6.28) indicates a steep hydraulic gradient in the northern and northeastern parts of the basin and gentle in the western and southern parts. Therefore, the general direction of groundwater movement throughout most of the Lower Omo Basin is from the North and Northeast to the South and Southwest.

In this study, isotope data constitute an independent indicator of the attribution of water to an aquifer level. For example, in the Hammer basement aquifer system (wells at Turmi with the depth of 46 and 82.5 m) are enriched in isotopes (Figure 6.29) reflecting the average value of precipitation ($\delta^{18}O$ =-0.21‰) indicating that at this area aquifer is a single layer of weathered regoliths and fractures (dot circle). Whereas, the isotopic signature of water from the Delta aquifer system (Quaternary sediments) are more erratic as manifested variation in their salinity. Water from Hand-dug wells, Shallow wells, and deep wells have relatively the same isotopic signature (bold circled) indicating that interconnection of the aquifer system.

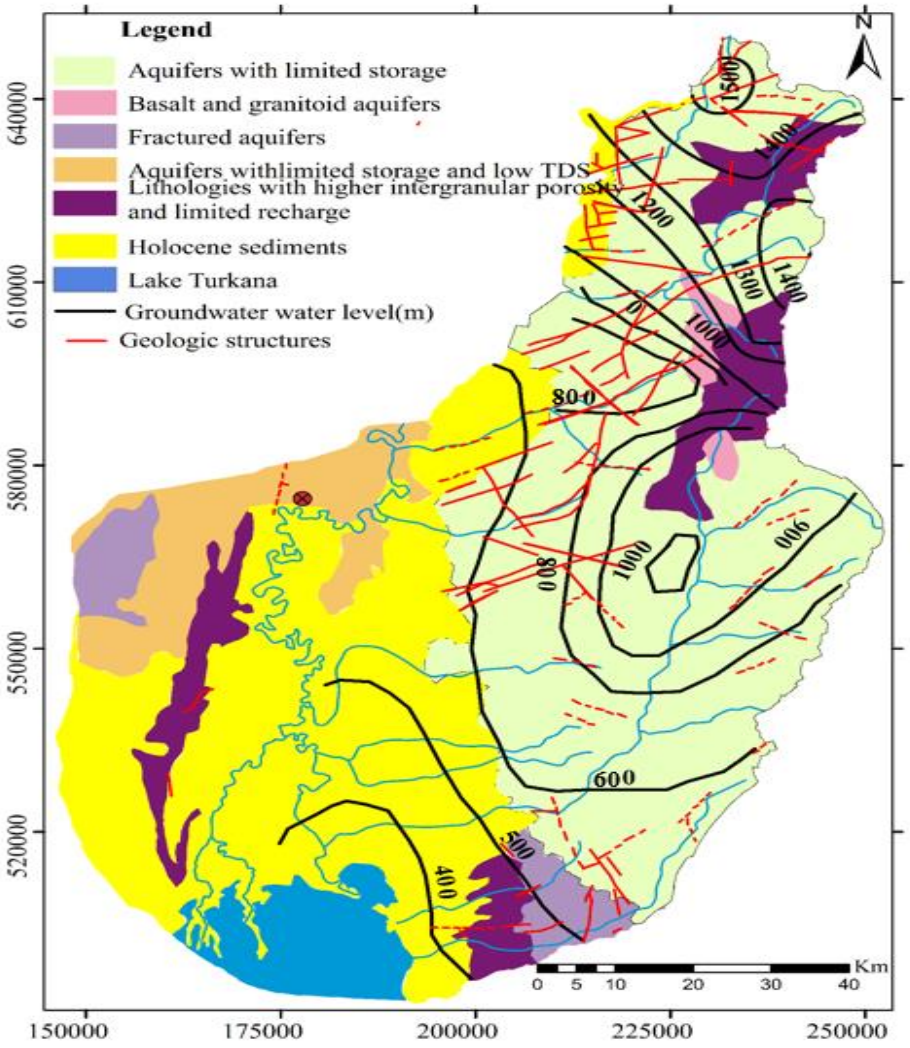

Figure 6.28 Water level map of the study area.

In the Quaternary sediment aquifer system, as wells depth increases, the isotope signature of groundwater from this aquifer system exhibit large variation indicating a multilayer aquifer system. The possible piezometric level of groundwater is varied in the Omo Delta aquifer system depends on the structural and depositional complexities of the Delta environment.

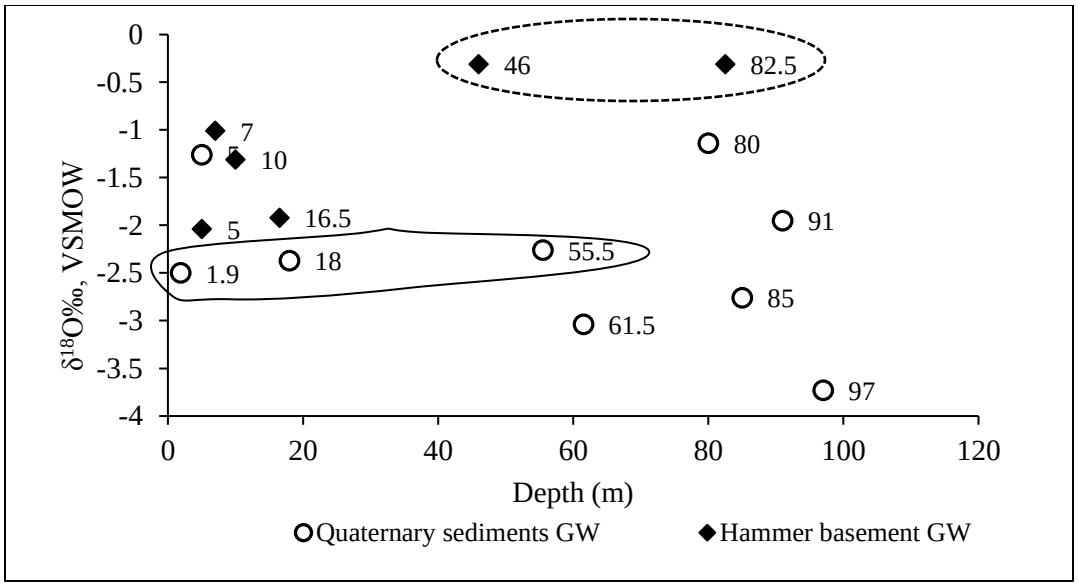

Figure 6.29 Relation between the isotope signature $\delta^{18}O‰$ and depth of the well.

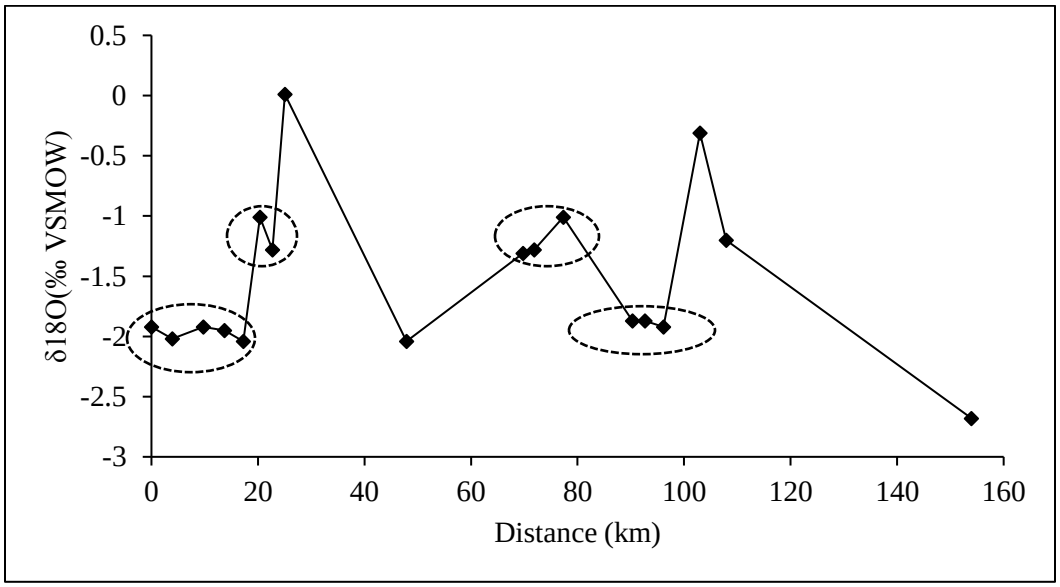

Figure 6.30 The spatial variation of isotope along the N-S groundwater flow direction. The section line is drawn in Figure 5.11

Figure 6.30 also shows that the isotopic signatures around Jinka (0-20kms) are similar indicating local flow system is prevailed at recharge areas. Similar observation can be made around Turmi (80-100kms). Whereas, in the other part of flow direction the isotope signature are different that indicating there is no dominant type of flow system in the region.

6.6. Groundwater Quality in the Study Area

6.6.1. General

The concentration of solutes and gases dissolved in the water as well as the matter suspended in and floating on the water determine the quality of water. Water quality is a result of the natural chemical and physical state of the water as well as any alterations that may have followed as a consequence of human activity (Fetter, 2001; WHO, 2008). The usefulness of water for a particular purpose is determined by its quality.

To specify the limitations of chemical and biological ingredients water quality standards are developed by scientists and provide basic scientific information about the effects of water pollutants on specific water use. They also describe water quality requirements for protecting and maintaining individual use. Water quality criteria are based on variables that characterize the quality of water and/or the quality of the suspended particulate matter, the bottom sediment, and the biota. Various water quality standards set a maximum limit for the concentration of a substance in a specific medium (i.e. sediment, water, or biota) which will be unsafe when the specific medium is used constantly for a single, particular purpose.

6.6.2. Groundwater Quality for Drinking Purposes

Water is vital to endure life, and a satisfactory (safe, adequate, and accessible) supply must be offered to all. Different Guidelines defines the safe drinking water as does not cause any substantial threat to health over a lifetime of consumption, as well as different sensitivities that may occur between life stages (WHO, 2008). Many consumers in developing countries like the study area utilize groundwater directly pumped from public wells without any treatment. Therefore, groundwater standards (guidelines) are especially important for evaluating groundwater quality of wells prior to consumption. Performing complete analysis of water from public groundwater wells and confirming that it is to standard before time as well is put into service should be mandatory. Periodical monitoring thereafter is also very important. During this study, the investigator found that, among the wells that are drilled for water supply, only 42% have water quality test report during the completion of drilling. The local woreda and Zone water development offices do not monitor periodical quality check-up. Many water schemes are developed by NGOs working on

relief and sustainable developments. Their main concern is the only provision of water for the needy, but quality issues are secondary, that is why many wells drilled in the Delta have abandoned only after the inauguration and the community return to the unsafe source due to their objectionable taste due to salinity.

Table 6-1 presents a comparison of the results of the physicochemical analysis of groundwater of the study area with the standard guideline values recommended by the World Health Organization (WHO, 2008) for drinking water purposes.

It is observed from the Table 6-1 that 17.1 and 15.8% of the samples for the Quaternary sediment and Hammer basement aquifers respectively show TDS values above the guideline value of 500mg/l while 34.3, 25.7, 17.1 and 25.7% of samples in the Quaternary sediment aquifer are characterized by Na^+, Cl^-, F^- and NO_3^- respectively. In Hammer basement aquifer groundwater, though the number of wells is twice as much as at the Quaternary sediment, the highest outlier values are observed in two wells. But the mean values are well below the limit of WHO indicating that most Basement aquifer groundwater is safe for drinking compared to the Quaternary sediment groundwater.

Nitrate concentration is higher in most wells that are sited at Delta. It reaches the groundwater as the result of agricultural activity (including the excess application of inorganic nitrogenous fertilizers and manures), from wastewater disposal and the oxidation of nitrogenous waste products in human and animal excreta, and including septic tanks (WHO, 2008). But in the case of Omo Delta, agricultural activity in the area of those wells that show high nitrate concentration is nonexistence rather during the field survey it is observed that a large number of cattle and herds of goats are residing close to these wells so that their manures can be the possible sources for the pollution.

Table 6-1 Statistical values of groundwater quality (zero value represent not detected).

Quaternary sediment groundwater							
Water Quality index	max	min	Range	Mean	WHO(2008)guideline (mg/l)	No. of Samples above the guideline value	% above the guideline value
TDS	6656	35.4	6620.6	1376.9	500	6	17.1
Na	1645.3	16.8	1628.5	313.2	200	12	34.3
Cl	1583.9	1.3	1582.6	272.4	250	9	25.7
F	5.9	0	5.9	1.2	1.5	6	17.1
SO4	131.2	0	131.2	44.3	250	0	0
NO3	344	0.9	343.1	33.5	25	9	25.7
PH	9.1	6.9	2.1	7.9	6.5-8.5	6	17.1
Hammer basement groundwater							
TDS	4100	28.5	4071.5	375.8	500	12	15.8
Na	120	4	116	37.2	200	0	0
Cl	155	1	154	10.9	250	0	0
F	3.5	0	3.5	0.8	1.5	2	2.6
SO4	560	0	560	34.1	250	2	2.6
NO3	16.5	0	16.5	2.5	25	0	0
PH	9.25	5.9	3.35	7.6	6.5-8.5	8	10.5

The World Health Organization recommends a maximum fluoride concentration of 1.5 mg/l; in case of hot waters (above 25 °C) or tropical countries with a high daily intake of drinking water, the value decreases to 0.7 mg/l (WHO 2004). High concentrations in fluoride affect human health. Fluoride may give rise to mild dental fluorosis at drinking-water concentrations between 0.9 and 1.2 mg/l (Bonetto et al., 2015). This is particularly true in warmer areas, where dental fluorosis occurs at low concentrations in the drinking water because of the greater amounts of water consumed (Office of Drinking Water 1985; WHO 1984). Fluoride can also have more serious effects on skeletal tissues (bones and teeth) in case of long-term ingestion, particularly, if drinking water contains 3–6 mg of fluoride per liter (WHO 1984). In the study area, tooth mottling is a common observation. 17.1 % of the samples in the Omo Delta show values exceeding the WHO maximum acceptable concentration of 1.5 mg/l. The 85.7% wells with high concentration of fluoride (>1.5 mg/l) have high TDS value ranged from 1254 to 6656mg/l.

6.6.3. Groundwater Quality for Irrigation Purposes

Irrigation water comprises different mixture of naturally occurring salts. Irrigated soils with such kind water will have a similar mix but generally at a higher concentration than in the applied water. The extent to which the salts accumulate in the soil will depend upon the irrigation management, the adequacy of drainage, and irrigation water quality. The presence of excessive salts in the soil results in loss of yield. Water with good to excellent quality used for irrigation purpose is unlikely to impose severe salinity constraints. When water quality is poor, controlling salinity become a difficult task. Increased salinity will resulted in accumulation of salts in root zone that affect the yields. Therefore, great care must be taken to leach out these salts from the root zone.

Irrigation agriculture is a common practice in most Deltas in the word, which are highly populated regions in the world (Al-agha et al., 2015). In the study area, the surface water is scarce except the Omo River. Therefore, using the groundwater as an alternative source for irrigation is expected in the near feature. In this study, an attempt has been made to determine the quality of groundwater for irrigation purposes from available data. Accordingly, SAR (Sodium Absorption Ratio) and percentage of sodium (Na %) and magnesium hazard (Mg %) are used for the groundwater quality assessment for irrigation purposes.

Sodium Adsorption Ratio (SAR) characterizes soil sodicity, which is a widely accepted index. It defines the ratio of sodium to calcium and magnesium in soil solution. The equation used to calculate Sodium Adsorption Ratio is expressed below, the unit of concentrations expressed in milliequivalents per liter (meq/L) analyzed from a saturated paste soil extract.

$$SAR = \frac{[Na^{+}]}{[Ca^{2+} + Mg^{2+}]^{0.5}}$$

Where the unit of concentration of the cations is expressed in meq/L.

The sodium adsorption ratio (SAR) parameter evaluates the sodium hazard in the soil in relation to magnesium and calcium concentrations. SAR values show significant variation between the Quaternary sediment (Delta aquifer) and Basement aquifer groundwaters. High range from 215.93 to 0.934 values exhibited in the quaternary sediment. Values greater than 2.0 indicate groundwater is unsuitable for irrigation purposes (Vasanthaviger et al. 2010, Ayuba et al., 2013). Only 11.4% of groundwater samples from Omo sediment aquifers are suitable for irrigation purposes. These

samples are obtained from wells that are close to "kaskie" (waddie beds). Whereas in hammer basement aquifers 59.7% of groundwater samples are suitable for irrigation purposes. Their value range from 6.043 to 0.189. According to the U. S. Salinity diagram classification of irrigation water (USLL, 1954), the groundwaters fall in the field of C1-S1, C2-S1 and C3-S1 (figure 6.33) indicating a low to high salinity hazard and low sodium (alkalinity) hazard.

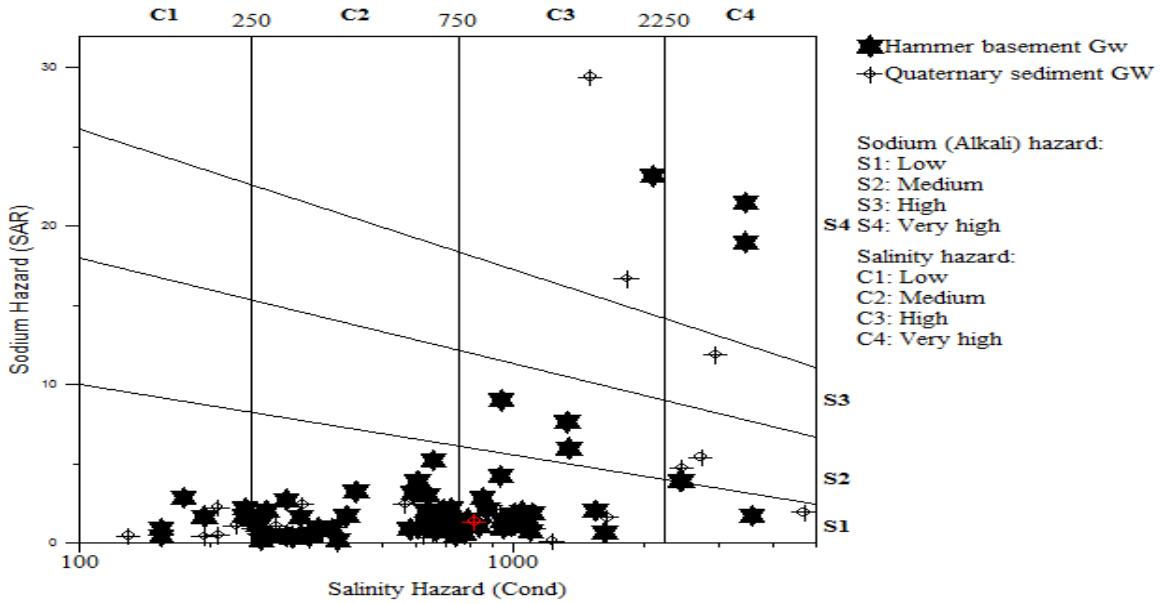

Figure 6.31 U.S. Salinity Classification of Groundwater for Irrigation (USLL, 1954) for the Study Area.

Sodium Percentage (Na %)

Sodium percentage (Na%) or Exchangeable Sodium Percentage (ESP) is the ratio of Na^+ to Ca^{2+}, Mg^{2+}, Na^+, and K^+ according to the following equation.

$$ESP = \frac{[Na+]}{[Ca^{2+} + Mg^{2+} + Na^{+} + K^{+}]}$$

Where the concentration of the cations is expressed in meq/l.

Sodium in soils is considered vital for determining groundwater suitability for irrigation purposes because sodium reacts with soil to reduce its permeability and support little or no growth (Vasanthaviger et al. 2010). Sodium salts in the soil, besides affecting the growth of plants directly, also affect soil structure, permeability, and aeration; which directly affect plant growth (Singh et

al. 2008). The Na% in the Delta sediment aquifer ranged from 99.14 to 11.69% and in Hammer sediment aquifers the Na% is ranged from 77.01 to 4.86%. Na% greater than 35% in groundwater is unsuitable for irrigation (Vasanthaviger et al. 2010). Accordingly, 14.3 and 67.5% of groundwater samples from the Quaternary sediment and Hammer basement are suitable for irrigation purposes (Annex 2).

Magnesium Hazard (MH) %

Magnesium hazard defines the relationship between magnesium and calcium concentration in groundwater (Ayuba et al., 2013). The MH% in the Delta sediment aquifer ranged from 76.92 to 6.49% and in Hammer sediment aquifers it ranged from 89.69 to 3.57%. MH % greater than 50% in groundwater is unsuitable for irrigation (Kacmaz and Nakoman, 2010). Accordingly, 40 and 76.3% of groundwater samples from the Quaternary sediment and Hammer basement are suitable for irrigation purposes (Annex 2).

From the discussion made in the previous section, it is possible to observe that groundwater in Omo Delta is challenged by high salt content and this saline nature also limits its use for both drinking and irrigation purposes. Therefore, the future plan of starting the mechanized agricultural activities in the area should consider conjunctive use of both surface and groundwater resources to minimize the problems arises from the use of saline groundwater for irrigation purposes.

6.7. Groundwater Management Challenges and Implication of the Work for Water Management

Within the concept of groundwater management, aspects related to quantity and quality of the resource may be distinguished. When water quantity is a primary concern, the quality governance issues is often not of primary interest. This explains the importance of the groundwater quality protection issues certainly growing. Indeed, in semi-arid and arid countries where recharge is scarce, eventually quantity needs are satisfied and quality issues become progressively more significant (FAO, 2016). Compared to water quantity, the water quality concern is under poor development. This is due to the great number of components and factors involved in water quality assessment, as well as to inconsistencies in the knowledge base, which is therefore often subject to interpretation.

For a correct evaluation of groundwater resources, a validated conceptual model on how the aquifer system functions are needed, including mass transport as the basis for water quality assessment. However, the information regarding aquifer recharge is very important, and it is often rather inexact. These are key issues for groundwater management that must be addressed to control groundwater development coherently and consistently.

As groundwater mostly used for drinking-water supply, quality issues are the backbone of management. This happens in relatively rich urban areas, and good quality groundwater without further treatment is wanted for urban supply. In poor areas, the lack of infrastructure makes quantity issues the main concern for management, except if serious threats to health appear due to the presence of natural hazardous substances and serious pollution. Except in certain coastal aquifers, peri-urban areas that depend on local water resources for human supply, intensively irrigated agricultural areas, and in general where natural groundwater contains solutes recognized as a health problem, such as arsenic (As) and fluoride (F) the water quality issues are often of secondary importance in aquifer governance (Mabrouk et al.,2013; Vengosh, 2014).

As the result of past action, the groundwater quality deterioration is a worldwide and growing concern. In addition, it is not easy to show groundwater quality evolution, worldwide or at a regional level, not only due to data scarcity but also to the difficulty of using an index that is able to reflect the different points of view. The evolution of a chemical characteristic at a given point does not always show the general trends. The chemical groundwater composition of recent groundwater is the result of climate–soil processes and lithological influences. These well-known processes (Custodio and Llamas, 1976; Appelo and Postma, 1993) control groundwater quality baseline or background (Custodio and Manzano, 2007; Edmunds and Shand, 2008).

Management of groundwater natural quality refers to management under conditions of poor quality and aims to preserve quality when there are threats from poor natural quality around, above, or below the aquifer. Thus, the first step for management is understanding the origin of the natural quality of the aquifer under consideration and of the other related surface and groundwater bodies. When there is some aquifer development-taking place, then the aquifer is disturbed, and this changes the flow pattern locally in small extractions, and affects the whole aquifer system for intensive development. It influences the groundwater displacement inside the aquifer through a sluggish but it taking place in sustained process. Besides, wells and other groundwater abstraction

works mix water from different layers. Their drilling and construction activities may disturb natural flow by introducing by-passes, when low permeability layers are penetrated without carefully grouting the space between the hole and the casing.

Delineation of the origin of the salinity problem is crucial for model prediction and thus water management and remediation (Vengosh, 2005). Proper management of available groundwater reserves is impossible without knowledge of the spatial distribution of fresh and saline groundwater and the processes that determine the evolution of salinity.

Groundwater salinity is becoming a serious water quality problem in areas that are subjected to intensive water abstraction in the coastal environment. A different situation causes aquifer salinity in arid areas is due to the existence of brackish to saline water held in the often-thick unsaturated zones. This water is the result of intensive evapo-concentration (water salinity increase due to evaporation and transpiration) of atmospheric salt deposition by highly efficient rainfall use by native vegetation.

Brackish and saline groundwater is relatively frequent in deep aquifers, especially in slowly renovating, confined aquifers, and as a consequence of recharge in arid environments. In coastal areas, saline and brackish groundwater is the result of natural seawater intrusion in permeable, thick and relatively poorly recharged aquifers, and the mixing with fresh groundwater in upper layers. In Delta environments and large saline lakes, periodical land flooding during heavy storms resulted in high salinity.

Understanding the origin of the natural quality of the aquifer under consideration, related surface water and groundwater resources are important to understand the origin of the natural quality problems arises from the natural process. In Omo Delta, due to excessive groundwater salinity, 50% of the wells drilled in this hydrogeologic feature are abandoned. (Figure 6.32). Unlike in other areas with significant oil, gas, or water resources. Investigations of groundwater in the Omo Delta area have been sporadic and the state of knowledge about this Deltaic aquifer relies mostly on the mapping of surficial geology and a limited number of groundwater tube wells.

Omo Basin in general and Lower Omo Basin, in particular, is considered as the development corridor for extensive irrigation activity have taking place and planned. The Ethiopian Government's announcement in early 2011 of large-scale commercial irrigation development in

the Lower Omo increased the potential for water abstraction from the Omo by a large margin (Avery et al., 2018). The "land investment deals" reported recent expectations of irrigation development in the Omo Basin (Figure 6.32); a very larger area of land under irrigation was now in prospect.

This kind of economic activity induces two kinds of changes in groundwater quality: introducing contaminants (chemical fertilizers, pesticides, and herbicides), which cause pollution and modifying recharge (where increase water table), as well as the flow and mass-transport characteristics of aquifers in the Delta groundwater system. In this case, understanding the cause of the current problem of groundwater salinity is dually important to tackle the expected salinity due to the change of land and water use in the Delta and its environs. Therefore, understanding the origin of salinity in the current geo-hydrologic condition can be used as a bench-mark to understand the functioning of the aquifer system in this dynamic water-land interface region.

The main aquifer is in the Delta formed by Quaternary deposits. The variation of the hydraulic parameters and salinity of the aquifer to the fact that these deposits took place under different deltaic conditions. These deposits represent different aggradations and degradation phases that were usually accompanied by lake level changes (Butzer, 1972). Omo Delta is characterized by spatially varying hydraulic conductivity for different locations and layers, which needs to be taken into account for a more accurate representation of the study area. There were not any studies with estimations of the hydraulic parameters for the overlying clay layer in literature.

In this study, attempts were made to investigate the origin of groundwater salinity, the interaction between the surface and groundwater in the area, the role of micro-geomorphologic features in the groundwater quality, the distribution of saline groundwater spatially and vertically based on available data, and a potential source of recharge and flow direction of groundwater in the Delta.

As the significance of groundwater as resources in the water supply system in the study area and the negative effect of salinization on their quality call for a meaningful approach to the study of groundwater salinity of the Delta. Earlier authors (Kebede, 2009; WAPCOS, 2007; Wood et.al. 2004) have mentioned the occurrence of saline groundwater. However, the questions of origin(s), the mechanism(s) that redistribute the saline groundwater, its lateral and vertical distribution, and how geomorphology of the area affects the distribution of salinity in groundwater were not fully

understood. This study with help of geochemical and stable water isotopic signatures tools, come up with a vital understanding of the source of salinity, their mechanism of distribution, surficial and vertical distributions in different geological settings. This investigation is used as a benchmark for this area regarding groundwater quality management in current and feature as the study of this type in the region.

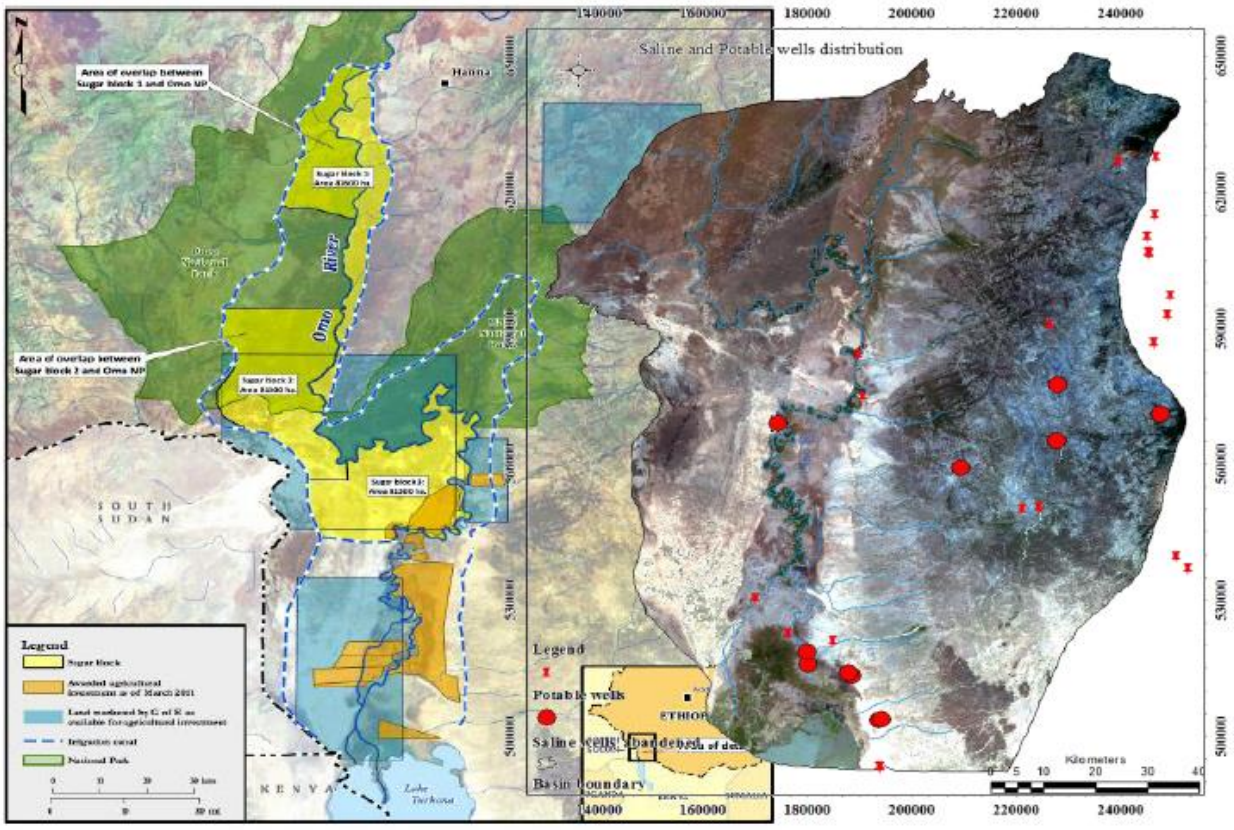

Figure 6.32 Lower Omo planned agricultural development (Source: Avery, 2012)(left). Distribution of saline (abandened) and potable wells in the study area (right).

7. CONCLUSIONS AND RECOMMENDATIOS

7.1. Conclusions

Omo River, the main drainage for the southwestern Ethiopian highlands, originates from western Ethiopian Plateau. It flows southward through a deep gorge to the Lower Omo Valley, a broad tectonic depression, and finally into Lake Turkana. The study area (Omo Delta and its environs) is located in Southwestern Ethiopia and covers 8,291 km^2 bounded by 489486N and 650706N latitude and 161659E and 252961E longitude. Omo Delta is located at the junction of the Omo River with Lake Turkana at the borders of Ethiopia, Kenya, and South Sudan. It has a total area of about 1600 square kilometers.

The main objective of this work is to characterize the source of salinity and mechanism(s) of salinization in the Omo Delta groundwater giving special emphasis on characterizing various morphological units and depositional environments recognized in the area and their implication on groundwater salinity. To achieve this objective converging evidences from the conventional hydrogeological investigation, litho-hydrostratigraphic relationships, water chemistry, isotope hydrology, and Radon (Rn-222) were used to set up the hydro-chemical framework of the study area.

Based on the evidence from the conventional hydrogeological investigation and litho-hydrostratigraphy, the main aquifer is in the Delta formed by Quaternary deposits. The variation of the hydraulic parameters for different locations and layers and salinity of the aquifer to the fact that these deposits took place under different deltaic conditions. These deposits represent different aggradations and degradation phases that were usually accompanied by lake level changes. The general direction of groundwater movement throughout most of the Lower Omo Basin is from the north and northeast to the south and southwest. The upper basement aquifers are unconfined whereas the lower Delta aquifer is confined. Groundwater movement and recharge is highly dependent on geomorphic features and depositional environments. Groundwater that is close to surface water sources (River and Wadies) is fresh relative to other farther away from it.

Different salinity scenarios characterize geomorphic features, like alluvial fans; the fan apex is characterized by fresh groundwater compared to fan toe, which is more saline. Due to the oscillation and repeated lake level rise and fall, the resulting stratigraphy is repeatedly of gravel,

coarse-sand, sand, and clay and silt lithological stratification. The thickness of the clay layer significantly affects the salinity of groundwater as it acts as the adsorption media and filtering membrane for groundwater in the Delta.

Based on the dominant cations and anions, the waters of the study area were classified into four major groups of chemical facies: Na- Ca- HCO_3, Na-Ca-SO_4 -HCO_3, Na-HCO_3 , and Na-Cl and 9 (nine) subgroups. The correlation matrixes of major anions, cations, and physical parameters of water indicate that elements chloride, sodium, fluoride, sulphate, and bicarbonates contributed by the process of mineralization. These ions have been dissolved into groundwater continuously and resulted in the rise of TDS/salinity. Using the Gibbs graph, the relation between the composition of water and its respective aquifer characteristics was determined. Accordingly, the dominant effects of precipitation, rock weathering, and evaporation on the geochemical evolution of groundwater in semi-arid and arid regions were explained. Rock weathering was the main mechanism controlling the chemical compositions of Hammer basement groundwater whereas; evaporation–crystallization is in the Quaternary sediment-Delta aquifer groundwater system. The calculated values of SI for anhydrite, aragonite, calcite, dolomite, gypsum, and halite vary between −4.98 and −0.78, between −4.77 and -0.54, and between −9.86 and -4.29 with averages of -2.88, -2.66 and -7.08, respectively. It shows that the groundwater in the study area was below the equilibrium with anhydrite, gypsum, and halite, indicating that these minerals are anticipated to dissolve. However, the SIs of aragonite, calcite, and dolomite range from −2.06 to 0.63, −1.91 to 0.76, and −1.16 to 2.64, with averages of -0.72, -0.58 and 0.74, respectively. Overall, the groundwater samples were dynamically saturated to over-saturated with aragonite, calcite, and dolomite, implying that the three major carbonate minerals may have affected the chemical composition of groundwater in the study area.

Cation exchange is an important process of water-rock interactions that influences the major ion composition of groundwater. In Omo Delta, the direct ionic exchange is a dominant process. The chloro-alkaline index was calculated and the effect of direction exchange is confirmed. Using Principal component analysis (PCA) and ion ratios relation important reactions and process that are responsible for the mineralization of groundwater is identified.

The stable isotopic signatures ($\delta^{18}O$ and $\delta^{2}H$) of different water sources revealed further evidence for the ideas concluded from the litho-stratigraphic relationships and hydrochemistry. The isotopic

composition of hand-dug wells and spring samples collected in the study area lies within a narrow range, confirming that these groundwater samples had the same recharge source. Shallow and deep groundwaters show similar isotopic compositions except those hand-dug wells recharged directly from Omo River suggesting a hydraulic connection between shallow groundwater and deep groundwater as observed from the chemical data. Hammer basement groundwater samples plotted along the global meteoric water line (GMWL) and Soddo LMWL, indicating that the Hammer basement groundwater is mainly of meteoric origin. In comparison with the other groundwater samples, hand-dug well samples are relatively enriched in stable isotopes; it deviates significantly from the LMWL. The Quaternary sediment groundwater samples distributed in two clusters. The first pattern is populated along the lower part GMWL indicating that these samples are from non-evaporated water, which is rapidly infiltrated, to the saturated zone, and middle part, which are shallow and hand-dug wells that have hydraulic interconnection with Omo River (recharged by Omo River). All wells with negative d-excess are characterized by higher EC (salinity value) provides evidence of recharge water evaporation before infiltration.

The radon survey conducted along Omo River stretch and wells close to it confirms in addition to isotopes that there is the interaction between the surface and groundwater. The radon-222 concentration in groundwater samples showed a very wide scale, ranging from 58.7 to 982.5Bq/m^3 compared to the River and Lake Water samples that are ranged from 18.65 to 105.2Bq/m^3 and 10.49 to 10.85Bq/m^3 respectively. The highest radon concentration was found in the samples that were collected from wells close to the Omo River. Indicating that these points represent groundwater discharge zones.

A comparison of the deuterium and chloride data provides a greater understanding of the scale of groundwater-surface water interaction processes. The chloride–deuterium plot suggests three types of groundwater occur in the Omo Delta. These are: (a) shallow groundwater from lacustrine plain close to Omo River, characterized by low chloride and relatively enriched δD that frequently recharged by river water, (b) groundwater from an alluvial fan, which is sometimes recharged by intermittent rivers ("Kaskie") during rainy seasons. These groundwaters are characterized by low chloride and depleted δD, representing areas that are recharged less frequently by surface water more frequently by high rainfall, and (c) highly saline groundwaters at lacustrine plain with very high chloride and lower δD, that never or rarely receive recharge from surface water. This result

also confirms that the interaction between surface and groundwater is taking place at different part of the Delta differently.

The hydrochemical evidences show that there is no significant signature of geochemical evolution that indicates the presence of continues or regional flow system along N-S and NE-SW hypothetical transects. The isotopic analysis under sections also shows that relatively depleted groundwater at Hammer basement and enriched groundwater at the Quaternary sediments reasonably indicates the absence of flow continuity between the two regions. Both hydrochemical and isotope techniques indicate the dominance of local recharge and flow system.

Finally, from converging evidence of geology, hydrogeology, hydrochemistry, and stable isotopes of water, three processes are responsible for the salinization of groundwater in Omo Delta: Salinity originated from water-rock interaction, evaporation at or near the surface and clay membrane filtration.

7.2. Recommendations

The results of this study suggest that further research is needed to fully characterize the geologic and hydrologic conditions and geochemical processes that control groundwater salinization and distribution in the area.

The work also faced limitations with regard to both data quantity and quality as well as to the spatial and temporal coverage of hydrological, hydrogeological, hydrochemical, and isotope data. To better understand and increase the knowledge on the hydrogeological framework of a complex system like the study area, proper utilization of existing records and generating new data having both temporal and spatial coverage is very crucial. The following points, if addressed, will help in alleviating the problem in future groundwater studies.

I. Most Groundwater wells constructed in the study area lack records on depth, water table, discharge, and lithologies encountered during drilling. Furthermore, some wells in the Delta are so saline that they are abandoned soon after construction. This makes the groundwater database in the region scarce and unreliable to use for research and/or scientific purposes. Therefore, important information on hydrogeological and hydrochemical information should be recorded to increase the groundwater database in the region.

II. The wells that drilled in the study area hardly conducted a Pump test. Therefore, the aquifer characterization parameters cannot be determined. This makes the determination of the groundwater dynamics in the Delta is a difficult task, which are important for delineation of aquifers vulnerable for salinization. Therefore, some test wells should be drilled on representative geomorphic features, and pump test should be conducted for wells drilled in the future.

III. Both surface and groundwater samples should be analyzed for tritium, $\delta^{14}C$, and $^{87}Sr/^{86}Sr$. Which can be used to determine the age of groundwater and flow paths and mixing relationships in regional flow systems.

IV. Isotopic and hydrochemical data of both rainfall and groundwater are useful in understanding a hydrologic system. In addition, temporal sampling of the rainfall should be made from GNIP stations, but there are no such stations in the study area. Therefore, establishing new stations in the basin could help to understand the different sources and events of the rainfall, circulation of the moisture, and its environmental conditions.

V. The present study only focused on the use of stable isotopes of water, major and minor elements to characterize salinization processes. These methods alone cannot provide a complete understanding of the salinity problem. Therefore, the important insights achieved in the course of this dissertation also provide scope for further work. In order to fully, characterize the salinity problem, a combination of geophysics, quantitative hydrogeology (hydraulic modeling), and geology are suggested.

REFERENCES CITED

Abriham Asha (2018). Hydrogeological system analysis of the Abaya Chamo Lakes basin, with special emphasis on using chemical and isotopic signatures.Unpublished PhD thesis, Addis Ababa Univeristy, Addis Ababa.

Addisu Deressa (2012). Hydrogeochemical and isotope Hydrology in Investigating Groundwater Recharge and Flow Processes, South Afar Eastern Ethiopia. Unpublish MSc thesis, Addis Ababa Univeristy, Addis Ababa.

Agroconsulting (2009). Environmental and Social Impact Assessment on Omo-Ghibe Downstream. EEPCO, Report no. AG 003, Addis Ababa.

Ait, Y., Abdelfattah, B., & Mbark, B. (2015). Origin and salinity of groundwater from interpretation of analysis data in the mining area of Oumjrane , Southeastern Morocco. Environmental Earth Sciences. DOI:10.1007/s12665-015-4467-7.

Al-agha, D. E., Closas, A., & Molle, F. (2015). Survey of groundwater use in the central part of the Nile Delta, Water and Salt Management in the Nile delta Project Report No. 1. IWMI, WMRI: Cairo.

Alcala, F. J., & Custodio, E. (2008). Using the Cl / Br ratio as a tracer to identify the origin of salinity in aquifers in Spain and Portugal. Journal of Hydrology 359,189–207. DOI: 10.1016/j.jhydrol.2008.06.028

Anderson, M. P. (2005). Heat as a groundwater tracer. Ground Water Association, 43(6), 951–968.

Antolino, D. J. (2011). Geochemical conditions and groundwater-surface water interactions within a municipal well field in Miami-Dade country. Published Msc thesis, Florida Atlantic University, Florida.

Arad, A. (1984). Relationship of salinity of Groundwater to Recharge in the Southern Kalahari Desert. Journal of Hydrology, 71, pp.225–238.

Assefa consult.(2015).Hydrogeological and Geophysical Investigation in Dasenech woreda, South Omo Zone, Techinical Report:Addis Ababa,p157.

Avery, S., Eng, C., & Env, C. (2018). Lake Turkana & the Lower Omo : Hydrological impacts of major Dam and Irrigation Developments, Report Volume I, African Studies Centre University of Oxford, London.

Ayenew, F. W. and T. (2016). Application of hydrochemical and isotopic techniques to understand groundwater recharge and flow systems in the Dawa River basin , southern Ethiopia. J Env Earth Sciences 75:1–17.

Basin, M., Cartwright, I., Weaver, T. R., & Fifield, L. K. (2006). Cl / Br ratios and environmental isotopes as indicators of recharge variability and groundwater flow: An example from the southeast Murray Basin, Australia. Chemical geology, 231, 38–56.

Bonetto, S., Luca, D. A. De, & Lasagna, M. (2015). Groundwater Distribution and Fluoride Content in the West Arsi Zone of the Oromia Region (Ethiopia). Springer 3,582-597. DOI:10.1007/978-3-319-09054-2

Butzer, K. (1972). Recent History of an Ethiopian Delta. The University of Chicago: USA.

Butzer, K. W. (1969). Some Late Cenozoic Sedimentary Formations of the Lower Omo Basin. Nature, 222(5199), 1132–1143.

Butzer, K. W. (1971). Geomorphological observations in the lower Omo basin, southwestern Ethiopia. Springers, 58,177–198.

Cecil D, Green J. (2000). Radon-222. In Cook PG, Herczeg AL, editors. Environmental tracers in subsurface hydrology. Norwell (MA): Kluwer Academic Publishers. p. 175-194.

Cerling, T. E., Levin, N. E., & Passey, B. H. (2011). Stable Isotope Ecology in the Omo-Turkana Basin. Evolutionary Anthropology, 237, 228–237.

Chorowicz, J. (2005). The East African rift system. Jornal of African Earth Science, 43, 379–410.

Clark, I. (1997). Environmental Isotopes in Hydrogeology. Retrieved from www.crcpress.com

Close, M. (2014). Analysis of Radon data from the Wairau River and adjoining Wairau Plains Aquifer New Zealand, Institute of Environmental Science and Research Report no.CSC14001: Marlborough District.

Coluccio, K., & Morgan, L. K. (2018). A review of methods for measuring groundwater-surface water exchange in braided rivers. Hydrol. Earth Syst. Sci, 18, pp42.

Constantz, J., Stewart, A. E., Niswonger, R., and Sarma, L. (2002). Analysis of temperature profiles for investigating stream losses beneath ephemeral channels. Water Resour. Res., 38 (12), 1316-1326.

C. J. Ebinger*, T. Yemane, D. J. Harding, S. Tesfaye, S. Kelley. (2000). Rift deflection , migration , and propagation : Linkage of the Ethiopian and Eastern rifts. Africa GSA Bulletin, v. 112; no. 2; pp. 163–176.

C.A.J. Appello and D. Postma. (2005). Geochemistry, Groundwater and Pollution. (2nd ed.). Amsterdam, the Netherlands.

Christian Leibundgut, Piotr Maloszewski, C. K. (2009). Tracers in Hydrology. A John Wiley & Sons, Ltd. West Sussex,UK.

Daniel Gamachu, 1977. Aspects of climate and water budget in Ethiopia, Addis Ababa University press, Addis Ababa, 71p.

Dansgard, W. (1964): Stable isotopes in precipitation. Tellus, 16 (4), 436–468.

Davis, S.N., Campbell, D.J., Bentley, H.W., Flynn, TJ. (1985): Ground Water Tracers. National Water Well Association, Worthington, Ohio, 200 p.

Davidson, A., (1983). The Omo River Project. Reconnaissance of Geology and Geochemistry of Parts of Ilubabor, Kefa, Gemu Gofa and Sidamo, Ethiopia. Ministry of Mines and Energy, Ethiopian Institute of Geological Surveys, Addis Ababa, Ethiopia.

Demlie, M., Ayenew, T., & Wohnlich, S. (2007). Comprehensive hydrological and hydrogeological study of topographically closed lakes in highland Ethiopia : The case of Hayq and Ardibo. Jornal of hydrology, (339),145–158.

Diab, H. M. (2019). Technical note accuracy and precision of RAD 7 and RAD H_2O accessories Radon detector in water measurement based on counting statistics for Sniff and normal. Romanian J. Biophys, 29, p30.

Dimova, N.T., Burnett, W.C., Chanton, J.P., Corbett, J.E., 2013. Application of radon-222 to investigate groundwater discharge into small shallow lakes. J. Hydrol., 486, 112–122.

Dongmei et al., 2011. (2011). Geochemical and isotopic evidence for palaeo-seawater intrusion into the south coast aquifer of Laizhou Bay, China. Applied Geochemistry, 26(5), 863–883.

DURRIDGE Company. (2019). User Manual For Electronic Radon Detector. Retrieved from www.durridge.com

Elango, L., & Kannan, R. (2007). Rock-water interaction. In Developments in Environmental Science. R. D. and R. H. (Eds) Elsevier Ltd.pp.229-243.

FAO. (2016). Thematic Papers on Groundwater-Synthesis Report, Rome.

FAO. (1995). <http://www.fao.org/waicent/faoinfo/agricult/agl/aglw/aquastat/ ethiopi.htm>

Fetter, C. W. (2001). Applied Hydrogeology (4th ed.). University of Wisconsin Oshkesh, USA, 598p.

Feibel, C. S. (2011). A Geological History of the Turkana Basin. Evolutionary Anthropology, 20, 206–216.

Flury, M.,Wai, N.N. (2003): Dyes as tracers for vadose zone hydrology. Reviews of geophysics, 41/1: 1–37.

Fitts, C. R. (2002). Groundwater Science. Elsevier Science Ltd, London, UK, 467p.

Fitzpatrick R.W., Merry, R.H., Cox, J.W. and McFarlane, J 2002. Effects of drainage on processes in saline soil profiles in the South East of South Australia. Proceedings for the 8th National Conference and workshop on: "Productive use and rehabilitation of saline lands (PUR$L)". Perth, Western Australia, September 16th to 20th, 2002. p. 299.

GAT, J. R. (1995). Stable Isotopes of Fresh and Saline Lakes. In D. I. and J. R. G. A. Lerman (Ed.), In Physics and Chemistry of Lakes (pp. 139–165). Berlin: Springer-Verlag.

Gat, J. R., & Carmi, I. (1970). Evolution of the Isotopic Composition of Atmospheric the Mediterranean Sea Area. Journal of geophysical research, 75(15), 3039–3048.

Glynn, P. D., & Plummer, L. N. (2005). Geochemistry and the understanding of ground-water systems. Hydrogeology Journal, 13, 263–287. DOI: 10.1007/s10040-004-0429-y

Guido Borzi, Carolina Tanjal, Lucía Santucci, E. C. (2019). Geochemical mechanisms controlling the isotopic and chemical composition of groundwater and surface water in a sector of the Pampean plain (Argentina). Science of the Total Environment, 683, 455–469.

Guida, M., Guida, D., & Guadagnuolo, D. (2013). Using Radon-222 as a Naturally Occurring Tracer to investigate the streamflow-groundwater interactions in a typical Mediterranean fluvial-karst landscape : the interdisciplinary case study of the Bussento river (Campania region, Southern Italy). Elsiever,12(2), 1234-1246.

Guseva, N. V, Kopylova, Y. G., Oidup, C. K., Arakchaa, K. D., & Rychkova, K. M. (2017). Formation of the chemical composition of brackish and brine groundwater in the Tuva depression and surrounding areas. Elsevier Ltd, 59(2), 135–143.

Hamada, H. (1999). Analysis of the Interaction between Surface Water. JARQ, 33, 261–265.

Hatch, M.A, Telfer, A.L.,., Burnell, R.A., Woods, J., Shintodewi, P.A., 2006. Atlas of Instream NanoTEM 2006. Australian Water Environments Report 45755d. Murray Darling Basin Commission (MBDC Publication 28/06), Canberra, Australia. 24p.

Heath, B. R. C. (1983). Basic Ground-Water Hydrology. USGS, Verginia, USA.

Hem, D. (1989). Study and Interpretation the Chemical Characteristics of Natural Water (4rd ed). USGS,Dallas, USA.

Hem, J. D. (1985). Study and Interpretation the Chemical of Natural of Characteristics Water(3rd ed.). USGS. Dallas.

Hiscock, K. M. (2005). Hydrogeology Principles and Practice. Blackwell Science Ltd, Malden, USA.

Http://isohis.iaea.org- Annual mean $\delta^{18}O‰$ of precipitation based on GNIP.

Http://www.soilgrids.org-Soil map of East Africa.

Huang, P., & Chen, J. (2012). Recharge sources and hydrogeochemical evolution of groundwater in the coal-mining district of Jiaozuo , China. Springer-Verlag, 20, 739–754.

Jamila et al. (2017). Characterization of Recharge Mechanisms and Sources of Groundwater Salinization in Ras Jbel Coastal Aquifer (Northeast Tunisia) Using Hydrogeochemical Tools , Environmental Isotopes , GIS , and Statistics. Hindawi, Journal of Chemistry, 2017, 1–19.

Jolliffe, I. T. (2002). Principal Component Analysis, Second Edition (2nd ed.). Springer Ltd. Kings university of Aberdeen,UK.

Khan, H. H., & Khan, A. (2019). Groundwater and Surface Water Interaction. Retrieved from https://doi.org/10.1016/B978-0-12-815413-7.00014-6

Kalbus, E., Reinstorf, F., & Schirmer, M. (2006). Measuring methods for groundwater, surface water, and their interactions, Hydrol. Earth Syst., 3, 1809–1850.

Kebede, S. (2004). Environmental isotopes and geochemistry in investigating groundwater and lake hydrology: cases from the Blue Nile basin & the Ethiopian Rift (Ethiopia). PhD Thesis, University of Avignon, France.

Kebede, S. (2005). Groundwater recharge, circulation, and geochemical evolution in the source region of the Blue Nile River, Ethiopia. Springer, 20, 1658–1676.

Kebede, S. (2013). Groundwater in Ethiopia Features Numbers and Opportunities. Springer, Verlag, Berlin.

Kebede, S., Abdalla, O., Sefelnasr, A., & Tindimugaya, C. (2016). Interaction of surface water and groundwater in the Nile River basin : isotopic and piezometric evidence. Hydrogeology Journal. DOI: 10.1007/s10040-016-1503-y

Kebede, S., Travi, Y., & Asrat, A. (2007). Groundwater origin and fl ow along selected transects in Ethiopian rift volcanic aquifers. Springer, DOI: 10.1007/s10040-007-0210-0.

Kelly, S. E., and Murdoch, L. C.(2003). Measuring the hydraulic conductivity of shallow submerged 5 sediments, Ground Water, 41(4), 431–439.

Kendall et al. (2001). Distribution of oxygen-18 and deuterium in river waters across the United States. Hydrological Processes, 15, 1363–1393.

L. Cary et al., E. (2015). Origins and processes of groundwater salinization in the urban coastal aquifers of Recife (Pernambuco , Brazil): A multi-isotope approach. Elsevier Ltd, (530–531), 411–429.

Leaney, F. W., & Herczeg, A. L. (2005). Groundwater – surface water interactions in a large semi-arid floodplain : implications for salinity management. Hydrol. Process, 19, 3063–3080.

Lee D. R., (1977). Device for Measuring Seepage Flux in Lakes and Estuaries, Limnol. Oceanogr.,15 22(1), 140–147.

Levin, N. E., Zipser, E. J., & Cerling, T. E. (2009). Isotopic composition of waters from Ethiopia and Kenya : Insights into moisture sources for eastern Africa. Journal of geophysical research, 114, 1–13.

Liu, F., Song, X., Yang, L., Zhang, Y., Han, D., Ma, Y., & Bu, H. (2015). Identifying the origin and geochemical evolution of groundwater using hydrochemistry and stable isotopes in the Subei Lake basin, Ordos energy base, Northwestern China. Jornal of Hydrology and Earth System Sciences, 19, 551–565 .

Li, S., Wang, G., Deng, W., Hu, Y., & Hu, W. (2009). Influence of hydrology process on wetland landscape pattern : A case study in the Yellow River Delta. Journal of Ecological Engineering 35, 1719–1726.

Liu, Y. (2018). A simplified method of developing a local meteoric water line equation for Beijing , China. Journal of Radioanalytical and Nuclear Chemistry, 315(3), 523–532.

M. B. Mabrouk, A. Jonoski, D. Solomatine, and S. Uhlenbrook,. (2013). A review of seawater intrusion in Solid the Nile Delta groundwater system – the basis for assessing impacts due to climate changes and water resources development. Hydrology and Earth System Sciences, 10,10873–10911.

Mammou, Ismail Chenini & Abdallah Ben Mercier, M. M. T. & E. (2010). Piezometric levels as possible indicator of aquifer structure : analysis of the data from Maknassy basin aquifer system (Central Tunisia). Arab J Geoscince, 3, 41–47.

Martindale, H. (2015). The use of radon and complementary hydrochemistry tracers for the identification of groundwater – surface water interaction in New Zealand. Unpublished Msc thesis, Massay Univeristy, New Zealand.

Martindale, H., & Raaij, R. Van Der. (2018). Investigation of groundwater-surface water interaction in the Te Arai River , Gisborne , using radon-222 and concurrent stream flow gauging. GNS Science Report, 2018/13, 27 p.

Mazor, E. (2004). Chemical and Isotopic Groundwater Hydrology (3rd ed.). Weizmann Institute of Science Rehovot, Israel.

Mccarthy, T. S. (2006). Groundwater in the wetlands of the Okavango Delta , Botswana , and its contribution to the structure and function of the ecosystem. Journal of Hydrology, 320, 264–282.

McDonnell, C. K. and J. J. (1998). Isotope tracers in Catchment Hydrology (1st ed.). Elsevier, Amesterdam, Netherlands.

McCallum, J.L., Cook, P.G., Berhane, D., Rumpf, C., McMahon, G.A.(2012). Quantifying groundwater flows to streams using differential flow gaugings and water chemistry. J. Hydrol. 416, 118–132.

Milzow, C., Kgotlhang, L., Bauer-gottwein, P., & Meier, P. (2009). The hydrology of the Okavango Delta , Botswana — processes , data and modelling. Hydrogeology Journal, 17, 1297–1328.

Ministry of Water Energy and Irrigation (MoWEI). (2008) Omo-Ghibe River Basin Master plan. Unpublished report, Addis Ababa.

Modibo et al. (2019). Assessing Groundwater Mineralization Process, Quality, and Isotopic Recharge Origin in the Sahel Region in Africa. MDPI, 11, pp19.

Mongelli, G., Monni, S., Oggiano, G., Paternoster, M., & Sinisi, R. (2013). Tracing groundwater salinization processes in coastal aquifers: a hydrogeochemical and isotopic approach in the Na-Cl brackish waters of northwestern Sardinia, Italy. Hydrology and Earth System Sciences, 17(7), 2917–2928.

Monjerezi, M. (2012). Groundwater Salinity in lower Shire River valley (Malawi) Hydro-geochemical and isotope constraints on sources and evolution. Elseiver, 26 (2011), 1399–1413.

Moore, R.D. (2004): Introduction to Salt Dilution Gauging for StreamflowMeasurement: Part 1. StreamlineWatershedManagement Bulletin, 7 (4), 20–23.

Morgenstern, U., Daughney, C.J.(2012). Groundwater age for identification of impacts of land-use intensification and natural hydrochemical evolution on groundwater quality – the National Groundwater Monitoring Programme of New Zealand. J. Hydrol., 456–457, 79–93.

Morrissey, A. (2014). Stratigraphic framework and Quaternary paleolimnology of the Lake Turkana Rift, Published Phd thesis, Syracuse University, Newyork.

Narany, T. S., Ramli, M. F., Aris, A. Z., Nor, W., Sulaiman, A., Juahir, H., & Fakharian, K. (2014). Identification of the Hydrogeochemical Processes in Groundwater Using Classic Integrated Geochemical Methods and Geostatistical Techniques , in Amol-Babol Plain , Iran. Hindawi Publishing, 2014,p15.

Naus, F. L., Schot, P., Groen, K., Ahmed, K. M., & Griffioen, J. (2019). Groundwater salinity variation in Upazila Assasuni (southwestern Bangladesh), as steered by surface clay layer thickness , relative elevation and present-day land use. Hydrology and Earth System Sciences, 23, 1431–1451.

NISSENBAUM, A. (Ed.). (1980).Hypersaline Brines and Evaporitic Environments. New York: Elsevier.

Peng Yi, Huan Luo, Li Chen, Zhongbo Yu, Huijun Jin, Xiaobing Chen, Chengwei Wan, Ala Aldahand, Minjie Zhenge, Q. H. (2018). Evaluation of groundwater discharge into surface water by using Radon-222 in the Source Area of the Yellow River , Qinghai-Tibet Plateau. Journal of Environmental Radioactivity, 192, 257–266.

Petelet-giraud, E., Négrel, P., Guerrot, C., Aunay, B., & Dörfliger, N. (2013). Origins and processes of salinization of a Plio-Quaternary coastal Mediterranean multilayer aquifer : the Roussillon Basin case study. *Procedia Earth and Planetary Science*, *7*, 681–684. https://doi.org/10.1016/j.proeps.2013.03.046

Pfahl, S., & Sodemann, H. (2014). What controls deuterium excess in global precipitation ? Jornal of Climate of Past, 10, 771–781.

Prajapati, M., Jariwala, N., & Agnihotri, P. (2018). Geochemical Evaluation of Groundwater in the Mandvi Taluka of Surat , India. Journal of Environmental Protection,9, 67–89.

Production, F. (2007). Tropical Deltas and Coastal Zones at the Land – Water Interface. Chu Thai Hoanh et.,al(Eds) pp.1-13.Cambridge:USA.

R.Ayuba et al., 2013. (2013). Assessment of Groundwater Quality of Lokoja Basement Area. Journal of Geological Society of India, 82, 413–420.

Rice, J. A. (1995). Mathematical Statistics and Data Analysis Second Edition (2nd ed.). University of California, Berkeley.

Richard A. Davis, Jr. (Eds). (1985). Coastal Sedimentary Environments(2nd ed). Springer-Verlag: New York Inc.

Rosenberry DO. 2008. A seepage meter designed for use in flowing water. Journal of Hydrology. 359(1-2):118-130.

Rusydi, A. F. (2018). Correlation between conductivity and total dissolved solid in various type of water. Earth and Environmental Science, 118,p7.

Saadi, R., Marah, H., & Hakam, O. K. (2018). Setting up a continuous monitor for the control of temporal variability of Rn in groundwater : Application to samples from Tadla Basin, Morocco. Journal of Materials and Environmental Sciences, 9(5), 1439–1445.

S. Baskaran a , T. Ransley a, R. S. B. a b & P. B. a. (2009). Investigating groundwater – river interactions using environmental tracers. Australian Journal of Earth Sciences, 56:1, 13-19.

Sahu, S., Ground, C., & Board, W. (2018). Aquifer salinization and ground water security in Puri urban area in the coastal tract of Odisha; understanding local geomorphology as a tool. ResearchGate, 17,pp15.

Samuel Y. Ganyaglo, Shiloh Osae, Tetteh Akiti, Thomas Armah, Laurence Gourcy, Tomas Vitvar, Mari Ito & Isaac A. Otoo (2017). Application of geochemical and stable isotopic tracers to investigate groundwater salinity in the Ochi-Narkwa Basin. Ghana, Hydrological Sciences Journal, DOI: 10.1080/02626667.2017.1322207

Santos, I.R., Peterson, R.N., Eyre, B.D., Burnett, W.C., (2010). Significant lateral inputs of fresh groundwater into a stratified tropical estuary: evidence from radon and radium isotopes. Marine Chem. 121 (1–4), 37–48.

Sasamoto, H., Yui, M., & Arthur, R. C. (2007). Estimation of in situ groundwater chemistry using geochemical modeling : A test case for saline type groundwater in argillaceous rock. 32, 196–208.

Scanlon, B. R., Healy, R. W., & Cook, P. G. (2002). Choosing appropriate techniques for quantifying groundwater recharge. Hydrogeology Journal, 10, 18–39.

Shaw, S.B., Eckhardt, D.A., 2012. An assessment of radon in groundwater in New York state. Health Phys. 103 (3), 311–316.

Shojaeya, G., Strip, G., Strip, G., & February, R. (2011). Hydro-Geochemical Characteristics of Groundwater beneath the Gaza Strip. Journal of Water Resource and Protection, 3, 341-348.

Smedley, W. M. E. & P. L. (1996). Groundwater geochemistry and health. British Geological Survey, 113, 91–105.

Saadu U., Wali K., Jega U., Ibrahim M. (2019). Hydrochemical characterization of shallow and deep groundwater in Basement Complex areas of southern Kebbi State , Sokoto Basin. Applied Water Science, 9, 1–36.

Taylor, P., Baskaran, T., Brodie, R. S., & Baker, P. (2009). Investigating groundwater – river interactions using environmental tracers. Australian Journal of Earth Sciences,8, 37–41.

Tefera Alemu (2017).Seismic Reflection Studies of South Omo Basin, Southwestern Ethiopia. Unpublished Msc thesis, Addis Ababa Univeristy.

Thomas C. Winter. (1998). Relation of streams, lakes, and wetlands to groundwater flow systems. U.S. Geological Survey, MS 413, 7:28–45

Tilahun Mammo (2012). Analysis of gravity field to reconstruct the structure of Omo basin in SW Ethiopia and implications for hydrocarbon potential. *Mar. Petrol. Geol*. **29**: 104-114.

Vengosh, A. (2014). Salinization and Saline Environments. In: Holland, H.D., Turekian, K.K. (Eds.), Treatise on geochemistry volume 9: Elsevier, pp. 1–35.

Vitvar, T., & Aggarwal, P. K. (1998). A Review of Isotope Application in Catchment Hydrology. In P. K. A. T. VITVAR (Ed.), Orgon, USA.

WHO. (2008). Guidelines for Drinking-water Quality (3rd ed., Vol. 1). World Health Organization: Geneva.

Worku, F. F., Werner, M., Wright, N., Zaag, P. Van Der, Demissie (2014). Flow regime change in an endorheic basin in southern Ethiopia. Hydrol. Earth Syst. Sci, 18, 3837–3853.

Woodroofe (2007). Evaluation of groundwater resources of the Omo-Ghibe basin for water supply project, Part I Report, Addis Ababa, pp189

Wynn, J. G., Campisano, C. J., Drapeau, M. S. M., Dumouchel, L., & Geraads, D. (2014). The Omo Mursi Formation : A window into the East African Pliocene. Journal of Human Evolution, 75, 64–79.

Xiaoyi Shi, Tao Pu, Yuanqing He, Cuishan Qi, Guotao Zhang (2017). Variability of Stable Isotope in Lake Water and Its Hydrological Processes Identification in Mt. Yulong Region. Water Resource Research, 9,p15.

Yang, L., Song, X., Zhang, Y., Han, D., Zhang, B., & Long, D. (2012). Characterizing interactions between surface water and groundwater in the Jialu River basin using major ion chemistry and stable isotopes. Hydrology and Earth System Sciences,16, 4265–4277.

Yi, P., Luo, H., Chen, L., Yu, Z., Jin, H., & Chen, X. (2018). Evaluation of groundwater discharge into surface water by using Radon-222 in the Source Area of the Yellow River, Qinghai-Tibet Plateau. Journal of Environmental Radioactivity, 192, 257–266.

Zhao, D., Wang, G., Liao, F., Yang, N., Jiang, W., & Guo, L. (2018). Groundwater-surface water interactions derived by hydrochemical and isotopic (222 Rn, deuterium, oxygen-18) tracers in the Nomhon area, Qaidam. Journal of Hydrology, 565, 650–661.

Appendices

Appendix 1. Water chemistry and Stable isotopes of groundwater samples. TDS, major and some minor ions are measured in mg/l.

Sample-code	source	X	Y	Z	EC (µs/cm)	TDS	T (0c)	ph	Na^+	Ca^{2+}	$Mg2^+$	K^+	Cl^-	F^-	Br-	$SO4^{2-}$	$HCO3^-$	$NO3^-$	RE%	δ2H(‰ VSMOW)	δ18O(‰ VSMOW)
OD1	SW	186873	519302	406	816	396	34.9	7.85	53.4	48.2	43.9	5.68	21.3	0.47	0.04	42	339.16	2.6	9.3	-10.2	-3.44
OD2	Sw	187527	519278	404	637	317	35.9	8.02	41.7	37.6	33.6	6.2	17.9	0.42	0	4.07	326	0.9	5.5	-11.3	-3.08
OD3	SW	188608	515958	401	693	322	39.4	8.02	53.2	23.4	16	56	8.3	0.67	0.04	50.9	260	8.2	4.7	-12.5	-3.73
OD4	SW	188769	514480	381	2430	1154	39.4	7.94	180.5	40.5	72.1	6.9	140.38	0.94	0.99	44.55	530.7	86	3.3	-11.2	-1.87
OD5	sw	188334	514243	372	3450	1579	37.8	7.98	495.5	12	24	7.68	847.26	0.64	0.1	50.93	232	13	-9.2	-10.8	-1.26
OD6	SW	191044	512218	388	591	676	37	8.25	51.3	18	1.2	6.2	19.1	0.61	0.04	34	146	2.6	-4.2	-9.5	-2.68
OD7	sw	191109	512013	398	603	295	36.9	8.33	124	24	32	26.4	21.3	0.65	0.15	28.4	434	12.8	7.7	-9	-2.65
OD8	SW	192451	506657	375	7071	3431	35.8	8.05	1406	9.15	7.24	6.32	1119.5	2.18	0.01	123.5	988.2	62	9.3	-11.7	-0.26
OD9	Pond	192641	494884	380	2240	1254	35.2	8.76	321.5	2.9	2.3	2	354.6	5.88	0	17.2	332.9	19.6	-6.2	-14.1	-2.5
OD10	SW	222264	549636	910	663	352	31.1	7.9	18.2	30.46	9.23	4.2	6.38	2.11	0.09	14.41	172.6	12.8	-4.9	2.7	-0.31
OD11	Sw	207846	555573	777	1052	526	31.5	7.32	93.4	70	57.1	8.6	5.2	2.26	0.17	67	665	4	0.1	-1.3	-1.32
OD12	SW	221505	569509	1117	638	333	29.4	7.7	24.2	16	2.4	4.8	17.2	0.74	0.01	8	98	0.9	-2.3	-0.7	-1.2
OD13	SW	223763	568179	1117	638	379	29.4	7.43	54.8	84	21.9	4.9	10.9	0.72	0.17	3	500	11.4	-1.3	-3.5	-1.87
OD14	HDW	228126	581102	1180	434	229	27.5	7.5	47.1	16	0	6.2	8.1	1.01	0.12	64	98	2.6	-3.3	-0.1	-1.31
OD15	SW	226290	578083	1136	726	171	29.1	7.81	57.5	80	29.2	4.1	13.2	0.75	0.11	3	537	4.8	-1.5	-1.1	-1.28
OD16	HDW	228246	572987	1109	738	379	28.5	6.53	12.3	37.68	10.21	3.9	9.5	1.16	0.08	17.7	155	1.8	2.4	5.7	-1.01
OD17	SW	235380	600233	1311	602	179	27.8	7.89	29	60	10.9	4.4	5.3	1.45	0.07	4	305	2.6	0.1	-6.1	-2.04
OD18	Sw	186022	521659	410	718	335	33.2	7.51	76	32	36	34.5	18.2	0.24	0.07	52.3	350.2	0.6	8.8	-3.5	-1.95
OD19	Sp	232601	637098	1448	341	173	21.9	7.96	17.4	56	3.6	5.2	10.4	0.87	0.11	6	220	8.8	-2.2	-1.6	-2.02
OD20	Sw	185519	522162	409	633	298	35.5	7.75	30.2	10	4.3	6.2	16.8	0.69	0.03	10	110	3.5	-4.5	4.9	0.01
OD21	Sw	184780	523746	399	1548	742	35.1	9.25	33.1	14	3.6	4.2	8.5	0.84	0	32	110	0.9	-3.4	-3.5	-1.92
OD22	sw	236938	633201	1416	945	453	24.1	7.5	63.1	98	29.2	5	16.9	0.71	0	31	561	16.3	-1.8	-3.5	-1.92
OD23	SW	167628	528254	370	1079	521	29.7	6.97	26.2	18	3.6	6.8	15	0.81	0.06	0	110	2.6	5.0	-3.5	-1.87
OD24	HDW	172546	531578	371	937	343	30.5	7.4	138.5	76.8	3.2	18.8	86.1	0.89	0.31	0	456	6.2	2.8	6.7	-0.4
OD25	HDW	172197	531152	370	7070	3239	33.6	7.14	262.1	178	48.9	28.8	249.9	1.55	0.02	125	1202	0.9	-8.0	6.3	-0.4
OD26	sw	172170	530378	373	635	308	30.4	8.23	84.2	50	4.9	10	58.3	0.32	0	1	336	2.6	-2.9	-0.5	-1.6
OD27	sw	186321	521188	409	1628	739	32.3	7.17	37	168	41.3	12	31.3	0.24	0.03	112	366	334.4	-3.0	-9.07	-2.77
OD28	Sw	182648	522929	383	2940	1332	34.8	8.52	193.2	6	8.5	4.8	269.2	0.36	0.12	4	110	1.8	-0.4	-3.6	-2.1
OD29	SW	184299	521592	396	1336	676	35.2	7.76	124	18	1.2	6.2	122.2	0.61	0.04	34	146	2.6	-0.6	-11.3	-2.89
OD30	Sw	182541	521233	384	5340	2523	34.6	8.68	410	20	2.4	6.6	168.2	3.78	0.02	42	872	1.8	-2.1	-10.4	-2.26
OD31	sw	520745	184857	407	655	266	34.9	8.08	110.4	20	8.5	5	60.1	0.61	0.08	16	312	39.2	-8.0	-10.9	-2.76
OD32	SW	183979	527736	383	852	411	35.8	8.12	85.6	21.3	29.3	8	28.4	0.97	0.05	36.2	292	2.6	7.5	-11.2	-3.08
OD33	SW	207753	555368	779	1012	506	31.8	7.2	84.4	76	51	8.2	1.3	2.38	0	46	647	11	0.6		

OD34	SW	183181	525531	382	6150	3444	35.6	7.27	1395	30	28.8	15.64	1322.3	0.66	0.01	131.24	817.4	35	8.8	-12.50	-3.12
OD35	SW	184951	520803		1348	755	35.7	7.26	200.75	30	33.5	7.98	31.47	0.4		62.6	520.4	222	-4.0		
OD36	SW	184894	523672		2100	1176	35.5	7.79	312.5	7.21	4	4.31	265	1.3		6.98	359.9	86	-2.1		
OD37	SW	184288	521605		940	526	36.3	7.73	168	14.4	7.25	5.72	22.05	0.53		115.58	192	97	6.2		
OD38	SW	194252	503743		10240	5734	32.6	7.93	1645.3	3.63	3.09	7.16	1583.9	4.6		54.19	988.2	62	6.3		
OD39	SW	192358	506450	393	7080	3965	35.1	7.69	1224.6	9.15	7.24	6.32	1119.5	1.5		68.2	822.3	13	7.3		
OD40	SW	188244	514042	372	3450	1932	32	7.55	560.3	12	24	7.68	847.26	0.44	0.1	44.55	325	86	-8.0	-10.6	
OD41	SW	188677	514268	383	2460	1377	36	7.13	180.5	40.5	72.7	6.9	140.38	0.31		44.55	528.26	86	3.6		
OD42	SW	188283	520978	432	2460	1377	35.2	6.91	165.3	39	32.4	7.18	137.54	0.3		4.07	339.16	97	3.8		
OD43	SW	183077	521404	391	1836	1108	33.5	9	172.4	4.8	2	143	168			65	224	20	6.5		
OD44	SW	184524	524728		1508	843	35.6	8.6	358	9.6	1	112	43			61	817.4	19.2	7.9		
OD45	SW	186039	521721		645	326	33.4	8	76	32	42	54	18			8	482	12	5.5		
OD46	SW	191007	511820		564	275	32.4	8.3	78	24	32	42	21			11	421	10	2.7		
OD47	SW	227146	526379	902	1120	560	24.7	8.32	32.1	78.5	11.2	5.2	1	2	0.16	50	318	0.3	0.8		
OD48	SW	241378	543432	1208	8320	4100	24	4.9	35	360	26.73	24.5	155	3.5	0.19	520	488	9.2	-2.3	-17.30	
OD49	SW	241935	608642	1392	260	130	20.2	7.2	24	78.4	34.24	14	7	0.51	0.03	62	336.2	1.6	7.5		
OD50	SW	364142	535433		284.6	143	18.9	7.18	28	32	12.15	4	9	0.87	0.02	0	231.8	1.8	-1.9	-0.1	
OD51	SW	240716	622407	1303	390	230	25.1	7.4	32	56	12.15	4.5	5	0	0.04	26	292.8	2.4	-1.9	-1.1	
OD52	SW	242163	624264	1315	327	196	25.1	7.26	56	24	9.72	9	3.5	0.63	0	0	244	0	6.6	5.7	
OD53	SW	238951	628225	1369	362	203	24.7	7.1	24	34	7.29	9	6.5	0.29	0.08	4	168	9.4	6.0	-6.1	
OD54	SW	235645	629432	1419	252	151.5	24.9	6.6	14	12	4.617		4.5	1.8	0.31	1	85.4	2.6	0.1	-3.5	
OD55	SW	246560	584609	958	209	126.4	25.4	6.99	12	36.2	4.86	6.5	7.5	0.83	0.55	0.16	146.4	6.6	3.2	-1.6	
OD56	SW	264397	576162	543	620	310	2.6	8.55	16	68	7.29	7.5	4.5	0.86	0.65	3	326.96	1.1	-6.4		
OD57	SW	274627	590530	562	584	293	24.1	8.57	24.4	48.6	16.8	15	2	0	0	0	261.08	0.7	9.6		
OD58	SW	248638	610128	1586	56.9	28.5	21.7	7.3	68	4	20.898	13.5	4.5	1.2	0.04	2	286.35	2.2	3.4		
OD59	SW	239793	611237	1381	1233	739	22	8.37	4	65.6	1.458		3.5	0	0.13	5.8	196	2.3	1.5		
OD60	SW	248575	611470	1600	1654	992	21	8.35	65.6	72	33.048	2.4	12.5	1	0.02	97.5	321	4.1	9.1		
OD61	SW	240034	611790	1392	651	378	21.5	7.6	24.6	58.4	43.74	12	2.5	0	0.04	1	452	1.5	2.7		
OD62	SW	282858	594422	608	4710	2830	21.6	8.72	58.4	51.2	10.692	1.8	8.75	1	0.25	64	324	1.1	-6.8		
OD63	HDW	172121	530402	380	930	558	22.4	7.24	51.2	26.3	18.6	37.5	4	0.06	0.15	1.7	362	2.9	-0.6	5.9	
OD64	SW	246529	577781	1338	194	115.7	20.9	8.02	8	22.4	3.402	4.2	3	0.4	0.07	1.5	124	5.5	-9.3		
OD65	SW	244596	579381	1308	129.8	64.9	27.4	7.1	8	16.8	4.86	1.6	3.5	0	0.23	0	109.8	0	-7.5		
OD66	SW	199810	545220	609	59	35.4	19	7.02	16.8	4.8	4.374	1.4	2	0	0.02	0	68.5	3.9	4.9		
OD67	HDW	240063	575274	1241	834	438	20.8	8.5	32	68	1.944	2	2	0.8	0	0	296	1.8	0.7	5.2	
OD68	HDW	240310	544852	1232	787	442	20.9	8	64	96	23.328	1.6	18	0.7	0.21	37.7	512.4	10	-1.5	9.30	

OD69	HDW	221550	550837		1098	648	21.9	8.1	26	42	28.7	0.0008	4	0.6	0.05	0	334.28	2.7	-0.1	
OD70	SW	225816	558914	975	890	450	28.7	7.2	80	48	24.3	1.4	37.5	0.99	0	0	506.3	0.1	-8.3	
OD71	SW	222857	557027	965	987	587	20.8	8.4	48	96	35.964	3.7	25	0.5	0.07	28.9	534.36	11	-1.4	-3.5
OD72	SW	228076	521014	890	870	440	24.6	8.62	96	88	41.31	3.8	34.8	1.08	0.09	32.8	527.04	0.9	7.9	-3.5
OD73	SW	263050	569924	540	240	120	25.4	7.27	64	44.4	36.45	4.5	11.25	0.66	0.09	28.6	367	0	8.1	-3.5
OD74	SW	221424	569604		1111	557	23.8	8.22	54.4	44	13.122	3.4	10	1.75	0.01	63	235	1	2.5	6.7
OD75	SW	234358	568267	1034	247	124	22.5	6.64	44	32	12.15		12.5	0	0.07	54.6	185.44	0.6	-0.2	6.3
OD76	SW	222718	551617	509	355	178	22.3	7.4	32	60	14.58	2.3	5	0	0.01	36.2	255.8	1.4	5.1	-0.5
OD77	SW	241863	553671	1232	60	30	23	5.9	60	6	5.346	1.3	2.5	0.1	0.05	24.6	142.3	1	7.2	-9.07
OD78	SW	218990	573110	1170	75.8	37.9		8	6	8	1.215	0.6	5		0.1	2	42.7	2.2	-8.4	
OD79	SW	219839	573609	1136	310	157.1	23.6	7.2	8	11.2	14.2	2.3	1.5	0.85	0.37	5	143	1.5	-7.8	
OD80	SW	221351	569395	1108	300	150	26	7.2	11.2	38.4	2.916	4.1	6.15	0.38	0.14	3	186.3	0	-8.9	
OD81	SW	221413	569306	1107	244	122	24.7	7.18	38.4	47.2	10.692	4.1	7.5	0.1	0.26	0	258.64	0.1	6.0	
OD82	SW	237296	540102	1130	383	192	25.2		27.2	49.6	12.15	4.7	8.4	0.19	0.1	34.3	219.6	1.6	2.3	-8.90
OD83	SW	228502	520339	880	248	125	21.6	6.9	49.6	32	33.048		7.5	0.55	0.17	54.4	256.6	3.3	7.5	
OD84	SW	228380	520152	881	194.3	97.5	23.3	6.8	40	20	14.58	1.3	2.5	0.5	0.1	3.1	247.9	1.2	-2.8	
OD85	SW	231332	543936	1006	950	480	26.5	8.6	32	56	20.4	7.5	1.25	3.1		24	342.2	0.2	-0.5	2.7
OD86	SW	231720	544459	1014	270	140	27.3	8.3	56	28	17.01	45	3.5	1.02	0.08	31	360	0.4	-1.9	-1.3
OD87	SW	222612	545757	870	259	129	22	7.32	28	40	3.888	4.5	15	0.27	4.33	27.3	126.88	16.5	4.5	-0.7
OD88	SW	220877	559899	1001	230	120	21.5	7.05	23.4	18.4	9.72	2.2	18.982	0.84	0	32.6	85.4	0	3.4	-3.5
OD89	SW	219795	557462	987	60.9	30.5	26.2	6.89	48.4	4	8.262	7.8	2.5	0.25	0.03	0.8	189	0	0.1	-0.1
OD90	SW	234991	570508	1134	395	198	25	6.9	4	44	4.86	1.9	1.25	1.33	0.05	12.4	178	2.5	-7.0	-1.1
OD91	SW	244257	573084	1334	324	163	25.1	6.9	44	44	5.832	13.2	2	0.13	0.39	14.7	234.24	1.6	7.7	
OD92	SW	228226	580880	1179	208	104	23.2	6.7	44	18.4	6.804	8.2	1.5	0.77	0	12	172.48	2.1	6.7	
OD93	SW	228025	580892	1179	358	180	22.4	6.82	18.4	28	5.832	7.8	3.5	0.91	0	13	161.2	2.6	-2.9	
OD94	SW	224265	559010	999	723	363	24	6.81	28	69.6	12.15	2	1.25	0.95	0.06	8	344.2	0.9	-0.8	5.3
OD95	SW	227507	579393	1155	413	207	22.5	6.99	48.2	46.4	8.6	2	7.5	0.54	0.41	22.1	256.7	0	3.0	
OD96	SW	228962	572414	1092	173.8	87.3	23.1	6.9	46.6	10.4	5.832	2.1	4	0	0.01	10.2	154.9	4.6	2.4	
OD97	SW	219931	573814	1137	741	372	24.8	7.14	24.5	62.4	2.916	5.6	3.5	1.48	0.24	3	286.2	0	-3.0	
OD98	SW	221758	561906	1022	668	334	24	6.74	62.4	73.6	19.683	4	1	0.86	0.22	1	457.5	1.7	3.6	
OD99	SW	210989	550340	802	300	150	22.2	8	73.6	32	14.094	0.1	1.25	1.44	0.07	32.3	287.2	1	4.8	-1.3
OD100	SW	243087	572249		580	290	25.5	8.85	20	20	12.15	4.5	17.5	1.49	0.24	78	73.2	0	-5.2	
OD101	SW	239543	544950	1163	3560	1780	24.3	7.65	120	320	30.132	14.5	75	0.76	0	560	475.8	0.3	5.4	9.30
OD102	SW	231627	526840	970	770	390	24.2	7.6	26	88	36.2	13.5	2.5	0.4	0.1	27	427	1.1	7.5	
OD103	BH	240029	625289	1301	362	206	23.1	8.43	24	15.23	19.197	6	8.15	0.2		15.85	158.65	8.2	3.8	4.9

OD104	BH	248718	611366	1654	636	363	24.3	8.63	37.24	14.83	29.16	5.08	6.5	0.14		35.4	236.9	2.3	0.8	-3.5	
OD105	BH	244589	618450	1303	340	194	22.5	8.47	20.3	38.08	46.58	5.08	17.02			18.73	289.7		9.4		
OD106	BH	229526	638762	1446	274	156	23.1	8.41	12.87	32.06	18.23	5.87	4.96	0.21		16.81	183.06		4.6	-2.55	-1.97
OD107	BH	228608	647279	1475	154	88	24.3	7.82	11.96	19.24	23.33	1.56	8.86			9.61	222.5		-8.4		
OD108	BH	230487	640387	1547	154	88	24.6	7.89	17.6	15.63	7.29	1.17	10.99	0.23		10.09	103.73		-0.9	-2.54	-1.92
OD109	BH	228731	572264	1079	263	150	23.5	8.42	5.98	37.68	17.5	3.91	9.57	0.52		17.77	155.6		7.4	5.7	-1.01
OD110	BH	235217	599988	1295	340	193	21.6	8.21	10.35	32.06	10.21	2.35	4.96			14.41	140.35		3.9		
OD111	HDW	172424	531184	399	2721	1551	22.6	9.05	125.54	32.87	4.86	3.91	173.5	0.62		62.8	169		-8.6	13.2	-2.37
OD112	HDW	224426	550369	895	241	137	25.6	8.23	53.4	30.46	9.23	14.86	6.38	0.46		14.41	267.34		1.3	2.7	-0.31

Appendix 2. Groundwater samples suitability for irrigation purposes from Quaternary sediment aquifers

Sample ID	X	Y	h(m)	Cond (µs/cm)	TDS (mg/l)	Na (meq/l)	K (meq/l)	Mg (meq/l)	Ca (meq/l)	SAR	Na%	MH%
D1	186873	519302	406	816	396	2.32	0.15	3.66	2.41	1.885	27.200	60.286
D2	187527	519278	404	637	317	1.81	0.16	2.8	1.88	1.676	27.256	59.829
D3	188608	515958	401	693	322	2.31	1.44	1.33	1.17	2.924	36.995	53.262
D4	188769	514480	381	2430	1154	7.85	0.18	6.01	2.03	5.538	48.872	74.793
D5	188334	514243	372	3450	1579	21.54	0.20	2	0.6	26.721	88.509	76.923
D6	191044	512218	388	591	676	2.23	0.16	0.1	0.9	4.461	65.806	10
D7	191109	512013	398	603	295	5.39	0.68	2.67	1.2	5.483	54.266	68.966
D8	192451	506657	375	7071	3431	61.13	0.16	0.60	0.46	118.704	98.039	56.874
D9	192641	494884	380	2240	1254	13.98	0.05	0.19	0.15	48.182	97.300	56.931
D23	167628	528254	370	1079	521	1.14	0.17	0.3	0.9	2.080	45.321	25
D24	172546	531578	371	937	343	6.02	0.48	0.27	3.84	5.943	56.753	6.494
D25	172197	531152	370	7070	3239	11.40	0.74	4.08	8.9	6.327	45.385	31.407
D26	172170	530378	373	635	308	3.66	0.26	0.41	2.5	4.293	53.634	14.040
D27	186321	521188	409	1628	739	1.61	0.31	3.44	8.4	0.935	11.693	29.064
D28	182648	522929	383	2940	1332	8.4	0.12	0.71	0.3	16.730	88.130	70.248
D29	184299	521592	396	1336	676	5.39	0.16	0.1	0.9	10.783	82.306	10
D30	182541	521233	384	5340	2523	17.83	0.17	0.2	1	32.546	92.867	16.667
D31	184857	520745	407	655	266	4.8	0.13	0.71	1	7.345	72.327	41.463
D32	183979	527736	383	852	411	3.72	0.21	2.44	1.07	3.975	50.067	69.629
D33	207753	555368	779	1012	506	3.67	0.21	4.25	3.8	2.587	30.760	52.795
D34	183181	525531	382	6150	3997.5	60.65	0.40	2.4	1.5	61.425	93.378	61.538
D35	184951	520803		1348	876.2	8.73	0.20	2.79	1.5	8.426	66.000	65.049
D36	184894	523672		2100	1365	13.59	0.11	0.33	0.36	32.623	94.411	48.042
D37	184288	521605		940	611	7.30	0.15	0.60	0.72	12.695	83.239	45.626
D38	194252	503743		10240	6656	71.53	0.18	0.26	0.18	215.931	99.137	58.656
D39	192358	506450	393	7080	4602	53.24	0.16	0.60	0.46	103.389	97.755	56.874
D40	188244	514042	372	3450	2242.5	24.36	0.20	2	0.6	30.216	89.701	76.923
D41	188677	514268	383	2460	1599	7.85	0.18	6.06	2.03	5.521	48.720	74.948
D42	188283	520978	432	2460	1599	7.19	0.18	2.7	1.95	6.666	59.786	58.065
D43	183077	521404	391	1836	1108	7.50	3.67	0.17	0.24	23.508	64.791	40.984
D44	184524	524728		1508	843	15.57	2.87	0.08	0.48	41.477	81.921	14.793
D45	186039	521721		645	326	3.30	1.38	3.5	1.6	2.926	33.756	68.627
D46	191007	511820		564	275	3.39	1.08	2.67	1.2	3.449	40.688	68.966
D66	199810	545220	609	59	35.4	0.73	0.04	0.36	0.24	1.879	53.284	60.298
D111	172424	531184	399	2721	1768.65	5.46	0.10	0.41	1.64	7.627	71.753	19.771

Appendix 3. Groundwater samples suitability for irrigation purposes from Hammer Basement aquifers

Sample ID	X	Y	h (m)	Cond (µs/cm)	TDS (mg/l)	Na (meq/l)	K (meq/l)	Mg (meq/l)	Ca (meq/l)	SAR	Na%	MH%
D47	227146	526379	902	1120	560	1.40	0.13	0.93	3.93	1.266	21.850	19.211
D48	241378	543432	1208	8320	4100	1.52	0.63	2.23	18.00	0.677	6.800	11.012
D49	241935	608642	1392	260	130	1.04	0.36	2.85	3.92	0.802	12.763	42.126
D50	364142	535433		284.6	143	1.22	0.10	1.01	1.60	1.506	30.958	38.756
D51	240716	622407	1303	390	230	1.39	0.12	1.01	2.80	1.425	26.156	26.557
D52	242163	624264	1315	327	196	2.43	0.23	0.81	1.20	3.435	52.075	40.299
D53	238951	628225	1369	362	235.3	1.04	0.23	0.61	1.70	1.374	29.133	26.327
D54	235645	629432	1419	252	151.5	0.61	0.00	0.38	0.60	1.227	38.200	39.071
D55	246560	584609	958	209	126.4	0.52	0.17	0.41	1.81	0.701	17.970	18.284
D56	264397	576162	543	620	310	0.70	0.19	0.61	3.40	0.695	14.210	15.159
D57	274627	590530	562	584	293	1.06	0.38	1.40	2.43	1.084	20.109	36.554
D58	248638	610128	1586	56.9	28.5	2.96	0.35	1.74	0.20	4.244	56.377	89.699
D59	239793	611237	1381	1233	739	0.17	0.00	0.12	3.28	0.189	4.864	3.572
D60	248575	611470	1600	1654	992	2.85	0.06	2.75	3.60	2.263	30.775	43.343
D61	240034	611790	1392	651	378	1.07	0.31	3.65	2.92	0.835	13.467	55.522
D62	282858	594422	608	4710	2830	2.54	0.05	0.89	2.56	2.734	42.064	25.819
D63	172121	530402	380	930	558	2.23	0.96	1.55	1.32	2.630	36.779	54.101
D64	246529	577781	1338	194	115.7	0.35	0.11	0.28	1.12	0.587	18.710	20.200
D65	244596	579381	1308	129.8	64.9	0.35	0.04	0.41	0.84	0.623	21.289	32.530
D67	240063	575274	1241	834	438	1.39	0.05	0.16	3.40	1.474	27.801	4.548
D68	240310	544852	1232	787	442	2.78	0.04	1.94	4.80	2.143	29.084	28.826
D69	221550	550837		1098	648	1.13	0.00	2.39	2.10	1.067	20.107	53.247
D70	225816	558914	975	890	450	3.48	0.04	2.03	2.40	3.307	43.811	45.763
D71	222857	557027	965	987	587	2.09	0.09	3.00	4.80	1.495	20.914	38.438
D72	228076	521014	890	870	440	4.17	0.10	3.44	4.40	2.981	34.456	43.895
D73	263050	569924	540	240	120	2.78	0.12	3.04	2.22	2.427	34.119	57.775
D74	221424	569604		1111	557	2.37	0.09	1.09	2.20	2.607	41.164	33.202
D75	234358	568267	1034	247	124	1.91	0.00	1.01	1.60	2.367	42.272	38.756
D76	222718	551617	509	355	178	1.39	0.06	1.22	3.00	1.355	24.558	28.826
D77	241863	553671	1232	60	30	2.61	0.03	0.45	0.30	6.043	77.009	59.759
D78	218990	573110	1170	75.8	37.9	0.26	0.02	0.10	0.40	0.737	33.552	20.200
D79	219839	573609	1136	310	157.1	0.35	0.06	1.18	0.56	0.527	16.177	67.878
D80	221351	569395	1108	300	150	0.49	0.11	0.24	1.92	0.662	17.675	11.234
D81	221413	569306	1107	244	122	1.67	0.11	0.89	2.36	1.852	33.221	27.407
D82	237296	540102	1130	383	192	1.18	0.12	1.01	2.48	1.266	24.660	28.991
D83	228502	520339	880	248	125	2.16	0.00	2.75	1.60	2.067	33.124	63.252
D84	228380	520152	881	194.3	97.5	1.74	0.03	1.22	1.00	2.337	43.615	54.853
D85	231332	543936	1006	950	480	1.39	0.19	1.70	2.80	1.312	22.870	37.778
D86	231720	544459	1014	270	140	2.43	1.15	1.42	1.40	2.901	38.007	50.311
D87	222612	545757	870	259	129	1.22	0.12	0.32	2.00	1.597	33.291	13.941
D88	220877	559899	1001	230	120	1.02	0.06	0.81	0.92	1.547	36.286	46.821
D89	219795	557462	987	60.9	30.5	2.10	0.20	0.69	0.20	4.465	65.908	77.490
D90	234991	570508	1134	395	198	0.17	0.05	0.41	2.20	0.216	6.150	15.547
D91	244257	573084	1334	324	163	1.91	0.34	0.49	2.20	2.335	38.745	18.094
D92	228226	580880	1179	208	104	1.91	0.21	0.57	0.92	3.138	52.988	38.130

D93	228025	580892	1179	358	180	0.80	0.20	0.49	1.40	1.165	27.720	25.769
D94	224265	559010	999	723	363	1.22	0.05	1.01	3.48	1.149	21.131	22.538
D95	227507	579393	1155	413	207	2.10	0.05	0.72	2.32	2.405	40.429	23.600
D96	228962	572414	1092	173.8	87.3	2.03	0.05	0.49	0.52	4.040	65.656	48.310
D97	219931	573814	1137	741	372	1.07	0.14	0.24	3.12	1.162	23.300	7.226
D98	221758	561906	1022	668	334	2.71	0.10	1.64	3.68	2.352	33.347	30.830
D99	210989	550340	802	300	150	3.20	0.00	1.17	1.60	3.842	53.538	42.332
D100	243087	572249		580	290	0.87	0.12	1.01	1.00	1.226	29.010	50.311
D101	239543	544950	1163	3560	1780	5.22	0.37	2.51	16.00	2.425	21.649	13.565
D102	231627	526840	970	770	390	1.13	0.35	3.02	4.40	0.830	12.711	40.674
D103	240029	625289	1301	362	235.3	1.04	0.15	1.60	0.76	1.358	29.323	67.750
D104	248718	611366	1654	636	413.4	1.62	0.13	2.43	0.74	1.818	32.903	76.620
D105	244589	618450	1303	340	221	0.88	0.13	3.88	1.90	0.734	12.982	67.091
D106	229526	638762	1446	274	178.1	0.56	0.15	1.52	1.60	0.633	14.602	48.657
D107	228608	647279	1475	154	100.1	0.52	0.04	1.94	0.96	0.610	15.002	66.898
D108	230487	640387	1547	154	100.1	0.77	0.03	0.61	0.78	1.299	35.034	43.737
D109	228731	572264	1079	263	171	0.26	0.10	1.46	1.88	0.284	7.022	43.632
D110	235217	599988	1295	340	221	0.45	0.06	0.85	1.60	0.575	15.182	34.674
D112	224426	550369	895	241	156.7	2.32	0.38	0.77	1.52	3.067	46.482	33.556
D10	222264	549636	910	663	352	0.79	0.11	0.77	1.52	1.045	24.797	33.556
D11	207846	555573	777	1052	526	4.06	0.22	4.76	3.50	2.826	32.384	57.619
D12	221505	569509	1117	638	333	1.05	0.12	0.20	0.80	2.104	48.370	20.000
D13	223763	568179	1117	638	379	2.38	0.13	1.83	4.20	1.941	27.921	30.290
D14	228126	581102	1180	434	229	2.05	0.16	0.00	0.80	4.579	68.106	0.000
D15	226290	578083	1136	726	171	2.50	0.11	2.43	4.00	1.971	27.660	37.824
D16	228246	572987	1109	738	379	0.53	0.10	0.85	1.88	0.647	15.871	31.111
D17	235380	600233	1311	602	179	1.26	0.11	0.91	3.00	1.276	23.871	23.241
D18	186022	521659	410	718	335	3.30	0.88	3.00	1.60	3.081	37.597	65.217
D19	232601	637098	1448	341	173	0.76	0.13	0.30	2.80	0.859	18.961	9.677
D20	185519	522162	409	633	298	1.31	0.16	0.36	0.50	2.835	56.345	41.748
D21	184780	523746	399	1548	742	1.44	0.11	0.30	0.70	2.878	56.507	30.000
D22	236938	633201	1416	945	453	2.74	0.13	2.43	4.90	2.026	26.884	33.182

Appendix 4. Lithostratigraphic column of Sabisa 1B (after Tullow oil, 2013).

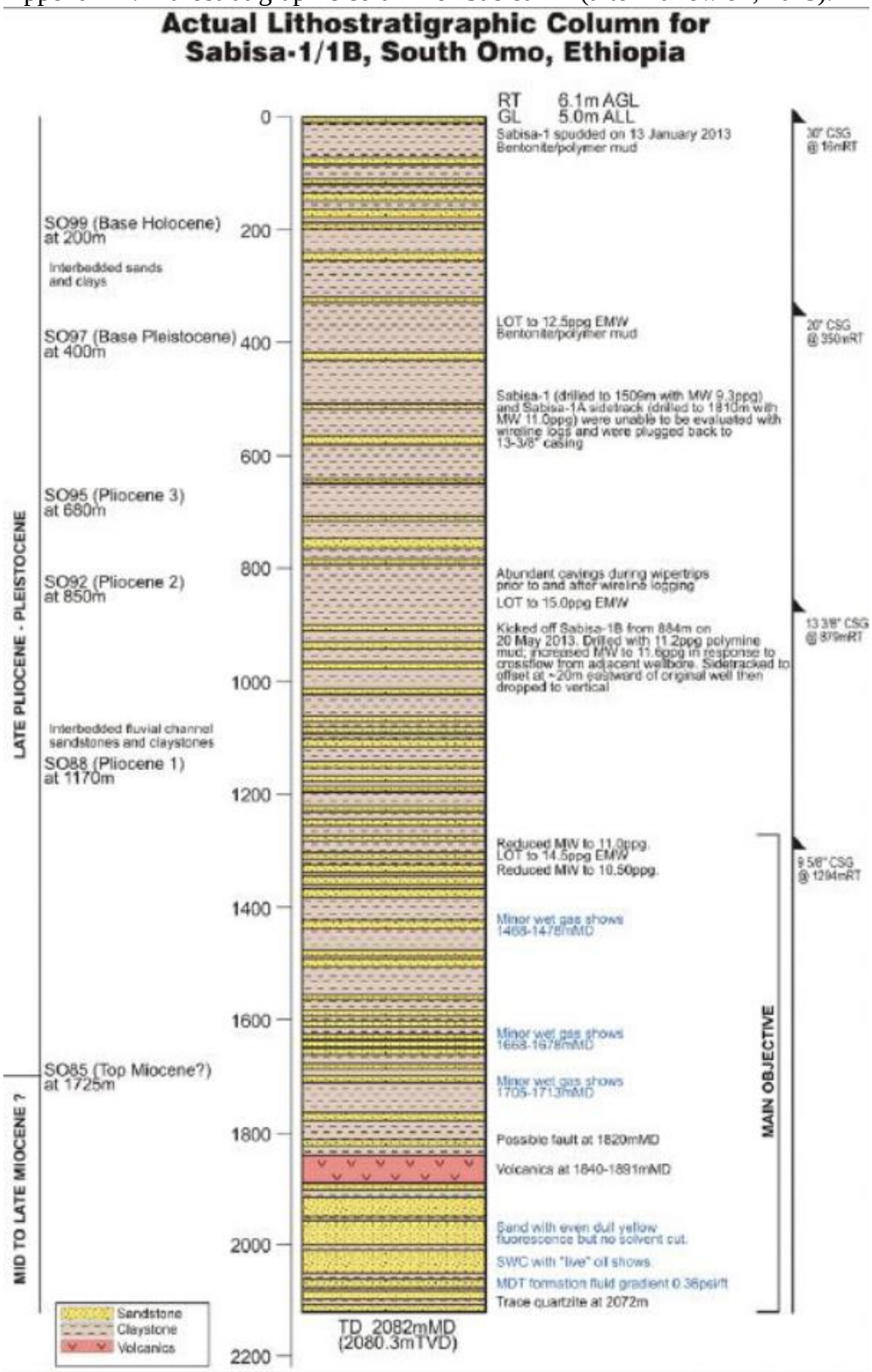

Appendix 5. Schoeller index values. Ion concentration expressed by (meq/l).

SampleID	aquifer-type	Na^+	K^+	Mg^{2+}	Ca^{2+}	Cl^-	$SO4^{2-}$	HCO3-	CAI1	CAI2	(Ca+Mg)-(HCO3+SO4)	Na+K-Cl
OD1	Qat.sedt	2.32	0.15	3.61	2.41	0.60	0.88	5.56	-3.11	-0.29	-0.41	1.87
OD2	Qat.sedt	1.81	0.16	2.77	1.88	0.50	0.08	5.34	-2.91	-0.27	-0.78	1.47
OD3	Qat.sedt	2.31	1.44	1.32	1.17	0.23	1.06	4.26	-15.03	-0.66	-2.84	3.52
OD4	Qat.sedt	7.85	0.18	5.93	2.03	3.95	0.93	8.70	-1.03	-0.42	-1.67	4.07
OD5	Qat.sedt	21.54	0.20	1.98	0.60	23.87	1.06	3.80	0.09	0.44	-2.29	-2.13
OD6	Qat.sedt	2.23	0.16	0.10	0.90	0.54	0.71	2.39	-3.44	-0.60	-2.10	1.85
OD7	Qat.sedt	5.39	0.68	2.63	1.20	0.60	0.59	7.11	-9.11	-0.71	-3.87	5.47
OD8	Qat.sedt	61.13	0.16	0.60	0.46	31.54	2.57	16.20	-0.94	-1.59	-17.72	29.76
OD9	Qat.sedt	13.98	0.05	0.19	0.15	9.99	0.36	5.46	-0.40	-0.69	-5.48	4.04
OD20	Qat.sedt	1.31	0.16	0.35	0.50	0.47	0.21	1.80	-2.11	-0.50	-1.16	1.00
OD21	Qat.sedt	1.44	0.11	0.30	0.70	0.24	0.67	1.80	-5.46	-0.53	-1.47	1.31
OD23	Qat.sedt	1.14	0.17	0.30	0.90	0.42	0.00	1.80	-2.11	-0.49	-0.61	0.89
OD24	Qat.sedt	6.02	0.48	0.26	3.84	2.43	0.00	7.48	-1.68	-0.55	-3.37	4.08
OD25	Qat.sedt	11.40	0.74	4.02		7.04	2.60		-0.72	-1.96	1.42	5.09
OD26	Qat.sedt	3.66	0.26	0.40	2.50	1.64	0.02	5.51	-1.39	-0.41	-2.63	2.28
OD27	Qat.sedt	1.61	0.31	3.40		0.88	2.33	6.00	-1.17	-0.12	-4.93	1.03
OD28	Qat.sedt	8.40	0.12	0.70	0.30	7.58	0.08	1.80	-0.12	-0.50	-0.89	0.94
OD29	Qat.sedt	5.39	0.16	0.10	0.90	3.44	0.71	2.39	-0.61	-0.68	-2.10	2.11
OD30	Qat.sedt	17.83	0.17	0.20	1.00	4.74	0.88	14.30	-2.80	-0.87	-13.97	13.26
OD32	Qat.sedt	3.72	0.21	2.41	1.07	0.80	0.75	4.79	-3.91	-0.56	-2.06	3.13
OD34	Qat.sedt	60.65	0.40	2.37	1.50	37.25	2.73	13.40	-0.64	-1.48	-12.26	23.81
OD35	Qat.sedt	8.73	0.20	2.76	1.50	0.89	1.30	8.53	-9.08	-0.82	-5.58	8.05
OD36	Qat.sedt	13.59	0.11	0.33	0.36	7.46	0.15	5.90	-0.83	-1.03	-5.36	6.23
OD37	Qat.sedt	7.30	0.15	0.60	0.72	0.62	2.41	3.15	-11.00	-1.23	-4.24	6.83
OD38	Qat.sedt	71.53	0.18	0.25	0.18	44.62	1.13	16.20	-0.61	-1.56	-16.89	27.10
OD39	Qat.sedt	53.24	0.16	0.60	0.46	31.54	1.42	13.48	-0.69	-1.47	-13.85	21.87
OD40	Qat.sedt	24.36	0.20	1.98	0.60	23.87	0.93	5.33	-0.03	-0.11	-3.68	0.69
OD42	Qat.sedt	7.19	0.18	2.67	1.95	3.87	0.08	5.56	-0.90	-0.62	-1.03	3.50
OD43	Qat.sedt	7.50	3.67	0.16	0.24	4.73	1.35	3.67	-1.36	-1.28	-4.62	6.43
OD44	Qat.sedt	15.57	2.87	0.08	0.48	1.21	1.27	13.40	-14.22	-1.17	-14.11	17.23
OD45	Qat.sedt	3.30	1.38	3.46	1.60	0.51	0.17	7.90	-8.25	-0.52	-3.01	4.18
OD46	Qat.sedt	3.39	1.08	2.63	1.20	0.59	0.23	6.90	-6.55	-0.54	-3.30	3.88
OD63	Qat.sedt	2.23	0.96	1.53	1.32	0.11	0.04	5.93		-0.52	-3.12	3.07
OD66	Qat.sedt	0.73	0.04	0.36	0.24	0.06	0.00	1.12	-12.60	-0.63	-0.52	0.71
OD10	Ham.bas	0.79	0.11	0.76	1.52	0.18	0.30	2.83	-4.00	-0.23	-0.85	0.72
OD11	Ham.base.	4.06	0.22	4.70	3.50	0.15	1.40	10.90	-28.23	-0.34	-4.10	4.13
OD12	Ham.base.	1.05	0.12	0.20	0.80	0.48	0.17	1.61	-1.43	-0.39	-0.78	0.69
OD13	Ham.base.	2.38	0.13	1.80	4.20	0.31	0.06	8.20	-7.17	-0.27	-2.26	2.20

OD14	Ham.base.	2.05	0.16	0.00	0.80	0.23	1.33	1.61	-8.67	-0.67	-2.14	1.98
OD15	Ham.base.	2.50	0.11	2.40	4.00	0.37	0.06	8.80	-6.01	-0.25	-2.46	2.23
OD16	Ham.base.	0.53	0.10	0.84	1.88	0.27	0.37	2.54	-1.37	-0.13	-0.19	0.37
OD17	Ham.base.	1.26	0.11	0.90	3.00	0.15	0.08	5.00	-8.20	-0.24	-1.19	1.22
OD18	Ham.base.	3.30	0.88	2.96	1.60	0.51	1.09	5.74	-7.17	-0.54	-2.27	3.68
OD19	Ham.base.	0.76	0.13	0.30	2.80	0.29	0.13	3.61	-2.04	-0.16	-0.64	0.60
OD22	Ham.base.	2.74	0.13	2.40	4.90	0.48	0.65	9.20	-5.03	-0.24	-2.54	2.40
OD31	Ham.base.	4.80	0.13	0.70	1.00	1.69	0.33	5.11	-1.91	-0.59	-3.75	3.24
OD33	Ham.base.	3.67	0.21	4.20	3.80	0.04	0.96	10.61	-104.95	-0.33	-3.57	3.84
OD41	Ham.base.	7.85	0.18	5.98	2.03	3.95	0.93	8.66	-1.03	-0.42	-1.58	4.07
OD47	Ham.base.	1.40	0.13	0.92	3.93	0.03	1.04	5.21	-53.28	-0.24	-1.41	1.50
OD48	Ham.base.	1.52	0.63	2.20			10.83	8.00		-0.11	-16.63	2.15
OD49	Ham.base.	1.04	0.36	2.82	3.92	0.20	1.29	5.51	-6.11	-0.18	-0.07	1.21
OD50	Ham.base.	1.22	0.10	1.00	1.60	0.25	0.00	3.80	-4.21	-0.28	-1.20	1.07
OD51	Ham.base.	1.39	0.12	1.00	2.80	0.14	0.54	4.80	-9.70	-0.26	-1.54	1.37
OD52	Ham.base.	2.43	0.23	0.80	1.20	0.10	0.00	4.00	-26.04	-0.64	-2.00	2.57
OD53	Ham.base.	1.04	0.23	0.60	1.70	0.18	0.08	2.75	-5.96	-0.38	-0.54	1.09
OD54	Ham.base.	0.61	0.00	0.38	0.60	0.13	0.02	1.40	-3.80	-0.34	-0.44	0.48
OD55	Ham.base.	0.52	0.17	0.40	1.81	0.21	0.00	2.40	-2.26	-0.20	-0.19	0.48
OD56	Ham.base.	0.70	0.19	0.60	3.40	0.13	0.06	5.36	-6.01	-0.14	-1.42	0.76
OD57	Ham.base.	1.06	0.38	1.38	2.43	0.06	0.00	4.28	-24.66	-0.32	-0.47	1.39
OD58	Ham.base.	2.96	0.35	1.72	0.20	0.13	0.04	4.69	-25.05	-0.67	-2.82	3.18
OD59	Ham.base.	0.17	0.00	0.12	3.28	0.10	0.12	3.21	-0.76	-0.02	0.07	0.08
OD60	Ham.base.	2.85	0.06	2.72	3.60	0.35	2.03	5.26	-7.27	-0.35	-0.97	2.56
OD61	Ham.base.	1.07	0.31	3.60	2.92	0.07	0.02	7.41	-18.56	-0.18	-0.91	1.31
OD62	Ham.base.	2.54	0.05	0.88	2.56	0.25	1.33	5.31	-9.49	-0.35	-3.20	2.34
OD64	Ham.base.	0.35	0.11	0.28	1.12	0.08	0.03	2.03	-4.39	-0.18	-0.66	0.37
OD65	Ham.base.	0.35	0.04	0.40	0.84	0.10	0.00	1.80	-2.94	-0.16	-0.56	0.29
OD67	Ham.base.	1.39	0.05	0.16	3.40	0.06	0.00	4.85	-24.61	-0.29	-1.29	1.39
OD68	Ham.base.	2.78	0.04	1.92	4.80	0.51	0.79	8.40	-4.57	-0.25	-2.47	2.32
OD69	Ham.base.	1.13	0.00	2.36	2.10	0.11	0.00	5.48	-9.03	-0.19	-1.02	1.02
OD70	Ham.base.	3.48	0.04	2.00	2.40	1.06	0.00	8.30	-2.33	-0.30	-3.90	2.46
OD71	Ham.base.	2.09	0.09	2.96	4.80	0.70	0.60	8.76	-2.10	-0.16	-1.60	1.48
OD72	Ham.base.	4.17	0.10	3.40	4.40	0.98	0.68	8.64	-3.36	-0.35	-1.52	3.29
OD73	Ham.base.	2.78	0.12	3.00	2.22	0.32	0.60	6.02	-8.14	-0.39	-1.39	2.58
OD74	Ham.base.	2.37	0.09	1.08	2.20	0.28	1.31	3.85	-7.71	-0.42	-1.88	2.17
OD75	Ham.base.	1.91	0.00	1.00	1.60	0.35	1.14	3.04	-4.43	-0.37	-1.58	1.56
OD76	Ham.base.	1.39	0.06	1.20	3.00	0.14	0.75	4.19	-9.30	-0.26	-0.75	1.31
OD77	Ham.base.	2.61	0.03	0.44	0.30	0.07	0.51	2.33	-36.52	-0.90	-2.11	2.57
OD78	Ham.base.	0.26	0.02	0.10	0.40	0.14	0.04	0.70	-0.96	-0.18	-0.24	0.14
OD79	Ham.base.	0.35	0.06	1.17	0.56	0.04	0.10	2.34	-8.63	-0.15	-0.72	0.36

OD80	Ham.base.	0.49	0.11	0.24	1.92	0.17	0.06	3.05	-2.42	-0.13	-0.96	0.42
OD81	Ham.base.	1.67	0.11	0.88	2.36	0.21	0.00	4.24	-7.40	-0.37	-1.00	1.56
OD82	Ham.base.	1.18	0.12	1.00	2.48	0.24	0.71	3.60	-4.51	-0.25	-0.83	1.07
OD83	Ham.base.	2.16	0.00	2.72	1.60	0.21	1.13	4.21	-9.21	-0.36	-1.02	1.95
OD84	Ham.base.	1.74	0.03	1.20	1.00	0.07	0.06	4.06	-24.17	-0.41	-1.93	1.70
OD85	Ham.base.	1.39	0.19	1.68	2.80	0.04	0.50	5.61	-43.97	-0.25	-1.63	1.55
OD86	Ham.base.	2.43	1.15	1.40	1.40	0.10	0.65	5.90	-35.40	-0.53	-3.75	3.49
OD87	Ham.base.	1.22	0.12	0.32	2.00	0.42	0.57	2.08	-2.15	-0.34	-0.33	0.91
OD88	Ham.base.	1.02	0.06	0.80	0.92	0.53	0.68	1.40	-1.01	-0.26	-0.36	0.54
OD89	Ham.base.	2.10	0.20	0.68	0.20	0.07	0.02	3.10	-31.72	-0.72	-2.24	2.23
OD90	Ham.base.	0.17	0.05	0.40	2.20	0.04	0.26	2.92	-5.32	-0.06	-0.58	0.19
OD91	Ham.base.	1.91	0.34	0.48	2.20	0.06	0.31	3.84	-38.96	-0.53	-1.47	2.20
OD92	Ham.base.	1.91	0.21	0.56	0.92	0.04	0.25	2.83	-49.25	-0.68	-1.60	2.08
OD93	Ham.base.	0.80	0.20	0.48	1.40	0.10	0.27	2.64	-9.14	-0.31	-1.03	0.90
OD94	Ham.base.	1.22	0.05	1.00	3.48	0.04	0.17	5.64	-35.03	-0.21	-1.33	1.23
OD95	Ham.base.	2.10	0.05	0.71	2.32	0.21	0.46	4.21	-9.16	-0.41	-1.64	1.94
OD96	Ham.base.	2.03	0.05	0.48	0.52	0.11	0.21	2.54	-17.46	-0.71	-1.75	1.97
OD97	Ham.base.	1.07	0.14	0.24	3.12	0.10	0.06	4.69	-11.26	-0.23	-1.39	1.11
OD98	Ham.base.	2.71	0.10	1.62	3.68	0.03	0.02	7.50	-98.95	-0.37	-2.22	2.79
OD99	Ham.base.	3.20	0.00	1.16	1.60	0.04	0.67	4.71	-89.95	-0.59	-2.62	3.17
OD100	Ham.base.	0.87	0.12	1.00	1.00	0.49	1.63	1.20	-1.00	-0.17	-0.83	0.49
OD101	Ham.base.	5.22	0.37	2.48		2.11	11.67	7.80	-1.65	-0.18	-16.99	3.48
OD102	Ham.base.	1.13	0.35	2.98	4.40	0.07	0.56	7.00	-19.97	-0.19	-0.18	1.41
OD103	Ham.base.	1.04	0.15	1.58	0.76	0.23	0.33	2.60	-4.22	-0.33	-0.59	0.97
OD104	Ham.base.	1.62	0.13	2.40	0.74	0.18	0.74	3.88	-8.55	-0.34	-1.48	1.57
OD105	Ham.base.	0.88	0.13	3.83	1.90	0.48	0.39	4.75	-1.11	-0.10	0.60	0.53
OD106	Ham.base.	0.56	0.15	1.50	1.60	0.14	0.35	3.00	-4.08	-0.17	-0.25	0.57
OD107	Ham.base.	0.52	0.04	1.92	0.96	0.25	0.20	3.65	-1.24	-0.08	-0.97	0.31
OD108	Ham.base.	0.77	0.03	0.60	0.78	0.31	0.21	1.70	-1.57	-0.25	-0.53	0.49
OD109	Ham.base.	0.26	0.10	1.44	1.88	0.27	0.37	2.55	-0.34	-0.03	0.40	0.09
OD110	Ham.base.	0.45	0.06	0.84	1.60	0.14	0.30	2.30	-2.65	-0.14	-0.16	0.37